ADVANCES IN MODERN WOVEN FABRICS TECHNOLOGY

Edited by **Savvas Vassiliadis**

INTECHWEB.ORG

Advances in Modern Woven Fabrics Technology
Edited by Savvas Vassiliadis

Published by InTech
Janeza Trdine 9, 51000 Rijeka, Croatia

Publishing Process Manager Niksa Mandic
Technical Editor Teodora Smiljanic
Cover Designer Jan Hyrat
Image Copyright meirion matthias, 2010. Used under license from Shutterstock.com

First published July, 2011
Printed in Croatia

A free online edition of this book is available at www.intechopen.com
Additional hard copies can be obtained from orders@intechweb.org

Advances in Modern Woven Fabrics Technology, Edited by Savvas Vassiliadis
p. cm.
ISBN 978-953-307-337-8

Contents

Preface IX

Part 1 Multifunctional Woven Fabrics 1

Chapter 1 **Electro-Conductive Sensors and Heating Elements Based on Conductive Polymer Composites in Woven Fabric Structures 3**
Irina Cristian, Saad Nauman, Cédric Cochrane and Vladan Koncar

Chapter 2 **Smart Woven Fabrics in Renewable Energy Generation 23**
Derman Vatansever, Elias Siores, Ravi L. Hadimani and Tahir Shah

Part 2 Computational Modelling and Structural Woven Fabrics 39

Chapter 3 **Mechanical Analysis of Woven Fabrics: The State of the Art 41**
Savvas Vassiliadis, Argyro Kallivretaki, Dimitra Domvoglou and Christofer Provatidis

Chapter 4 **Finite Element Modeling of Woven Fabric Composites at Meso-Level Under Combined Loading Modes 65**
Mojtaba Komeili and Abbas S. Milani

Chapter 5 **Multiaxis Three Dimensional (3D) Woven Fabric 79**
Kadir Bilisik

Part 3 Design and Appearance of Woven Fabrics 107

Chapter 6 **Functional Design of the Woven Filters 109**
Cioară Lucica and Cioară Ioan

Chapter 7 **Color and Weave Relationship in Woven Fabrics 129**
Kavita Mathur and Abdel-Fattah M. Seyam

Part 4 Advanced Properties of Woven Fabrics 151

Chapter 8 **Sensory and Physiological Issue 153**
Laurence Schacher, Sourour Bensaid, Selsabil El-Ghezal Jeguirim and Dominique Adolphe

Chapter 9 **Superhydrophobic Superoleophobic Woven Fabrics 179**
Hoonjoo Lee and Jeffery Owens

Chapter 10 **The Flame Retardant Nomex/cotton and Nylon/Cotton Blend Fabrics for Protective Clothing 197**
Charles Q. Yang and Hui Yang

Chapter 11 **Liquid Transport in Nylon 6.6. Woven Fabrics Used for Outdoor Performance Clothing 211**
A. B. Nyoni

Preface

Woven fabric: a simple structure, with complex properties and a unique behaviour! Two sets of interlaced yarns, the warp and the weft, in various patterns result in this valuable fibrous product. The woven fabrics are highly deformable, especially in bending and shearing. Consequently, they were the only materials fulfilling the requirements of the body protection, providing simultaneously a high level of comfort. The same basic production principles are adopted from the time of the hand crafted production until today for the industrialized products. The early use of the woven fabrics was mainly in clothing and domestic applications. The so called technical applications in the past were rare (sails, tents etc). Gradually, more and more technical applications appeared. In the last period an explosive use of the woven fabrics in new application fields is being observed. In parallel to the common traditional clothing and domestic commodities, very important high value added technical products have been designed and produced.

Currently, the use of woven fabrics is being continuously expanded in fields including medical, military, structural, telecommunications, electronic, aerospace etc. applications. Thus the importance of the woven fabrics increases constantly. The specific and critical character of the technical applications imposed a dynamic change in the fields of the design, engineering, production and testing. The traditional empirical approach has been replaced by the careful modelling, calculation of the properties, prediction of the behaviour and the final evaluation of the performance. The modern approach is reflected on the majority of the recent research results, the patents and the scientific publications of the academic and industrial research community.

The new technological position and role of the woven fabrics causes important changes and evolutions in some key fields. Therefore the four sections of the current book correspond to the most influenced thematic areas:

- Multifunctional character
- Computational modelling and structural elements
- Design and appearance
- Advanced properties

The first section focused on the multifunctional character of the woven fabrics consists of two chapters. The heat sensors and the heating elements based on the use of conductive fibres, incorporated in woven fabrics are presented in the first chapter. The

important issue of the energy harvesting is the topic covered by the second chapter. Piezoelectric fibres are used in woven fabrics and their imposed mechanical deformations result in the generation of electrical power.

The second section consists of three chapters and deals with the computational modelling and structural elements. Chapter three comprises a thorough examination of the mechanical modelling of the woven fabrics and leads to the state-of-the-art of the computational mechanical modelling in various scales. The use of the finite elements method for the prediction of the mechanical behaviour of woven fabric composites at meso-level and under combined loading modes, is the subject of the fourth chapter. The overview of the production methods and the classification of the multiaxis three-dimensional fabrics are the subject of the fifth chapter.

The third section contains three chapters and includes design and appearance issues. The computer supported functional design of the woven filters with the respective applications are presented in the sixth chapter. The automatic recognition of the woven fabrics based on the computational image processing method of the texture analysis is the subject of the seventh chapter. The eighth chapter involves the examination of the color and weave design relationship in woven fabrics made from colored yarns.

The fourth section, about the advanced properties of woven fabrics, consists of four chapters. The sensory and physiological issues as major and strategic design factors involving artificial neural networks and fuzzy logic tools is the topic of the ninth chapter of the book. In the tenth chapter is presented a theoretical and practical approach of the super-hydrophobic and super-oleophovic woven fabrics. The finishing techniques for the production of flame retardant Nomex/cotton, nylon/cotton and polyester/cotton blend fabrics for protective clothing is described in chapter eleven. In the twelfth chapter exists the presentation of the liquid transport issues for Nylon 6.6 woven fabrics used for outdoor performance clothing.

The authors of the twelve chapters are widely known for their expertise. They have been invited to contribute in this book because of their international reputation in their particular fields. Every single chapter though has a pioneering and innovative character corresponding to the respective state-of-the-art. The result is a highly interdisciplinary book with breaking through contents.

From the current position, I would like to thank the authors for their valuable contribution, prompt response and cooperation during the preparation of the book. The open access publishing principle is a new and powerful tool for the free and worldwide dissemination of the scientific knowledge. I wish and hope that the current open access book will serve better and more efficiently the future readers.

Savvas G. Vassiliadis
TEI Piraeus
Greece

Part 1

Multifunctional Woven Fabrics

1

Electro-Conductive Sensors and Heating Elements Based on Conductive Polymer Composites in Woven Fabric Structures

Irina Cristian[1,2,3], Saad Nauman[1,2],
Cédric Cochrane[1,2] and Vladan Koncar[1,2]
[1]*University Lille Nord de France*
[2]*ENSAIT, GEMTEX, F-59100 Roubaix*
[3]*Technical University GHEORGHE ASACHI of Iaşi*
[1,2]*France*
[3]*Romania*

1. Introduction

The use of intelligent materials which are capable of reacting to external stimuli is growing in the field of textiles. Conductive materials, metals as well as conducting polymers, are already being used in many textile applications, like antistatic materials, electromagnetic interference shielding, heating, transport of electrical signals, sensors etc.
Conductive polymers are some of the developments which seem to respond to specific properties of textile materials, like flexibility and deformability. Two sub-classes of conductive polymers can be identified: intrinsically conductive polymers and conductive polymer composites.
Inherently conducting polymers are composed of polymer chains containing long conjugated double bonds which give rise to highly conducting properties, and they have been considered as promising materials (Heeger, 2002; Kumar et al., 1998). Inherently conducting polymers are suitable for applications in many domains of intelligent textiles, but they present some substantial disadvantages, like infusibility or insolubility in common organic solvents, weak mechanical properties and poor procesability. However, advanced solution processing of this class of polymers has been developed significantly over the last decade to improve their low solubility. For example, chemical modification of monomers with dopants has enhanced the solubility in the case of polythiophene and polyaniline (Haba et al., 1999; Gettinger et al., 1995).
For their part, composite conductive polymers are obtained by blending (generally by melt mixing) an insulating polymer matrix (thermoplastic or thermosetting plastic) with conductive fillers like carbon black, carbon fibres or nanotubes, metallic particles or conductive polymers. The presence of filler particles in the matrix may have a negative impact on the mechanical properties of the final composite (Krupa et al., 2001; Novak et al., 2002). Instead of this, the development in the field of composite conductive polymers seems therefore to be a promising approach for intelligent textiles own to simplicity of preparing and to their low cost.

In this chapter, two applications (sensor and actuator) based on coating of textile materials with conductive polymer composites are presented. Several different coating techniques for intelligent textile structures exist - the one chosen for both applications was developed in our laboratory (Cochrane et al., 2007, 2010) based on dispersed carbon black particles (Printex® L6) in a polymer solution (Styren-Butadien-Styren or latex), using a solvent.

In the first part of this chapter, a new approach of NDE (Non Destructive Evaluation) using fibrous sensors inserted inside composite woven reinforcements during their weaving is presented. The use of 3D woven fabrics as the reinforcing medium for composites is becoming a popular choice, due to various advantages such as reduced cost and shorter production cycle, greater design flexibility and superior mechanical properties (Kamiya et al., 2000). Recently, these high performance composites reinforced with 3D structures have found wide applications in various industrial areas such as aerospace, aircraft, automobile, civil engineering etc. Good quality and reliability are basic requirements for advanced composite structures which are often used under harsh environments. To improve their performance, the cure monitoring of technological process is clearly necessary. At the same time, in service NDE is also needed to keep these structures operating safely and reliably.

A novel flexible piezoresistive fibrous sensor has been developed and optimized for in situ structural deformation sensing in carbon composites. Those sensors were inserted as weft in 3D-woven interlock reinforcement, during the weaving process on a special weaving loom. The reinforcement was then impregnated in epoxy resin and was later subjected to quasi static tensile loading. It was found that the sensor was able to detect deformations in the composite structure until rupture since it was inserted together with reinforcing tows.

The morphological and electromechanical properties of the fibrous sensors have been analyzed using tomography and yarn tensile strength tester. An appropriate data acquisition module has also been developed and used for data acquisition and its further treatment. The results obtained for carbon composite specimens under standard testing conditions have validated in situ monitoring concept using our fibrous textile sensors.

The second part of this chapter presents a woven fabric containing an original heating element. Textile actuators like heating fabrics can find applications in numerous and varied fields such as sports, leisure, medical and automotive (Droval et al., 2005; El-Trantawy et al., 2002). Usually actuators need heavy power supplies that are rarely flexible and lightweight which badly affects wearability. Our heating element is designed to adapt to flexible structures. Metallic yarns, used as electrodes are integrated in a woven structure in a comb-teeth arrangement. These electrodes are connected to a power supply. A thin conductive coating is applied on the fabric surface and on the electrode arrangement, in order to ensure uniform heat distribution. The coating is a composite material based on aqueous latex dispersed with carbon black as filler. The heating element (comb electrodes and electro-conductive coating) can thus adopt the desired pattern. This is an important aspect of our heating element as it allows integration of the heating element in various fabrics designed for varied and diverse applications. In our research the distance between electrodes remained unchanged, the only variable value being the percentage of filler. The results regarding the power consumption and textile surface temperature for different filler content were registered. From these results, optimum filler content for heating application was defined. A thermal image of the heating fabric operating at low voltage is given, in order to demonstrate the efficiency of our system. A more precise measurement of surface temperature is thus possible. For applied voltage of 15 V, the maximum temperature gained

was about 50 °C. The thermal image also demonstrates the homogeneity of heating provided by our system. Potential applications of these self heating fabrics include garments designed to provide thermal comfort and antifreeze safety.

2. Electro-conductive sensors for on-line measurements of structural deformation in composites reinforced with 3D-woven fabrics

Weaving technique has been used for a long time in order to obtain technical textile products for industrial applications. An important use of this technology is for the manufacturing of 3D reinforcements using high performance fibres (carbon, glass, aramid etc.). 3D reinforcement based composites, in combination with high-performance fibres, are being increasingly used in the aerospace industry (Ko, 2007). Particular advantages of these fabrics mentioned in the literature include better through the thickness properties, better out of plane properties, high impact resistance, enhanced delamination resistance, resistance to crack propagation, impact/fracture resistance, improved post impact mechanical properties, damage tolerance, dimensional stability, ease of fabrication and minimal need of cutting, lay up and joining.

Regarding these properties it can be safely concluded that 3D woven fabrics constitute the most promising class of reinforcements for composite materials for high tech structural applications. To improve their performance, the cure monitoring of technological process is clearly necessary. At the same time, in-service non destructive evaluation is also needed to keep these structures operating safely and reliably. Non destructive evaluation techniques have been developed in the past including ultrasonic scanning, acoustic emission, shearography, stimulated infrared thermography, fibre brag grating sensors and vibration testing etc. (Black, 2009). The challenge today is to develop new low cost techniques which can perform on-line structural health assessment starting from the manufacture of composite structure to the real service of these structures in the field. Moreover, the non destructive evaluation techniques have to be integrated in the design phase and sensors should be inserted during the fabrication of composites, in order to improve accuracy and reduce their costs. The classical non destructive evaluation techniques are difficult to adapt. They are not well suited for on-line structural health monitoring, because of difficulties in making in situ implementation.

One possible solution is to use intelligent textile materials and structures which provide real possibility for on-line and in situ monitoring of structural integrity. Such intelligent materials are made by coating or treating textile yarns, filaments or fabrics with nanoparticles or conductive & semi-conductive polymers giving them special properties.

A review of piezoresistive sensing approaches already being applied to measure strain in fabrics/composites shows that several sensing mechanisms exist (Dharap et al., 2004; Lorussi et al., 2005; Scilingo et al., 2003; Fiedler et al., 2004). These approaches may be categorized on the basis of manufacturing technology as nanotube networks, use of carbon tows for self-sensing and semi-conductive coatings.

Nanotubes have been investigated in detail for use as sensing mechanisms, both for smart textile applications and for structural health monitoring of composites. Significant challenges still exist in their development, for example the efficient growth of macroscopic-length carbon nanotubes, controlled growth of nanotubes on desired substrates, durability of nanotube based sensors and actuators, effective dispersion in polymer matrices and their orientation. Therefore, there is a need to develop both experimental and analytical techniques to bridge the

nano and macro scales towards optimization so as to use nanotube networks as sensors inside macroscale (fabric) or mesoscale (tow) composites (Li et al., 2005).
Carbon fibre reinforced composites offer a unique possibility of using carbon tows as sensing network because of their conductivity. However such an approach can only be used for conductive fibre based composites. Moreover, before applying such an approach for structural health monitoring it is imperative to understand the deformation mechanism of the reinforcement. Any anomaly in the deformation mechanism can threaten the sensing mechanism's validity and efficacy.
Concerning semi conductive coatings, they are easy to realize and can be made wash resistant. Their use as percolation networks for sensing in structural health monitoring applications is quite promising and needs to be further investigated.
Present study is aimed at designing, developing and optimizing piezoresistive fibrous sensors realized from semi-conductive coatings, suited for composites structural parts containing 3D reinforcement. Our sensors can be embedded inside the reinforcement during weaving and they have all the characteristics of a traditional textile material (flexible, lightweight and are capable of adopting the geometry of the reinforcement and become its integral part).
Embedding such an intelligent piezoresistive sensor inside the reinforcement during weaving process is the most convenient and cost effective way of insertion of a sensor for structural health monitoring.
Development and optimization of such piezoresistive sensors has been carried out in order to render them sensitive enough to measure in situ strains inside the composite part. Sensitivity is important as the targeted application usually undergoes very low strains and even such low strains and/or vibrations during the life time of composite parts are critical. Often they are used in areas where structural integrity can not be compromised (aircraft wings, bodies etc).

2.1 Sensor design and optimisation

As coating solution, the conductive polymer composite based on dispersion of carbon black particles (Printex® L6) in polymer (Evoprene® 007) solution, using chloroform as a solvent was chosen (Cochrane et al, 2007, 2010).
In order to characterize the sensitivity and adherence of the coating on different substrates, the 35 % carbon black solution was coated on different yarns (71 tex cotton spun yarns; 482.3 tex polyethylene monofilament and 25 tex polyamide monofilament). Visual inspection of the surfaces of the coated yarns shows that the coating is more uniform for synthetic monofilaments compared to cotton yarns. The cotton yarns absorb the conductive solution, which penetrates inside the pores and interstices much like a dye. This particular phenomenon could be a source of non homogeneity in sensor electrical and mechanical properties, as the spun yarn is non uniform as compared to filaments, the coating and thus the resistivity achieved could be non uniform. Moreover the greatest inconvenience with coated cotton spun yarns is their low sensitivity during the initial tensile loading phase.
The resistance values were measured on 12 coated samples of each variant using a multimeter. The resistivities were then calculated using the yarn/filament fineness, yarn/filament lengths and these measured resistance values. Fig. 1 gives a comparison of calculated resistivity values of conductive layer deposited on different fibrous substrates. It can be seen that coated polyethylene filaments show relatively lower dispersion of resistivity as compared to coated poyamide filaments.

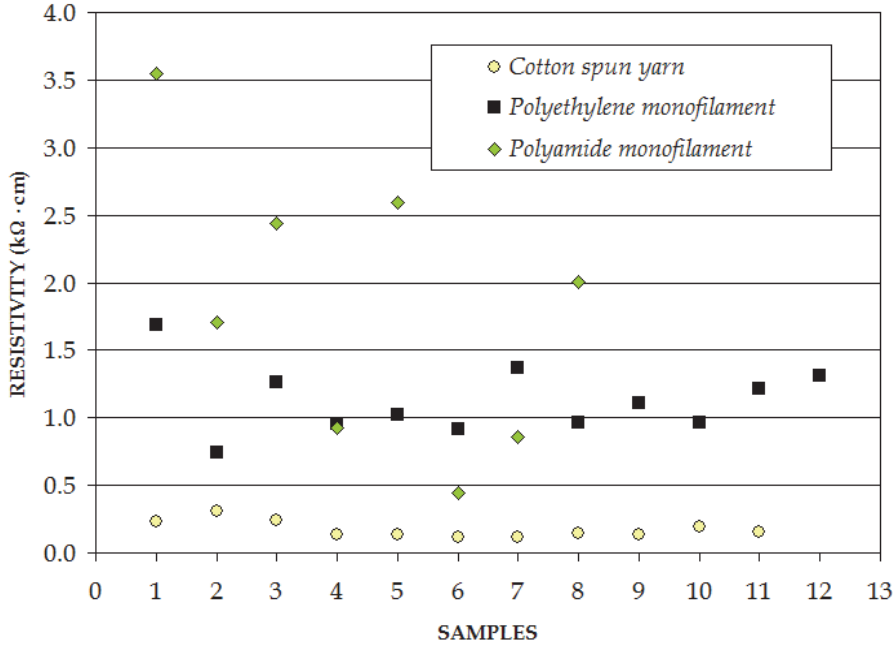

Fig. 1. Resistivity values calculated for different substrates coated with 35 wt.- % carbon black solution

In order to carry out tensile tests on coated yarns and monofilaments, MTS 1/2 tester was used. Samples underwent quasi static tensile loading at a constant test speed of 5 mm/min. For the purpose of electrical resistance variation measurement during the tensile testing, a simple voltage divider circuit and Keithley KUSB-3100 data acquisition module were employed. Fig. 2 shows some of the results for electrical resistance variation, expressed as normalised resistance ($\Delta R/R$) during tensile testing, obtained using different substrates for coating.

Initial resistance of the coating on cotton yarns is much lower then monofilaments. But since the cotton spun yarns are inherently irregular, the coatings obtained are not homogenous and the results for different coated yarns vary widely in their response to tensile loading (Fig. 2-a). Due to particular fineness of the polyamide monofilament it was found that slight non homogeneity in coating on the surface can result in breakdown of conductive path as is obvious from Fig. 2-b. As a result, the behaviour of polyamide is highly inconsistent. Polyethylene monofilaments provide a reasonably good compromise as the substrate. The coatings on polyethylene are easy to achieve due to good substrate/conductive solution interfacial properties. As the curves in Fig. 2-c show, the polyethylene coatings are reproducible as the curves for all the four samples are nearly identical as opposed to polyamide and cotton. Therefore, polyethylene monofilament was chosen for sensor development.

The two ends of the coated polyethylene filaments were additionally coated with silver paint and fine copper wire was attached to the two ends with the help of this paint (as

shown in the Fig. 3). In this way, secure connections were realized enabling the reduction of the contact resistance to the minimum.

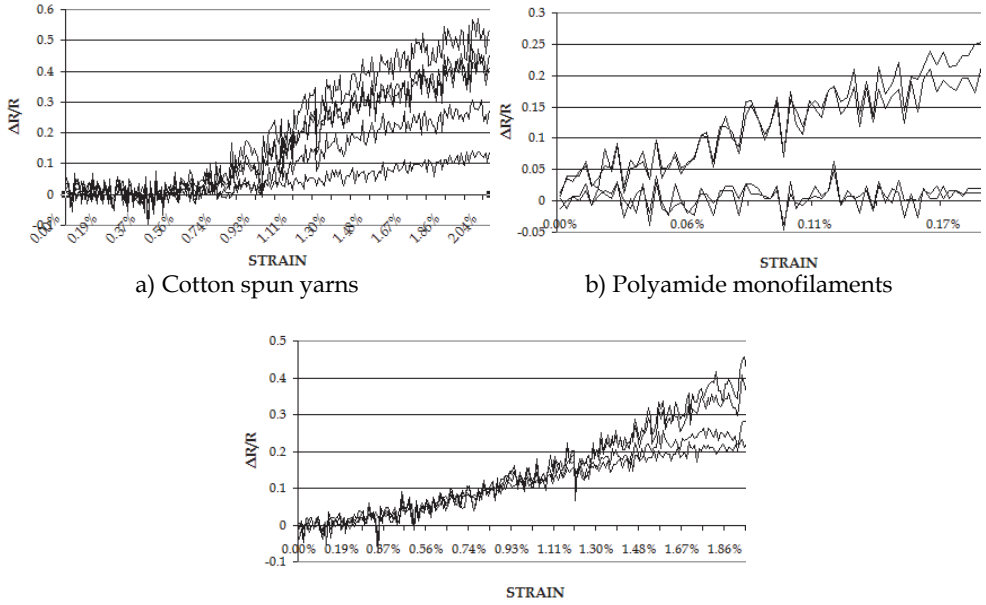

a) Cotton spun yarns

b) Polyamide monofilaments

c) Polyethylene monofilaments

Fig. 2. Electrical resistance variation during tensile strength tests on different yarn and filament substrates coated with 35 wt.-% carbon black solution

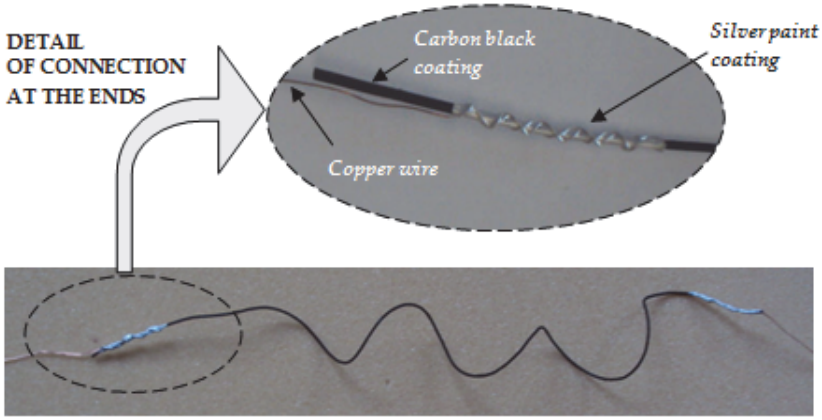

Fig. 3. Carbon black coated sensor with polyethylene substrate

Sensor structural and geometrical parameters along with initial electrical resistance are shown in Table 1.

No.	PARAMATER	UM	VALUE
1	Linear density of the filament	g/km	48.23
2	Diameter of the filament	mm	0.70
3	Average width of the sensor cross section	mm	1.68
4	Average thickness of the sensor cross section	mm	1.26
5	Aspect ratio of the sensor (width/thickness)	-	1.33
6	Initial resistance of the sensor	kΩ	43.3

Table 1. Sensor properties

For insertion in conductive fibre based reinforcements like that woven using carbon multifilament tows, the sensor was coated with Latex Abformmasse supplied by VossChemie® so as to insulate the sensor from surrounding carbon tows.
Prepared in this way, the sensor with polyethylene substrate was tested again on MTS 1/2 tester, under quasi static tensile loading at a constant test speed of 5 mm/min. The same Keithley® KUSB-3100 data acquisition module was employed for the purpose of voltage variation during tensile testing. This time, a special set-up containing a Wheatstone bridge and an amplifier was used to measure unknown variable resistance of the sensor as a function of output voltage. As is obvious from curves presented in Fig. 2-a, b and c, the simple voltage divider circuit is not adequate for the measurement of resistance change in case of sensors developed here. These piezoresistive sensors produce a very small percentage change in resistance in response to physical phenomena such as strain. Moreover the output signal has considerable noise. Generally, a bridge measures resistance indirectly by comparison with a similar resistance. Wheatstone bridges offer an attractive solution for sensor applications as they are capable of measuring small resistance changes accurately (Wilson, 2004).
Fig. 4 shows schematic diagram of the data acquisition module developed and used for data acquisition and its further treatment.

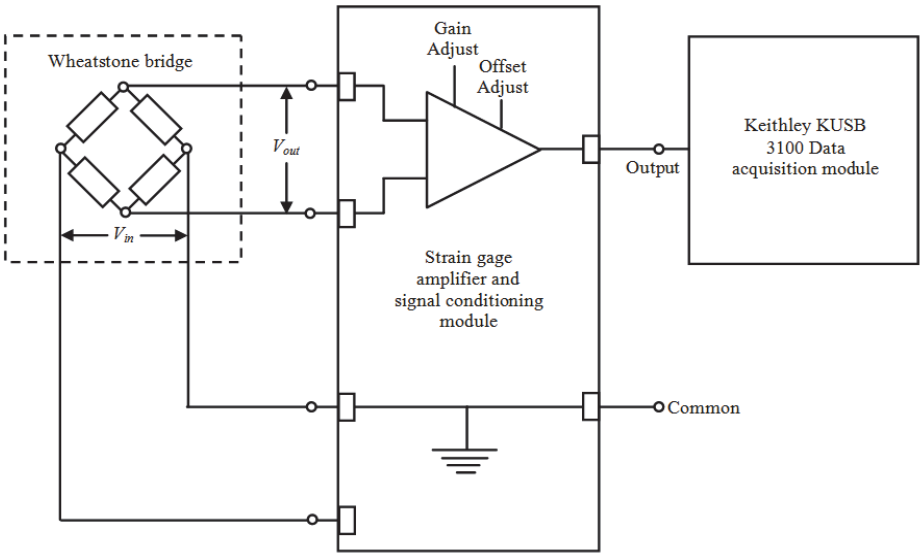

Fig. 4. Schematic of instrumentation amplifier (INA 101) connected to Wheatstone bridge

The resistance variation data thus obtained for different test results was treated for noise reduction using a low pass filter. The resultant stress-strain-resistance relationship curve up to 2.75 % elongation of the out of composite sensor (before insertion in the reinforcement) is shown in Fig. 5.

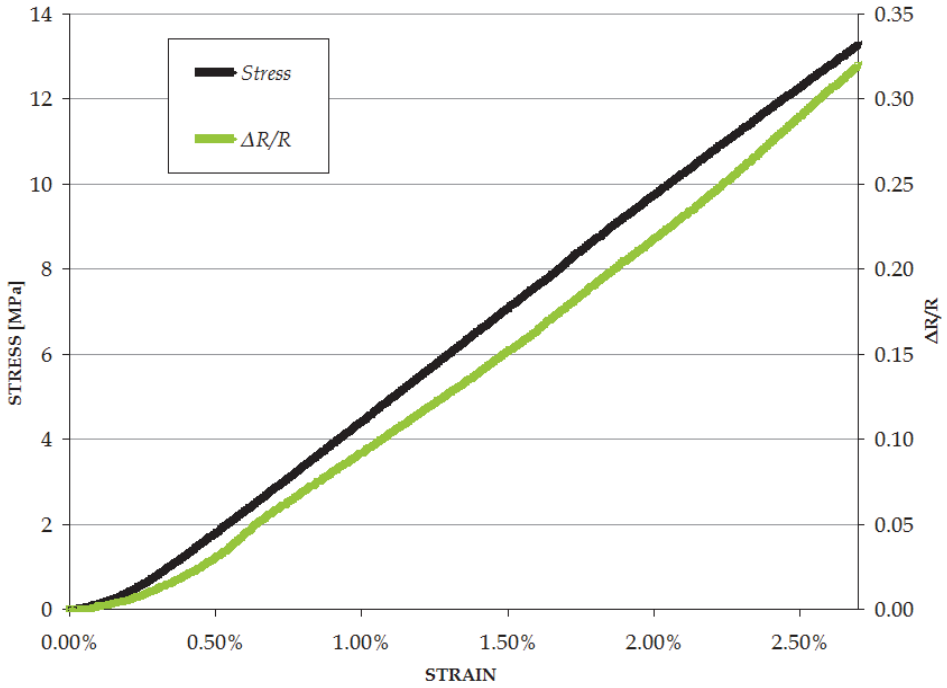

Fig. 5. Normalized resistance and stress against strain for sensor outside composite

It may be noticed in Fig. 5 that the stress vs. strain curve has the same shape as normalised resistance (ΔR/R) vs. strain curve. This validates electromechanical properties of our fibrous sensor for strains ranging from 0 to 2.75 %.

In Fig. 6, the hysteresis results of the sensor for 10 cycles have been given. The sensor underwent 0.5 % extension at a constant test speed of 5 mm/min, followed by compression in each cycle. The sensor follows the extension and compression patterns in each cycle.

The hysteresis is high for the first cycle which reduces gradually and for the 10th cycle the sensor exhibits almost linear behaviour.

2.2 Sensor insertion in carbon woven reinforcement

An orthogonal/layer to layer warp interlock with 13 weft layers and 12 warp layers was chosen as woven structure (Fig. 7-a) and than was woven on a modified conventional loom (Patronic B60 ARM). 6K multifilament carbon tows (supplied by Hercules Inc.) having 200 tex was used in both direction – warp and weft. Yarn densities were 24 yarns/cm in warp direction and 170 yarns/cm in weft direction. The thickness and areal density of resulted reinforcement were 6.5 mm and 3908 g/m^2, respectively.

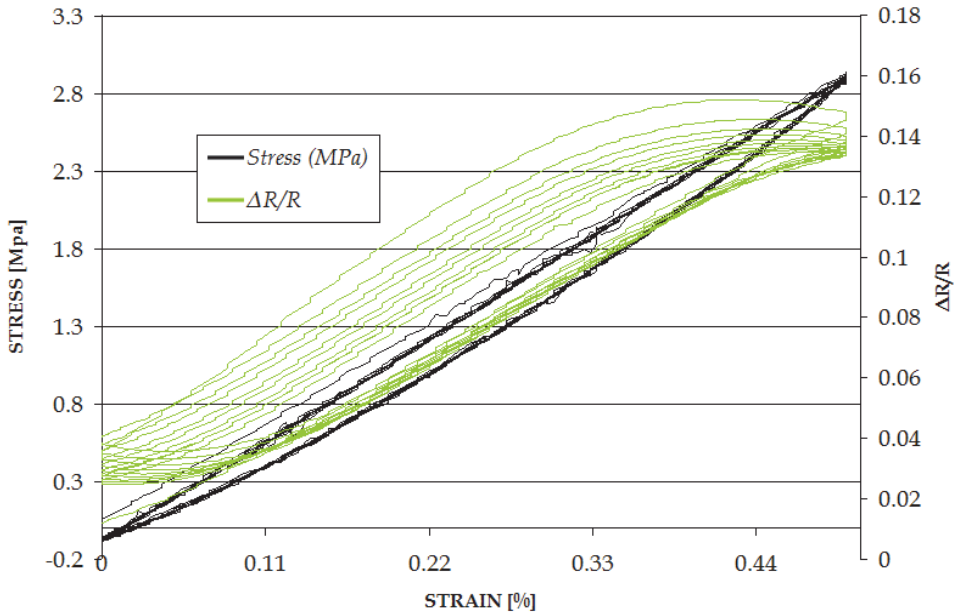

Fig. 6. Normalized resistance (ΔR/R) and stress against strain for sensor (Hysteresis 10 cycles at 0.5 % extension)

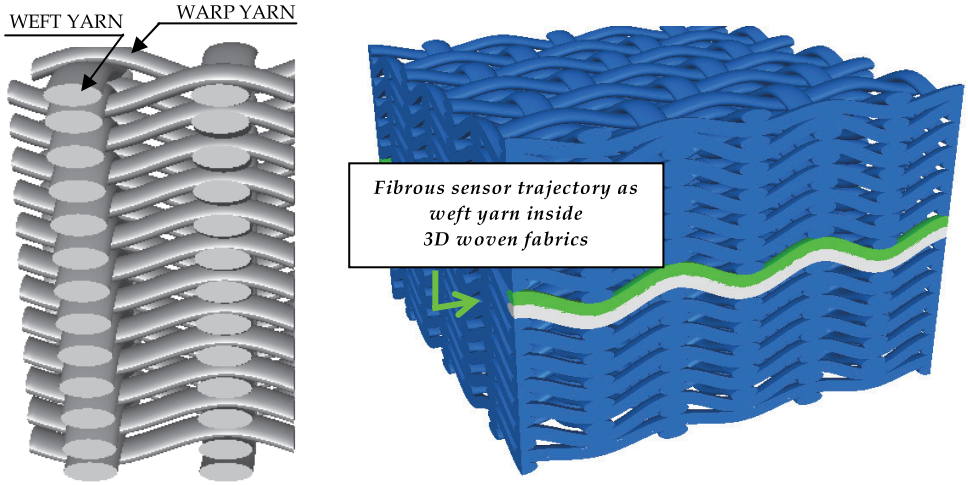

a) The weave repeat b) The path of the sensor inside woven fabric

Fig. 7. Interlock weave structure used as reinforcement – graphical representation (TexGen software)

Sensors can be inserted in warp or weft directions during weaving. Given the technical complications associated with sensor insertion in warp direction during weaving on a loom,

insertion in weft direction has been carried out for preliminary studies. The placement of sensor in the reinforcement was decided so that the sensor was inserted in the middle of the structure related to thickness (Fig. 7-b).
The sensor was inserted during the weaving process, as a weft yarn and it follows the same trajectory as the carbon weft yarns inside the reinforcement. In Fig. 8, off the loom dry reinforcement photograph have been shown. Latex coated sensor connections can be seen protruding from the reinforcement.

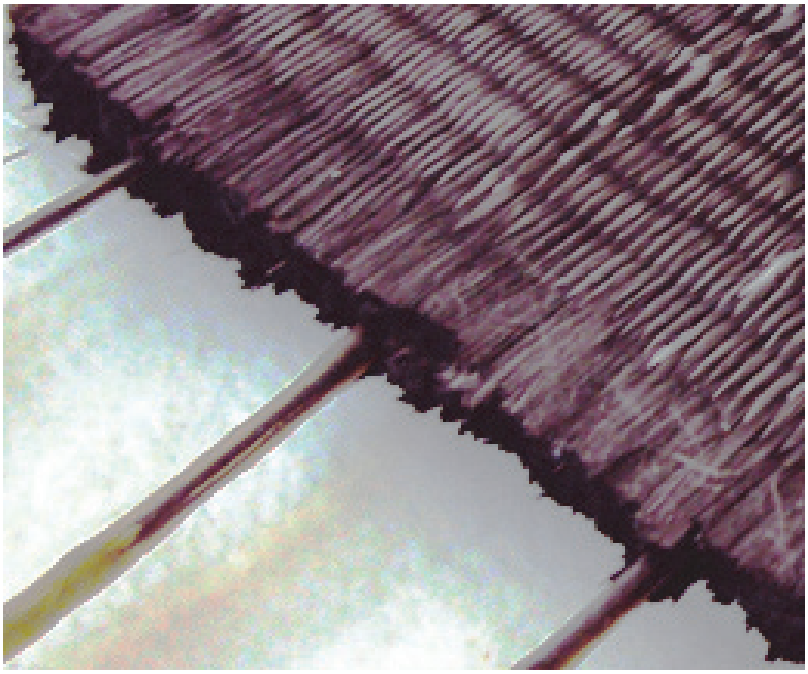

Fig. 8. Reinforcement with protruding sensor connections

2.3 Carbon woven reinforcement impregnation and testing

After weaving, the reinforcement was carefully removed from the loom and was impregnated using vacuum bag infusion process in order to make the composite part stiff. The resin employed was epoxy Epolam® 5015. The two connections of the sensor which remain outside the reinforcement at the two ends were carefully separated from the rest of the mould. This was done by creating two vacuum sub moulds inside the larger mould so that the resin may not impregnate the two connections of the sensor. The impregnated composite samples were cut into slabs of 25 X 2.5 cm (Fig. 9).
The composite specimens were tested on Instron 8500 tester. Tensile strength tests were performed on the composite specimens (according to ISO 527-4, 1997) in the weft direction i.e., the direction parallel to the inserted sensor. The same Wheatstone bridge was used for resistance variation measurement. The configuration of the testing equipment was also kept the same. The composite structural part was tested at constant test speed of 5 mm/min. The composite underwent traction until rupture.

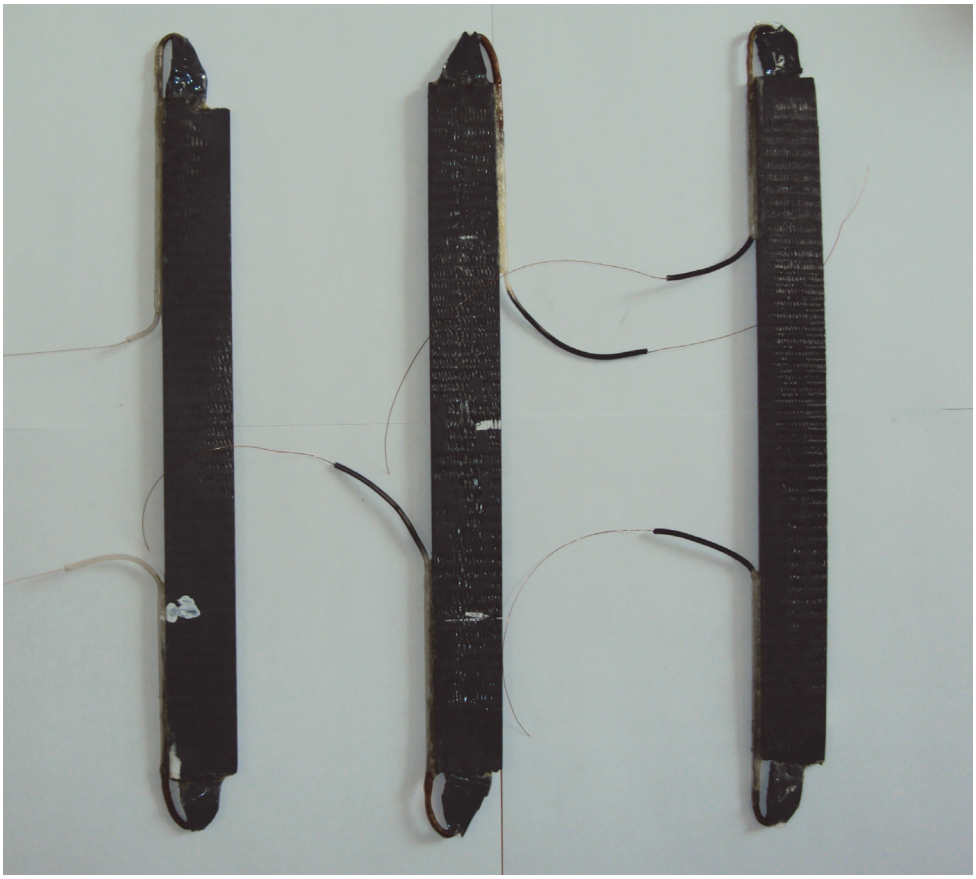

Fig. 9. Textile composite sample containing fibrous piezo-resistive sensor

2.4 On-line measurements of sensor in woven fabric composites - Results

Resultant stress-strain-resistance relationship curve is shown in Fig. 10. It can be observed that the normalized resistance follows the stress-strain curve. The stress-strain-resistance curve can be divided into four regions: *the initial stiff region* - where the composite exhibits toughness against the applied load represented by high slope; *the tows straightening region; the second stiff region* and the *zone of rupture*. The rupture occurred at the strain of 0.52 %, after which the tensile strength tester came back to its initial position at the same speed (5 mm/min). Since the fibrous sensor has not been broken, the normalised resistance ($\Delta R/R$) decreased until zero as the tester returned to its initial position. However this decrease was not linear because the sensor was still intact while the resin-sensor interface was partially damaged which caused its non linear behaviour.

Due to the high difference in yarn densities (24 warp yarns/cm vs. 170 weft yarn/cm), the weft tows are highly crimped. In the initial stiff region micro-cracks start appearing as the composite specimen undergoes traction but the interface at resin and multifilament tows is still intact. That is why the composite exhibits rigid behaviour. In Fig. 10 it can be observed

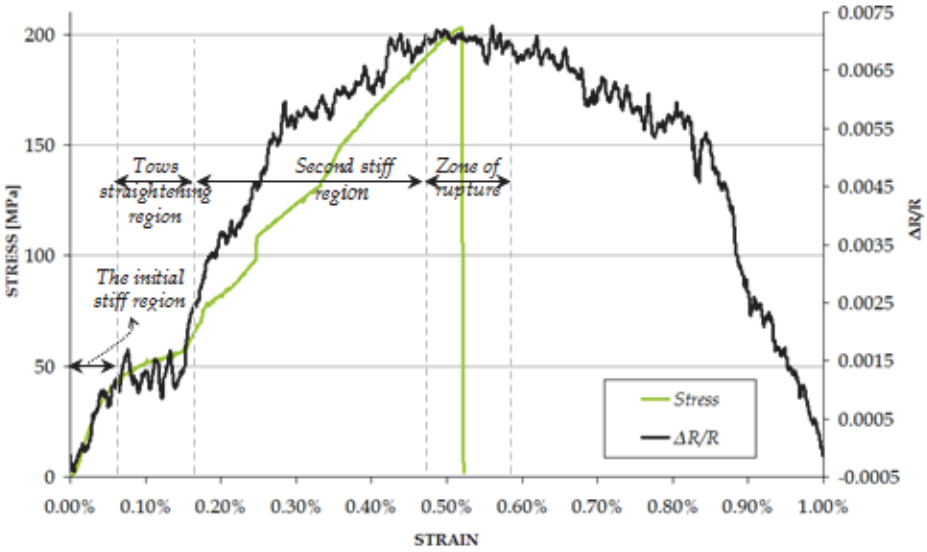

Fig. 10. Normalized resistance and stress against strain for sensor inside composite

that after the initial stiff region the highly crimped tows tend to straighten due to increasing tensile load in the second region. In this region the micro-cracks give way to relative slippage of highly crimped tows in their sockets i.e., the resin-tow interface is relatively weakened. It can also be remarked that the sensor resistance follows the stress strain curve, but in the second region the electrical resistance curve is noisier as compared to other regions of the curve which might signify the slippage of tows as well as the sensor in their sockets. This second region is followed by the third region called the second stiff region where the tows are locked in their sockets. In this region the tows resist the applied load and exhibit stiff behaviour as they regain some of their initial stiffness after the straightening of tows in the second region. The electrical resistance varies almost linearly with the applied load, in this region. The third region is followed by the zone of rupture of the composite in which the electrical resistance, having attained the highest value starts dropping down. The normalized resistance starts dropping after the rupture. The fact that the sensor resistance attains its initial value after the rupture signifies that the sensor, owing to its elastic properties, is not destroyed with the composite. This fact was confirmed by tomographical image of the samples which underwent traction, shown in Fig. 11-a) and b). Sensor cross section and its path at and near the zone of rupture can be observed.

In Fig. 11-a) and b) it can be observed that the sensor-resin interface has a lot of voids. These are caused by poor resin-sensor interfacial properties. The insulating medium on the sensor surface needs to have good adherence with the epoxy resin and carbon fibre reinforcements. Damage that occurred at the main rupture zone has propagated along the sensor boundary giving rise to de-bonding of the sensor. A kink in the sensor can be observed which is caused by the relaxation of sensor as it tries to regain its original dimensions after the tensile loading damages the composite sample. The insulation coating around the sensor renders it thick as well which is undesirable for high performance composite materials as thick insulation coatings might adversely affect the mechanical properties.

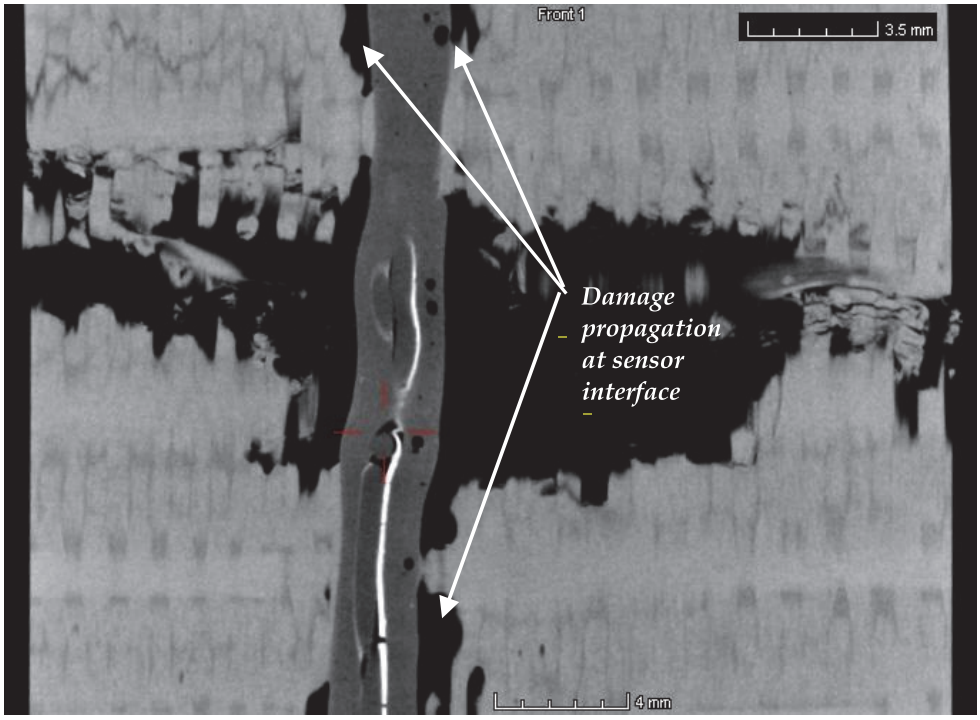

a) Frontal view

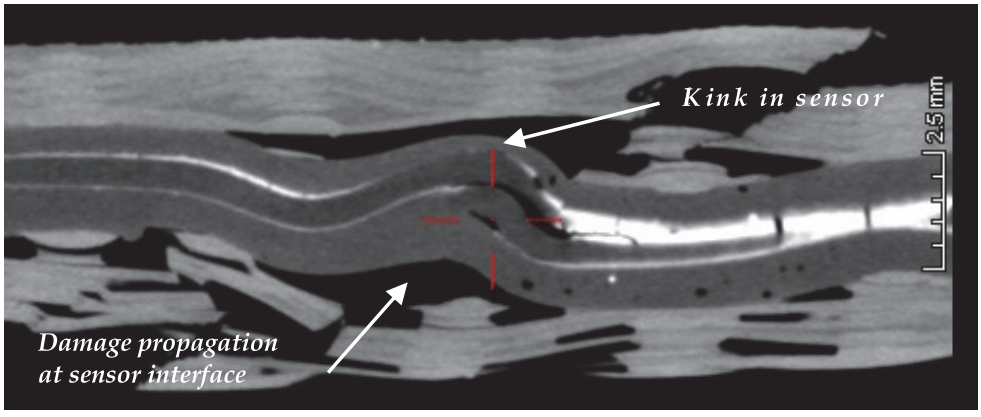

b) Longitudinal section

Fig. 11. Tomographical images of sensor inside a tested sample near the zone of rupture

3. Heating elements based on conductive polymer composite

The second part of this chapter presents a woven fabric containing an original heating element. Textile actuators like heating fabrics can find applications in numerous and varied

fields such as sports, leisure, medical and automotive (Droval et al., 2005; El-Tantawy et al., 2002). In garments, wearability is affected because of the use of metallic components (heating wire and/or heating track on polymer flexible substrate), that are rarely elastic, flexible and lightweight. Nevertheless, these metallic, non-textile elements can be replaced by other conductive fibres such as silver plated polyamide fibres. In that case, the heating textile becomes lightweight, but very expensive (WarmX GmbH). In all the cases, heating systems need heavy power supplies. Thus, it is very important to develop heating textile systems able to work at low voltage.

Our heating element is designed to adapt to woven flexible structures. Additional metallic yarns, used as electrodes, are integrated in a woven structure (or sewn into textile) in a comb-teeth arrangement. Function of these electrodes is to connect heating textile to a power supply and to distribute the current in the conductive coating layer applied on the fabric surface. The comb-teeth electrode arrangement is specially designed to ensure uniform heat distribution. The coating is realized with a composite material based on aqueous latex dispersed with carbon black (CB) as filler. The heating element (comb electrodes and electro-conductive coating) can thus adopt the desired pattern. This is an important aspect of our heating element as it allows integration of the heating element in various fabrics designed for varied and diverse applications.

3.1 Materials and methods

Comb structure was made with stainless steel yarns (2 x 275 x 12 µm from Bekintex®). The average yarn count was 500 Tex, with a resistivity of 14 ohm/m. These yarns were either woven or sewn on an existing fabric. The common feature of all the configurations is that only one comb-teeth structure was used (Fig. 12). The textile fabric was woven on a hand loom (ARM loom equipped with Selectron command box). A plain weave was chosen. Cotton yarns were used in warp and weft having densities of 27 and 10 yarns/cm respectively. The stainless steel yarns were introduced manually during the weaving process according to the pattern (Fig. 12).

Samples with heating surface (*i.e.* L x l in Fig. 12) larger than 180 cm² were prepared. In typical samples, the dimension *L* was about 140 mm while *l* was about 150 mm. In this study, the distance between electrodes (*lp*) remained unchanged: i.e., 20 mm.

The coating was made using a conductive polymer composite (CPC) composed of carbon black (CB, Printex ® L6, Degussa), a synthetic rubber latex solution (Kraton® IR-401, Kraton Polymers) a dispersing agent (Disperbyk®-2010, SPCI) and water.

The preparation procedure is as follows: the dispersing agent is put into water and the CB particles are gradually added while mixing continuously. The polymer is finally added while mixing gently in order to avoid too strong shearing. The coating was then applied on the fabric with a magnetic coating table equipped with a magnetic bar as scraper. 12 samples were prepared with different CB content: 2.5, 5.0, 7.5, 10.0, 15.0, 20.0, 30.0, 35.0, 40.0, 45.0, 50.0 and 60.0 wt.-%. These contents were calculated from the total weight CB + Latex solution. After coating the woven fabric samples were dried at 50 °C for 12 hours. For all the samples, the thickness of the final coating layer was 450 ± 50 µm.

For each coating surface resistivity was measured using four-point probe (MR-1 Surface resistance meter, Schuetz Messtechnik). The aim of these measurements is to determine the percolation threshold and the minimum CB content which allows sufficient electrical conduction for our application.

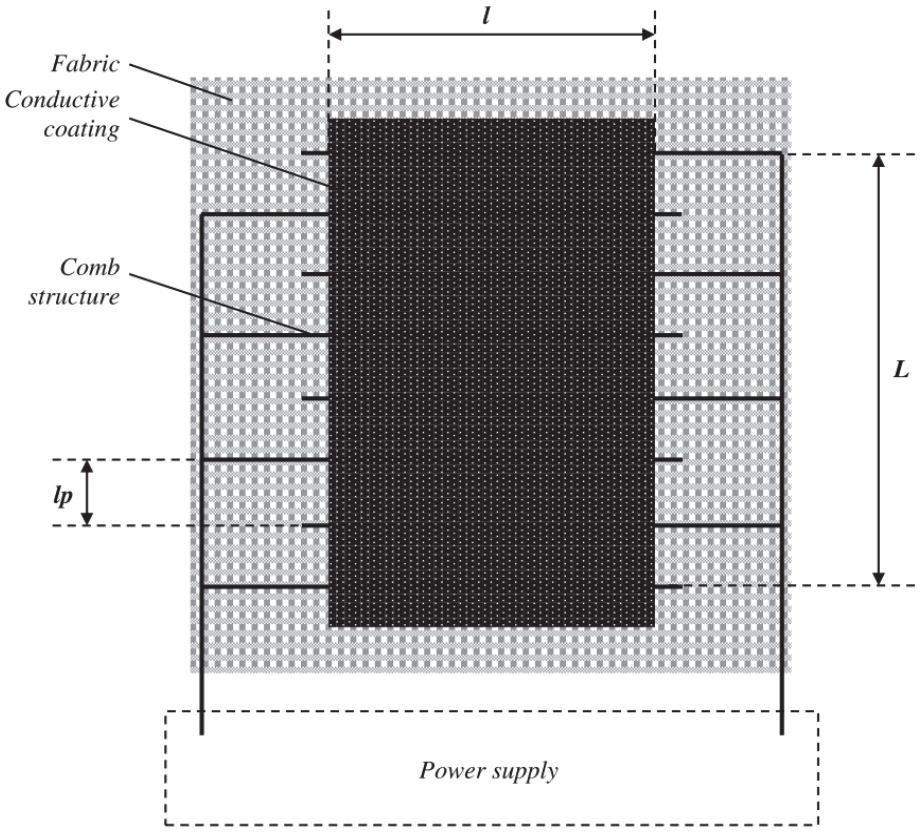

Fig. 12. General structure (comb-teeth pattern and conductive coating) of heating textile element

To characterize heating effect of the samples, 2 processes were used:

- Feeding of the heating element with variable voltage supply (10, 15, 20 and 24 V). The surface temperature was recorded using thermocouple at 15 minute intervals at 5 different locations of the fabric. The average temperature was calculated from 5 measurements. Ammeter was used to determine the power consumption (W) of the heating element. This consumption is expressed in mW/cm² (taking into consideration the surface area of each sample),
- Feeding of the heating element with constant voltage supply (15 V) in conjunction with an IR camera (Agema ThermoVision 900). This camera took an IR image every 20 seconds.

3.2 Results

Fig. 13 shows electrical resistivity of coatings plotted against filler (CB) content in the latex solution. As expected, it is possible to identify the percolation threshold from this plot, which lies at 12 ±1 wt.-%. The form of the plot is in accordance with the typical behaviour of systems consisting of percolation networks (Kirkpatrick, 1973).

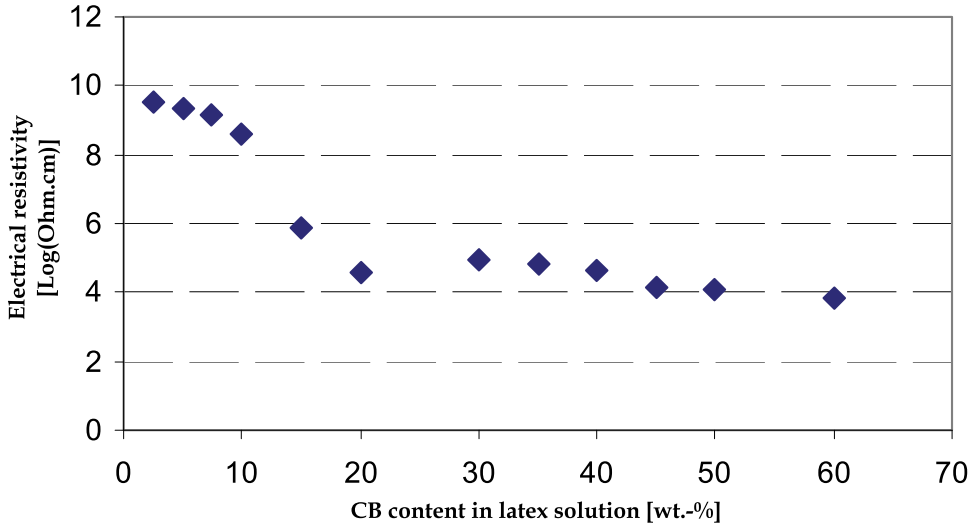

Fig. 13. Electrical resistivity of the coating vs. CB content in the latex solution

This threshold value in wt.-% is expressed for liquid latex solution. Liquid latex contains approximately 63 % of dry material by weight. Thus, the corrected value of percolation threshold is near 18 wt.-%. This value is relatively higher than the value reported in literature for similar systems, (Grunlan et al. 1999, 2001). In our study, process of dispersion (including rupture of CB aggregate) and coating on fabric is not yet optimized. Obtained results show that 15 wt.-% of CB is necessary to obtain à conductive coating. Nevertheless, Fig. 13 shows that between 15 and 40 wt.-% resistivity is not optimal: therefore it is necessary to fill the composite at least by 45 wt.-% to obtain lower resistivity.

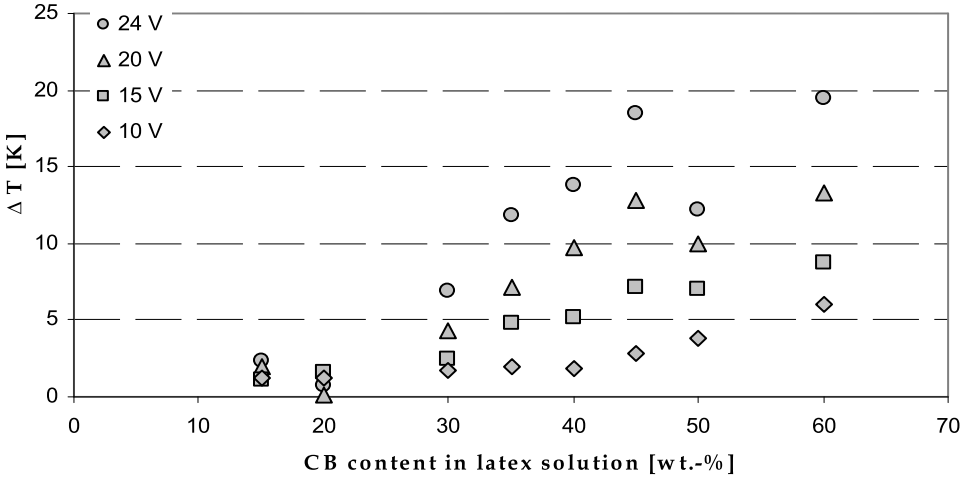

Fig. 14. Surface temperature vs. CB content for feeding voltage of 10, 15, 20 and 24 V

Fig. 14 shows surface temperature of coating plotted against the filler content (in liquid latex) for several feed voltages (10, 15, 20 and 24 V). Temperature on the graph (ΔT) is expressed as difference between measured temperature and room temperature (between 20 and 22 °C). No elevation of temperature was recorded for sample under 30 wt.-% of CB. For CB content between 30 wt.-% and 45 wt.-%, ΔT increases with the CB content. Above 45 wt.-% of CB, ΔT does not increase significantly with filler addition. These results are in agreement with the previous remarks concerning resistivity vs. CB content.
These results show that the best content of CB was, in our case, 45 wt.-%. Under this value heating effect was non optimal. Above this value addition of CB does not increase heating ability.
Maximum value of ΔT (near 20 K) was registered for sample voltages of 24 V and CB content of 45 wt.-% and 60 wt.-%. Fig. 15 shows that for these heating elements, electrical input power was close to 250 mW/cm².

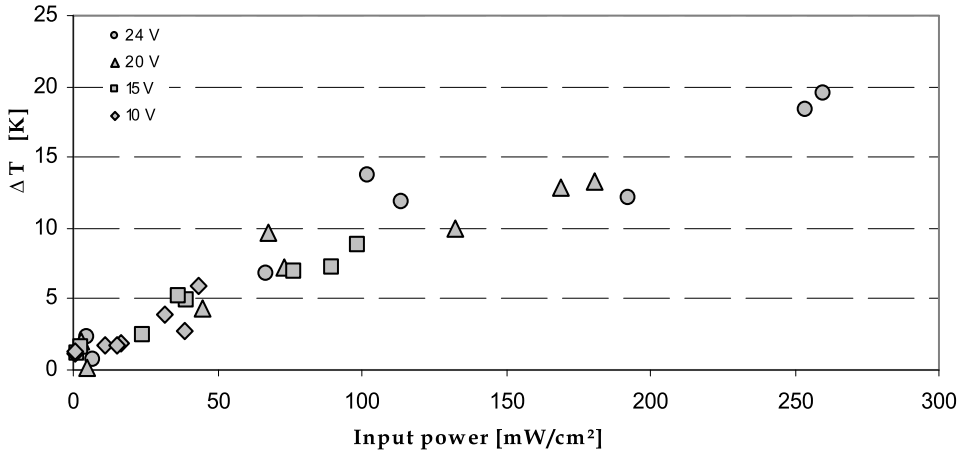

Fig. 15. Increase of surface temperature (ΔT) vs. power consumption of heating element

Infrared images show the distribution of heat in the structure (comb electrodes and conductive coating) vs. time. Fig. 16 shows temperature of sample with 60 wt.-% of CB from t = 0 s (Fig. 16-a) to t = 180 s (Fig. 16-f). Feeding voltage was constant and was equal to 15 V.
Fig. 16 shows that comb structure (stainless steel yarn) heats first after switching on. The maximum temperature of this yarn was about 70 °C. This temperature is achieved after 120 s. CB coating heats relatively slowly but it can be conjectured that after 120 s the temperature of all the surface area exceeds 35 °C while it exceeds 40 °C after 180s. This behaviour is expected since stainless steel yarns have better thermal conductivity than carbon based composite.

4. Conclusion

The sensor based on conductive polymer composite, developed for in situ measurements on carbon fibre based woven fabric composite, is capable of detecting strain in the structure. The electrical resistance variation in the sensor follows the deformation pattern of the composite, mainly due to its sensitivity to its environment and because of the fact that it is

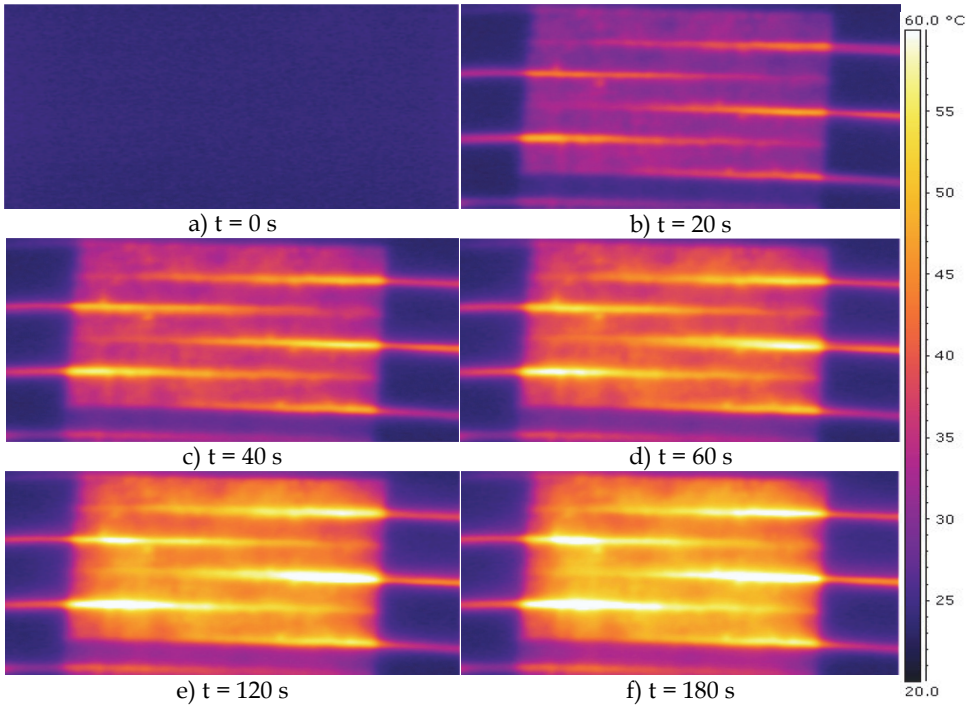

Fig. 16. IR image of 60 wt.-% CB heating element from a) t = 0 s to f) t = 180 s, voltage = 15V

integrated in the structure and follows the fibre architecture of the reinforcement. It has been shown that the integrated textile sensors inside the reinforcement can be used as in situ strain gages for the composite materials. Moreover, if the placement of these sensors inside the reinforcement is carefully chosen, they can be used to follow the local deformation pattern so as to better understand the deformation mechanisms and predict life time of the composite parts. At present the sensors have been tested for tensile loading. Tensile strength tests were chosen to demonstrate the basic features of this novel SHM approach. In the future these sensors will be used for bending and fatigue tests on similar 3D carbon fibre woven reinforcement based composites. However optimisation of sensors needs to carried out in order to prepare finer sensors having negligible affect on reinforcement geometrical and mechanical properties. For carbon fibre based reinforcements which require an insulation coating on the sensor surface, a better and finer coating needs to be applied. In view of the test results presented, it can be concluded that these sensors can be used for in situ health monitoring of various types of composites for industrial applications (aeronautics, automotive etc).

We have also developed a heating element based on original comb-teeth structure (stainless steel electrode) and electro-conductive coating composed of latex and carbon black. Comb structure can be either woven or sewn into the fabric. Final product is flexible and lightweight. This study has show that ideal carbon content of the coating was 45 wt.-% in a latex solution. Our heating elements (about 200 cm^2) allow increasing the temperature (ΔT) by 20 K with low voltages (between 15 and 24 V). Temperature homogeneity of heating

elements is better than those of heating elements made with only stainless steel yarns because in the later case, heat is only produced and localized at conductive yarns. Moreover, our system is cost efficient because we used a few stainless steel yarns.
The next step of this study would allow, in the first place, the optimization of composite preparation (liquid Latex + CB) and secondly the realization of larger heating elements (> 0.5 m^2). Potential applications of these heating elements can be found in garments (to improve thermal comfort), in transportation where heating is required for passenger comfort and in certain industrial systems (antifreeze).

5. Acknowledgements

This research was partially financed by Interreg IV via TRITEX (Transfer of Research and Innovations in TEXtiles) program (FLV1.1.1). Special acknowledgments to Textile Department Laboratory from UGENT (Belgium) for electrical measurements (part 3.) and use of IR camera.

6. References

Black, S. (2009). Structural health monitoring: Composites get smart, Composites World, http://www.compositesworld.com/articles/structural-health-monitoring-composites-get-smart

Cochrane, C., Koncar, V., Lewandowski, M., & Dufour, C. (2007). Design and development of a flexible strain sensor for textile structures based on a conductive polymer composite. Sensors, Vol. 7, pp. 473-492.

Cochrane, C., Lewandowski, M., & Koncar, V. (2010). A Flexible Strain Sensor Based on a Conductive Polymer Composite for in situ Measurement of Parachute Canopy Deformation. Sensors, Vol. 10, pp. 8291-8303.

Dharap, P., Zhiling L., Nagarajaiah, S. & Barrera, E.V. (2004). Nanotube film based on single-wall carbon nanotubes for strain sensing, Nanotechnology, vol. 15, pp. 379-382.

Droval, G., Glouannec, P., Feller, J.F., & Salagnac, P. (2005). Simulation of electrical and thermal behavior of conductive polymer composites heating elements. Journal of Thermophysics, Vol. 19, No. 3, pp. 375-381.

El-Tantawy, F., Kamada, K., & Ohnabe, H. (2002). In situ network structure, electrical and thermal properties of conductive epoxy resin–carbon black composites for electrical heater applications. Materials Letters, Vol. 56, pp. 112-126.

European Standard NF EN ISO 527-4 (1997), Plastiques - Détermination des propriétés en traction, Partie 4 : Conditions d´essai pour les composites plastiques renforcés de fibres isotropes et orthotropes.

Fiedler, B., Gojny, F. H., Wichmann, M. H. G, Bauhofer, W. & Schulte, K. (2004). Can carbon nanotubes be used to sense damage in composites?, Annales de chimie, 29, p. 81-94.

Gettinger, C.L., Heeger, A.J., Pine, D.J. & Cao, Y. (1995). Solution characterization of surfactant solubilized polyaniline. Synth. Met., 74, pp. 81-88.

Grunlan, J., Gerberich, W., & Francis, L. (2001). Lowering the percolation threshold of conductive composites using particulate polymer microstructure. Journal of applied polymer science, Vol. 80, No. 4, pp. 692-705.

Grunlan, J., Gerberich, W., & Francis, L. (1999). Electrical and mechanical property transitions in carbon-filled poly(vinylpyrrolidone). Journal of materials research, Vol. 14, No. 11, pp. 4132-4135.

Haba, Y., Segal, E., Narkis, M., Titelman, G.I. & Siegmann, A. (1999). Polymerization of aniline in the presence of DBSA in an aqueous dispersion. Synth. Met., 106, 59-66.

Heeger, A.J. (2002). Semiconducting and metallic polymers: the fourth generation of polymeric materials. Synth. Met. No. 125, pp. 23-42.

Kamiya, R., Cheeseman, B. A., Popper, P. & Chou, T.-W. (2000). Some recent advances in the fabrication and design of three-dimensional textile preforms: a review. Composites Science and Technology, Vol. 60, pp. 33-47.

Kirkpatrick, S. (1973). Percolation and conduction. Reviews of Modern Physics, Vol. 45, No. 4, pp. 574-588.

Ko, F. (2007). 3-D textile reinforcements in composite materials, 3-D Textile Reinforcements In Composite Materials. vol. null: Woodhead Publishing Limited.

Krupa, I. & Chodak, I. (2001). Physical properties of thermoplastic/graphite composites. Europ Polym J., 37, pp. 2159-2168.

Kumar, D., & Sharma, R.C. (1998). Advances in conductive polymers. Eur. Polym. J. No. 34, pp. 1053-1060.

Li, C., Thostenson, E. T. & Chou, T. W. (2008). Sensors and actuators based on carbon nanotubes and their composites: A review, Composites Science and Technology, vol. 68, pp. 1227-1249.

Lorussi, F., Scilingo, E. P., Tesconi, M., Tognetti, A. & De Dossi, D. (2005). Strain sensing fabric for hand posture and gesture monitoring, IEEE Transactions On Information Technology In Biomedicine, vol. 9, pp. 372-381.

Novak, I., Krupa, I. & Chodak, I. (2002). Investigation of the correlation between electrical conductivity and elongation at break in polyurethane-based adhesives. Synth. Met., 131, 93–98.

Scilingo, E. P., Lorussi, F., Mazzoldi, A. & De Rossi, D. (2003). Strain-sensing fabrics for wearable kinaesthetic-like systems, IEEE sensors journal, vol. 3, pp. 460-467.

Wilson, J. (2004). Sensor signal conditioning, Sensor Technology Handbook. vol. null: Newnes Publishing Limited.

www.nottingham.ac.uk/~emxmns/texgen.htm, consulted on 10/01/2011

www.datasheetdir.com/INA101-Instrumentation-Amplifiers, consulted on 06/05/2010.

2

Smart Woven Fabrics in Renewable Energy Generation

Derman Vatansever, Elias Siores, Ravi L. Hadimani and Tahir Shah
University of Bolton, Institute for Materials Research and Innovation
United Kingdom

1. Introduction

Initially, the first purpose of fabric making was only for covering the body and sheltering. However, with a growing population and ever improving advanced technologies, today's fabrics are mostly used for fashion and performance thus enhancing the standard of people's everyday life and enjoyment.
Most of the technologies which increase the standard of living also increase carbon emission and adversely affect human life indirectly. Warming buildings, using cars, provide hot water, cooking food etc. need energy generated by using coal, gas, fuel or electricity. Burning gas and fuel accelerate the threat of nature and eventually contribute to global warming. Even electricity generation causes carbon emission unless it is generated by using renewable energy sources. Interest in providing renewable usable electrical power from the environment has grown, particularly in the elimination of battery usage, because of their sizeable dimensions, weight and limited lifetime.
Since global warming is being considered as the biggest danger for the nature, many scientists and researchers have brought a new breath to their researches. As almost all areas of renewable science and technology, researchers are now working in the field of textile fabrics capable of generating green electricity.
Undoubtedly, weaving is the oldest fabric making method which has been a part of human life for protection from nature's elements and hazards. It is now possible to produce smart woven fabrics by combining the oldest fabric making method with smart fibre material technologies. The chapter named "Smart Woven Fabrics in Renewable Energy Generation" contains a brief introduction to smart materials, focusing on piezoelectricity and polymer based piezoelectric fibre production. The rest of the chapter explains how to produce smart woven structures by integrating smart fibres into the fabric during weaving process and examples for possible applications for energy regeneration from nature's elements are given.

2. Brief introduction to weaving and looms

2.1 Vertical and horizontal looms

The first loom consisted of only a branch of a tree that is parallel to the ground. In this simple design, warp threads were directly fastened to the branch of a tree and held parallel to each other under tension caused by tied stones at the other end of the warps. The weft threads work from right to left and left to right by passing through hanging warps until the

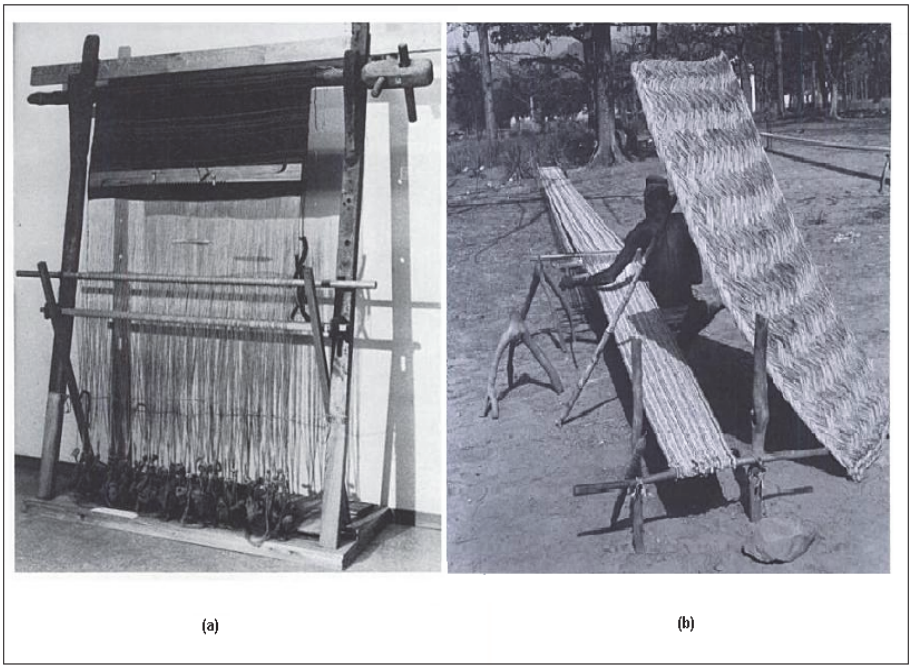

Fig. 1. (a) A vertical warp-weighted loom used in Iceland, reconstructed and set up before 1914, National Museum of Iceland-Photograph by Gilsli Gestsson (Broudy, 1979), (b) a horizontal ground loom used in Northen Cameroon-Photograpgh by René Gardi (Broudy, 1979).

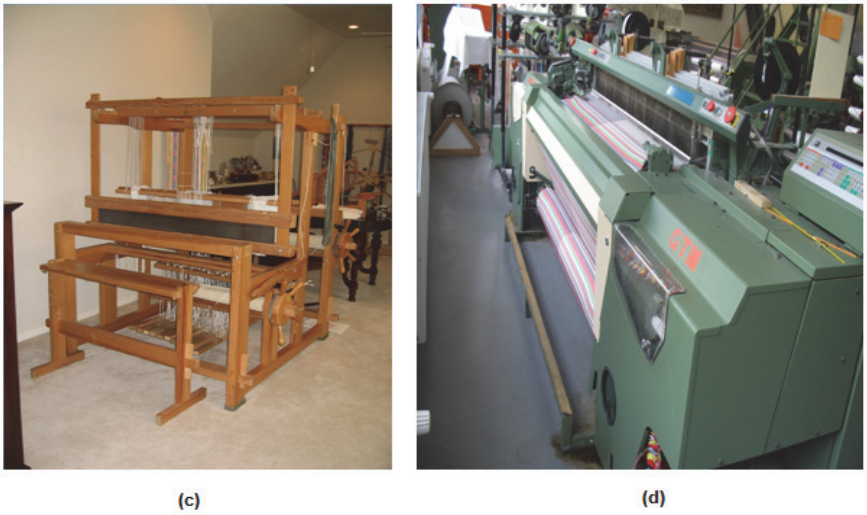

Fig. 1. (c) An example of laboratory scale hand looms and (d) an example of automated looms (wikipedia, 2011).

designed fabric is composed. Later, a simple framework was made of tree branches to form a vertical loom to use for indoor as well as outdoor.
Figure 1 (a and b) show examples for early vertical loom and horizontal looms and Figure 1 shows a laboratory scale hand loom (c) and automated loom (d). Warp threads are attached to heddles and held parallel to each other on the loom and weft thread is held by a shuttle. The heddles keep warp threads apart so that the shuttle could pass through easily and cary the thread from left to right and right to left so that the weft will work over and under warp threads to form a fabric. Movements of the heddles on hand looms are controlled by pedals beneath the loom.
Current generation looms (Fig. 1d) are fully automated. Movements of the heddles are automatically controlled according to the fabric design sent via a computing system. The important parameters, such as tension, speed, temperature etc., are measured and/or controlled by the controlling systems. Thus, any errors that occur during the fabric production are immediately detected.

2.2 Main weaving constructions

Weaving is one of the traditional fabric making methods. There are two sets of threads, warp threads and weft threads which form a fabric by being interlaced row by row. Weaving has three main construction techniques; plain weaving, twill weaving and satin weaving. Any other techniques developed are variations of these main techniques.
Plain weave is created by interlacing the weft across the warp threads and for this at least 2 heddles are needed. Weft thread goes under a warp thread and then over the next one so that the equal amount of weft and warp is seen on both surfaces of the woven fabric.
Twill weave is created by interlacing two or more weft threads over and under one or more warp threads so that at least three heedles are needed to make a twill woven fabric. In twill wovens, parallel diagonal ribs are formed from left to right or from right to left that depends on the formation, woven fabric is characterised and named as “S“ or “Z“ twill, respectively. If a twill woven has more warps than the wefts on the fabric face is known as warp faced twill and if it has more wefts on the fabric face, it is known as weft faced twill.
Satin weave is created by floating four or more yarns before a single interlacing occurs and at least 5 heddles are needed to make a satin woven fabric. The warp or weft threads pass across many threads in such a way, like 4/1, 5/1, 7/1 etc., that the face of the woven fabric is mostly covered with either warp or weft threads and known as warp satin or weft satin, respectively.
Depending on the construction of the weave and characteristics of the used warp and weft threads, fabric properties may vary. Count of the used fibres/yarns determines the fabric density which affects the weight, feel, appearance, thickness etc. Variable properties are many and can be found in the literature (Gioello, 1982). They include:

- Weight
- Hand and feel
- Drapeability
- Appearance
- Covering power
- Surface texture
- Body fit

- Thickness
- Lustre
- Strength
- Flexibility / pliability
- Resiliency
- Warmth
- Affinity to dyestuff

Fabrics created by using plain weave technique are tough compared to twill and satin weave. The fabrics made by twill weaving technique are more pliable and drapable than plain weave fabrics but not as pliable as satin weave. However, strength of plain woven fabrics is higher than both twill and satin woven fabrics.

3. Smart materials and piezoelectricity

A smart material is one that shows extraordinary response when subjected to a stimulus. Piezoelectric materials are considered as smart materials because of their ability to generate electricity against the stimulus which is mechanical strain or vibration (Fig.2a). This property of piezoelectric materials is known as direct piezoelectric effect. The reverse effect is also possible in that this material undergoes a slight deformation in shape when a small electrical field is applied (Fig.2b).

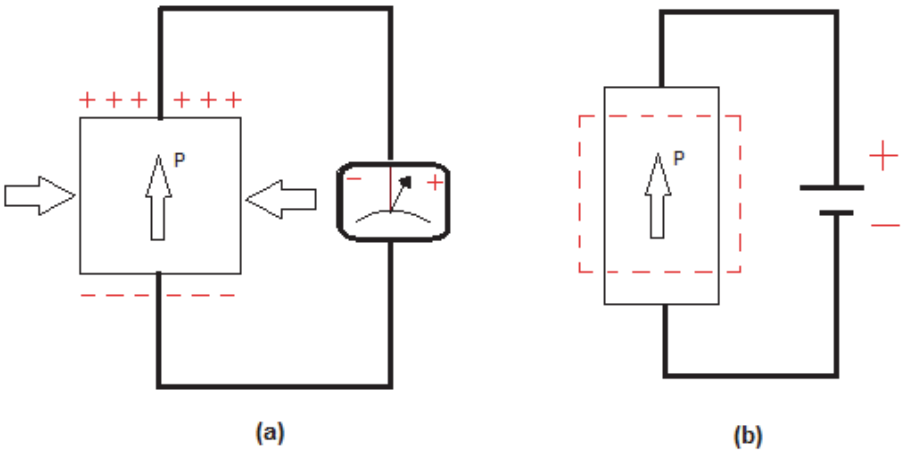

Fig. 2. (a) Direct piezoelectric effect; mechanical energy is converted to form electrical energy, (b) Converse piezoelectric effect; electrical energy causes deformation in the shape of piezoelectric material.

Direct piezoelectric effect of the materials is also known as "generator effect" or "sensor effect". The terms "motor effect" and "actuator effect" are also used to mean converse piezoelectric effect of the piezoelectric material. It should also be pointed out that the piezoelectric effect can be induced when heat or cooling is involved, in which case this phenomenon is termed thermoelectric or pyroelectric effect.

Direct piezoelectric effect is mainly used for energy harvesting. The term "Energy Harvesting" is used to describe the process of extracting energy from the environment and the extracted energy is converted and stored in the form of electrical energy.
Although energy harvesting technologies have been known for many years, increasing concern about global warming has led to intensive research for alternative energy sources including piezoelectrics. With an increasing concern about global warming, piezoelectricity has gained a significant importance and intensive research and development efforts are being made for extracting energy from the environment [Umeda et al., 1997; Sodano et al., 2004; Mateu & Moll, 2005].

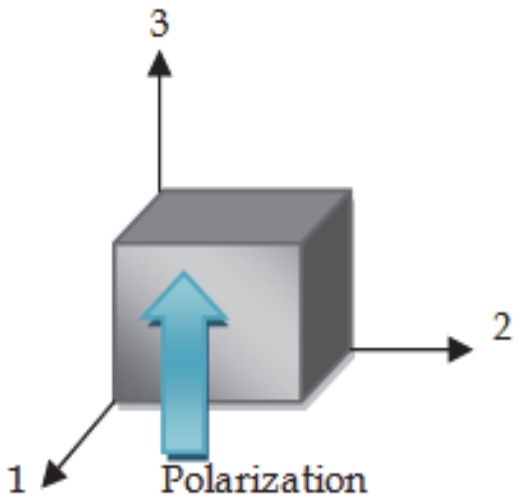

Fig. 3. Defining the modes of piezoelectric material

The generated electrical charge of a piezoelectric material under a mechanical stress can be formulated in terms of dielectric displacement, D (charge per unit area, C/m²) [Schwartz, 2002; Granstrom et al., 2007; Swallow et al., 2008]

$$D_i = d_{ij}\sigma_j \tag{1}$$

where "d_{ij}" is the piezoelectric charge coefficient (C/N) and "σ_j" is the stress (N/m²). "i" is the direction of polarization and takes terms 1–3 and "j" is the direction of applied stress having subscripts 1–6 (Fig. 3).
In Figure 3, numbers 1, 2 and 3 present x,y and z axes of piezoelectric material, respectively. Modes 31 and 33 are two coupling modes of piezoelectric materials that when a force is applied in the perpendicular direction to the poling direction, the piezoelectric voltage coefficient acts in the mode 31. When a force is applied in the parallel direction to the poling direction, the piezoelectric voltage coefficient acts in the mode 33 which generally yields a higher coupling coefficient (k) [Roundy et al., 2005; Baker et al., 2007; Anton & Sodano 2007; Patel et al., 2010] which is the ability of piezoelectric materials to convert mechanical energy into electrical energy and vice versa, and can be defined by,

$$k = \sqrt{\frac{Y}{\varepsilon} d} \tag{2}$$

where "ε" is dielectric constant and "Y" the elastic modulus of the material.
Piezoelectric voltage coefficient (g) relating the electric field generated by an applied mechanical stress and relationship between the piezoelectric charge coefficient and piezoelectric voltage coefficient can be expressed as [Jordan & Ounaies, 2001],

$$gij = dij \,/\, \varepsilon_0 \mathrm{Kj} \tag{3}$$

where; "ε_0" is the permittivity of free space (8.85x10-12 F/m) and "Kj" is the relative dielectric constant of the material.
Since the discovery of piezoelectricity in ceramics [Shirane & Suzuki, 1952; Jaffe et al., 1971] and polymers [Kawai, 1969], various studies have been carried out on structural changes [Ramos et al., 2005; Sencadas 2006], poling [Seo et al., 1985; Holstein et al., 1999; Neagu et al., 1999; Parvanova & Nadoliisky 2005] and applications, such as sensors [Tzou & Tseng 1990; Sirohi & Chopra 2000], actuators [Baz & Poh 1988; Schmidt et al., 2006], energy harvesting [Sodano & Inman 2004; Shu & Lien 2006; Granstrom et al., 2007; Ramadass & Chandrakasan 2010] and so on. PZT has been pre-eminent due to its piezoelectricity among other piezoelectric materials, with a piezoelectric coefficient (d_{33}) of 220pC/N [Hellwege, 1996] while PVDF exhibits much lower piezoelectric coefficient of $d_{33} \approx 35$pC/N [Sencadas et al., 2006; De-Qing, 2008; Jain et al., 2010; Patel et al., 2010]. However, flexible nature of polymers adds extra versatility for applications against ceramic based piezoelectric materials.
With the invention of new polymers exhibiting piezoelectric and better mechanical properties, the scope of application has widened. Both ceramic and polymer based piezoelectric materials have found a wide range of application in many areas. Ceramic based piezoelectric materials, in general, have a higher piezoelectric constant compared to polymer based piezoelectric materials. However, polymer based piezoelectric materials have an advantage of being flexible which makes them preferable for many applications, particularly for wearable applications. This flexibility can also result in better conversion of energy in certain applications.

3.1 Flexible piezoelectric fibres

There are many naturally occurring piezoelectric structures, such as cane sugar, tendon, silk, bones etc., but polymers are not natural piezoelectric materials. However, polymers such as polyvinylidene fluoride (PVDF), polyproplylene (PP), polyethylene terephthalate (PET), odd numbered polyamides (PA11, PA9, PA7, PA5) etc. can be made piezoelectric (Kawai, 1969; Newman et al. 1980; Dunn & Carr, 1988; Harrison & Ounaies, 2001).
Siores et al (2010) were the first to develop and patent a continuous process for making piezoelectric fibres by extruding suitable polymers. To produce piezoelectric PVDF fibres via a continuous process on the melt extruder, granular PVDF was fed to extruder screw which was heated above melting point of the polymer. To gain the piezoelectricity, molecular chain of the PVDF fibre must be re-oriented and transformed from non-piezoelectric α-phase to piezoelectric β-phase by applying a high stretching ratio (Sencadas et al., 2006), heat (Neagu et al., 1999) at the stretching region and high voltage (Holstein et al., 1999 & Ramos et al., 2005), simultaneously.

3.1.1 Fibre extrusion and poling

High purity PVDF polymer granules are fed a melt extruder. The extrusion temperature is kept at 195°C which is 20°C higher than the melting point of PVDF inside the feeding screw. The temperature is slightly higher at the die, 205°C, where the fibre is extruded. The extruded fibre is then air cooled with a blower and water cooled on the initial stage rollers which help in further cooling of the extruded fibre.

Poling is a critical step for piezoelectric fibre generation. Temperature, drawing ratio and applied electric field play a crucial role in the amount of polarisation. Highest polarisation charge coefficient was given in the literature (Sessler, 1981; Wegener et al., 2002).

The drawing of fibres takes place at the rollers, which have heating coil inside to vary the temperature during stretching of fibres. The temperature of these rollers is maintained constant on PVDF fibre when it leaves the roller and an appropriate electric field applied on PVDF fibre while being drawn.

Fig. 4. Piezoelectric polyvinylidene fluoride (PVDF) filament production via a continuous process using a melt extruder

Figure 4 shows the continuous process of producing piezoelectric polymer in a customised melt extruder. This is a less expensive and less time consuming method for preparing piezoelectric polymer fibres in that all process variables are applied simultaneously. Detailed information on polymer based piezoelectric fibre production via a continuous process has been reported (Siores et al, 2010).

3.1.2 Testing of generated piezoelectric fibres

Generated polymer fibres, shown in Figure 5, are embedded in between two thin sheets of aluminium or copper which act as electrodes. The fibres are placed close to each other such that the top electrode would not contact the bottom one. The top and bottom electrodes act as positive and negative terminals for the energy generating polymer piezoelectric device.

Poled PVDF fibres generate about 5 V_{oc} when a moderate mechanical stimulus is applied on to the fibres. The obvious advantage of producing flexible piezoelectric fibres is to be able to produce large area active surfaces by incorporating piezoelectric fibres in wearable technologies. However, to generate enough electricity for wearable applications to power small electronic devices, produced flexible piezoelectric fibres need to be used in a fabric structure such as woven, knitted, nonwoven and 3D structures.

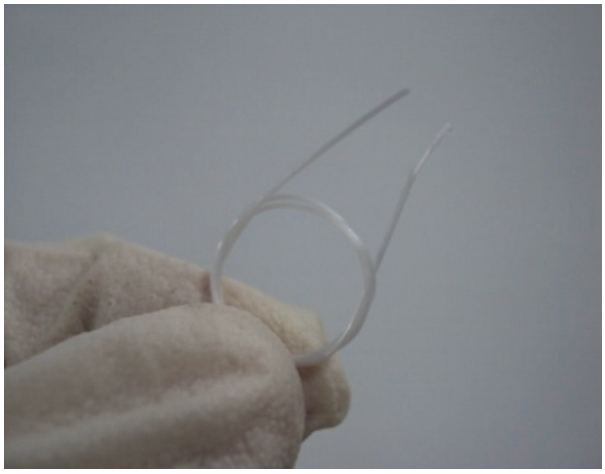

Fig. 5. Polymer based flexible piezoelectric fibre generated by a continuous process using the melt extruder.

4. Smart woven fabrics

Each fabric making method has its own special attributes which help us to find most applicable fabric structure and method for a specific application. By weaving polymer based piezoelectric fibres into woven fabrics, smart piezoelectric fabrics can be produced and used for many responsive applications.

Weaving is one of the best fabric making techniques that can be used for smart fabric production. Warp threads can be located at the heddles with different orders and wefts are travelled through warps by shuttle(s). The position of heddles designates where wefts will be going over or under the warps.

While a fabric is being designed, expectations from the final fabric are taken into consideration. For smart piezoelectric fabrics, depending on expected energy generation from the final product, weaving designs can be variable. In this case, intersection of piezoelectric (the charge generator) and conductive (the charge carrier) fibres is crucial. One piezoelectric fibre can interlace more than one conductive fibre. One conductive fibre can also interlace more than one piezoelectric fibre. However, one conductive fibre can only interlace the same pole of the each piezoelectric fibre.

A number of weaving designs are studied below for smart woven fabrics. Conductive fibres and conventional (non-conductive) fibres are needed alongside piezoelectric fibres. Because piezoelectric fibres carry negative charges on one side along its length and positive charge on the other side, a conductive material is needed to carry the charge produced by

movements of the piezoelectric fibres. Conductive wires would add extra rigidity to the fabric which is an undesirable outcome for most textile structures.
The best alternative to undesirable wires may be conductive fibres are produced and patented (Perera & Mauretti, 2009). It is claimed (Mauretti & Perera, 2010) that conductive filaments are flexible, non-toxic and conformable for wearable applications. Electrical conductivity of metallised synthetic (acrylic) conductive textile yarns is widely studied (Vassiliadis et al., 2004, 2009, 2010). Mechanical and electrical properties of metallised conductive yarn are controlled by blending conventional and conductive fibres in the yarn and changing the ratio of fibres in the blend. The way piezoelectric, conductive and conventional fibres are integrated into fabric structure by weaving technique, gives a good indication of the performance of resultant fabric. When more piezoelectric fibres are used in the fabric, this results in higher energy generation by movement and mechanical strain. However, to be able to carry as much charge as it is possible, the right number of conductive fibres need to interlace with piezoelectric fibres.
The possible woven fabric designs for energy generation for wearable textiles are shown in this chapter. Blue lines represent piezoelectric fibres while red lines represent conductive and grey lines show non-conductive conventional fibres. This is the simplest weaving pattern produced by plain weaving technique. However, by integrating piezoelectric and conductive fibres into this basic structure, the resultant woven fabric becomes a smart fabric which can harvest energy from the natural sources.

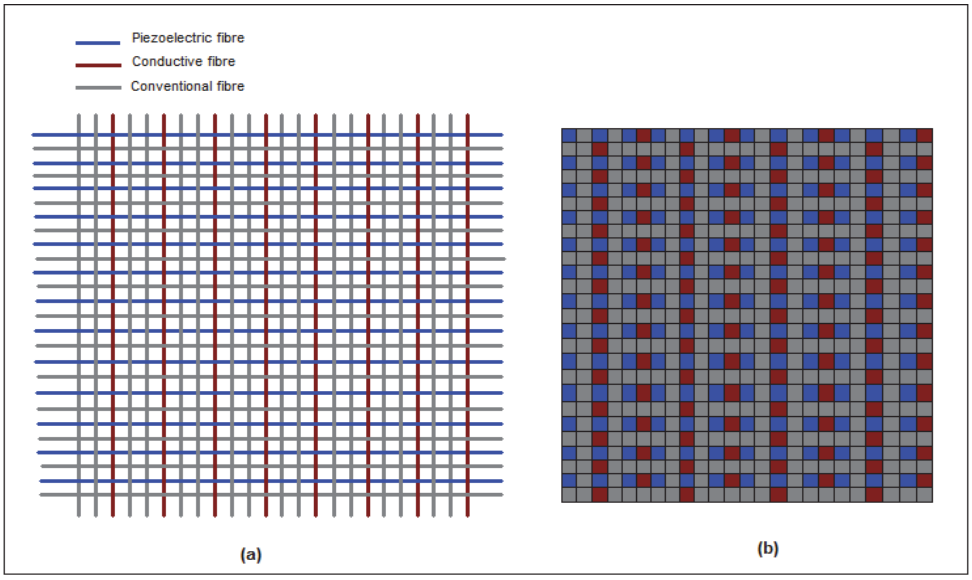

Fig. 6. (a) Smart woven fabric design 1 consisting of piezoelectric, conductive and non-conductive conventional fibres, (b) Face of the woven fabric consisting of piezoelectric, conductive and non-conductive fibres

Polymer based piezoelectric fibres can be used as either weft or warp into the woven structure and conductive fibres can be used as negative and positive electrodes for charge transfer so that the resultant fabric can produce energy for micro powered electronics.

The main advantage of the use of polymer based piezoelectric material in this application is its flexibility and the fact that it can easily be incorporated in the woven structures without causing any problem. It is impossible to integrate existing ceramic based piezoelectric fibres into similar structures because these fibres are rigid and brittle thus can cause major problems in the weaving process. For the first design shown in Figure 6(a), 2 heddles are needed to locate conductive and non-conductive fibres/yarns and 2 shuttles, the one with piezoelectric fibres/yarn and the other with non-conductive conventional fibres/yarn. In the warp direction, 2 conventional fibres are located between conductive fibres. Conductive fibres act as negative and positive electrodes.
If a number is given to each warp from left to right, odd numbered warps are located on the first heddle and even numbered warps are located on the second heddle. During the shuttles' travel along the loom's width, according to design, while the first conductive fibre only interlaces with negative pole of piezoelectric wefts, second conductive warp interlaces only positive pole of the piezoelectric filling fibres/yarns. Thus, any short circuit is avoided. Figure 6(b) shows interlace of warp and weft threads and possible appearance on face of the fabric. If the used fibres counts are the same and the warps and wefts are located with an exact sequence, the resultant fabric will contain 24% piezoelectric, 16% conductive and 60% non-conductive conventional fibres/yarns.

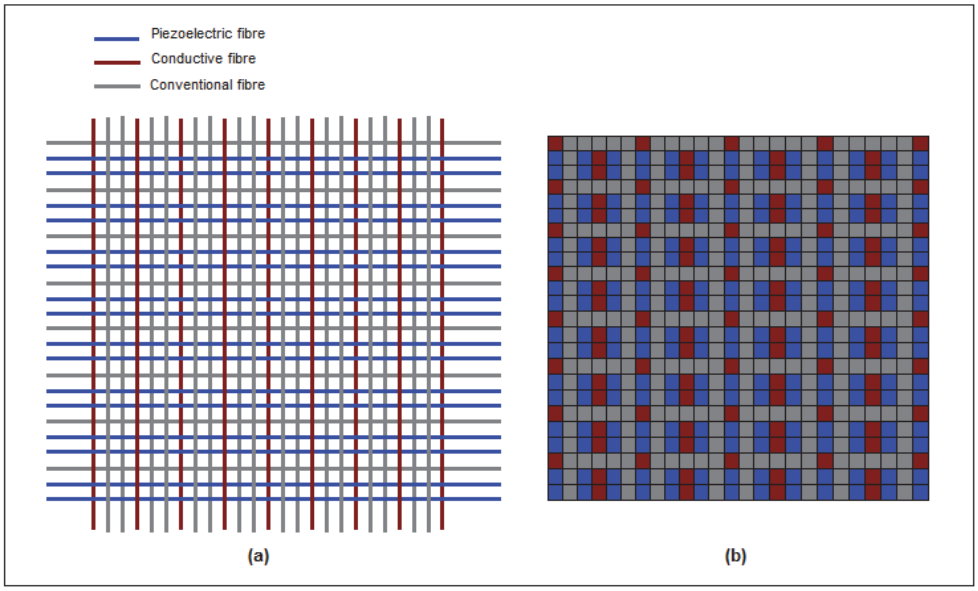

Fig. 7. (a) Smart woven fabric design 2 consisting of piezoelectric, conductive and non-conductive conventional fibres, (b) Face of the woven fabric consisting of piezoelectric, conductive and non-conductive fibres

The design shown in Figure 7(a) needs 2 heddles to locate conductive and non-conductive fibres/yarns and 2 shuttles, the one with piezoelectric fibres/yarn and the other with non-conductive conventional fibres/yarn. If a number is given to each warp from left to right, odd numbered warps are located on the first heddle and even numbered warps are located on the second heddle.

During the shuttles travel along the loom's width according to the design, the first heddle is kept in place, second heddle is uplifted so that warps are kept apart and shuttle travels through easily. Shuttle carrying piezoelectric fibre travels twice and then the other shuttle which carries non-conductive conventional fibres/yarn travels once. The whole process is repeated until the desired fabric structure is created. Thus, the first conductive warp only interlaces with negative charged sides of piezoelectric wefts, second conductive warp interlaces only with the positive charged sides of the piezoelectric filling fibres/yarns.
Figure 7(b) shows interlace of warp and weft threads and possible appearance on face of the fabric. If the used fibres counts are the same and the warps and wefts are located with an exact sequence, the resulted fabric will contain 34% piezoelectric, 18% conductive and 48% non-conductive conventional fibres/yarns.

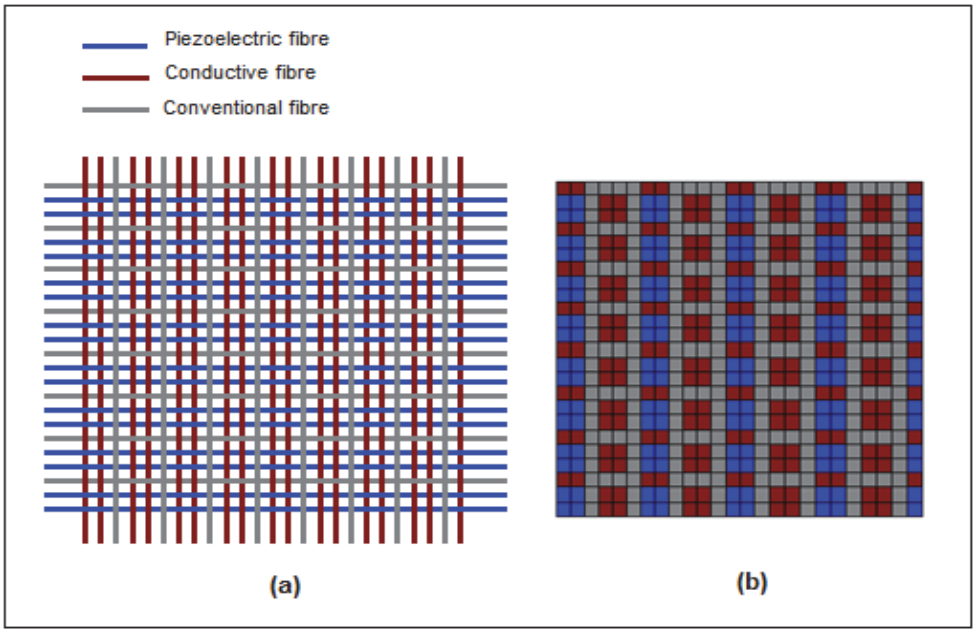

Fig. 8. (a) Smart woven fabric design 3 consisting of piezoelectric, conductive and non-conductive conventional fibres, (b) Face of the woven fabric consisting of piezoelectric, conductive and non-conductive fibres

The design shown in figure 8(a) needs 2 heddles to locate conductive and non-conductive fibres/yarns and 2 shuttles, the one with piezoelectric fibres/yarn and the other with non-conductive conventional fibres/yarn. If we give a number to each warp from left to right, 1st, 2nd, 7th, 8th, 13th, 14th, 19th, 20th and 25th warps are located on the first heddle and other warps are located on the second heddle.
According to design in figure 8(a), while first heddle is kept in place, second heddle is uplifted so that warps can be kept apart from the first heddle's warps and shuttle, which carries piezoelectric fibres/yarn, can easily travel through. The shuttle which carries piezoelectric fibre travels twice and then the first heddle is uplifted while the second heddle

is lowered so that the other shuttle which carries non-conductive conventional fibres/yarn travels once through the warps. The same movements are carried out with the same order again and again until a fabric structure is created. Thus, all the conductive warps on the first heddle only interlace with negative pole of piezoelectric wefts and all the conductive warps on the second heddle interlace only with positive pole of the piezoelectric wefts.
Figure 8(b) shows interlace of warp and weft threads and possible appearance on face of the fabric. If the used fibres' counts are the same and the warps and wefts are located with an exact sequence, the resultant fabric will contain 34% piezoelectric, 34% conductive and 32% non-conductive conventional fibres/yarns.

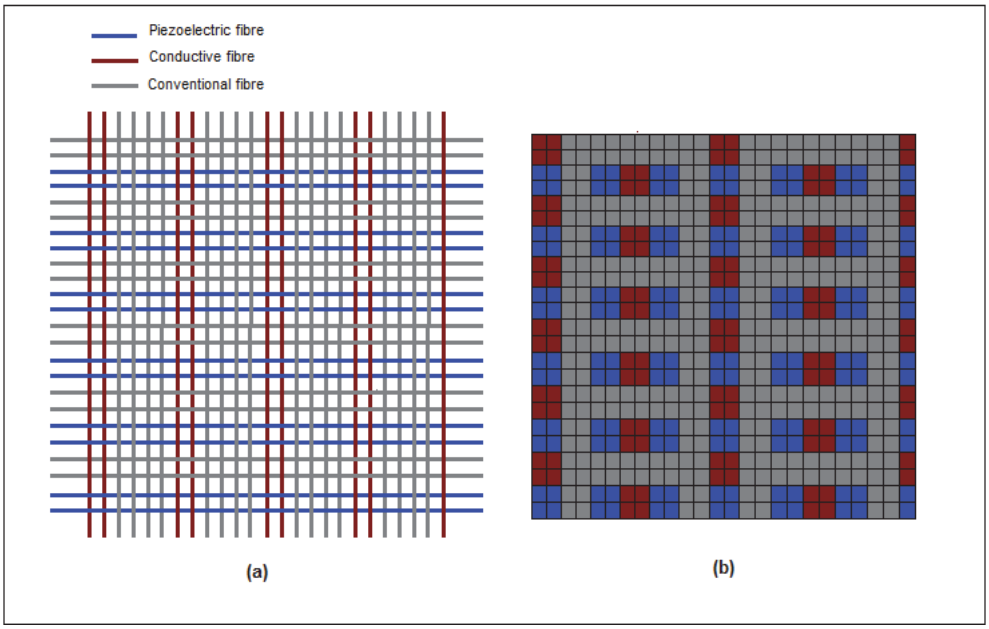

Fig. 9. (a) Smart woven fabric design 4 consisting of piezoelectric, conductive and non-conductive conventional fibres, (b) Face of the woven fabric consisting of piezoelectric, conductive and non-conductive fibres

The design shown in Figure 9(a) needs 2 heddles to locate conductive and non-conductive fibres/yarns and 2 shuttles, the one with piezoelectric fibres/yarn and the other with non-conductive conventional fibres/yarn. If we give a number to each warp, 1st, 2nd, 5th, 6th, 9th, 10th, 13th, 14th, 17th, 18th, 21st, 22nd and 25th warps are located on the first heddle and others are located on the second heddle.
During the first shuttle's travel along the loom width, the first heddle is kept in place and the second heddle is uplifted so that warps can be kept apart from the first heddle's warps and shuttle which carries piezoelectric fibres/yarn can easily travel through. The shuttle carrying piezoelectric fibre travels twice and then the first heddle is uplifted while the second heddle is lowered so that the other shuttle which carries non-conductive conventional fibres/yarn travels twice through the warps. The same movements are carried out in the same order again and again until a fabric structure is created. Thus, all the

conductive warps on the first heddle only interlace with negative pole of piezoelectric wefts and all the conductive warps on the second heddle interlace only with positive pole of the piezoelectric wefts.
Figure 9(b) shows interlace of warp and weft threads and possible appearance on face of the fabric. If the used fibres counts are the same and the warps and wefts are located with an exact sequence, the resultant fabric will contain 26% piezoelectric, 18% conductive and 56% non-conductive conventional fibres/yarns.

5. Conclusions

Polymer based piezoelectric fibres can be used as either weft or warp into the woven structure and conductive fibres can be used as negative and positive electrodes for charge transfer, therefore the resultant fabric can produce energy to power small electronic devices.
The advantage of polymer based piezoelectric fibre is their flexibility so that they can easily be used in woven structures. It is impossible to integrate existing ceramic based piezoelectric fibres into a similar structure since they are brittle.
For all four fabric designs studied in this chapter, interlace of piezoelectric and conductive fibre/yarn is significant. In a woven fabric structure, one piezoelectric fibre can interlace with more than one conductive fibre and one conductive fibre can also interlace with more than one piezoelectric fibre. However, to avoid any short circuit, one conductive fibre can only interlace with the same pole of the each piezoelectric fibre.
Since the fibres are considered having the same thickness, in the first design, piezoelectric and conductive fibres interlace 96 times in the fabric. The times of interlace of piezoelectric and conductive fibres are 153 for the second design whilst it is 289 and 117 times for the third and forth fabric designs, respectively. Therefore, the highest energy generation is expected from the third design when they all designs are subjected to the same amount of mechanical stimulus.
Smart piezoelectric woven fabrics can be used where they can be subjected to mechanical strain/stress or vibrations. Depending on the application and energy need, smart piezoelectric woven fabrics can be used to produce whole textile structure or only a part of it. For instance, tents, awnings and umbrellas can be wholly made of smart piezoelectric fabrics and produce electricity under rain as well as wind. However, waterproof finishing is needed if the fabric will be used for outdoor applications.
Energy generated by piezoelectric materials is always in the form of AC, therefore a small rectifier is needed for the conversion of the generated energy (AC) into usable energy (DC) for low power electronics.
The best weaving technique for smart piezoelectric fabric is plain weaving and its derivatives. Possible smart woven fabric designs are not limited. Depending on energy need, different fabric designs can be made with less or more interlacing. Other existing fabric making methods (other than weaving) such as embroidery can also be used to produce smart fabrics.

6. References

Anton, S.R. & Sodano, H.A. (2007). *Smart Mater. Struct.,* V.16, R1-R7.

Baker, J.; Roundy, S. & Wright, P. (2005). *Proc. 3rd Int. Energy Conversion Engineering Conf.,* pp. 959-970.

Baz, A.; Poh, S. (1988). Performance of an active control system with piezoelectric actuators, *J. Sound and Vibration*, V.126, No.2, pp. 327-343.

Broudy, Eric. (1979). *The Book of Looms: A History of the Handloom from Ancient Times to the Present*, University Press of New England, ISBN 0-87451-649-8, New York, USA

De-Qing, Z. (2008). *Chinese Physics Letters,* V.25, p. 4410.

Dunn, P. E. & Carr, S. H. (1988). Piezoelectricity in nylon 5,7, IEEE Proceedings 6th International Symposium on Electrets, DOI 10.1109/ISE.1988.38559

Gioello, D.A. (1982). *Understanding Fabrics from Fiber to Finished Cloth*, Fairchild Publications, ISBN 87005-377-9, New York, USA

Granstrom, J.; Feenstra, J.; Sodano, H.A. & Farinholt, K. (2007). Energy harvesting from a backpack instrumented with piezoelectric shoulder straps, *Smart Materials Structures*, V.16, pp. 1810-1820.

Harrison, J. S.; Ounaies, Z. (2001). Piezoelectric Polymers, *NASA/CR-2001-211422,* ICASE Report No. 2001-43

Hellwege, K.H. & Hellwege A.M. (Eds.) (1996). *Ferroelectrics and Related Substances: Oxides*, Landolt Bornstein New Series, Springer, Berlin.

Holstein, P.; Leister, N.; Weber, U.; Geschke, D. & Binder, H. (1999). A Combined Study of Polarization Effects in PVDF, *10th International Symposium on Electret. IEEE*

Jaffe, B.; Cook, W.R. & Jaffe, H. (1971). *Piezoelectric Ceramics*, Academic Press, London.

Jain, A.; Kumar, J.S.; Mahapatra, D.R. & Kumar, H.H. (2010). Proceedings of SPIE – The International Society for Optical Engineering 7647.

Jordan, T.L. & Ounaies, Z. (2001). NASA ICASE Report No. 2001-28.

Kawai, H. (1969). The piezoelectricity of poly(vinylidene fluoride), *Jpn. Journal of Applied Physics*, V.8, pp. 975-976

Mateu, L.; Moll, F. (2005). *J. Intell. Mater Syst. Struct.*, V.16, pp. 835-845.

Mauretti, G. J. & Perera, W. R. (2010). iCon Conductive Filaments, *Proceeding of Textile Institute Centenary Conference,* Manchester, UK, November 3-4, 2010

Neagu, E. R.; Hornsby, J. S. & Das-Gupta D. K. (1999). Analysis of Polarization ans Space Charge in Thermally Poled PVDF, *10th International Symposium on Electrets, IEEE,* pp. 87-90

Newman, B. A.; Chen, P.; Pae, K. D. & Scheinbeim, J. I. (1980). Piezoelectricty in Nylon 11, Journal of Apllied Physics, V.51, No.10, pp.5161-5164, DOI 10.1063/1.327283

Parvanova, V.D. & Nadoliisky, M.M. (2005). Polarization Processes in PZT Ceramics, *Bulg. J. Phys.*, V.32, pp. 45-50.

Perera, W. R. & Mauretti, G. J. (2009). *Microwires, Methods for Their Production, and Products Made Using Them*, US Patent Number 20090260848 A1

Ramadass, Y.K. & Chandrakasan, A.P. (2010). An Efficient Piezoelectric Energy Harvesting Interface Circuit Using a Bias-Flip Rectifier and Shared Inductor, *IEEE Journal of Solid-State Circuits*, V.45, No.1, pp. 189-204.

Ramos, M. M. D.; Correia, H. M. G. & Lanceros-Mendez, S. (2005). Atomistic modelling of processes involved in poling of PVDF, *Computational Materials Science,* V.33, pp. 230

Roundy, S.; Wright, P.K.; & Rabaey, J. (2003). *Computer Communications,* V.26, pp. 1131-1144.

Schmidt, V.H.; Lediaev, L. & Polasik, J. (2006). Piezoelectric Actuators Employing PVDF Coated with Flexible PEDOT-PSS Polymer Electrodes, *IEEE Transactions on Dielectrics and Electrical Insilation*, V.13, No.5, pp. 1140-1148.

Schwartz, M. (2002). *Encyclopaedia of Smart Materials Vol.1-2*, pp. 780-792.

Sencadas, V.; Moreira, V.M.; Lanceros-Mendez, S.; Pouzada, A.S. & Gregorio Jr. R. (2006). α-to-β Transformation on PVDF Films Obtained by Uniaxial Stretch, *Materials ScienceForum 514-516*, pp. 872-876

Sencadas, V.; Filho, R.G. & Lanceros-Mendez, S. (2006). *J. Non Cryst. Solids* V.352, pp. 2226

Seo, J.W.; Ryoo, K.S. & Lee, H.S. (1985). Characteristics of Charge Traps and Poling Behaviour of Poly(Vinylidene Fluoride), *Bulletin of Korean Chemical Society*, V.6, No.4, pp. 218-221.

Sessler, G.M. (1981). Piezoelectricity In Polyvinylidene fluoride, *J. Acoust. Soc. Am.*, V.70, pp. 1596-1608.

Shirane, G. & Suzuki, K. (1952). Crystal structure of Pb(Zr-Ti)O_3, *J. Phys. Soc. Jpn.*, V.7.

Shu, Y.C. & Lien, I.C. (2006). Analysis of Power Output for Piezoelectric Energy Harvesting Systems, *Smart Materials Structures*, V.15, pp. 1499-1512.

Siores, E.; Hadimani, R. L. & Vatansever, D. (2010). *Piezoelectric Polymer Element & Production Method & Apparatus Therefor.* GB Patent Application Number 1015399.7

Sirohi, J. & Chopra, I. (2000). Fundamental Understanding of Piezoelectric Strain Sensors, *J. Intelligent Mater. Systems and Struc.*, V.11, pp. 246-257.

Sodano, H. A.; Inman, D. J. & Park, G. (2004). *Shock Vib. Digest*, V.36, pp.197-205.

Sodano, H.A. & Inman, D.J. (2004). A Review of Power Harvesting from Vibration Using Piezoelectric Materials, *The Shock and Vibration Digest,* V.36, No.3, pp. 197-205.

Swallow, L. M.; Luo, J. K.; Siores, E.; Patel, I. & Dodds, D. (2008). *Smart Mater. Struct.*, V.17

Tzou, H.S. & Tseng, C.I. (1990). Distributed piezoelectric sensor/actuator design for dynamic measurement/control of distributed parameter systems: A piezoelectric finite element approach, *J. Sound and Vibration*, V.138, pp. 17-34.

Umeda, M.; Nakamura, K.; Ueha, S. (1997). *Jpn. Journal of Applied Phys.*, V.36, pp.3146-3151.

Vassiliadis, S; Provatidis, Ch.; Prekas, K. & Rangoussi, M. (2004). Electrically Conductive Spun Yarns, Proc. of the Xth International Izmir Textile and Apparel Symposium, pp.37-49, Izmir, Turkey

Vassiliadis, S.; Rangoussi, M.; Meimaris, D.; Prekas, K. & Provaditis Ch. (2009). Electrically Conductive Spun Yarns and their Contact Behaviour, *Proceedings of the International Conference on Intelligent Textiles and Mass Customisation*, Casablanca, Morocco

Vassiliadis, S.; Prekas, K.; Rangoussi, M.; Absalon, K. & Maillard, J. (2010). The Conductive Spun Yarns as Electrical Components, *Proceedings of the XIIth International Izmir Textile and Apparel Symposium*, pp.333-338, Izmir, Turkey

Wegener, M.; Künstler, W.; Richter, K. & Gerhard-Multhaupt, R. (2002). Ferroelectric polarization in stretched piezo- and pyroelectric poly(vinylidene fluoride-hexafluoropropylene) copolymer films, *J. Appl. Phys*., V.92, pp.7442-7447.

Wikipedia, online access from http://en.wikipedia.org/wiki/Loom#Handloom (Jan. 2011)

Part 2

Computational Modelling and Structural Woven Fabrics

3

Mechanical Analysis of Woven Fabrics: The State of the Art

Savvas Vassiliadis[1], Argyro Kallivretaki[1],
Dimitra Domvoglou[1] and Christofer Provatidis[2]
[1]*Department of Electronics, Technological Education Institute of Piraeus,*
[2]*School of Mechanical Engineerin, National Technical University of Athens,*
Greece

1. Introduction

The automation and integration of processes in the textile industry is dictated by the increasing need to offer specialized products at optimum quality and low cost, satisfying at the same time the fast cycles of fashion trends or in the case of technical applications the delivery of products of high qualiy and of exact properties. Under these premises, computer engineering tools, such as computer-aided engineering (CAE) and computer-aided design (CAD), have recently gained attention. The revolutionary role of CAE and CAD tools in the textile industry is the guaranty that the final product meets the set specifications, optimizing thus the quality control procedure. Moreover, the prediction of the properties and the aesthetic features of the product before the actual fabrication can essentially benefit the textile research community [Hu and Teng, 1996]. Especially nowadays that textile materials can be used for the production of a wide range of technical products, such as reinforcements in composites for aerospace or marine applications or textiles for medical applications, the prediction of the end-product's mechanical properties is of major importance. Furthermore, the textile raw materials are processed under low-stress conditions and it is thus reasonable to assume that the knowledge of the possible modifications introduced via the manufacturing process is necessary for the final product realization (Hu, 2004).

Textiles are flexible, anisotropic, inhomogeneous, porous materials with distinct visco-elastic properties. These unique characteristics makes textile structures to behave essentially different compared with other engineering materials. Moreover, textiles are characterized by an increased structural complexity. Their properties mainly depend on a complicated combination of their structural units and their interactions. The complicated nature of the textiles' mechanics makes them ideal candidates for a mechanical analysis using computer-based methods.

This paper focuses on the investigation of the modeling attempts of woven fabrics. The woven fabrics' weave patterns as well as the deformation mechanisms of their consistent yarns make these structures modelling extremely challenging (Parsons et al., 2010). An extended literature review of the computational models for the deformation of woven fabrics is presented. Based on these models, the difficulties towards a comprehensive model for textile structures are highlighted. Taking into account the existent literature, the perspective of developing a widely accepted integrated CAE environment for textiles (Hearle, 2006), is also extensively discussed.

2. Textile structures and their mechanical behavior

Since this study focuses on the investigation of the existent woven fabrics' simulation techniques, some introductory remarks concerning the basic structural units of these unique substrates, are thought to be extremely useful. Textile fabrics are made of interlaced yarns which consist of the basic element of every textile product, the fibres. Fabrics are classified according to their manufacture process as knitted, woven and non-woven.
The computational representation of textiles is hindered by the geometrical complexity of the textiles' basic structural units (fibres and yarns) as well as of the fabrics' weaving and knitting patents. The aforementioned characteristics of the textiles woven fabrics result in complicated deformations even in cases of simple loading. For example, the tensile deformation of a spun yarn corresponds to the superposition of bending, tensile and compression of the constituent helically arranged fibres. Furthermore, contact phenomena, as sticking and sliding interaction, should be also taken into account in the mechanical deformation analysis increasing thus further the complexity of the mechanical study.
Fabric mechanics study often leads to the introduction of models with simplifying assumptions. The yarn, which is usually assumed as a homogeneous material, is considered as the basic structural unit of the fabrics. The elastic properties of the homogeneous yarn result from the elastic properties of the fibres and include the non-linear structural synergy of them within the yarn body. Even if the yarns are assumed as homogeneous materials, the contact phenomena dominate the deformation procedure of the fabrics. Actually, the friction effects support the stability of the textile structures. The contact phenomena have also a great significance for the stress and strain distribution in a fabric subjected to deformation. The friction energy losses appear during the load transferring along threads. Thus, very often, uneven load distribution appears within the textile structures.
Due to the large deflection effects and the nonlinearity of the textile structures' deformation phenomena, the fabrics mechanics study requires special attention. The relative large deformation of the fabrics arises from the flexibility of the textile fibres and yarns as well as from the structural details and the way of the load application. The yarns present high deformability which results from the low values of packing factor (the ratio of the fibres volume to the total volume of the yarn). The air trapped between the fibres is easily removed during the axial loading imposing the reduction of the apparent yarn cross sections and thus the high deformation of the yarns which is obviously transferred to the fabrics. Moreover the pattern of the fabrics itself and especially the structure of the fabrics, supports the development of high deformations. From the structural point of view the fabric pattern can be considered as a multi-body system of yarns. The tensile deformation of the fabric corresponds to the synthesis of two processes, the bent yarns' straightening and their subsequent elongation. The first process dominates in the lower loading stage and the second process appears upon the increase of the load. Thus the load-deflection curves of a textile structure subjected to tensile deformation is strongly nonlinear. The nonlinearity is also supported from the change of the contact status between the yarns, the large deflection effects observed even within the unit cell of the fabric and finally the material nonlinearities

2.1 Technical applications of textiles

Although conventional textiles are primarily used for clothing, the use of a variety of raw materials as well as the development of new manufacturing processes led to a considerable expansion of their possible applications. The importance of aesthetic and decorative

characteristics of textiles has been decreased by the new materials' performance and functionality. The growing recognition of the textiles potentials led to revolutionary new technical applications which according to Techtextiles (the international Trade exhibition for technical textiles) are (Horrocks, 2000):
Agrotech: agricultural (nonwoven for wind protection)
Buildtech: building and construction (awning, concrete reinforcements)
Clothtech: clothing (garments)
Hometech: household (curtains, wall covering)
Indutech: industrial applications textiles (filters)
Medtech: medical (bandages, sutures)
Mobitech: mobility (ropes, seat covers)
Oekotech: eco-friendly textiles (recyclable composites)
Packteck: packaging (nets, wrappings)
Protech: protection (bullet-proof jackets, uniforms)
Sportech: sports and leisure (carbon-fibre composites for racquet frames)
Geotech: geotextiles (nonwovens for drainage, reinforcement)
Over the last decades there is also an intensive need for high-tech materials with "life functions". Consequently, research interest has been moved towards the development of textile-based structures which change their properties in response to an external stimulus, offering products with increased functionalities. The so called "intelligent", "smart" textiles in conjunction with the wearable electronics usually consisting of electronic modules incorporated into textiles, support activities in military, telemedicine or rehabilitation (Rossi et al. 2006; Tang, 2007; Cho et al., 2009). Textiles' flexibility, indicative of the wearer's comfort, makes them ideal candidates for interfaces in contact with the human skin. Based on these assumptions, a large number of wearable electronic systems have been developed (Dunne et al., 2005; Xu et al., 2008; Tognetti et al., 2006). Smart textiles development requires the synergistic action of different disciplines such as textile science and engineering, natural sciences, material science, mechanical engineering, electrical and computer engineering and informatics, making this promising research area extremely challenging. Furthermore, the attention attracted by this dynamic sector of textile research is thought to make a contribution towards a cost effective commercialization of innovative textile-based products aiming in the improvement of people's quality of life.

(a) (b) (c)

Fig. 1. Technical applications of textiles (a) Fabric for solar protection used in the Paul Klee museum, (soltis-textiles, 2011), (b) DuPont's Kevlar® XP™ developed for hard armor applications, (DuPont, 2011), (c) Space suit developed by ILD Dover (ilddover, 2011)

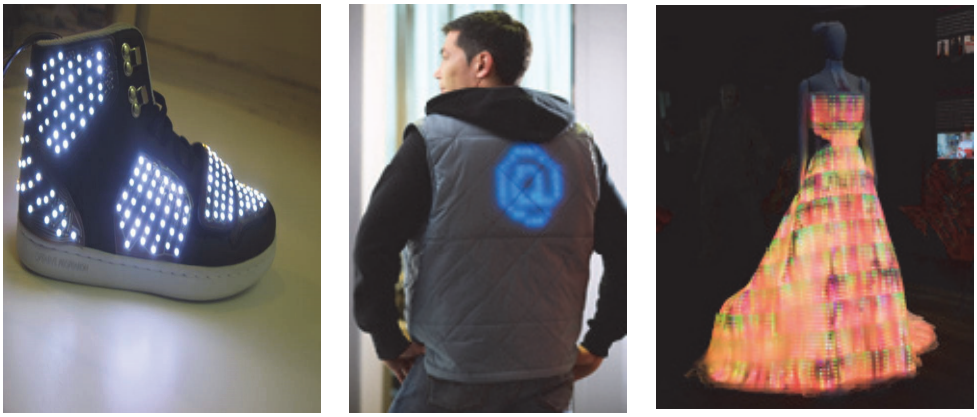

(a) (b) (c)

Fig. 2. Smart textiles (a) Interactive Led dance shoe by Moritz Waldemeyer (waldemeyer, 2011) (b) Luminate textiles by Phillips (smarteconomy, 2006), (c) Led Dress by Cute Circuit (crunchwear, 2010)

3. Mechanical modelling of the textile structures

3.1 Classification of the modelling approaches

During the last decades, several methods were adopted for the mechanical modelling and analysis of the textile structures. A basic classification, according to the modelling method used, divides them into the analytical and numerical or computational approaches. The dominant engineering design culture played important role for the development and the succession of these approaches. Classical modelling methods find in textiles an attractive application field. Another essential classification of the modelling of the textile structures is made according to the scale of the model. There is micromechanical, mesomechanical and the macromechanical modelling. The micromechanical modelling stage focuses on the study of the yarns, tows even fabrics taking into account the structure, orientation and mechanical properties of the constituent fibres. The mesomechanical modelling, on the other side, studies the mechanical characteristics of the fabric unit cell considering the yarns as homogenous structures. Finally the macromechanical modelling stage is reffered to the prediction of mechanical performance of the fabric in complex deformations, as drape, studing the fabric as a continuum material.

Although the mentioned modelling stages were developed as distinct analysis approaches, their integration in a compound modelling approach was directly rised. Thus the textile society implemented a modelling hierarchy (Takano et al., 1999; Lomov et al. 2004; Bogdanovich, 2006) based on three modelling scales: the micromechanical modelling of yarns, the mesomechanical modelling of the fabric unit cell and the macromechanical modelling of the fabric sheet (Figure 3).

According to the integrated textile modelling concept, the only inputs in the total design procedure are the fibre properties, the yarn structure and the fabric structure. In the first modelling stage, the fibre properties and the yarn structure (yarn type, number of fibres, orientation) are introduced as input parameters for the mechanical analysis of the yarn and the calculation of the yarn properties. Then the yarn properties are transferred in the second

modelling stage. The selection of the required yarn properties and their attribution in the modelled yarns corresponds to a homogenization procedure that connects the two individual stages. Moreover the woven fabric structure is introduced in the mesomechanical modelling stage. At the current stage the yarns are represented as continuum structures and the analysis is limited on the study of the fabric unit cell. Then a second homogenization stage is required for the connection of the second and the third modelling stage, defining the required properties of the unit cell and their attribution in the continuum fabric models. Finally the macromechanical modelling stage based on the generation of simplified structure (usually continuum material) predicts the mechanical performance of of extended fabric pieces in complex deformations. Each individual modelling procedure such as their interface presents significant obstacles.

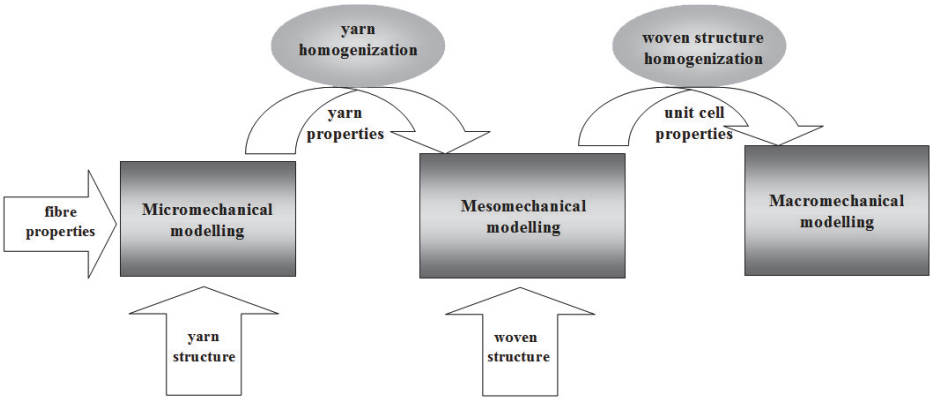

Fig. 3. Integrated textile modelling.

3.2 Classification of the deformations

The substantial difficulty arising in textile mechanics consists in the calculation of the superposed deformations in the microscopic scale. Even a simple deformation of the woven fabric, for example a tensile deformation, incures a complex deformation mechanism of straightening, tensile, compression and sliding of yarns in the mesoscopic scale and respective deformations of fibres in the microscopic scale. Moreover the percentage of the deformation increases when it is referred to the microscopic scale since the subjected structures are smaller. For example, a 5 % shear deformation of a fabric could impose a huge displacement of the constituent fibres. Thus a simple deformation in the macroscopic scale corresponds to complex deformations in the microscopic scale. However the classification of the deformations is based on the macroscopic level. Thus the tensile, shear, bending and compression of the fabric sheet are considered simple deformations. The complex deformation of fabrics is mainly referred to the drape test. The performance of a fabric in drape is very interesting for the aesthetic effects and the dynamic functionality. The fabrics have the ability to undergo large, recoverable draping deformations by bending in single and double curvature providing a sense of fullness and a graceful appearance. Especially when the fabrics are used as reinforcement materials for the construction of composites, drape is very important since it determines the formability of the fabric in the matrix. The

drapeability of the fabric reinforcement offers the advantage of bending around double-curvature mould producing complex shaped composite parts.

4. Analytical modeling

The first mechanical modelling and analysis attempts of the textile structures started about a hundred years ago. The earliest publication probably is from R. Haas in the report of the National Advisor Committee for Aeronautics in 1918 (Haas, 1918). It is worth to mention that NACA is the early form of the today's NASA of the US. This publication is the translation from the German of the original article dated back on 1913 appeared in a German Journal. The work of Haas is of great importance. Although it is the first known, it is characterized by its integrated character. It brings together the theoretical and practical aspects up to the testing and application topics. However the work of Haas remained unknown for a long perod while the work of Peirce (Peirce, 1937) was considered as the starting reference for the analytical mechanical modelling of the textile structures. The researchers focused on the application of the existent analytical methods already used in other sectors of engineering. The main characteristic is the balance between the simplifications introduced and the precision of the modelling. The energy methods and the elastica theory are dominating in these attempts.

4.1 Micromechanical modelling of simple deformations

In the field of the analytical modelling of the textile yarns, several investigations focused on multi-filament twisted yarns. Purpose of these investigations was the prediction of the response of a twisted yarn when subjected to a certain deformation. It was supposed that the mechanical parameters such as the load-elongation curve of the constituent fibres, the twist density, the initial specific volume etc are given. The analysis focused on the correlation of the macroscopic distortion of the yarn with the microscopic response of the constituent fibres. A basic challenge in the modelling of the yarns is the balance between the realistic formulation and the idealization required for a theoretically treatable model. In the most cases the yarn was considered as being made of continuous filaments of circular cross-sections and constant linear density along their length. All the fibres were assumed to have identical properties and to be perfectly elastic. The cylindrical-helix model of Hearle et al. (Hearle et al., 1959), the conical-helix model of Önder and Başer (Önder & Bacer, 1996) and the statistical model of Komori (Komori, 2001) approached the yarn mechanical modelling from different points of view, depending on the considered alignment of the fibres. The tensile, bending and torsional behaviour of the yarns were approached using the force, the stress-analysis and the energy methods (Backer, 1952; Platt et al., 1959; Freeston & Schoppee, 1975; Choi & Tandon, 2006; Park & Oh, 2006).

4.2 Mesomechanical modelling of simple deformations

Starting point for the analytical modelling of woven fabrics was the uniaxial/biaxial deformation of the plain woven structure. The proposed approaches were based on three principal underlying geometrical models of plain weave (Dastoor et al., 1994). The "flexible thread" model of Peirce (Peirce, 1937) assumed the yarns infinitely flexible, incompressible and inextensible, without bending rigidity and having circular cross-sections (Figure 4, Figure 5). The analytical transcendental equations proposed by Peirce for the systematic

description of his model cannot easily give a solution. Thus graphical and nomographic tools were presented in order to support the users. Peirce's model has been modified later towards a better representation of the real fabric structure. Thus the assumptions of the race-track (Figure 6) or elliptical (Figure 7) yarn cross-sections (Kemp, 1958; Olofsson, 1964b) were adopted for the fabric modelling. The concept of the elastica model (Peirce, 1937), in continue, introduced the yarn bending rigidity in the analysis. According to this model the shape of yarn axis can be obtained by treating the yarns as elastic slender rods subjected to transverse point forces, equidistant but alternating in direction. In general, the mentioned models and their later modifications used the equilibrium, energy or elastica method for the mechanical analysis.

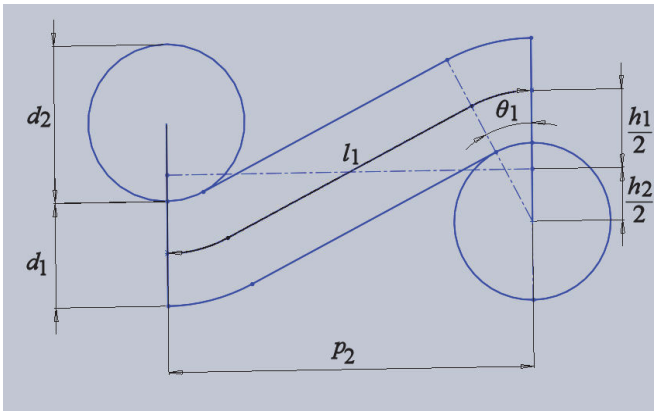

Fig. 4. Plain woven geometry proposed by Peirce.

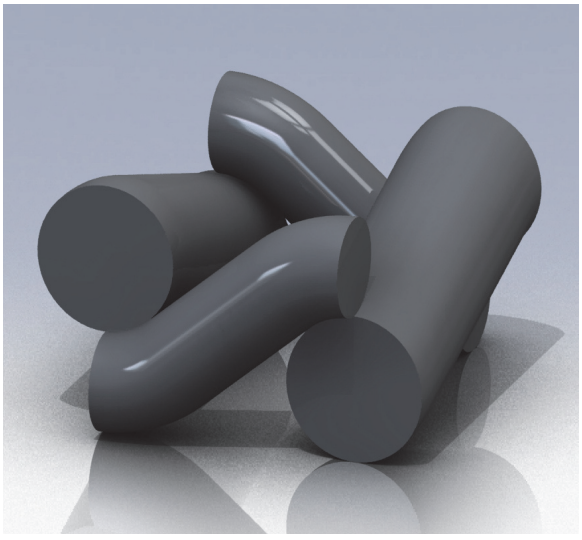

Fig. 5. 3D representation of woven model proposed by Peirce.

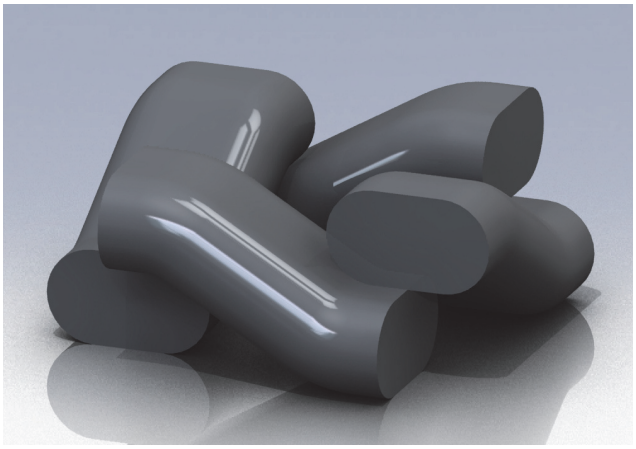

Fig. 6. 3D representation of woven model proposed by Kemp.

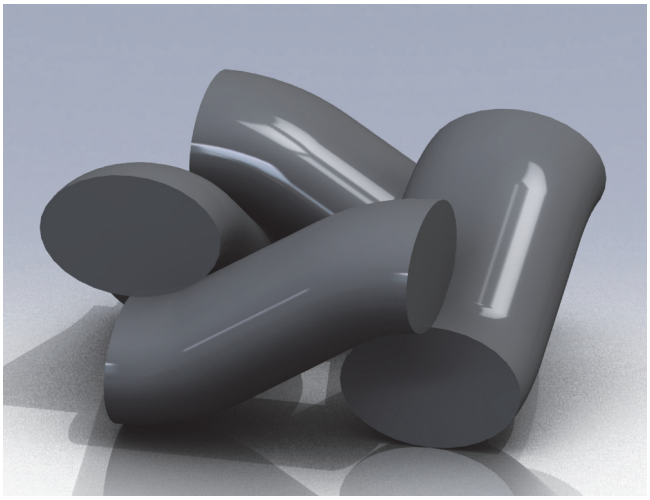

Fig. 7. 3D representation of elliptic model proposed by Olofsson.

An approach including the effect of crimp and yarn extension, based on a flexible thread model was proposed by Freeston et al. (Freeston et al., 1967). The yarns were assumed as homogenous, linear elastic materials with linear work-hardening. An elastica model declining from the assumption of the standard shape yarn cross-section was published by Olofsson (Olofsson, 1964a). The shape of the cross-section of the yarns was considered as a function of the forces acting on them and the degree of set. The mathematical analysis was given on equilibrium conditions, on stress-strain relationships in extension and compression and on energy in bending. The effect of fabric set was included, also, in the work of Grosberg and Kedia (Grosberg & Kedia, 1966; Grosberg, 1966). They adopted an energy method on small deformation for the investigation of the initial load extension modulus of completely relaxed woven fabrics, while the yarns were assumed inextensible and

incompressible. Another approach based on the elastica theory including linear extensibility of the yarns was given by Dastoor et al. (Dastoor et al., 1994). They assumed the yarns to be homogeneous, weightless slender rods, frictionless and undeformed by shear forces. In addition the yarns were considered as having circular section which does not deform under external forces. A computational implementation was adopted for the solution of the equilibrium equations. The large biaxial deformation of partially and completely set plain woven fabrics was presented by Huang (Huang, 1979b; Huang, 1979a). His approach was based on the elastica model of yarns in the undeformed fabric and the combined action of extension and bending was considered for the fabric deformation. The introduction of bilinear moment-curvature relation (due to the sliding of the fibres within the yarn) in combination to the contact deformation of the yarns increases the reliability of the study. The "sawtooth" geometrical model was proposed by Kawabata *et al*. (Kawabata et al., 1973). The mechanical analysis was based on the force equilibrium and the displacement of the warp and weft yarns in the thickness direction of the fabrics at the contact point of the crossing threads. Although the geometrical representation of the unit cell was approximant, the deformation effect at the cross-over points was taken into account. Most of the models described assume an unrealistic invariable cross-sectional yarn shape along the yarn path, where Gong et al. (Gong et al. 2010), in a recent study moves towards a more realistic representation of woven yarns, suggesting an ellipse model with a variable yarn cross-sectional shape based on the various parameters, including fibre type, yarn count, yarn twist factor and cover factor. An alternative geometric model of woven fabric, based on the yarns' packing density as well as general fabric data, has been suggested by Dolatabadi and Kovař (Dolatabadi & Kovař, 2009).

4.3 Mesomechanical modelling of complex deformations

The concept of the complex deformations on a mesomechanical scale is extremely marginal. It is almost impossible to simulate on the scale of the unit cell the effects occurring during the drape of a fabric. The so called mesomechanical models for the complex deformation of the fabrics mainly refer to the bending behaviour of the fabrics. The first study in complex deformations of fabrics was conducted by Peirce (Peirce, 1937). He proposed an energy method for the analysis of 2D fabric bending. The analysis was based on the calculation of the change of the strain energy of the unit cell after the bending deformation. For the analysis the yarns were assumed to be of circular cross-section and incompressible and distributed forces were considered at the cross-sections of the yarns. Many researchers (Behre, 1961; Dahlberg, 1961; Lindberg et al., 1961; Abbott et al., 1971; Abbott et al., 1973) studied and reported the nonlinear nature of bending and shear properties. The approach adopted by Grosberg (Grosberg, 1966) incorporated the effects of friction into the strip 2D bending analysis. Many relative research actions were carried out in continue contributing to the understanding of drape to some extent. But the 2D drape assessment cannot fully reflect the more complex 3D double curvature deformations of drape (Lo et al., 2002).

Shanahan et al. (Shanahan et al., 1978) accented the necessity of the complete drape treatment based on the structural mechanics shell theory. They also defended the consideration of anisotropic constitutive laws for the fabric sheet. Amirbayat and Hearle (Amirbayat & Hearle, 1989) used aspects of the shell theory in their theoretical investigation of the complex buckling. They correlated the drape shape with the bending, membrane and potential energies. From their investigation they concluded that drape is also influenced by other parameters such us the full set of anisotropic in-plane membrane, out-of-plane bending, cross term elastic constants, and the nonlinearity of the materials behaviour.

4.4 Macromechanical modelling of complex deformations

Many publications appeared in the past dealing with the macromechanical modelling of the complex deformations of the fabrics. For many years this specific area has concentrated the interest of many very important researchers. The most representative of them are referenced below.

An approach of the elastica theory for the analysis of complex deformations of fibres and fibre assemblies has been proposed by Konopasek (Konopasek, 1980a, 1980b, 1980c). It was based on the concept of planar and spatial elastica as developed respectively by Euler and Kirchhoff. Phenomena corresponding to the nonlinear behaviour of material, friction-elasticity, elastic-plasticity, and visco-elasticity were introduced in the analysis. The planar elastica theory was applied for the analysis of the large deflections of a yarn in a plane and the cylindrical bending of a fabric treated as sheet material. The spatial elastica was applied in the analysis of fibre buckling and crimp. The solution of the system of the resulted nonlinear differential equations was supported by computational tools.

An alternative approach to the theoretical mechanics of static drape of fabrics based on the differential geometry of surfaces was published by Lloyd et al. (Lloyd et al., 1996). They developed a computationally convenient implementation of the theoretical mechanics of fabrics. The fabrics themselves were treated as 2D continua represented by a surface without considerable thickness embedded in the 3D Euclidean space. The mechanical properties of the fabric were assigned to the model. The shape of the surface was described for both the deformed and the undeformed state by the means of the differential geometry of the surface. The strain values were deduced from the differences in the differential geometry expressions for the two extreme states. The strain values were correlated to the applied forces by the constitutive equations that express the mechanical properties of the material.

The differential geometry of surfaces for the dynamical modelling of fabric deformations was used for the approach of the problem by J. and R. Postle (Postle & Postle, 1996). The surface was considered as a series of twisted curves generated into the 3D Euclidean space. The differential geometry parameters incorporated the mechanical properties of the material (fabric) relating these mechanical properties to the changes in curvature as the surface was transformed into another surface. The deformation of the surface from the initial state to the final was mathematically modelled using the concept of homotopy. Bäcklund transformations were chosen for the solution of the nonlinear partial differential equations of the dynamic system.

Trying to combine the theoretical study to the experimental knowledge, Stump and Fraser (Stump & Fraser, 1996) analyzed the drape of a circular fabric sample over the circular disk of the drapemeter. They proposed an elastic ring-theory model of the draped fabric and used an energy analysis associated with the various large post-buckled deformations of the ring. Aim of their investigation was the study of the ability of the fabrics to present different configurations when they are draped under exactly the same conditions. The explanation of this ability was based on the calculation of the energy that corresponds to the various symmetric configurations.

4.5 Evaluation of the analytical approaches

The review of the literature of the analytical methods for the mechanical analysis of textile structures demonstrates the absence of a successful globally accepted technique suitable for the textile design. The basic drawbacks of the analytical methods result from the simplifying assumptions implemented in order to generate a low-complexity geometry and mechanical

problem. Thus the two-dimensional approach for the mesomechanical modelling, the attribution of isotropic elastic properties in the yarn models, the assumption of linear and isotropic properties in the macromechanical model introduces significant inaccuracies in the textile modelling. However the basic disadvantage of analytical approaches is the difficulty in handling in respect to the time consumption, the application field in terms of structures and materials, and the integration of the individual stages (micro, meso, macro). On the other side the analytical approaches accented the modelling difficulties of textile mechanics, the basic considerations and roadmap for an integrated design procedure.

5. Numerical modeling

The enormous computational power arose from the development of the computer systems and the expansion of advanced commercial software codes for the analysis of mechanical problems was guiding the textile design towards the numerical approaches. Mainly the Finite Element (FEM) and Boundary Element Method (BEM) were used for the mechanical modelling of the textile structures (Hu & Teng, 1996).

5.1 Micro- and mesomechanical modelling of simple deformations

The first attempts in the computer based mesomechanics of textiles dealt with the 2D and 3D representation of the plain woven structure. The geometry proposed by Haas and then by Peirce was the starting point for the solid geometrical modelling since the numerical techniques succeed the solution of the complex system of equations. Keefe et al. (Keefe et al., 1992) based on Peirce's geometry presented the solid model of the plain woven fabric. They also extended the model for various compactions and fabric angles. Later comparative studies examined the accuracy of the geometrical models for use in the numerical modelling of fabrics (Provatidis & Vassiliadis, 2002, 2004, Provatidis et al., 2005).

The first studies in mechanical analysis of textiles focused on the tensile deformation of the plain woven unit cells. The initial use of computational methods in textile mechanics was oriented towards the numerical solution of the complex analytical expressions. The use of numerical methods, as FEM, BEM etc, for the achievement of a rigorous approach for the textile micro- and mesomechanical analysis appeared in a later stage. Obstacles for the successful use of numerical methods were mainly the large displacement effects and the nonlinearity related with the deformations of textiles and the convergence problems arose. Munro et al. (Munro et al., 1997a) proposed a new approach for the application of FEM to the aligned fibre assembly problem. Three dimensional 8-node elements with cuboid shape in the neutral configuration and 6 degrees of freedom (DOF) per node employed for the investigation. The approach attempted to separate the various energy contributions to the element stiffness, allowing the user to specify their properties individually. This technique was successful in the easy introduction of nonlinear material properties in the solid model. The approach of Munro et al. (Munro et al., 1997b) was verified qualitatively by modelling realistic yarn situations. The yarn models were meshed by dividing them into layers where the layer interfaces were surfaces perpendicular to the yarn axis. Each layer was split into a number of finite elements ranging from 1 to 22. Initial configurations were arranged so that the fibres within the elements followed idealized helical-yarn geometry. A multi-layer yarn model consisting of 9 elements per layer was subjected to axial extension and axial compression. The model presented the expected, in terms of quality, deformation behaviour. Thus the necking of the yarn piece was caused by the helical winding of the fibres appeared during extension. Moreover the elements of the model were opened significantly during the

axial compressing test since the fibres were buckled to avoid compression of the fibre material.

The advance and easy manipulation of CAD tools, in the last few years, allowed the construction of 3D solid models of textile structures. By the use of the attributes of these tools, such as numerical interpolations, mirroring abilities etc. the representation of the structures became feasible. A yarn modelling approach based on the assumprion of helicoid filaments of a constant helix radius and a circular filament cross-section for the loose and a dense structure are presented in the Figure 8 and Figure 9 respectively.

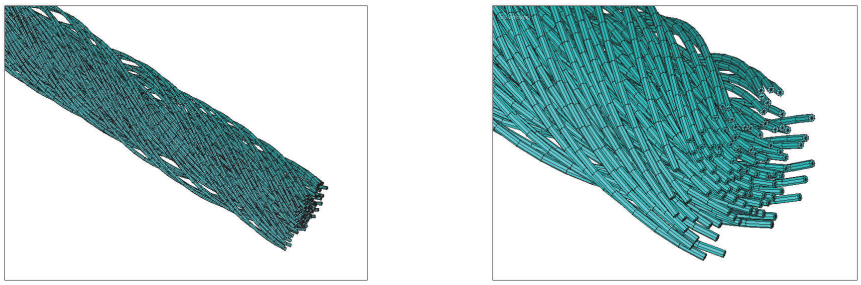

Fig. 8. Beam model of filaments in random locations for loose yarn structure.

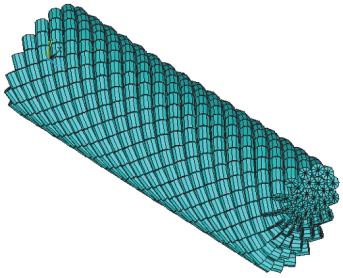

Fig. 9. Beam FE model of 50-filament twisted yarn (Vassiliadis et al., 2010).

Parametric solid modelling software packages are currently available allowing the construction of complex woven structures (Figure 11). The complete design flexibility provides the selection of weave pattern, yarn size or spacing. The yarn representation is still based on the assumption of the homogenous material for the simplification of modelling and the computational time saving (Toney, 2000). The advance moreover of the FEA codes allowed the mechanical simulation of the unit cells of the modelled textile structures. The mesomechanical modelling of textile structures was improved by the employment of advanced finite elements types and libraries of material properties including linear, nonlinear, elastic, plastic, viscoelastic, isotropic, orthotropic, anisotropic options etc. Additionally the introduction of contact algorithms and large strain effects was essential for the realistic results of the simulated tests. Lin et al. (Lin et al. 2008) studied the mechanical behavior of woven fabrics under compression implementing the finite element analysis using solid elements and nonlinear material properties. Furthermore, Durville (Durville, 2010) approached the textile simulation of woven structures' problem at the fibres scale by

means of 3D beam model, providing interesting data useful in the incorporation of fibres in composites structures.
Significant progress noticed in the modelling of complex structures of fabrics. Tarfaoui and Akesbi (Tarfaoui & Akesbi, 2001) presented the model of the twill woven fabric and the mechanical simulation using the FEM. The unit cell is composed by three warp yarns that intersect with three weft yarns, presenting a different type of crimp. Furthermore, B-spline curve methods have been successfully used to model woven yarns (Turan & Baser, 2010 Jiang & Chen, 2010).

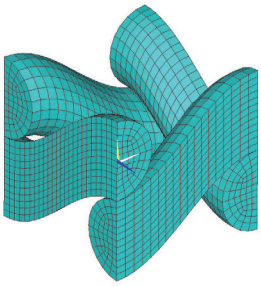

Fig. 10. Solid FE model of unit cell of plain woven structure.

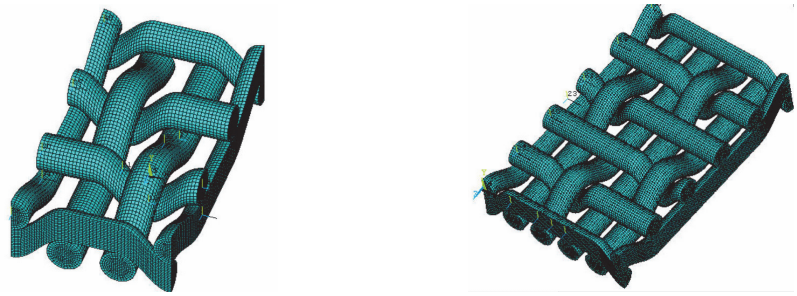

Fig. 11. Solid FE model of unit cell of twill (left) and satin (right) woven structure (Vassiliadis et al., 2008).

Intensive researches were conducted in the field of woven fabrics composites due to their progressive spread in industrial applications. Actually the exceptional characteristics of woven fabrics composites, as high stiffness and strength, light-weight and efficient manufacturability are determinant for their expansion in automotive, marine and aerospace industry. Zhang and Harding presented one of the first numerical studies for the evaluation of the elastic properties of the plain woven composite structures (Zhang & Harding, 1990). Their approach was based on a strain energy method applied to a one-direction undulation model using the FEM. The drawback of this approach, reported also by the authors, was the consideration of the tow undulation in one-direction that is a non-realistic assumption for woven fabrics. Naik expanded the above approach taking into account the strand cross-section geometry, possible gap between two adjacent strands and the two-direction undulation geometry (Naik & Ganesh, 1992). Actually his detailed model demands a large

number of geometrical parameters to describe the undulation and varying thickness of the tow structure. The evolution of numerical methods in the next years produced the first 3D finite element models of the plain woven composites. Whitcomb studied the effect of quadrature order, mesh density and material degradation on the predicted failure resulting from the in-plain loading (Whitcomb & Srirengan, 1996).
The 3D solid modelling of the composite structure consists in the generation of the volumes representing the woven unit cell and an external volume (with the apparent dimensions of the composite unit cell). Then subtracting volumes of the woven structure from the external volume, the volume of the matrix material is resulted (see figure 12).

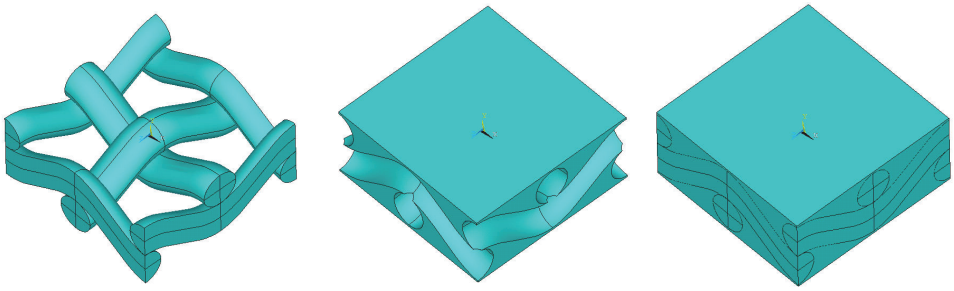

Fig. 12. Geometrical model of composite woven structure (woven reinforcement, matrix, composite)

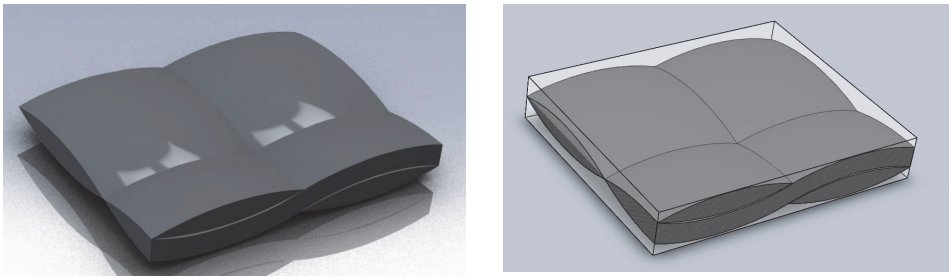

Fig. 13. Geometrical model of a woven structure of tows and a composite structure.

Several approaches were based on the prediction of the homogenized elastic properties of fabric composites using the unit cell of the composite structure. The geometrical representation of the tows was based on certain assumptions such as circular, elliptic, compressed hexagonal and lenticular cross-section areas were considered (Figure 13). The used tows (usually made of glass or carbon fibres) were assumed as transverse isotropic material and the matrix (usually resin) as isotropic material. The homogenized elastic properties of the unit cell results from the mesomechanical analysis using FEM. A relative approach proposed by Ng et al. (Ng et al., 1998) has ben applied for the prediction of the in-plane elastic properties of a single layer 2/2 twill weave fabric composite. The compressed hexagonal shape was considered for the tow cross-section. The modelling and mechanical analysis was programmed using the ANSYS Parametric Design Language (APDL). The 8-node solid elements with 3 degrees of freedom (translational) per node were used.

Indicatively a model of approximately 52000 finite elements and 12000 nodes was generated. The contact areas generated during the subtracting operation (for the generation of matrix material) were assigned to be shared entities for both the yarn and the matrix volumes, to ensure the transmission of loading. Choi and Tamma (Choi & Tamma, 2001) dealt with the prediction of the in-plane elastic properties of a composite structure reinforced with plain woven fabric. The predicted elastic properties were used in continue for the damage analysis of the laminated composite structures. The superposition principle was applied for the evaluation of homogenised properties of the woven fabric composite. The generated model of composite unit cells consists of 520 wedge elements for the yarns and 256 brick elements for the matrix. The progressive damage was evaluated simulating the in-plane tensile and shear deformation introducing a respective incrementing load. The degradation of elastic moduli and Poisson ratios was considered for the mechanical damage analysis.

A main framework for the multi-scale modelling of woven composite structures for the damage prediction was proposed by Kwon (Kwon, 1993, 2001; Kwon & Hamilton, 1995; Kwon & Roach, 2004) and implemented in several following investigations. It is worth to mention that the damage of a laminated textile composite is presented as a matrix damage, fibre brakeage, fibre – matrix debonding or laminated debonding (delamination). The proposed multi-scale approach is based on the integration of three individual modules: the fibre-strand module, the strand-fabric module and the lamination module. The fibre-strand module aims at the evaluation of the effective elastic properties of a unidirectional composite strand exploiting the material properties and structure of the constituent fibres and matrix. Moreover the current stage relates the stresses and strains of the strand with the stresses and strains of the fibre and matrix materials thus the damage criteria can be applied. The strand-fabric module focuses on the evaluation of the effective properties of the woven fabric composite (unit cell) exploiting the material properties of the unidirectional composite strand. In addition the current stage relates the stresses and strains of the composite structure with the stresses and strains of the strand. Finally the lamination module evaluates the effective properties of the laminated composite structure (multiple layer) using the material properties of the composite lamina. A classical lamination theory or a higher order theory is implemented in this stage. Thus the stresses and strains developed on the laminated composite structure are correlated with the stresses and strains of the lamina.

An innovative research in the field of fabric composites is conducted in the K.U. Leuven, initially focusing on the generalized description of the internal structure of the textile reinforcement. Lomov and his colleagues developed a model for the internal geometry of 2D- and 3D-weaves based on a minimum number of topological data and yarn mechanical properties. The mechanical model applies a yarn deformation energy minimization algorithm to predict the internal geometry of any 2D- and 3D-weave. This approach was systematically extended to 2D- and 3D-woven, two- and three-axial braided, weft knitted and non-crimp warp-knit stitched fabrics and laminates and incorporated in the Wise-Tex software package (Verpoest & Lomov, 2005; Lomov et al., 2000; Lomov et al., 2001). Regarding the damage analysis of the composite structures a three-level hierarchy was proposed: the micro-, meso- and macro-level. The micro-level defines the arrangement of fibres in the representative volume of the impregnated yarn. The meso-level describes the internal structure of the reinforcement and variations of the fibre direction and volume fraction within the yarn. Finally the macro-level defines the 3D geometry of the composite part and the distribution of the reinforcement properties.

5.2 Macromechanical modelling of complex deformations

The macromechanical modelling of fabrics or cloth modelling, as usually referred, attracted the interest of the textile community in the last decades. Many investigators attempted to approach computationally the macromechanical performance of fabrics for several purposes from the prediction of the drape behaviour of the fabric up to the virtual mode show (Gray, 1998). Depending on the purpose served and the application field different techniques were developed. The basic classification of the developed techniques is divided into computer animation models (graphic models) and the engineering design models. Many numerical techniques including the particle-based model, the deformable node-bar model and the FEM were developed for the engineering design of fabrics. Most of the efforts were focused on the prediction of the drapeability of fabrics.

The used FEM for the drape simulation were based on a variety of element types from simple rods to complex shell elements. Collier (Collier et al., 1991) studied the drape behaviour of fabrics using a nonlinear FEM based on the classical nonlinear plate theory. The fabric was assumed to be two dimensional. It was considered as a linear elastic material with orthotropic anisotropy, where the symmetry lines are aligned in the warp and weft directions. Many corrective actions were assigned the following years by the researchers in the classical finite element techniques in order the realistic performance of fabrics to be approached.

The FEM and flexible thin shell theory was employed by Chen and Govindaraj (Chen & Govindaraj, 1995) to simulate the fabric drape. Their approach provides nonlinear solution since large displacements appear during drape test. Thus the loads are applied incrementally to the system, and at each step, the equilibrium equation system is solved by a Newton-Raphson method. The nonlinearity was handled by calculating the stiffness matrix in each step as a function of the displacement vector. The fabric was considered continuous orthotropic material. A 9-node, doubly curved shell element with 5 DOF per node was used for the simulation.

The simulation of the 3D drape test based on the FEM was also approached by Kang and Yu (Kang & Yu, 1995). The woven fabric was assumed to be an elastic material with orthotropic anisotropy. The fabric was considered as a thin flexible plate under the plane stress condition, and the transverse shear strain was included in the formulation. Since large displacements and large rotations are developed during draping, the drape phenomenon was considered as geometrically nonlinear and respectively the nonlinear analysis was adopted for the simulation. The Green-Lagrangian strains and the second Piolar-Kirchhoff stresses were used for the analysis. The formulation of the FEM was based on a total Lagrangian approach. 4-node quadrilateral elements were used with 5 DOF in each node. In order to avoid the shear locking phenomenon which is commonly observed in the thin plane analysis, a transverse shear strain interpolation method was applied. Almost the same approach was proposed by Gan et al. (Gan et al., 1995). In their analysis 8-node shell elements were used with 5 DOF per node. The adopted technique in this approach for the elimination of locking was a reduced integration with zero energy mode control.

For the minimization of the computational power required for the simulation of fabric drape, a FEM using simple beam elements with 6 DOF per node was proposed by Ascough et al. (Ascough et al., 1996). The used beam elements include mass and stiffness properties and can represent iso- or orthotropic cloth properties. The large displacement effects were achieved with the addition of a geometric or initial stress matrix to the elastic stiffness

matrix to form the element characteristic matrix. Newmark's method was used to allow a time-stepping approach to the solution, with the advantage that the mesh geometry can be updated at each step. The proposed analysis includes also interaction of the cloth with the body form. Checks for a collision detection of material elements with the body model are made following each time step of the drape simulation. An iterative calculation process is executed until contact rather than penetration of cloth element with the body model occurs.
An approach for the drape simulation of woven fabrics quite different from the traditional macromechanical methods was proposed by Breen et al. (Breen et al., 1994). The cloth was modelled as a collection of particles that conceptually represent the crossing points of warp and wefts threads in a plain weave. Important mechanical interactions that determine the behaviour of woven fabric are discretized and lumped at these crossing points. The various yarn-level structural constraints are represented with energy functions that capture simple geometric relationships between the particles. These energy functions account for the four basic mechanical interactions of yarn collision, yarn stretching, out of plane bending, and trellising. The simulation was implemented as a three-phase process operating over a series of discrete time steps. The first phase for a single time step calculates the dynamics of each particle and accounts the collisions between particles and surrounding geometry. The second phase performs an energy minimization to enforce inter-particle constraints. The third phase corrects the velocity of each particle to account for particle motion during the second phase.

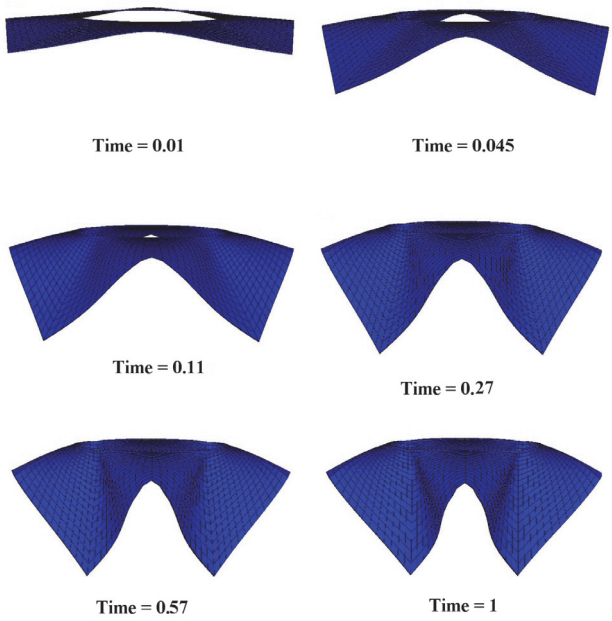

Fig. 14. Deformed FE model of square fabric in drape test (Provatidis et al., 2009).

Stylios et al. (Stylios et al., 1995; Stylios et al., 1996) proposed a node-bar model for the drape modelling of fabrics. The deformable elements were defined as consisting of one deformable

node with a number of rigid bars. Thus the patch of cloth is divided into a grid (the patch is divided as a series of elements, which can be of equal or unequal sizes). The material properties of the continuum in all elements are lumped together at these deformable nodes by integrating all the energies within those elements. The total energy density was considered as the sum of strain, kinetic energy density, and the energy density introduced by external and boundary forces. Viscoelastic terms were added in the energy equation. The cloth motion in continue was determined using the Euler-Lagrange equations.
The finite volume method employed by Hu et al. (Hu et al., 2000) for the drape modelling of fabrics. The mesh lines were aligned along the warp and weft direction producing rectangular internal volumes and triangular or quadrilateral boundary volumes in a circular fabric sheet. The equilibrium equations of the fabric sheet derived using the principle of stationary total potential energy. Geometric nonlinearity and linear elastic orthotropic material properties of the fabric were considered in the formulation. The full Newton-Raphson iteration method with line searches was adopted for the solution of the resulting nonlinear algebraic equation.

5.3 Evaluation of the numerical methods

The adoption of computational techniques in textile mechanics is essential to face and overcome the objective difficulties, as the geometrical representation, the complex deformations, the particular material properties, the contact phenomena and the large deflection effects. Moreover, the advanced computer based tools are suitable for the virtual representation of a product performance under loading. That is a significant facility for the textile designers since a realistic sense from the mechanical up to the aesthetic attributes can be provided.
Most of the mesomechanical modeling approaches implemented the finite element method using solid FE. The yarns were assumed as homogenous material with transverse isotropic elastic properties. The attribution of the yarn properties constitutes basic factor for the accuracy of the mesomechanical modelling stage. Thus the equivalent performance of the homogenous yarn, considering the discrete structure, in the tensile and bending deformation is required at least for the reliable attribution of yarn models. It is remarkable that most of the proposed models omitted the calculation of the real value of the yarn bending rigidity and its attribution at the modelled yarn.
The macromechanical modelling approaches are grouped in two basic categories. The first corresponds to the investigations based on the experimental measurement of the mechanical properties of fabrics and the generation of equivalent models describing their bending performance and drapeability (Collier et al., 1991; Ascough et al., 1996; Stylios et al., 1995; Hu et al., 2000; Araujo et al., 2004). The second category focused on the computational analysis of fabrics in the mesoscopic level and the generation of models presenting equivalent in-plane elastic properties (Ng et al., 1998; Choi & Tamma, 2001; Lomov et al., 2007).
The basic drawback encountered in the existing modelling approaches concerns the collaboration of the different modelling stages (micro, meso, macro) for the development of an integrated design procedure of the textile structures. Thus the modelling of the structure in the mesoscopic level should incorporate the micromechanical performance of the yarns. Whereas the modelling of the structure in the macroscopic level should incorporate the mesoscopic performance of the unit cells and therefore the microscopic performance of the

yarns. Consequently the collaboration of the discrete modelling stages is attainable generating realistic models and attributing the equivalent properties.

6. Conclusions

An extended review was conducted over the textile mechanical modelling area. It is obvious that despite the about 70 years of actual research it's not possible to conclude in an Integrated Computer Aided Engineering Environment. The absence of a global tool was remarked, that aggravates the textile design procedure in terms of time and cost.
The structural hierarchy of the textile structures (fibre – yarn – fabric) is correlated with the high level of complexity presented in the modelling procedure and the mechanical analysis of them. The difficulties are increased due to the high divergence of the dimensions corresponding to the fabric sheet (10^{-1} to 10^{0} m) and the structural elements (fibre diameter, 10^{-5} m). The modelling complexity resulted from the structural hierarchy of textiles is faced adopting a relative modelling hierarchy. Thus three basic modelling scales were developed: the micromechanical modelling of yarns, the mesomechanical modelling of the fabric unit cell and the macromechanical modelling of the fabric sheet. The modular modelling of the textile woven fabrics is a systematic method to overcome the complexity of the mechanical structure and the nature of the materials involved. The global evolution of the modelling approaches seem to converge in this stepwise method and thus indicate a likely way towards the desired Textile Computer Aided Engineering environment.

7. References

Abbott, G.M., Grossberg, P. and Leaf, G.A.V., (1971) The mechanical properties of woven fabrics, part VII: hysteresis and bending of woven fabrics. Textile Research Journal, Vol.41, No.4, pp. 345-348.

Abbott, G.M., Grosberg, P. and Leaf, G.A.V., (1973) The elastic resistance to bending of plain-woven fabrics. Journal of the Textile Institute, Vol.64, No.3), pp. 346-362.

Amirbayat, J. and Hearle, J.W.S., (1989) The anatomy of buckling of textile fabrics: Drape and conformability of dimensionless groups. Journal of the Textile Institute, Vol.80, pp. 51-70.

Araujo, M., Fangueiro, R. and Hong, H., (2004) Modelling and simulation of the mechanical behaviour of weft-knitted fabrics for technical applications. Part IV: 3D FEA model with a mesh of tetrahedric elements. Autex Research Journal, Vol.4, No.2, pp. 72-80.

Ascough, J., Bez, H.E. and Bricis, A.M., (1996) A simple beam element, large displacement model for the finite element simulation of cloth drape. Journal of the Textile Institute, Vol.87, No.1, pp. 152-165.

Backer, S., (1952) The mechanics of bent yarns. Textile Research Journal, 22(5), pp. 668-681.

Behre, B., (1961) Mechanical properties of textile fabrics, part I: Shearing. Textile Research Journal, Vol.31, No.2), pp. 87-99.

Bogdanovich, A.E., (2006) Multi-scale modeling, stress and failure analyses of 3-D woven composites. Journal of Materials Science, Vol.41, No.20), pp. 6547-6590.

Breen, D.E., House, D.H. and Wozny, M.J., (1994) Predicting the drape of woven cloth using interacting particles. Computer Graphics, Vo.4, pp. 365-372.

Chen, B. and Govindaraj, M., (1995) Physically based model of fabric drape using flexible shell theory. Textile Research Journal, Vol.65, No.6, pp. 324-330.

Cho, G., Lee, S. and Cho, J., (2009) Review and reappraisal of smart clothing. International Journal of Human-Computer Interaction, Vol.25, No.6, pp. 582-617.

Choi, J. and Tamma, K.K., (2001) Woven fabric composites, Part I: Predictions of homogenized elastic properties and micromechanical damage analysis. Int. J. Numer. Meth. Eng,Vol.50, pp. 2285-2298.

Choi, K.F. and Tandon, S.K., (2006) An energy model of yarn bending. Journal of the Textile Institute, Vol.97, No1, pp. 49-56.

Collier, J.R., Collier, B.J., O'Toole, G. and Sargand, S.M., (1991) Drape prediction by means of finite-element analysis. Journal of the Textile Institute, Vol.82, No1, pp. 96-107.

Dahlberg, B., (1961) Mechanical properties of textile fabrics Part II: Buckling. Textile Research Journal, Vol.31, No.2, pp. 94-99.

Dastoor, P.H., Ghosh, T.K., Batra, S.K. and Hersh, S.P., (1994) Computer-assisted structural design of industrial woven fabrics part III: modelling of fabric uniaxial/biaxial load-deformation. Journal of the Textile Institute, Vol.85, No.2, pp. 135-137.

Dunne, E. L., Brady, S., Smyth, B. and Diamond, D., (2005) Initial development and testing of a novel foam-based pressure sensor for wearable sensing. Journal of NeuroEngineering and Rehabilitation, Vol.2, No.4, pp.1-7.

Freeston, W.D., Platt, M.M. and Schoppee, M.M., (1967) Mechanics of elastic performance of textile materials. XVIII. Stress-strain response of fabrics under two-demensional loading. Textile Research Journal, Vol.37, No.11, pp. 948-975.

Freeston, W.D. and Schoppee, M.M., (1975) Geometry of Bent Continuous-Filament Yarns. Textile Research Journal, Vol.45, No.12, pp. 835-852.

Gan, L., Ly, N.G. and Steven, G.P., (1995) A study of fabric deformation using nonlinear finite elements. Textile Research Journal, Vol.65, No.11, pp. 660-668.

Gray, S., (1998) In virtual fashion. IEEE Spectrum, Vol.35, No.2, pp. 18-25.

Grosberg, P., (1966) The mechanical properties of woven fabrics, Part II: The bending of woven fabrics. Textile Research Journal, Vol.36, No.3, pp. 205-211.

Grosberg, P. and Kedia, S., (1966) The Mechanical Properties of Woven Fabrics, Part I: The Initial Load Extension Modulus of Woven Fabrics. Textile Research Journal, Vol.36, No.1, pp. 71-79.

Haas, R. and Dietzius, A. (1918) The stretching of the fabric and the shape of the envelope in non-rigit ballons. Annual Report, Report No. 16, National Advisory Committee for Aeronautics, pp.149-271 (originally published in German as: Haas, Rudolf und Alexander Dietzius, Stoffdehnung und Formaenderung der Huelle bei Prall-Luftschiffen. Untersuchungen im Luftschiffbau der Siemens-Schukkert-Werke, 1913, Luftfahrt und Wissenschaft, Hft. 4.)

Hearle, J.W.S., (2006) Engineering design of textiles. Indian Journal of Fibre and Textile Research, Vol.31, No.1, pp. 134-141.

Hearle, J.W.S., El-Behery, H.M.A.E. and Thakur, V.M., (1959) The mechanics of twisted yarns: Tensile properties of continuous-filament yarns. Journal of the Textile Institute, Vol.50, pp. T83-T111.

Horrocks A. R. and Anand, S. C. (Eds.)(2000) Handbook of Technical Textiles, Woodhead Publishing, 978-1-85573-385-5.

http://smarteconomy.typepad.com/smart_economy/2006/09/lumalive_a_smar.html

http://www.crunchwear.com/cute-circuit-galaxy-led-dress/

http://www.ilcdover.com/Space-Suits/

http://www2.dupont.com/Kevlar/en_US/index.html
http://www.soltis-textiles.com/
http://waldemeyer.com/projects/fashion/interactive-led-dance-shoe-disney/
Hu, J. L., (2004) Structure and mechanics of woven fabrics, Woodhead Publishing Limited, 1 85573 904 6.
Hu, J., Chen, S.-. and Teng, J.G., (2000) Numerical drape behavior of circular fabric sheets over circular pedestals. Textile Research Journal, Vol.70, No.7, pp. 593-603.
Hu, J.L. and Teng, J.G., (1996) Computational fabric mechanics: Present status and future trends. Finite Elements in Analysis and Design, Vol.21, No.4, pp. 225-237.
Huang, N.C., (1979a) Finite Biaxial Extension of Completely Set Plain Woven Fabrics. Journal of Applied Mechanics, Transactions ASME, Vol.46, No.3, pp. 651-655.
Huang, N.C., (1979b) Finite biaxial extension of partially set plain woven fabrics. International Journal of Solids and Structures, Vol.15, No.8, pp. 615-623.
Jayaraman, S., Kiekens, P. and Grancaric, A. M. (Eds). (2006). Intelligent Textiles for Personal Protection and Safety, IOS Press Inc., 1586035991.
Kallivretaki, A., (2010) Three-dimensional micromechanical models of textile fabrics, PhD Thesis, National Technical University of Athens.
Kang, T.J. and Yu, W.R., (1995) Drape simulation of woven fabric by using the finite-element method. Journal of the Textile Institute, Vol.86, No.4, pp. 635-648.
Kawabata, S., Niwa, M. and Kawai, H., (1973) Finite-Deformation Theory of Plain-Weave Fabrics - 1. The Biaxial-Deformation Theory. Journal of the Textile Institute, Vol.64, No.1, pp. 21-46.
Keefe, M., Edwards, D.C. and Yang, J., (1992) Solid modeling of yarn and fiber assemblies. Journal of the Textile Institute, Vol.83, No.2, pp. 185-196.
Kemp, A., (1958) An extension of Peirce's cloth geometry to the treatment of non-circular threads. Journal of the Textile Institute, Vol.49, No.1, pp. T44-T48.
Komori, T., (2001) A generalized micromechanics of continuous-filament yarns part I: Underlying formalism. Textile Research Journal, Vol.71, No.10, pp. 898-904.
Konopasek, M., (1980a) Classical elastica theory and its generalizations. In: J.W.S. Hearle, J.J. Thwaites and J. Amirbaya, eds, Mechanics of flexible fibre assemblies, Nato Advanced Study Institutes Series, Series E: Applied Science - No. 38. USA: Sijthoff & Noordhoff, pp. 255-274.
Konopasek, M., (1980b) Computational aspects of large deflection analysis of slender bodies. In: J.W.S. Hearle, J.J. Thwaites and J. Amirbaya, eds, Mechanics of flexible fibre assemblies, Nato Advanced Study Institutes Series, Series E: Applied Science - No. 38. USA: Sijthoff & Noordhoff, pp. 275-292.
Konopasek, M., (1980c) Textile application of slender body mechanics. In: J.W.S. Hearle, J.J. Thwaites and J. Amirbaya, eds, Mechanics of flexible fibre assemblies, Nato Advanced Study Institutes Series, Series E: Applied Science - No. 38. USA: Sijthoff & Noordhoff, pp. 293-310.
Kwon, Y.W., (1993) Calculation of effective moduli of fibrous composites with micro-mechanical damage. Composite Structures, Vol.25, No.1-4, pp. 187-192.
Kwon, Y.W., (2001) Multi-level approach for failure in woven fabric composites. Advanced Engineering Materials, Vol.3, No.9, pp. 713-717.
Kwon, Y.W. and Hamilton, B.H., (1995) Micro/macro-analysis of damage evolution in plate bending of composites. Proceedings of the 1995 ASME International Mechanical

Engineering Congress and Exposition; San Francisco, CA, USA; November 1995, Vol.321,pp. 1-9.

Kwon, Y.W. and Roach, K., (2004) Unit-cell model of 2/2-twill woven fabric composites for multi-scale analysis. CMES - Computer Modeling in Engineering and Sciences, Vol.5, No.1, pp. 63-72.

Lindberg, J., Behre, B. and Dahlberg, B., (1961) Mechanical properties of textile fabrics, Part III: Shearing and buckling of various commercial fabrics. Textile Research Journal, Vol.31, No.2, pp. 99-122.

Lloyd, D.W., Mete, F. and Hussain, K., (1996) An approach to the theoretical mechanics of static drape. International Journal of Clothing Science and Technology, Vol.8, No.3, pp. 43-58.

Lo, W.M., Hu, J.L. and Li, L.K., (2002) Modeling a fabric drape profile. Textile Research Journal, Vol.72, No.5, pp. 454-463.

Lomov, S.V., Gusakov, A.V., Huysmans, G., Prodromou, A. and Verpoest, I., (2000) Textile geometry preprocessor for meso-mechanical models of woven composites. Composites Science and Technology, Vol.60, No.11, pp. 2083-2095.

Lomov, S.V., Huysmans, G., Luo, Y., Parnas, R.S., Prodromou, A., Verpoest, I. and Phelan, F.R., (2001) Textile composites: Modelling strategies. Composites - Part A: Applied Science and Manufacturing, Vol.32, No.10, pp. 1379-1394.

Lomov, S.V., Ivanov, D.S., Verpoest, I., Zako, M., Kurashiki, T., Nakai, H. and Hirosawa, S., (2007) Meso-FE modelling of textile composites: Road map, data flow and algorithms. Composites Science and Technology, Vol.67, No.9, pp. 1870-1891.

Munro, W.A., Carnaby, G.A., Carr, A.J. and Moss, P.J., (1997a) Some Textile Applications of Finite-element Analysis. Part I: Finite Elements for Aligned Fibre Assemblies. Journal of the Textile Institute, Vol.88, No.4, pp. 325-338.

Munro, W.A., Carnaby, G.A., Carr, A.J. and Moss, P.J., (1997b) Some Textile Applications of Finite-element Analysis. Part II: Finite Elements for Yarn Mechanics. Journal of the Textile Institute, Vol.88, No.4, pp. 339-351.

Naik, N.K. and Ganesh, V.K., (1992) Prediction of on-axes elastic properties of plain weave fabric composites. Composites Science and Technology, Vol.45, No.2, pp. 135-152.

Ng, S.-., Tse, P.-. and Lau, K.-., (1998) Numerical and experimental determination of in-plane elastic properties of 2/2 twill weave fabric composites. Composites Part B: Engineering, Vol.29 No.6, pp. 735-744.

Olofsson, B., (1964a) A general model of a fabric as a geometric-mechanical structure. Journal of the Textile Institute, Vol.55, No.11, pp. T541-T557.

Olofsson, B., (1964b) The Setting of Wool Fabrics - A Theoretical Study. Journal of the Textile Institute, Vol.20, pp. 272-273.

Önder, E. and Bacer, G., (1996) A comprehensive stress and breakage analysis of staple fiber yarns Part I: Stress analysis of a staple yarn based on a yarn geometry of conical helix fiber paths. Textile Research Journal, Vol.66, No.9, pp. 562-575.

Park, J.-. and Oh, A.-., (2006) Bending rigidity of yarns. Textile Research Journal, Vol.76, No.6, pp. 478-485.

Parsons, E. M., Weerasooriya, T., Sarva, S. and Socrate, S., (2010) Impact of woven fabric: Experiments and mesostructure-based continuum-level simulations. Journal of the Mechanics and Physics of Solids, Vol.58, pp. 1995-2021.

Peirce, F.T., (1937) The geometry of cloth structure. Journal of the Textile Institute, Vol.28, No. T45, pp.43-77.

Platt, M.M., Klein, W.G. and Hamburger, W.J., (1959) Mechanics of elastic performance of textiles materials, part XIV: Some aspects of bending rigidity of single yarns. Textile Research Journal, Vol.29, pp. 611.

Postle, J.R. and Postle, R., (1996) Modelling fabric deformation as a nonlinear dynamical system using Bäcklund Transformations. International Journal of Clothing Science and Technology, Vol.8, No.3, pp. 22-42.

Provatidis, C. and Vassiliadis, S., (2002) On the numerical estimation of the mechanical behaviour of fabrics, 2nd AUTEX World Textile Conference, 2002, , pp. 88-97.

Provatidis, C.G. and Vassiliadis, S.G., (2004) On the performance of the geometrical models of fabrics for use in computational mechanical analysis. International Journal of Clothing Science and Technology, Vol.16, No.5, pp.434-444.

Provatidis, C.G., Vassiliadis, S.G. and Anastasiadou, E.A., (2005) Contact mechanics in two-dimensional finite element modelling of fabrics. International Journal of Clothing Science and Technology, Vol.17, No.1, pp.29-40.

Provatidis, C., Kallivretaki, A. and Vassiliadis, S., (2009) Fabric Drape Simulation using FEM, Proceedings of the South-East European Conference on Computational Mechanics, SEECCM, Rhodes, Greece, June 2009.

Shanahan, W.J., Lloyd, D.W. and Hearle, J.W.S., (1978) Characterizing the elastic behaviour of textile fabrics in complex deformation. Textile Research Journal, Vol.48, pp. 495-505.

Stump, D.M. and Fraser, W.B., (1996) A simpified model of fabric drape based on ring theory. Textile Research Journal, Vol.66, No.8, pp. 506-514.

Stylios, G., Wan, T.R. and Powell, N.J., (1995) Modeling the dynamic drape of fabrics on synthetic humans, a physical, lumped-parameter model. Int. J. Clothing Sci. Technol., Vol.7, No.5, pp. 10-25.

Stylios, G.K., Wan, T.R. and Powell, N.J., (1996) Modelling the dynamic drape of garments on synthetic humans in a virtual fashion show. International Journal of Clothing Science and Technology, Vol.8, No.3, pp. 95-112.

Takano, N., Uetsuji, Y., Kashiwagi, Y. and Zako, M., (1999) Hierarchical modelling of textile composite materials and structures by the homogenization method. Modelling and Simulation in Materials Science and Engineering, Vol.7, No.2, pp. 207-231.

Tang, S. L. P., (2007) Recent developments in flexible electronics for monitoring applications. Transactions of the Institute of Measurement and Control, Vol.29, pp. 283-300.

Tarfaoui, M. and Akesbi, S., (2001) Numerical study of the mechanical behaviour of textile structures. International Journal of Clothing Science and Technology, Vol.13, No.3-4, pp. 166-175.

Toney, M.M., (2000) Computer modeling of fibrous structures. Journal of the Textile Institute, Vol.91, No.3, pp. 133-139.

Tognetti, L. A., Carbonaro, N., Zupone, G. and De Rossi, D., (2006) Characterization of novel data glove based on textile integrated sensors. Proceedings of the 28th IEEE, EMBS Annual International Conference, pp.2510-2513.

Vassiliadis, S., Kallivretaki, A., Grancaric, A.M., Giannakis, S. and Provatidis, C., (2008) Computational modelling of twill and satin woven structure, Proc. of the World Conference AUTEX 2008, June 2008, Biella, Italy.

Vassiliadis, S., Kallivretaki, A. and Provatidis, C., (2010) Mechanical modelling of multifilament twisted yarns. Fibers and Polymers, Vol.11, No.1, pp. 89-96.

Verpoest, I. and Lomov, S.V., (2005) Virtual textile composites software WiseTex: Integration with micro-mechanical, permeability and structural analysis. Composites Science and Technology, Vol.65(15-16 SPEC. ISS.), pp. 2563-2574.

Whitcomb, J. and Srirengan, K., (1996) Effect of various approximations on predicted progressive failure in plain weave composites. Composite Structures, Vol.34, No.1, pp. 13-20.

Xu, P.J., Zhang, H. and Tao, X.M., (2008) Textile-structured electrodes for electrocardiogram. Textile Progress, Vol.40, No.4, pp. 183-213.

Zhang, Y.C. and Harding, J., (1990) A numerical micromechanics analysis of the mechanical properties of a plain weave composite. Computers & Structures, Vol.36, No.5, pp. 839-844.

4

Finite Element Modeling of Woven Fabric Composites at Meso-Level Under Combined Loading Modes

Mojtaba Komeili and Abbas S. Milani
School of Engineering, University of British Columbia, Canada

1. Introduction

Woven fabrics are among the most important materials used in today's modern industries. Next to their high mechanical properties, they are easy to handle in the dry or pre-impregnated pre-forms, offer good drape-ability and are particularly suited for manufacturing of doubly curved components, membranes, inflatable structures, etc (Cavallaro et al., 2003; 2007). In the dry form, fabrics can be formed into a variety of three-dimensional (3D) shapes and then consolidated with resin via resin transfer molding (RTM) or other manufacturing processes (Boisse et al., 2007). Reliable models capable of predicting the mechanical behaviour of woven fabric materials are not fully developed yet. The biggest challenge in this regard is perhaps the multi-scale nature of the fabric materials. Dry fabrics at macro level are composed of numerous yarns interlaced into each other. The yarns usually have characteristic length in the scale of millimetres and their interaction and behaviour at the fabric level can greatly influence the macro-level material behaviour (Guagliano and Riva, 2001). Yarns themselves are heterogeneous media made of bundles of very thin and long fibers. Figure 1 shows different hierarchical levels in a woven fabric along with their typical dimensions.

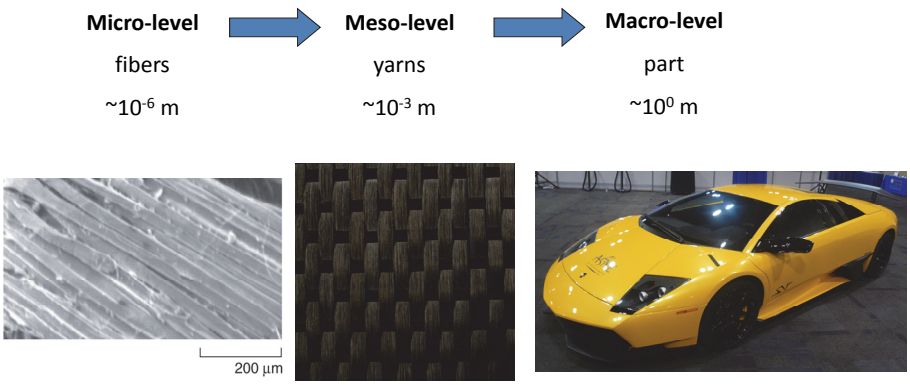

Fig. 1. 3 Hierarchical levels in woven fabrics

Among different material scales, meso-level modeling of woven fabrics is known to be a strong tool for predicting their effective mechanical properties at macro-level (Peng and Cao, 2002). It can also be useful for studying their local deformation mechanisms that occur during different manufacturing processes and loading conditions. Of different modeling techniques, the 3D finite element modeling is found to be of great interest to the researchers in the field. However, the multi-scale nature of fabrics makes the applicable numerical procedures different from those of the conventional finite element method. The fact that fabric yarns are heterogeneous media formed by bundles of fibres, and that the loose bounding between fibers in each yarn allows them to slide on each other, makes a considerable distinction in postulating the yarns' constitutive models as well as the numerical procedures applied to analyze their deformation.

(Kawabata et al., 1973; 1973a; 1973b) presented general theories for modeling woven fabric unit cells using bar and stiffness elements. Their sample model was based on the geometrical simplifications on a unit cell along with some parameters that were determined from experiments. Boisse et al., (1997) used the above model and developed a finite element simulation of a dry fabric forming process. Bi-axial tension tests were used to identify the unknown parameters in the constitutive model of the fabric unit cell. In order to develop more accurate models with more insight towards the local deformation phenomena in fibre yarns, Gasser et al. (2000) developed a 3D finite element model of a unit cell under bi-axial tension. Their results were compared to a set of bi-axial tests and satisfactory agreements were obtained. One of the most important features in their approach was to link the meso-level material model to the micro-level behaviour of yarns. For example, quasi-zero shear modulus and Poisson's ratio, crushing transverse behaviour of yarns, and the update of direction of material orientation during deformation were taken into account. Later on, the model was extended to simulate the in-plane shear behaviour of dry fabrics (Badel et al., 2007) and an algorithm for implementing a hypoelastic constitutive model was presented by Badel et al. (2008; 2009). For implementation of these models in numerical packages, the explicit solver of Abaqus has been frequently used. Recently, Komeili and Milani (2010) used a modified version of the aforementioned algorithm to implement an implicit integrator in Abaqus, which led to an increased accuracy and significantly decreased the simulation run time.

Based on the brief review above, it appears that the meso-level finite element modeling of fabrics has been mostly based on individual axial tension and shear modes. Other researchers have also looked at the homogenization of yarn properties at micro/meso levels, but again under individual deformation modes (Chen et al., 2001; Peng and Cao, 2002). Similarly, at macro-level, Xue et al. (2003), followed by Peng and Cao (2005), developed a constitutive material model for the dry fabric sheets. The model was based on a non-orthogonal local coordinate system whose in-plane axis is coincident with the weft and warp yarns of the fabric. To identify the unknown material parameters, the model was fitted to the experimental data from individual bi-axial and bias-extension tests. Nonetheless, during actual forming processes, a complex combination of the axial and shear deformation modes may be experienced by woven fabrics (Boisse, 2010). Cavallaro et al. (2007) developed a new test fixture with the capability of applying simultaneous axial tension and shear deformation modes to the fabric specimens, which could be advantageously used for a more reliable identification of constitutive modes that are used for simulation of composite forming processes.

The aim of the present work is to first present a general meso-level fabric unit cell model using an implicit integrator in Abaqus. To this end, modifications to the original model developed by Badel et al. (2008) are required. Then, the effect of combined loading on the response of a typical fabric unit cell is studied under different axial-shear combined loading modes. The axial loading is induced through controlled displacement/stretch along the yarns and the shear is applied through controlled rotation on the boundaries of the unit cell (i.e., simulating the picture frame test).

2. Modeling

A typical glass plain-weave fabric was selected (Figure 2). Because of its simple textile architecture and balanced properties, this type of fabric has found a wide range of applications in the composite industries.

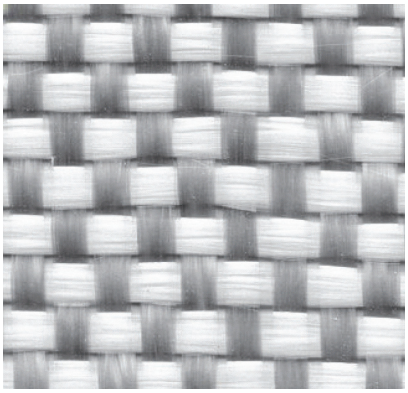

Fig. 2. A typical balanced plain weave fabric (Boisse, 2010).

2.1 Geometry

As mentioned earlier, the meso-level structure of a woven fabric consists of numerous yarns interlaced into each other to construct the whole fabric structure. In order to model such a complex material system (especially if the goal is to find the equivalent/effective material properties at a fabric level) it may be neither necessary nor computationally feasible to consider all individual yarns and their interactions. Instead, a representative volume element (also known as unit cell) may be considered as a sub-model of the whole fabric structure. Based on a given fabric type and the loading mode, different unit cell models have been employed in the literature (Boisse et al., 2006; Peng et al., 2004). Figure 3a shows the unit cell employed in the present study. The geometrical construction of the yarns in the model is based on the sinusoidal curves shown in Figure 3b and defined via Eqs. (1)-(5).

$$y_1(x) = \frac{h}{2}\left[cos\frac{\pi x}{s} + 1 \right] \quad (0 < x < s) \tag{1}$$

$$y_2(x) = \frac{h}{2}\left[cos\frac{\pi x}{s} - 1 \right] \quad (0 < x < s) \tag{2}$$

$$y_3(x) = -h\cos\frac{\pi x}{\beta} \quad \left(0 < x < \frac{w}{2}\right) \tag{3}$$

$$y_4(x) = -h\cos\left[\frac{\pi\left(x-(s-\beta)\right)}{\beta}\right] \quad \left(s-\frac{w}{2} < x < s\right) \tag{4}$$

$$\beta = \frac{\pi w}{2\arcsin\left[\sin^2\left(\frac{\pi w}{4s}\right)\right]} \tag{5}$$

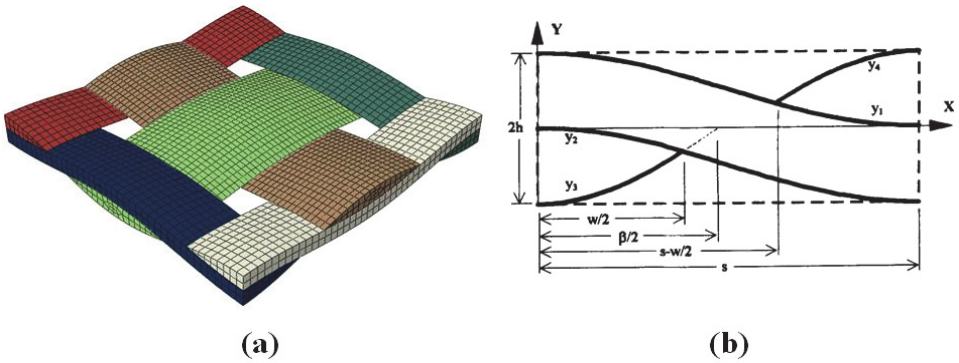

(a) (b)

Fig. 3. (a) Schematic of the unit cell; (b) the yarn generating lines (Mcbride and Chen, 1997); For the current model, $\mathbf{w} = 2.11\,\mathbf{mm}$, $\mathbf{h} = 0.5$ and $\mathbf{S} = 5.13$ are used. This means that the total length of the unit cell is $2\mathbf{S} = 0.26\,\mathbf{mm}$.

2.2 Material

The multi-scale nature of woven fabrics at meso-level means that the material behaviour of yarns is dependent on the attributes of micro-level fibrous structure. This, in turn, justifies using particular constitutive models of yarns with a close attention to the characteristics of fibers and their interactions at a lower material level. First, fiber yarns cannot have considerable tolerance for shear, compression or bending. This is due to the fact that yarns are made of bundles of thousands of very thin fibers which can slide on each other in the dry form. In addition, the high length to diameter ratio of yarns makes it almost impossible to carry compression without buckling. On the other hand, fibers can go under high tension in the axial direction of yarns. Indeed, the latter property is one of the main reasons for a fabric demonstrating superior mechanical properties. In the transverse direction, however, the yarn behaviour is more intricate. At the initiation of loading, there may be noticeable gaps/voids between the fibers in the cross section of yarns, but with increasing the load they vanish and the fibers begin side-to-side contacts (Figure 4). This phenomenon makes the transverse stiffness of yarns non-linear/strain dependant. It is not straightforward to directly measure a yarn's transverse stiffness during fabric deformation. Consequently, inverse identification methods along with experimental measurements are commonly used

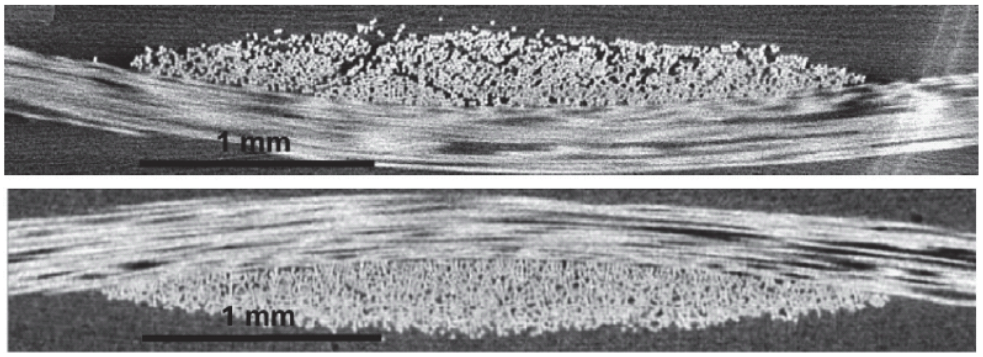

Fig. 4. The X-ray image from cross section of fibrous yarns (top) before loading; (bottom) after loading (Badel et al., 2008)

to arrive at strain-dependant relationships for the yarns' transverse stiffness parameters (Gasser et al., 2000; Badel et al., 2008).

The general form of material properties in the current model are adapted from (Komeili and Milani, 2010) which were extracted by matching the numerical simulations to the experimental measurements by Buet-Gautier and Boisse (2001) under axial tension and by Cao et al. (2008) under shear loading. The properties used for a simultaneous extension-shear are summarized in the following stiffness matrix:

$$[\boldsymbol{C}]=\begin{bmatrix} E_{11} & 0 & 0 & 0 & 0 & 0 \\ 0 & E_{22} & 0 & 0 & 0 & 0 \\ 0 & 0 & E_{33} & 0 & 0 & 0 \\ 0 & 0 & 0 & G & 0 & 0 \\ 0 & 0 & 0 & 0 & G & 0 \\ 0 & 0 & 0 & 0 & 0 & G \end{bmatrix} \tag{6}$$

$$E_{11}(\varepsilon_{11})=\begin{cases} 100\ \text{MPa} & \varepsilon_{11} < 1.0\times10^{-3} \\ 5\ \text{GPa} & 1.0\times10^{-3} \le \varepsilon_{11} < 1.6\times10^{-3} \\ 50\ \text{GPa} & 1.6\times10^{-3} \le \varepsilon_{11} \end{cases} \tag{7}$$

$$E_{tt}=2.5\times10^{5}\left|\varepsilon_{tt}\right|\varepsilon_{11}^{2}+3.0 \quad \text{MPa} \tag{8}$$

$[\boldsymbol{C}]$ is the stiffness matrix, E_{11} and ε_{11} are the axial stiffness and strains; E_{tt}, ε_{tt}, $tt=\{22,33\}$ are the transverse stiffness and strains, respectively. G is the shear modulus of the yarns which for dry fabrics should be small compared to the axial and transverse stiffness values. Here $G=60\,MPa$ as been selected merely for numerical stability purposes (Gasser et al., 2000); although the shear modulus is at the same order of magnitude as the other two stiffness values in the beginning of loading, it becomes less significant as E_{11} and E_{22} increases with the loading magnitude.

The material model of Eqs (6)-(8) was implemented in the Abaqus finite element software via a UMAT (implicit) user-defined subroutine. In doing so, however, it was noted that the

large difference between the stiffness in the yarn axial direction compared to the transverse and shear stiffness values highlights the extreme importance of applying proper material orientation updates during loading steps. The point is that the material properties should be defined in a frame which is rotating with the fiber direction in the yarns. On the other hand, conventional methods in the finite element codes use other (e.g., Green & Naghdi, 1965; Jaumann, 1911) methods for updating the material orientation under large deformation. The problem can be handled with user-defined material subroutines. Subsequently, two approaches may be implemented to ensure that the material properties during stress updates is based on the frame attached to the fibers: (1) Either the stiffness matrix defined along the fiber direction can be transformed to the current working frame of the finite element software, or (2) the stress in the working frame of the software can be transformed to the frame of the fiber and transformed back to the working frame after applying the stress updates in the fiber frame. The details of each method are available in (Badel et al., 2008) and (Komeili and Milani, 2010); the former reference employed an explicit and the latter reference an implicit integrator.

2.3 Periodic boundary conditions

A single isolated unit cell cannot be considered as a good representative of the whole fabric structure unless the effect of adjacent cells is taken into account. In other words, suitable kinematic (or dynamic) conditions should be applied on the perimeter of the unit cell where it is attached to the adjacent cells. These conditions are often called periodic boundary conditions. They are very similar (though different) to symmetric boundary conditions. A thorough discussion on their mathematical details and implementation under individual loading modes is given in (Badel et al., 2007).

The method that has been used in this study is based on the periodic boundary conditions reported in (Peng and Cao, 2002). According to their work, the side surfaces of yarns should remain plane and normal to the unit cell mid surface during deformation. More details of the latter kinematic conditions on unit cells are also given in (Komeili and Milani 2010).

2.4 Loading boundary conditions

There is a variety of test setups used for the axial tension and shear testing of woven fabrics (Buet-Gautier and Boisse, 2001; Cao et al., 2008). On the other hand, experimental setups for the combined loading modes are new and limited. First, it should be defined how a combined loading mode is exerted on a fabric specimen. For example, having a bi-axial load on a fabric where the axial loads does not rotate with the rotation of the yarns and stays parallel to its original direction during deformation, even after the shear load is applied, may be considered a special case of combined loading. As another example, one may consider a combined loading condition where the direction of the axial load rotates and realigns along the yarn direction. For a practical analysis of fabrics, the latter case of stretching in the yarn direction is more important than the former case of stretching yarns along a (fixed) off-axis direction (Boisse 2010). A new test setup capable of applying combined loading in the form of shear and biaxial stretching along the yarns (Figure 5) has been developed in (Cavallaro et al., 2007).

In order to simulate the unit cell of the fabric under such combined loading in the aforementioned Abaqus model, a set of kinematic couplings were applied around the unit cell to satisfy the periodic boundary conditions. Namely, the shear loading has been applied

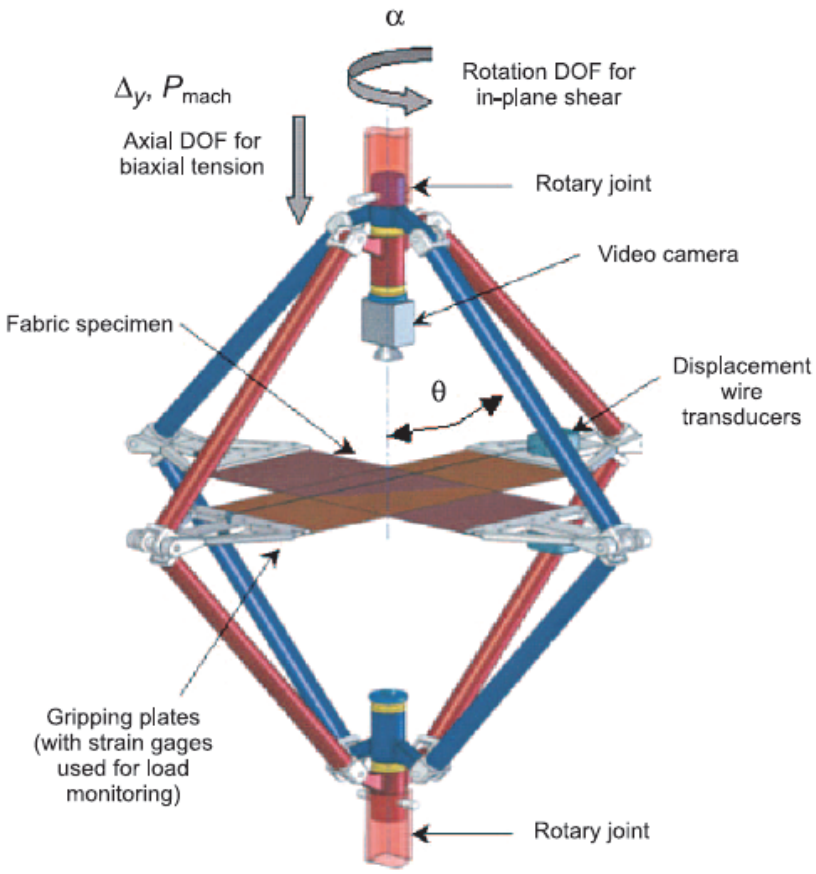

Fig. 5. Experimental fixture for applying combined shear and axial tension on fabrics (Cavallaro et al., 2007).

via rotation on one of the yarn sides and the rest of unit cell boundaries have linked to follow this movement through a periodic boundary condition. For the axial tension, connector elements between the two corners of each side yarn have been used (they can be seen as solid lines around the unit cell in Figure 6). The connector elements are chosen from the Abaqus library and provide an axial degree-of-freedom between their reference nodes. The axial distance between the nodes can be changed to apply/simulate stretching on the yarns. The reference points are not part of the yarns geometry, but they are kinematically connected to the nodes on the cross sectional surfaces of yarns (i.e., the side surfaces of the unit cell) to implement the periodic and loading boundary conditions. Moreover, there are four reference points on the mid-points of the side lines to impose the kinematic conditions on the middle yarns. The latter reference points are also connected to the corner points by kinematic constraints. Figure 6 shows the aforementioned conditions schematically. Eventually, the material resistance to deformation in the form of reaction moment from the rotation boundary condition and the normal force from the axial connector elements are

calculated and reported in the post processing of simulations. They can then be used in the normalized form and compared with experimental results.

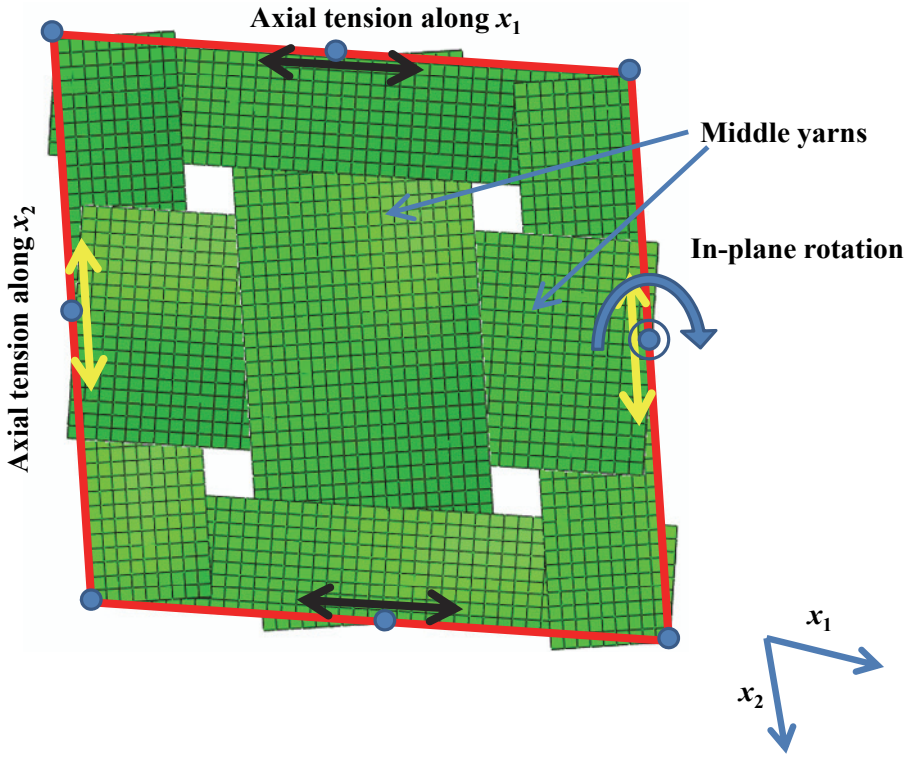

Fig. 6. The loading boundary conditions used on the unit cell to model the deformation under a combined loading mode; Circles show the location of reference points.

3. A preliminary validation

In order to validate the model with the existing data in the literature, it is compared to two basic cases where the unit cell is under pure bi-axial tension and shear (Komeili and Milani, 2010). Figure 7 shows the results of these comparisons. In the same figure, a set of actual picture frame test data, collected at the Hong Kong University of Science and Technology (HKUST), is replicated from (Cao et al., 2008). For the axial mode, however, data with the same unit cell geometrical parameters was not available. The differences between the resultant forces and moments in each mode can be related to the type of the unit cell used, shear stiffness of yarns, the method of applying boundary/loading conditions, and other details of the two finite element models in controlling their convergence (e.g. hourglass stiffness, mesh size, etc). In addition, one may redo the inverse identification of the yarn model using the current model. However, as the main goal of this chapter is to highlight the relative effect of combined loading on the mechanical characterization of woven fabrics (i.e.,

compared to the individual deformation modes), the current model and material properties are used without a loss of generality of the approach.

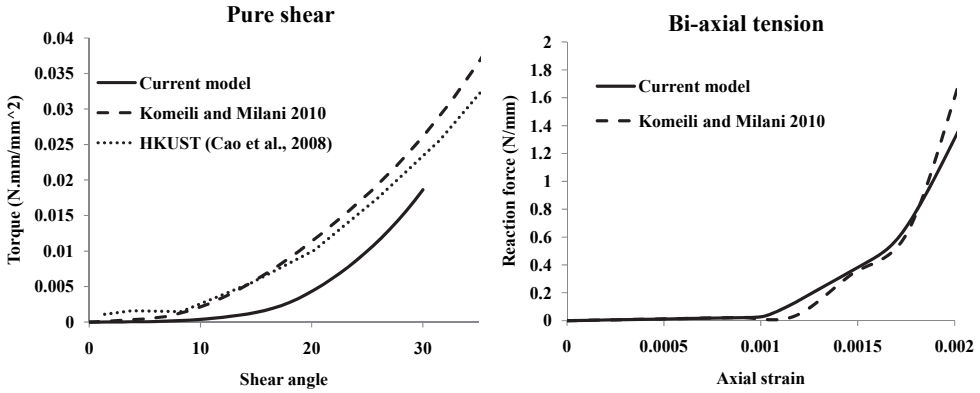

(a) (b)

Fig. 7. A validation of the current model under (a) pure bi-axial and (b) shear mode.

4. The effect of combined loading

In this section the effect of combined loading on the response of the material is analysed, when compared to those obtained from the individual biaxial and shear modes under the same loading magnitude. Figure 8 shows the effect of combined loading on the reaction force in the bi-axial tension and the reaction moment under shear loading. The amount of normalized reaction moment while the fabric is under combined loading has increased up to four times. It has also caused ~12% higher axial reaction force under an identical stretching magnitude.

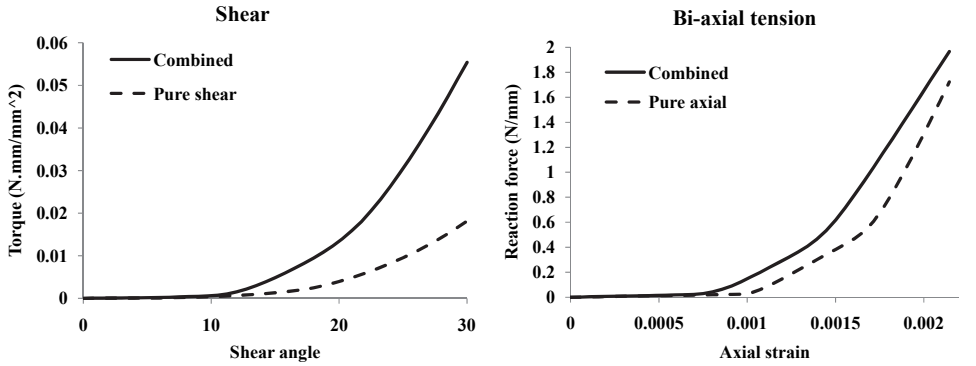

(a) (b)

Fig. 8. The effect of combined loading on the reaction force and moment when compared to the individual (a) shear and (b) biaxial modes. The difference between curves in each graph indicates the presence of additional local deformation phenomena/ interactions between shear and axial modes under combined loading.

The obtained numerical results from bi-axial loading well agree with what has been suggested through experimental measurements in the literature. Namely, Boisse, et al. (2001) and Buet-Gautier and Boisse (2001) argued that the effect of shear strain on the axial behaviour of plain fabrics is not considerable. In other words, it may be concluded that the small effect of shear deformation on the axial behaviour (~12%) can be considered as an inherent material noise in the experimental data. On the other hand, Cavallaro et al. (2007) reported that having the yarns under pretension in axial direction can greatly affect the subsequent shear behaviour of the fabrics, which is in fact the case from the simulation results in Figure 8.

After assessing the effect of combined loading on the basic normal and shear response of the fabric, another important notion may be studied. The question is, "Does the sequence of loading steps affect the response too?" In other words, if the axial loading is applied first, followed by the shear loading, or vice versa, are the resultant reaction force and moments the same as those when the two loadings are applied simultaneously?

To study the latter effect, let us define a normalized loading parameter α. It ranges from 0 to 1, where 0 refers to the initiation of loading and 1 represents the end of loading. For example, during a simultaneous/combined loading:

$$\theta(\alpha) = \alpha\,\theta_{max}; \quad \varepsilon(\alpha) = \alpha\,\varepsilon_{max} \tag{9}$$

where θ and ε, are the shear angle and axial strain in each step of loading and θ_{max} and ε_{max}, are the corresponding maximum values. Similarly, for the shear loading followed by the axial loading at $\alpha = \frac{1}{2}$ we have:

$$\theta(\alpha) = \left(R(\alpha) - R\left(\alpha - \frac{1}{2}\right)\right)\theta_{max}; \quad \varepsilon(\alpha) = R\left(\alpha - \frac{1}{2}\right)\varepsilon_{max} \tag{10}$$

where,

$$R(x) = \begin{cases} 2x & x \geq 0 \\ 0 & x < 0 \end{cases}$$

For the opposite case where the axial loading is followed by the shear loading, we may write:

$$\theta(\alpha) = R\left(\alpha - \frac{1}{2}\right)\theta_{max}; \quad \varepsilon(\alpha) = \left(R(\alpha) - R\left(\alpha - \frac{1}{2}\right)\right)\varepsilon_{max} \tag{11}$$

Results of the new simulations are presented in Figure 9. It can be clearly seen that for the shear response, the sequence of the loading affects the resultant moment up to four times. However, the axial response is still less sensitive to the effect of deformation from the shear mode and the loading sequence. The results also indicate that if the shear deformation is applied to the specimen first, the shear reaction moment is decreased substantially. Moreover, during the step that the pure shear is applied, there seems to be a small reaction force in the form of tension. This is perhaps due to the fact that during shearing, the sliding of yarns on each other and their replacement in the fabric affect their waviness/crimp. In

turn, the crimp interchange would induce a small axial stretch in some regions of yarns, especially if they are constrained at their ends (like in the picture frame test).

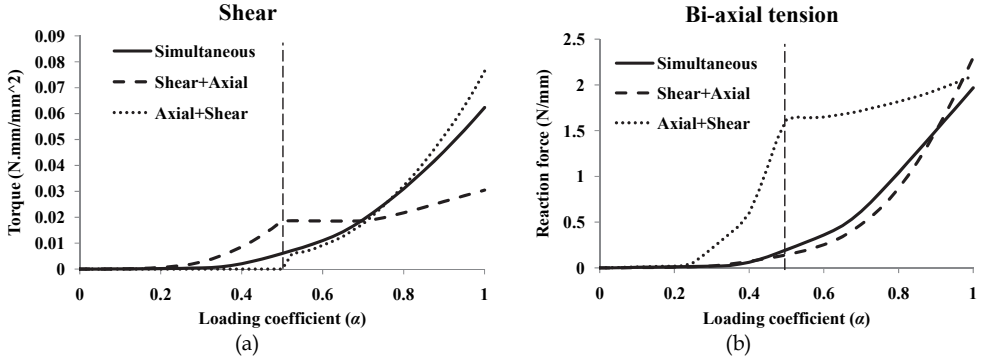

Fig. 9. The effect of loading sequence on the response of (a) shear and (b) axial deformation; the second loading step is applied after the dashed line for Axial+Shear and Shear+Axial cases.

The results in Figure 9 can also be linked to the constitutive model of yarns. Recalling Eq. (8), the transverse stiffness is a function of yarns' axial and transverse strains (crushing formula). The bi-axial stretching induces axial strain in the yarns, which leads to an increase in the yarns' transverse stiffness. In turn, the normal contact forces at the yarns cross over regions are increased, leading to a higher contribution from friction to the total reaction force. However, the opposite effect is not true. Under the bi-axial mode, the shear deformation (before locking point) does not induce considerable axial and transverse stretches in the yarns. Previously, using a sensitivity analysis under individual deformation modes, it was also reported by Komeili and Milani (2010) that the effect of transverse stiffness on the fabric response in the shear mode is considerable whereas it is ignorable in the bi-axial mode.

5. Summary

A numerical finite element model of a plain weave fabric unit cell at meso-level is developed. The model is capable of simulating specimens under simultaneous axial loading along the yarn directions and the fabric shearing. It can be a useful tool for predicting the meso-level local deformation phenomena in woven fabrics under complex loading conditions, as well as for developing equivalent material models at macro-level for fast simulation of fabric forming processes. Two fundamental deformation modes (shear and equi-biaxial stretching) are applied through two separate kinematics boundary conditions to facilitate extracting the contributions from each mode on the total resultant force and moment.

The analysis on the effect of combined loading has been conducted in two ways. First, the force and moment response of the unit cell under a predefined combined loading with a specific shear angle and axial strain is compared to those of the pure shear and axial modes. It was of interest to see if there is any interaction effect between the fundamental axial and shear deformation mechanisms when a combined loading is applied. Results showed that

this interaction in fact exists and it has a dramatic effect on the ensuing reaction moment response (shear rigidity), but it is less important for the axial reaction force. Second, the effect of applying combined loading in two sequential steps was scrutinized. Again, the shear deformation response showed high sensitivity to the sequence of loading if it is applied before the axial deformation. Moreover, it was noted that during shear deformation there is a small tension reaction force, even though no stretching is applied to the yarns. This is perhaps due to the crimp interchanges along with the imposed boundary conditions on the end surfaces of yarns.

In summary, the above mentioned results show a high level of nonlinear interactions between the material response in the axial tension and shear modes. This can be directly related to the geometrical nonlinearities that exist in woven fabrics at meso-level and the effect of crimp interchanges during loading. After each stage of loading, the rearrangement of yarns in the fabric and their interactions should occur before yarns can go through further stretching/shearing. Under the combined loading, the crimp changes due to each loading mode can affect the reaction from the other mode. If loads are applied in sequence (e.g., shear followed by biaxial tension), the crimp changes in each step can affect the global response due to the effect from the previous loading step. Considerably different magnitudes of the shear moment were found between two cases where the shear and bi-axial deformations are applied at the same time and where the shear is applied after the axial loading. This observation clearly showed the higher sensitivity of the shear response to the crimp interchanges. On the contrary, because the axial reaction forces are more related to the stretching in the yarns, the shear deformation has minor influence on their axial force magnitudes. The effect of axial tension on increasing the transverse stiffness of yarns is deemed to be the main reason for the presence of interactions between the axial tension and shear deformation under combined loading modes. Further experimental and/or numerical studies are needed to scrutinize and validate the reported effects.

6. Acknowledgment

The authors would like to acknowledge financial support from the Natural Sciences and Engineering Research Council (NSERC) of Canada.

7. References

Badel, P, Vidalsalle, E, & Boisse, P (2007) Computational determination of in-plane shear mechanical behaviour of textile composite reinforcements. *Computational Materials Science* 40: 439-448.

Badel, P, Vidalsalle, E, & Boisse, P (2008) Large deformation analysis of fibrous materials using rate constitutive equations. *Computers & Structures* 86: 1164-1175.

Badel, P, Vidalsalle, E, Maire, E, & Boisse, P (2008) Simulation and tomography analysis of textile composite reinforcement deformation at the mesoscopic scale. *Composites Science and Technology* 68: 2433-2440.

Badel, P, Gauthier, S, Vidal-Sallé, E, & Boisse, P. (2009) Rate constitutive equations for computational analyses of textile composite reinforcement mechanical behaviour during forming. *Composites Part A: Applied Science and Manufacturing* 40: 997-1007.

Boisse, P, Zouari, B, & Daniel, J (2006) Importance of in-plane shear rigidity in finite element analyses of woven fabric composite preforming. *Composites Part A: Applied Science and Manufacturing* 37: 2201-2212.

Boisse, P, Borr, M, Buet, K, Cherouat, A (1997) Finite element simulations of textile composite forming including the biaxial fabric behaviour. *Composites. Part B: Engineering* 28: 453–464.

Boisse, P, Gasser, A, Hivet, G (2001) Analyses of fabric tensile behaviour: determination of the biaxial tension–strain surfaces and their use in forming simulations. *Composites Part A: Applied Science and Manufacturing* 32: 1395-1414.

Boisse, P (2010) Simulations of Woven Composite Reinforcement Forming. *Woven Fabric Engineering*, pp 387-414. SCIYO.

Boisse, P, Akkerman, R, Cao, J, Chen, J, Lomov, S, & Long, A (2007) Composites Forming. *Advances in Material Forming - Esaform 10 years on material forming*. Springer, Paris.

Buet-Gautier, K, & Boisse, P. (2001) Experimental analysis and modeling of biaxial mechanical behavior of woven composite reinforcements. *Experimental Mechanics* 41: 260–269.

Cao, J, Akkerman, R, Boisse, P, Chen, J, Cheng, H, Degraaf, E, Gorczyca, J, Harrison, P, Hivet, G, Launay, J (2008) Characterization of mechanical behavior of woven fabrics: Experimental methods and benchmark results. *Composites Part A: Applied Science and Manufacturing* 39: 1037-1053.

Cavallaro, PV, Sadegh, AM, & Quigley, CJ (2007) Decrimping Behavior of Uncoated Plain-woven Fabrics Subjected to Combined Biaxial Tension and Shear Stresses. *Textile Research Journal* 77: 403-416.

Cavallaro, PV, Johnson, ME, & Sadegh, AM (2003) Mechanics of plain-woven fabrics for inflated structures. *Composite Structures* 61: 375–393.

Chen, J., Lussier, D, Cao, J., & Peng, X. (2001) Materials characterization methods and material models for stamping of plain woven composites. *International Journal of Forming Processes* 4: 269–284.

Gasser, A, Boisse, P., & Hanklar, S (2000) Mechanical behaviour of dry fabric reinforcements. 3D simulations versus biaxial tests. *Computational Materials Science* 17: 7–20.

Guagliano, M, & Riva, E (2001) Mechanical behaviour prediction in plain weave composites. *Journal of strain analysis for engineering design* 36: 153-162.

Kawabata, S, Niwa, M, & Kawai, H (1973) Finite-deformation theory of plain-weave fabrics - 1. The biaxial-deformation theory. *Journal of the Textile Institute* 64: 21-46.

Kawabata, S, Niwa, Masako, & Kawai, H (1973a) Finite-deformation theory of plain-weave fabrics - 2. The uniaxial-deformation theory. *Journal of the Textile Institute* 64: 47-61.

Kawabata, S, Niwa, Masako, & Kawai, H (1973b) Finite-deformation theory of plain-weave fabrics - 3. The shear-deformation theory. *Journal of the Textile Institute* 64: 62-85.

Komeili, M, & Milani, AS (2010) *Meso-Level Analysis of Uncertainties in Woven Fabrics*. VDM Verlag, Berlin, Germany.

Mcbride, TM, & Chen, Julie (1997) Unit-cell geometry in plain-weave during shear deformations fabrics. *Composites Science and Technology* 57: 345-351.

Peng, X, & Cao, J (2005) A continuum mechanics-based non-orthogonal constitutive model for woven composite fabrics. *Composites Part A: Applied Science and Manufacturing* 36: 859-874.

Peng, X, Cao, J, Chen, J., Xue, P, Lussier, D, & Liu, L (2004) Experimental and numerical analysis on normalization of picture frame tests for composite materials. *Composites Science and Technology* 64: 11-21.

Peng, X., & Cao, J. (2002) A dual homogenization and finite element approach for material characterization of textile composites. *Composites Part B: Engineering* 33: 45–56.

Xue, P, Peng, X, & Cao, J (2003) A non-orthogonal constitutive model for characterizing woven composites. *Composites Part A: Applied Science and Manufacturing* 34: 183-193.

5

Multiaxis Three Dimensional (3D) Woven Fabric

Kadir Bilisik
Erciyes University Department of Textile Engineering
Turkey

1. Introduction

Textile structural composites are widely used in various industrial sections, such as civil and defense (Dow and Dexter, 1997; Kamiya et al., 2000) as they have some better specific properties compared to the basic materials such as metal and ceramics (Ko & Chou 1989; Chou, 1992). Research conducted on textile structural composites indicated that they can be considered as alternative materials since they are delamination-free and damage tolerant (Cox et al, 1993; Ko & Chou 1989). From a textile processing viewpoint they are readily available, cheap, and not labour intensive (Dow and Dexter, 1997). The textile preform fabrication is done by weaving, braiding, knitting, stitching, and by using nonwoven techniques, and they can be chosen generally based on the end-use requirements. Originally three dimensional (3D) preforms can be classified according to fiber interlacement types. Simple 3D preform consists of two dimensional (2D) fabrics and is stitched depending on stack sequence. More sophisticated 3D preforms are fabricated by specially designed automated loom and manufactured to near-net shape to reduce scrap (Brandt et. al., 2001; Mohamed, 1990). However, it is mentioned that their low in-plane properties are partly due to through-the-thickness fiber reinforcement (Bilisik and Mohamed, 1994; Dow and Dexter, 1997; Kamiya et al., 2000). Multiaxis knitted preform, which has four fiber sets as ±bias, warp(0˚) and weft(90˚) and stitching fibers enhances in-plane properties (Dexter and Hasko, 1996). It was explained that multiaxis knitted preform suffers from limitation in fiber architecture, through-thickness reinforcement due to the thermoplastic stitching thread and three dimensional shaping during molding (Ko & Chou 1989).
Multiaxis 3D woven preform is developed in the specially developed multiaxis 3D weaving and it's in-plane properties are improved by orienting the fiber in the preform (Mohamed and Bilisik, 1995; Uchida et al, 2000). The aim of this chapter is to review the 3D fabrics, production methods and techniques. Properties of 3D woven composites are also provided with possible specific end-uses.

2. Classifications of 3D fabrics

3D preforms were classified based on various parameters. These parameters depend on the fiber type and formation, fiber orientation and interlacements and micro and macro unit cells structures. One of the general classification schemes has been proposed by Ko and Chou (1989). Another classification scheme has been proposed depending upon yarn

Direction	Three dimensional weaving			
	Woven		Orthogonal nonwoven	
	Cartesian	Polar	Cartesian	Polar
2 or 3	Angle interlock • Layer-to-layer • Through-the- thickness	Tubular	Weft- insertion	Weft-winding and sewing
	Core structure • Rectangular • Triangular • Double layer • Angularly oriented • Diamond			
3	Plain • Plain weft laid-in • Plain binder laid- in	Plain • Plain radial laid-in • Plain circumferential laid-in	Open- lattice Solid	Tubular
	Twill • Twill weft laid-in • Twill binder laid-in	Twill • Twill radial laid-in • Twill circumferential laid-in		
	Satin • Satin weft laid-in • Satin binder laid-in	Satin • Satin radial laid-in • Satin circumferential laid-in		
4	Plain • Plain laid-in	Plain • Plain radial laid-in • Plain circumferential laid-in	Corner across Face across Derivative structures • Corner- Face-Orthogonal • Corner- Face • Face-Orthogonal • Corner-Orthogonal	Tubular
	Twill • Twill laid-in	Twill • Twill radial laid-in • Twill circumferential laid-in		
	Satin • Satin laid-in	Satin • Satin radial laid-in • Satin circumferential laid-in		

5	Plain • Plain laid-in	Plain • Plain radial laid-in • Plain circumferential laid-in	Solid	Tubular
	Twill • Twill laid-in	Twill • Twill radial laid-in • Twill circumferential laid-in		
	Satin • Satin laid-in	Satin • Satin radial laid-in • Satin circumferential laid-in		
6 to 15	Rectangular array	Rectangular array	Rectangular array	Rectangular array
	Hexagonal array	Hexagonal array	Hexagonal array	Hexagonal array

Table 1. The classification of three dimensional weaving based on interlacement and fiber axis (Bilisik, 1991).

interlacement and type of processing (Khokar, 2002a). In this scheme, 3D woven preform is divided into orthogonal and multiaxis fabrics and their process have been categorized as traditional or new weaving, and specially designed looms. Chen (2007) categorized 3D woven preform based on macro geometry where 3D woven fabrics are considered solid, hollow, shell and nodal forms. Bilisik (1991) proposes more specific classification scheme of 3D woven preform based on type of interlacements, yarn orientation and number of yarn sets as shown in Table 1. In this scheme, 3D woven fabrics are divided in two parts as fully interlaced 3D woven and non-interlaced orthogonal woven. They are further sub divided based on reinforcement directions which are from 2 to 15 at rectangular or hexagonal arrays and macro geometry as cartesian and polar forms. These classification schemes can be useful for development of fabric and weaving process for further researches.

3. 3D Fabric structure and method to weave

3.1 2D fabric

2D woven fabric is the most widely used material in the composite industry at about 70%. 2D woven fabric has two yarn sets as warp(0˚) and filling(90˚) and interlaced to each other to form the surface. It has basically plain, twill and satin weaves which are produced by traditional weaving as shown in Figure 1. But, 2D woven fabric in rigid form suffers from its poor impact resistance because of crimp, low delamination strength because of the lack of binder fibers (Z-fibers) to the thickness direction and low in-plane shear properties because no off-axis fiber orientation other than material principal direction (Chou, 1992). Although through-the-thickness reinforcement eliminates the delamination weakness, this reduces the in-plane properties (Dow and Dexter, 1997, Kamiya et al., 2000). On the other hand, uni-weave structure was developed. The structure has one yarn set as warp (0˚) and multiple warp yarns were locked by the stitching yarns (Cox and Flanagan, 1997).

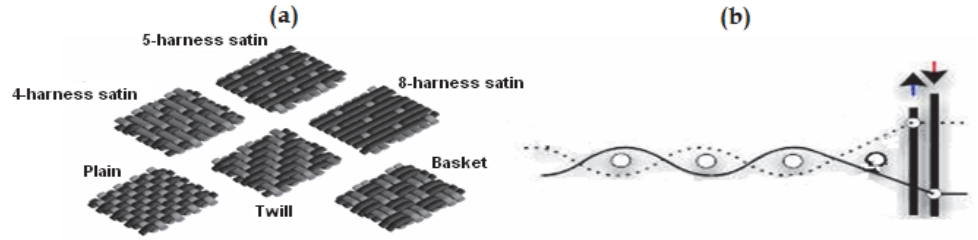

Fig. 1. 2D various woven fabrics (a) and schematic view of processing (b) (Chou, 1992).

Bi-axial non-crimped fabric was developed to replace the unidirectional cross-ply lamina structure (Bhatnagar and Parrish, 2006). Fabric has basically two sets of fibers as filling and warp and locking fibers. Warp positioned to 0˚ direction and filling by down on the warp layer to the cross-direction (90˚) and two sets of fibers are locked by two sets of stitching yarns' one is directed to 0˚ and the other is directed to 90˚. Traditional weaving loom was modified to produce such fabrics. Additional warp beam and filling insertions are mounted on the loom. Also, it is demonstrated that 3D shell shapes with high modulus fibers can be knitted by weft knitting machine with a fabric control sinker device as shown in Figure 2.

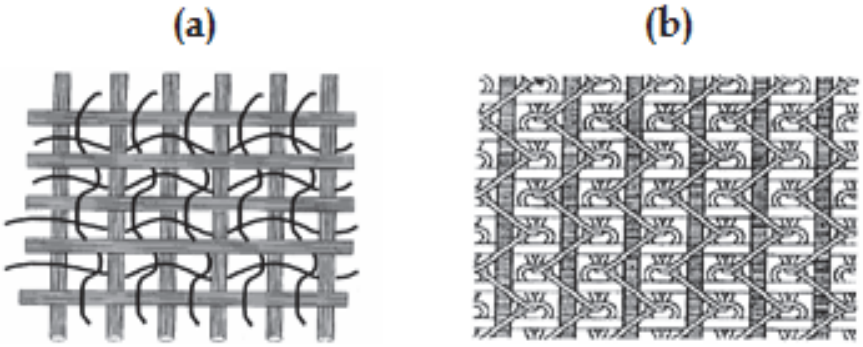

Fig. 2. Non-interlace woven fabric (a) and warp inserted knitted fabric (b) (Bhatnagar & Parrish, 2006).

3.2 Triaxial fabrics

Triaxial weave has basically three sets of yarns as ±bias (±warp) and filling (Dow, 1969). They interlaced to each other at about 60˚ angle to form fabric as shown in Figure 3. The interlacement is the similar with the traditional fabric which means one set of yarns is above and below to another and repeats through the fabric width and length. Generally, the fabric has large open areas between the interlacements. Dense fabrics can also be produced. However, it may not be woven in a very dense structure compared to the traditional fabrics. This process has mainly open reed. Triaxial fabrics have been developed basically in two variants. One is loose-weave and the other is tight weave. The structure was evaluated and concluded that the open-weave triaxial fabric has certain stability and shear stiffness to ±45˚ direction compared to the biaxial fabrics and has more isotropy (Dow and Tranfield, 1970).

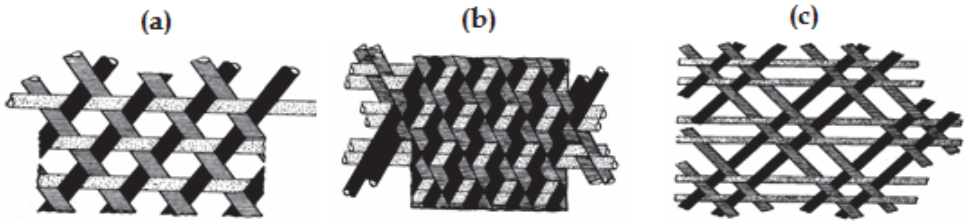

Fig. 3. Triaxial woven fabrics; loose fabric (a), tight fabric (b) and one variant of triaxial woven fabric (c) (Dow, 1969).

The machine consists of multiple ±warp beams, filling insertion, open beat-up, rotating heddle and take up. The ±warp yarn systems are taken from rotating warp beams located above the weaving machine. After leaving the warp beams, the warp ends are separated into two layers and brought vertically into the interlacing zone. The two yarn layers move in opposite directions i.e., the front layer to the right and the rear layer to the left. When the outmost warp end has reached the edge of the fabric, the motion of the warp layers is reversed so that the front layer moves to the left and the rear layer to the right as shown in Figure 4. As a result, the warp makes the bias intersecting in the fabric. Shedding is controlled by special hook heddles which are shifted after each pick so that in principle they are describing a circular motion. The pick is beaten up by two comb-like reeds which are arranged in opposite each other in front of and behind the warp layers, penetrate into the yarn layer after each weft insertion and thus beat the pick against the fell of the cloth.

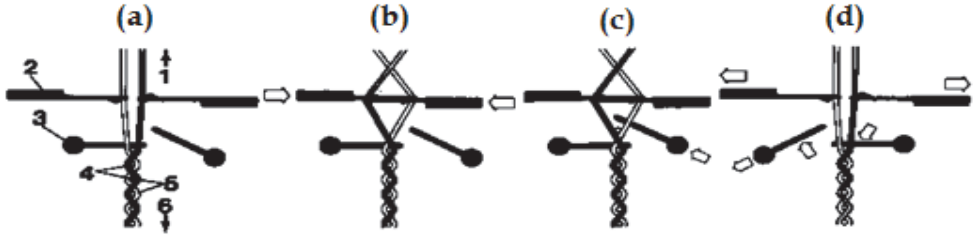

Fig. 4. The schematic views of weaving method of triaxial woven fabrics; bias orientation (a), shedding (b), beat-up (c) and take-up (d) (Dow, 1969).

A century ago, the multiaxis fabric, which has ±bias, warp(axial) and filling, was developed for garment and upholstery applications (Goldstein, 1939). The yarn used in weaving is slit cane. The machine principal operation is the same with triaxial weaving loom. A loom consists of bias creel which is rotated; ±bias indexing and rotating unit; axial warp feeding; rigid rapier type filling insertion and take up units.

Tetra-axial woven fabric was introduced for structural tension member applications. Fabric has four yarn sets as ±bias, filling and warp (Kazumara, 1988). They are interlaced all together similar with the traditional woven fabric. So, the fabric properties enhance the longitudinal direction. The process has rotatable bias bobbins unit, a pair of pitched bias cylinders, bias shift mechanism, shedding unit, filling insertion and warp (0°) insertion units. After the bias bobbins rotate to incline the yarns, helical slotted bias cylinders rotate to shift the bias one step as similar with the indexing mechanism. Then, bias transfer

mechanism changes the position of the end of bias yarns. Shedding bars push the bias yarns to make opening for the filling insertion. Filling is inserted by rapier and take-up advances the fabric to continue the next weaving cycle.
Another tetra-axial fabric has four fiber sets as ±bias, warp and filling. In fabric, warp and filling have no interlacement points with each other. Filling lays down under the warp and ±bias yarns and locks all yarns together to provide fabric integrity (Mamiliano, 1994). In this way, fabric has isotropic properties to principal and bias directions. The process has rotatable bias feeding system, ±bias orientation unit, shedding bars unit, warp feeding, filling insertion and take-up. After bias feeding unit rotates one bobbin distance, ±bias system rotates just one yarn distance. Shedding bars push the ±bias fiber sets to each other to make open space for filling insertion. Filling is inserted by rapier and take-up delivers the fabric. The fabric called quart-axial has four sets of fibers as ±bias, warp and filling yarns as shown in Figure 5. All fiber sets are interlaced to each other to form the fabric structure (Lida et al, 1995). However, warp yarns are introduced to the fabric at selected places depending upon the end-use.

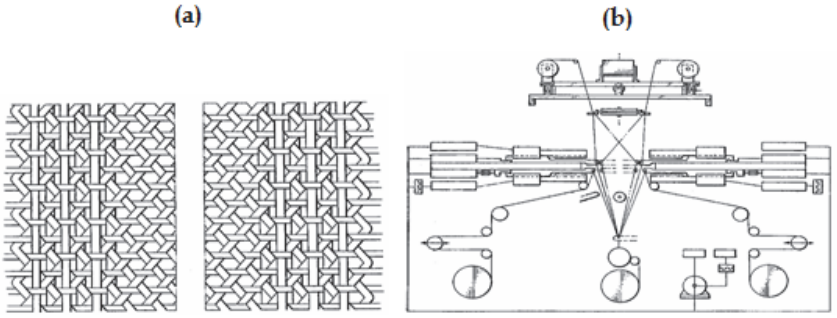

Fig. 5. Quart-axial woven fabric (a) and weaving loom (b) (Lida et al., 1995).

The process includes rotatable ±bias yarn beams or bobbins, close eye hook needle assembly, warp yarn feeding unit, filling insertion unit, open reed for beat-up and take-up. After the ±bias yarns rotation just one bobbin distance, heddles are shifted to one heddle distance. Then warp is fed to the weaving zone and heddles move to each other selectively to form the shed. Filling insertion takes place and open reed beats the filling to the fabric formation line. Take-up removes the fabric from the weaving zone.

3.3 3D orthogonal fabric

3D orthogonal woven preforms have three yarn sets: warp, filling, and z-yarns (Bilisik, 2009a). These sets of yarns are all interlaced to form the structure wherein warp yarns were longitudinal and the others were orthogonal. Filling yarns are inserted between the warp layers and double picks were formed. The z-yarns are used for binding the other yarn sets to provide the structural integrity. The unit cell of the structure is given in Figure 6.
A state-of-the-art weaving loom was modified to produce 3D orthogonal woven fabric (Deemey, 2002). For instance, one of the looms which has three rigid rapier insertions with dobby type shed control systems was converted to produce 3D woven preform as seen in Figure 7. The new weaving loom was also designed to produce various sectional 3D woven preform fabrics (Mohamed and Zhang, 1992).

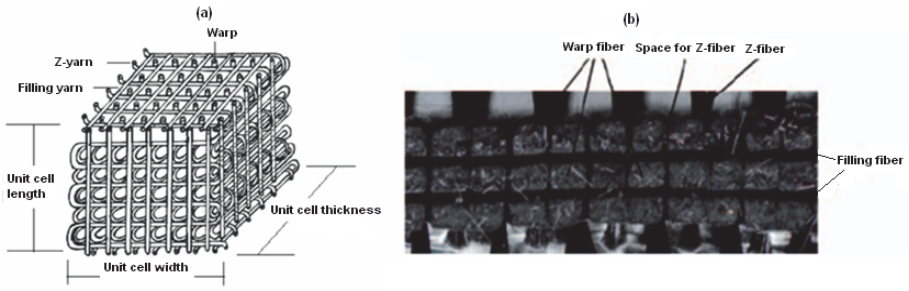

Fig. 6. 3D orthogonal woven unit cell; schematic (a) and 3D woven carbon fabric perform (b) (Bilisik, 2009a).

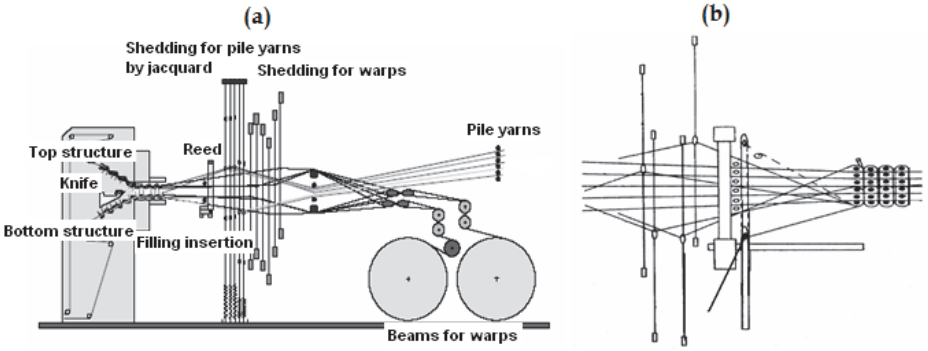

Fig. 7. Traditional weaving loom (a) and new weaving loom (b) producing 3D orthogonal woven fabrics (Deemey, 2002; Mohamed and Zhang, 1992).

On the other hand, specially designed weaving looms for 3D woven orthogonal woven preform were developed to make part manufacturing for structural applications as billet and conical frustum. They are shown in Figure 8. First loom was developed based on needle insertion principle (King, 1977), whereas second loom was developed on the rapier-tube insertion principle (Fukuta et al, 1974).

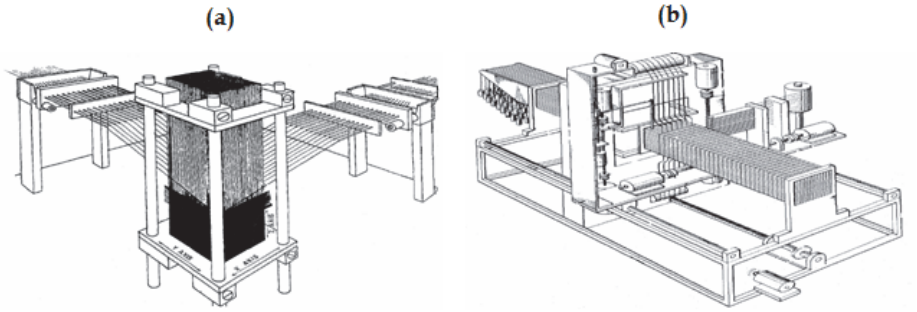

Fig. 8. 3D weaving looms for thick part manufacturing based on needle (a) and rapier (b) principles (King, 1977; Fukuta et al, 1974).

3D angle interlock fabrics were fabricated by 3D weaving loom (Crawford, 1985). They are considered as layer-to-layer and through-the-thickness fabrics as shown in Figure 9. Layer-to-layer fabric has four sets of yarns as filling, ±bias and stuffer yarns (warp). ±Bias yarns oriented at thickness direction and interlaced with several filling yarns. Bias yarns made zig-zag movement at the thickness direction of the structure and changed course in the structure to the machine direction. Through-the-thickness fabric has again four sets of fibers as ±bias, stuffer yarn (warp) and fillings. ±Bias yarns are oriented at the thickness direction of the structure. Each bias is oriented until coming to the top or bottom face of the structure. Then, the bias yarn is moved towards top or bottom faces until it comes to the edge. Bias yarns are locked by several filling yarns according to the number of layers.

Fig. 9. 3D angle interlock fabrics (a) and schematic view of 3D weaving loom (b) (Khokar, 2001).

Another type of 3D orthogonal woven fabric, which pultruded rod is layered, was introduced. ±Bias yarns were inserted between the diagonal rows and columns for opening warp layers at a cross-section of the woven preform structure (Evans, 1999).
The process includes ±bias insertion needle assembly, warp layer assembly and hook holder assembly as shown in Figure 10. Warp yarns are arranged in matrix array according to preform cross-section. A pair of multiple latch needle insertion systems inserts ±bias yarns at cross-section of the structure at an angle about 60˚. Loop holder fingers secure the bias loop for the next bias insertion and passes to the previous loop.

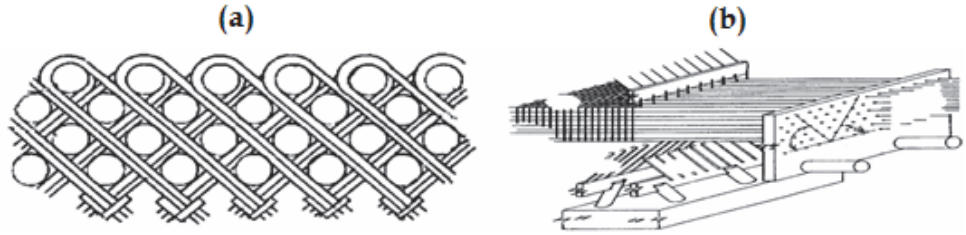

Fig. 10. 3D orthogonal fabric at an angle in cross-section (a) and production loom (b) (Evans, 1999).

3D circular weaving (or 3D polar weaving) was also developed (Yasui et al., 1992). A preform has mainly three sets of yarn: axial, radial and circumferential for cylindrical shapes and additional of the central yarns for rod formation as shown in Figure 11. The device has a rotating table for holding the axial yarns, a pair of carriers which extend vertically up and

down to insert the radial yarn and each carrier includes several radial yarn bobbins and finally a guide frame for regulating the weaving position. A circumferential yarn bobbin is placed on the radial position of the axial yarns. After the circumferential yarn will be wound over the radial yarn which is vertically positioned, the radial yarn is placed radially to the outer ring of the preform. The exchanging of the bobbins results in a large shedding motion which may cause fiber damage.

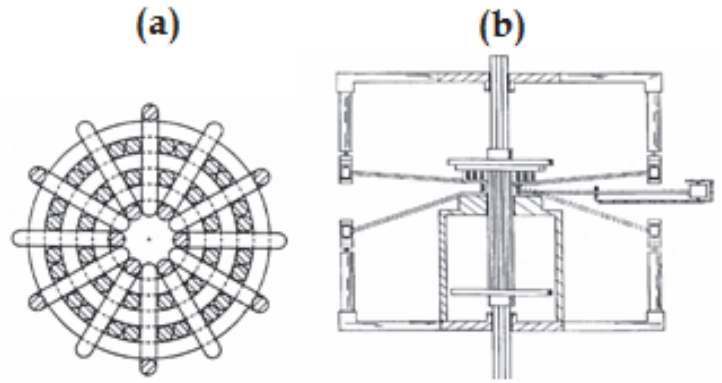

Fig. 11. 3D circular woven perform (a) and weaving loom schematic (b) (Yasui et al., 1992).

3D orthogonal woven fabrics at various sectional shapes as T, I and box beams were fabricated by modified 2D weaving loom (Edgson and Temple, 1998). Fabric has ±bias, warp and filling yarns. During weaving, ±bias fibers were placed at web of the T shape. Flange section has warp and filling and connected part of the ±bias fibers. The process is realized on a traditional two rapier insertion loom. ±Bias fibers' sets were placed to the web by jacquard head. ±Bias yarns were connected during weaving of the flange section.
A laminated structure in which biaxial fabric was used as basic reinforcing elements has been developed (Homma and Nishimura, 1992). The fabric was oriented at ±45˚ in the web section with low dense warp layers, whereas fabric orientation 0˚ means warp direction in the flange with high dense warp layers. Plies were formed above the arrangement to produce I-beam in use as structural elements of aircrafts fuselage.

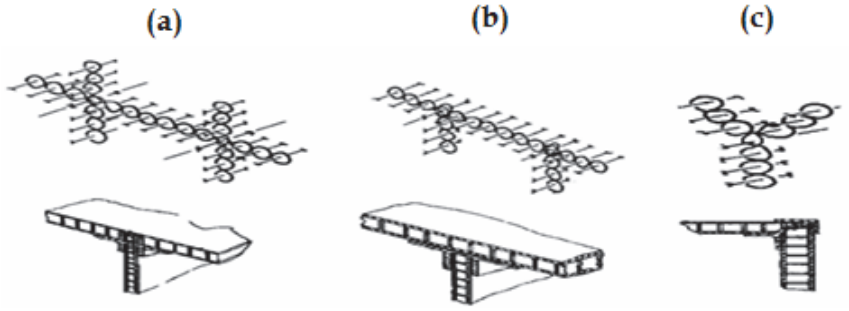

Fig. 12. 2D shaped woven connectors as H-shape (a), TT-shape (b) and Y-shape (c) (Abildskow, 1996).

A 2D woven plain fabric base laminated connector was developed. It was joined adhesively to the spar and sandwiched panel at the aircraft wing (Jonas, 1987). Integrated 2D shaped woven connector fabric was developed to join the sandwiched structures together for aircraft applications (Abildskow, 1996). The 2D integrated woven connector has warp and filling yarns. Basically, two yarn sets are interlaced at each other. Z-fibers can be used based on connector thickness. The connector can be woven as Π, Y, H shapes according to joining types as shown in Figure 12. Rib or spars as the form of sandwiched structures are joined by connector with gluing.

3.4 Multiaxis 3D fabric

Multiaxis 3D woven fabric, method and machine based on lappet weaving principles were introduced by Ruzand and Guenot (1994). Fabric has four yarn sets: ±bias, warp and filling as shown in Figure 13. The bias yarns run across the full width of the fabric in two opposing layers on the top and bottom surfaces of the fabric, or if required on only one surface. They are held in position using selected weft yarns interlaced with warp binding yarns on the two surfaces of the structure. The intermediate layers between the two surfaces are composed of other warp and weft yarns which may be interlaced.

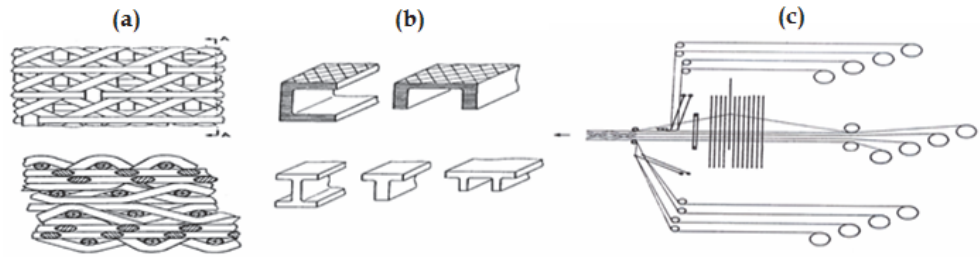

Fig. 13. Multiaxis 3D woven fabric (a), structural parts (b) and loom based on lappet weaving (c) (Ruzand and Guenot, 1994).

The basis of the technique is an extension of lappet weaving in which pairs of lappet bars are used on one or both sides of the fabric. The lappet bars are re-segmented and longer greater than the fabric width by one segment length. Each pair of lappet bars move in opposite directions with no reversal in the motion of a segment until they fully exceeds the opposite fabric selvedge. When the lappet passes across the fabric width, the segment in the lappet bar is detached, its yarns are gripped between the selvedge and the guides and it is cut near the selvedge. The detached segment is then transferred to the opposite side of the fabric where it is reattached to the lappet bar and its yarn subsequently connected to the fabric selvedge. Since a rapier is used for weft insertion, the bias yarns can be consolidated into the selvedge by an appropriate selvedge-forming device employed for weaving. The bias warp supply for each lappet bar segment is independent and does not interfere with the yarns from other segments.

A four layers multiaxis 3D woven fabric was developed (Mood, 1996). That fabric has four yarn sets: ±bias, warp and filling. The ±bias sets are placed between the warp (0˚) and filling (90˚) yarn sets so that they are locked by the warp and filling, where warp and filling yarns are orthogonally positioned as shown in Figure 14. The bias yarns are positioned by the use of special split-reeds together and a jacquard shedding mechanism with special heddles. A

creel supplies bias warp yarns in a sheet to the special heddles connected to the jacquard head. The bias yarns then pass through the split-reed system which includes an open upper reed and an open lower reed together with guides positioned in the reed dents. The lower reed is fixed while the upper reed can be moved in the weft direction.

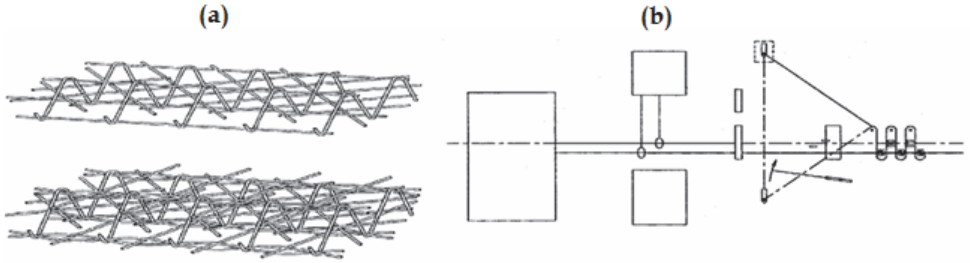

Fig. 14. Four layers multiaxis woven fabric (a) and Jacquard weaving loom (b) (Mood, 1996).

The jacquard head is used for the positioning of selected bias yarns in the dents of the upper reed so that they can be shifted transverse to the normal warp direction. The correct positioning of the bias yarns requires a series of such lifts and transverse displacements and no entanglement of the warp. A shed is formed by the warp binding yarn via a needle bar system and the weft is inserted at the weft insertion station with beat-up performed by another open reed.

Another multiaxis four layer fabric was developed based on multilayer narrow weaving principle (Bryn et al., 2004). The fabric, which has ±bias, warp and filling yarn sets, is shown in Figure 15. The fabric was produced in various cross-sections like ⊥, ╥, □. Two sets of bias yarns were used during weaving and when +bias yarns were reached the selvedge of the fabric then transverse to the opposite side of the fabric and become –bias. All yarns were interlaced based on traditional plain weave.

A narrow weaving loom was modified to produce the four layers multiaxis fabric. The basic modified part is bias insertion assembly. Bias yarn set was inserted by individual hook. The basic limitation is the continuous manufacturing of the fabric. It is restricted by the bias yarn length. Such structure may be utilized as connector to the structural elements of aircraft components.

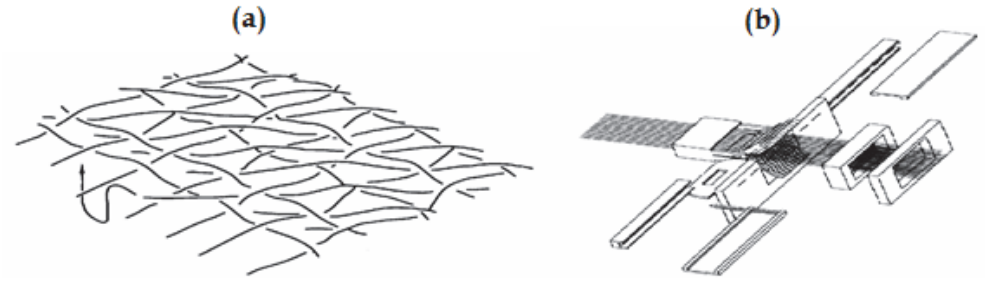

Fig. 15. Four layers multiaxis woven fabric (a) and narrow weaving loom (b) (Bryn et al., 2004).

A multiaxis weaving loom was developed to produce four layers fabric which has ±bias, warp and filling yarns as shown in Figure 16. The process has warp creel, shuttle for filling insertion, braider carrier for +bias or –bias yarns, open reed and take-up. Bias carriers were moved on predetermined path based on cross-sectional shape of the fabric. Filling is inserted by shuttle to interlace with warp as it is same in the traditional weaving. Open reed beats the inserted filling to the fabric fell line to provide structural integrity (Nayfeh et al., 2006).

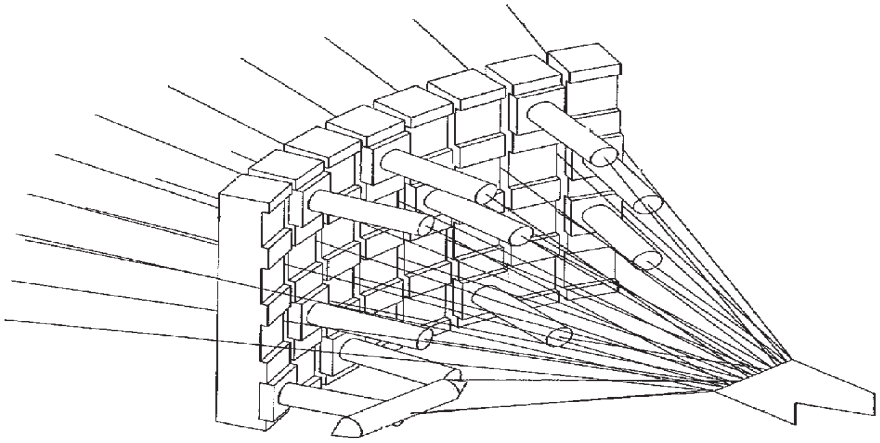

Fig. 16. Schematic view of multiaxis weaving loom (Nayfeh et al., 2006).

A multiaxis structure and process have been developed to produce the fabrics. The pultruded rods are arranged in hexagonal array as warp yarns as shown in Figure 17. Three sets of rods are inserted to the cross-section of such array at an angle about 60˚. The properties of the structure may distribute isotropically depending upon end-use (Kimbara et al., 1991).

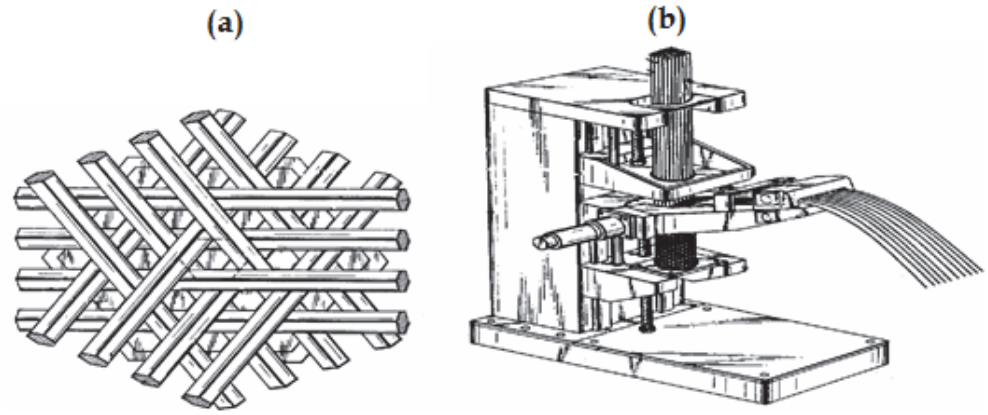

Fig. 17. Multiaxis pultruded rod fabric (a) and devise to produce the fabric (b) (Kimbara et al., 1991).

A fabric has been developed where ±bias yarns are inserted to the traditional 3D lattice fabric's cross-section at an angle of ±45° (Khokar, 2002b). The fabric has warp, filling, Z-yarn which are orthogonal arrangements and plain type interlaced fiber sets were used as (Z-yarn)-interlace and filling-interlace as shown in Figure 18. The ±bias yarns are inserted to such structure cross-section at ±45°. The fabric has complex internal geometry and production of such structure may not be feasible.

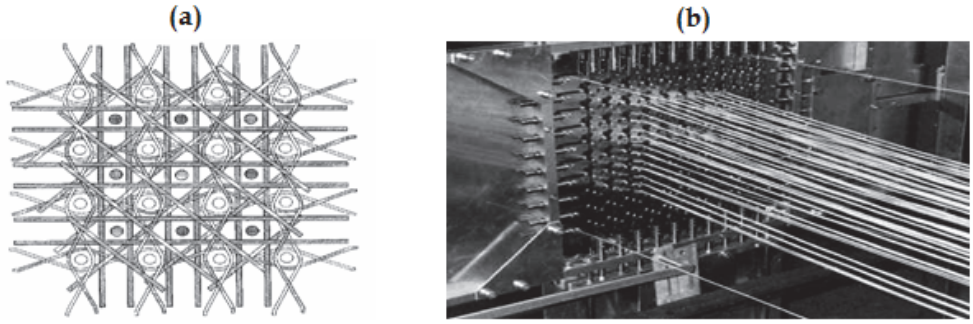

Fig. 18. The fabric (a) and specially designed loom to fabricate the multiaxis 3D fabric (b) (Khokar, 2002b).

Anahara and Yasui (1992) developed a multiaxis 3D woven fabric. In this fabric, the normal warp, bias and weft yarns are held in place by vertical binder yarns. The weft is inserted as double picks using a rapier needle which also performs beat-up. The weft insertion requires the normal warp and bias layers to form a shed via shafts which do not use heddles but rather have horizontal guide rods to maintain the vertical separation of these layers. The binders are introduced simultaneously across the fabric width by a vertical guide bar assembly comprising a number of pipes with each pipe controlling one binder as shown in Figure 19.

The bias yarns are continuous throughout the fabric length and traverse the fabric width from one selvedge to the other in a cross-laid structure. Lateral positioning and cross-laying of the bias yarns are achieved through use of an indexing screw-shaft system. As the bias yarns are folded downwards at the end of their traverse, there is no need to rotate the bias yarn supply. So, the bias yarns can supply on warp beams or from a warp creel, but they must be appropriately tensioned due to path length differences at any instant of weaving. The bias yarn placement mechanism has been modified instead of using an indexing screw shaft system, actuated guide blocks are used to place the bias yarns as shown in Figure 20.

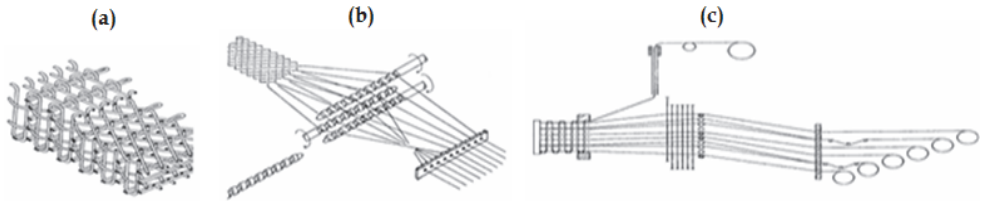

Fig. 19. The multiaxis 3D woven fabric (a), indexing mechanism for ±bias (b) and loom (c) (Anahara and Yasui, 1992).

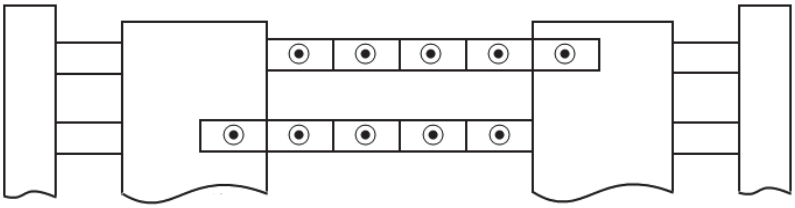

Fig. 20. Guide block mechanism for ±bias yarns (Anahara and Yasui, 1992).

A folded structure of the bias yarns results in each layer having triangular sections which alternate in the direction of the bias angle about the warp direction due to the bias yarn interchanges between adjacent layers. The bias yarns are threaded through individual guide blocks which are controlled by a special shaft to circulate in one direction around a rectangular path. Obviously, this requires rotation of the bias yarn supply.
Uchida et al. (1999) developed the fabric called five-axis 3D woven which has five yarn sets: ±bias, filling and warp and Z-fiber. The fabric has four layers and sequences: +bias, –bias, warp and filling from top to bottom. All layers are locked by the Z-fibers as shown in Figure 21.

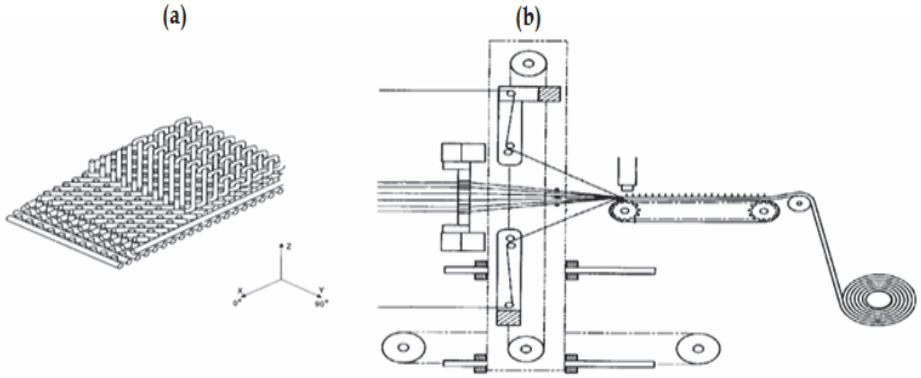

Fig. 21. Five-axis fabric (a) and newly developed weaving loom (b) (Uchida et al., 1999).

The process has bias rotating unit, filling insertion, Z-yarn insertion, warp, ±bias and Z-fiber feeding units, and take-up. A horizontally positioned bias chain rotates one bias yarn distance to orient the yarns, and filling is inserted to the fixed shed. Then Z-yarn rapier inserts the Z-yarn to bind all yarns together and all Z-yarn units are moved to the fabric fell line to carry out the beat-up function. The take-up removes the fabric from the weaving zone.
Mohamed and Bilisik (1995) developed multiaxis 3D woven fabric, method and machine in which the fabric has five yarn sets: ±bias, warp, filling and Z-fiber. Many warp layers are positioned at the middle of the structure. The ±bias yarns are positioned on the back and front faces of the preform and locked the other set of yarns by the Z-yarns as shown in Figure 22. This structure can enhance the in-plane properties of the resulting composites.

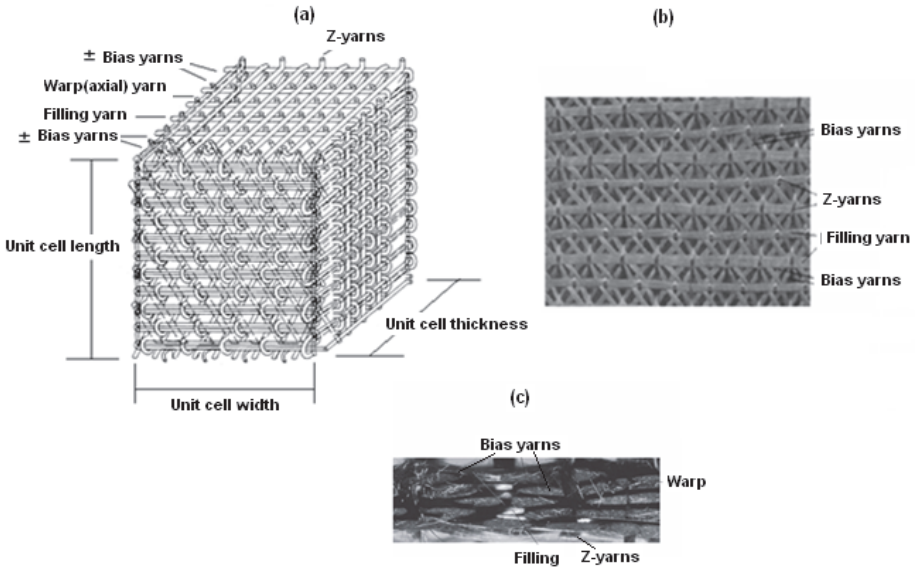

Fig. 22. The unit cell of multiaxis fabric (a), top surface of multiaxis small tow size carbon fabric (b) and cross-section of the multiaxis carbon fabric (c) (Mohamed and Bilisik, 1995; Bilisik, 2010a).

The warp yarns are arranged in a matrix of rows and columns within the required cross-sectional shape. After the front and back pairs of the bias layers are oriented relative to each other by the pair of tube rapiers, the filling yarns are inserted by needles between the rows of warp (axial) yarns and the loops of the filling yarns are secured by the selvage yarn at the opposite side of the preform by selvage needles and cooperating latch needles. Then, they return to their initial position as shown in Figure 23. The Z-yarn needles are inserted to both front and back surface of the preform and pass across each other between the columns of the warp yarns to lay the Z-yarns in place across the previously inserted filling yarns. The filling

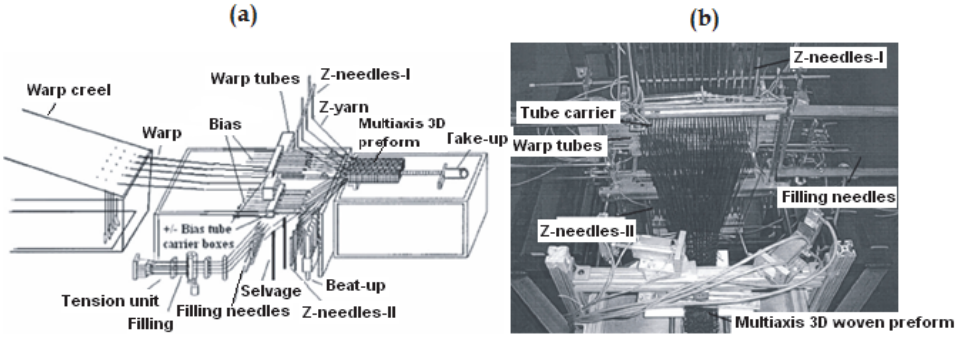

Fig. 23. Schematic view of multiaxis weaving machine (a) and top side view of multiaxis weaving machine (b) (Mohamed and Bilisik, 1995; Bilisik, 2010b).

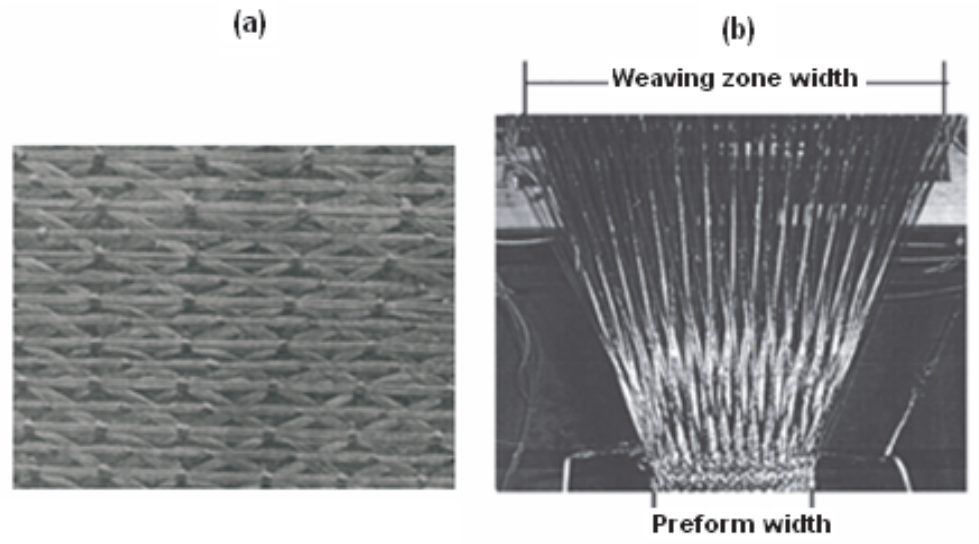

Fig. 24. Top surface of multiaxis large tow size carbon fabric (a) and weaving zone of the multiaxis weaving machine (b) (Bilisik, 2009a).

is again inserted by filling insertion needles and secured by the selvage needle at the opposite side of the preform. Then, the filling insertion needles return to their starting position. After this, the Z-yarns are returned to their starting position by the Z-yarn insertion needles by passing between the columns of the warp yarns once again and locking the bias yarn and filling yarns into place in the woven preform. The inserted filling, ±bias and Z-yarns are beaten into place against the woven line as shown in Figure 24, and a take-up system moves the woven preform.

Bilisik (2000) developed multiaxis 3D circular woven fabric, method and machine. The preform is basically composed of the multiple axial and radial yarns, multiple circumferential and the ±bias layers as shown in Figure 25. The axial yarns (warp) are arranged in a radial rows and circumferential layers within the required cross-sectional shape. The ±bias yarns are placed at the outside and inside ring of the cylinder surface. The filling (circumferential) yarns lay the between each warp yarn helical corridors. The radial yarns (Z-fiber) locks the all yarn sets to form the cylindrical 3D preform. A cylindrical preform can be made thin and thick wall section depending upon end-use requirements.

A process has been designed based on the 3D braiding principle. It has machine bed, ±bias and filling ring carrier, radial braider, warp creel and take-up. After the bias yarns are oriented at ±45˚ to each other by the circular shedding means on the surface of the preform, the carriers rotate around the adjacent axial layers to wind the circumferential yarns. The radial yarns are inserted to each other by the special carrier units and locked the circumferential yarn layers with the ±bias and axial layers all together. A take-up system removes the structure from the weaving zone. This describes one cycle of the operation to weave the multiaxial 3D circular woven preform. It is expected that the torsional properties of the preform could be improved because of the bias yarn layers.

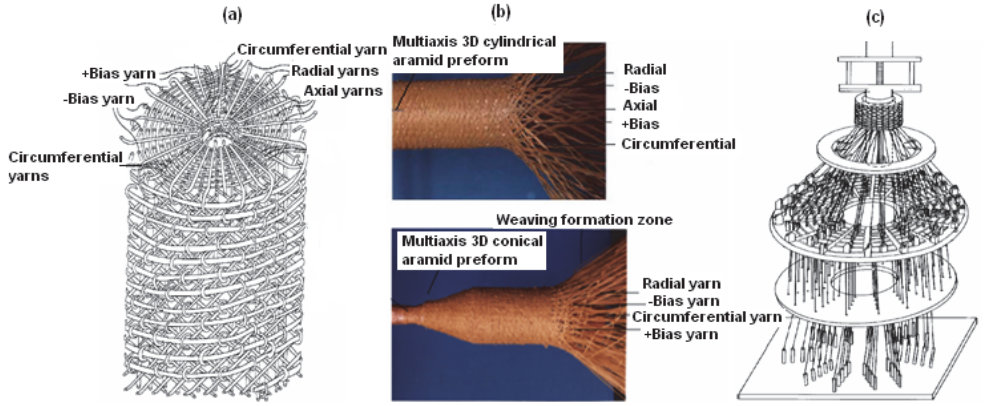

Fig. 25. The unit cell of multiaxis 3D circular woven fabric (a), Multiaxis 3D aramid circular woven fabric (b) and the weaving loom (c) (Bilisik, 2000; Bilisik, 2010c).

3.5 Multiaxis 3D knitted fabric

Wilkens (1985) introduced a multiaxis warp knit fabric for Karl Mayer Textilmaschinenfabric GmbH. The multiaxis warp knit machine which produces multiaxis warp knit fabric has been developed by Naumann and Wilkens (1987). The fabric has warp (0˚ yarn), filling (90˚ yarn), ±bias yarns and stitching yarns as shown in Figure 26. The machine includes ±bias beam, ±bias shifting unit, warp beam feeding unit, filling laying-in unit and stitching unit. After the bias yarn rotates one bias yarn distance to orient the fibers, the filling lays-in the predetermined movable magazine to feed the filling in the knitting zone. Then the warp ends are fed to the knitting zone and the stitching needle locks the all yarn sets to form the fabric. To eliminate the bias yarn inclination in the feeding system, machine bed rotates around the fabric. The stitching pattern, means tricot or chain, can be arranged for the end-use requirements.

Hutson (1985) developed a fabric which is similar to the multiaxis knitted fabric. The fabric has three sets of yarns: ±bias and filling (90˚ yarn) and the stitching yarns lock all the yarn sets to provide structural integrity. The process basically includes machine track, lay down fiber carrier, stitching unit, fiber feeding and take-up. The +bias, filling and –bias are laid according to yarn layer sequence in the fabric. The pinned track delivers the layers to the stitching zone. A compound needle locks the all yarn layers to form the fabric.

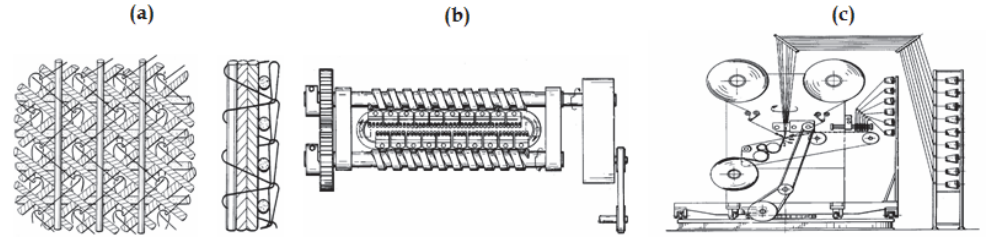

Fig. 26. Top and side views of multiaxis warp knit fabric (a) (Wilkens, 1985), bias indexing mechanism (b), warp knitting machine (c) (Naumann and Wilkens, 1987).

Wunner (1989) developed the machine produces the fabric called multiaxis warp knit for Liba GmbH. It has four yarn sets: ±bias, warp and filling (90° yarn) and stitching yarn. All layers are locked by the stitching yarn in which tricot pattern is used as shown in Figure 27. The process includes pinned conveyor bed, fiber carrier for each yarn sets, stitching unit, yarn creels and take-up.

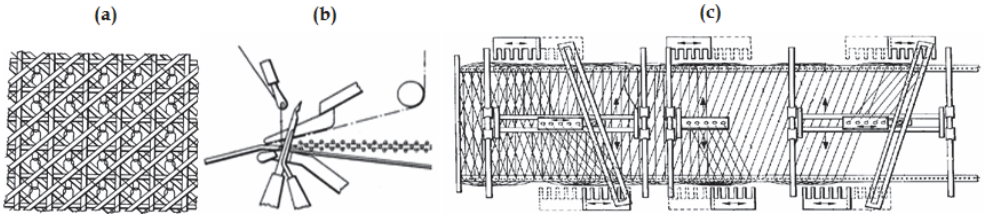

Fig. 27. Warp knit structure (a), stitching unit (b) and warp knit machine (c) (Wunner, 1989).

A multiaxis warp knit/braided/stitching type structure for aircraft wing-box has been developed by NASA/BOEING. The multiaxis warp knit fabric is sequence and cuts from 2 to 20 layers to produce a complex aircraft wing skin structure. Then, a triaxial braided tube is collapsed to produce a stiffener spar. All of them are stitched by the multi-head stitching machine which was developed by Advanced Composite Technology Programs. The stitching density is 3 columns/cm. The complex contour shape can be stitched according to requirements as shown in Figure 28. When the carbon dry preform is ready, resin film infusion technique is used to produce the rigid composites. In this way, 25 % weight reduction and 20 % cost savings can be achieved for aircraft structural parts. In addition, the structures have high damage tolerance properties (Dow and Dexter, 1997).

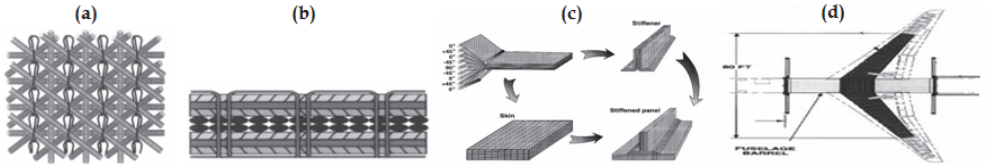

Fig. 28. Warp knit structure (a), multilayer stitched warp knit structure (b), layering-stitching-shaping (c) and application in airplane wing structure (d) (Dow and Dexter, 1997).

3.6 Comparison of fabric and methods

Kamiya et al. (2000) compared the multiaxis 3D woven fabrics and methods based on the bias fiber placement and uniformity, the number of layers and through-the-thickness (Z-yarn) reinforcements. It is concluded that the biaxial fabric/stitching, and the multiaxis knitted fabric and methods are readily available. It is recommended that multiaxis 3D woven fabrics and methods must be developed further. More general comparison is carried out and presented in Table 2. As seen in Table, multiaxis 3D fabric parameters are the yarn sets, interlacement, yarn directions, multiple layer and fiber volume fraction. The multiaxis 3D weaving process parameters are the bias unit, manufacturing type as continuous or part, yarn insertion, packing and development stage. It is realized that the triaxial fabrics and 3D woven fabrics are well developed and they are commercially available. But multiaxis 3D woven fabric is still early stage of its development.

Fabric	Yarn sets	Interlacement	Yarn directions	Multiple layer	Fiber volume fraction	Development Stage
Ruzand and Guenot, 1994	Four	Interlace, plain	Warp/weft/±Bias In-plane	Four layers	Low or Medium	Commercial stage
Anahara and Yasui, 1992 Uchide et al., 2000	Five	Non-interlace	Warp/Weft/±Bias /Z-yarn In-plane	More than four layers	Low	Prototype stage
Mohamed and Bilisik, 1995	Five	Non-interlace	Warp/Weft/±Bias /Z-yarn In-plane	More than four layers	Medium or High	Prototype stage
Khokar, 2002b	Five	Interlace, plain	Warp/Weft/±Bias /Z-yarn Out-of-plane	More than four layers	Low or Medium	Prototype stage
Bryn et al., 2004 Nayfeh et al., 2006	Four	Interlace, plain	Warp/Weft/±Bias In-plane	Four layers	Low or Medium	Prototype stage
Yasui et al., 1992	Four	Non-interlace	Axial/Circumferential + or – Bias	Five layers	Medium	Prototype stage
Bilisik, 2000	Five	Non-interlace	Axial/Circumferential/±Bias/Z-yarn	More than four layers	High	Early Prototype stage
Wilkens, 1985	Four	Non-interlace	Warp/Weft/±Bias /Stitched yarn	Four layers	Medium or High	Commercial stage
Wunner, 1989	Four	Non-interlace	Warp/Weft/±Bias /Stitched yarn	Four layers	Medium or High	Commercial stage

Table 2. Comparison of the multiaxis 3D fabrics and methods.

4. Multiaxis fabric properties and composites

4.1 Triaxial fabric

Scardino and Ko (1981) reported that the fabric has better properties to the bias directions compared to the biaxial fabric which has warp (0˚ yarn) and filling (90˚ yarn) to interlace each other at principal directions. Comparisons have revealed a 4-fold tearing strength and 5-fold abrasion resistance compared with a biaxial fabric with the same setting. Elongation and strength properties are roughly the same. Schwartz (1981) analyzed the triaxial fabrics

and compared with the leno and biaxial fabrics. He defined the triaxial unit cell and proposed the fabric moduli at crimp removal stage. It is concluded that the equivalency in all fabrics must be carefully defined to explore usefulness of the triaxial fabric. Schwartz (1981) suggested that when the equivalence is determined, triaxial fabric has better isotropy compare to the leno and plain fabrics. Isotropy can be considered on the fabric bursting and tearing strengths, shearing and bending properties. Skelton (1971) proposed the bending rigidity relations depending upon the angle of orientation. Triaxial fabric is independent of the orientation angle for bending. It is isotropic. Skelton (1971) noted that the 3-ply, 95 tex nylon and graphite yarns are used to do the comparable triaxial and biaxial fabrics. The stability of the triaxial fabric is much greater than that of an orthogonal fabric with the same percent open area. The triaxial fabric exhibits greater isotropy in its bending behavior and a greater shear resistance than a comparable orthogonal fabric.

4.2 General properties of 3D fabrics

The 3D woven fabrics are designed for composite structural component for various applications where structural design depends on loading conditions. Their basic parameters are fiber and matrix properties; total and directional volume fraction; preform types; yarn orientation in the preform and preform geometry. These parameters together with end-use requirements determine the preform manufacturing techniques. Many calculation techniques have also been developed by the aid of computer supported numerical methods in order to predict the stiffness and strength properties and understand the complex failure mechanism of the textile structural composite (Chou, 1992).

4.3 Multiaxis 3D and 3D orthogonal fabric process-property relations

Gu (1994) reported that the take-up rate of the 3D weaving effects the directional and total volume fraction of 3D woven fabrics. A high packing density can be achieved if the beat-up acts twice to the fabric formation line. Friction between brittle fiber such as carbon and parts of weaving machine must be kept low to prevent the filament breakages. Bilisik (2009a) identified the most related process-product parameters. These are the bias angle, width ratio, packing, tension and fiber waviness. The bias angle is the angle between bias fiber and warp fiber to the machine direction. The bias fiber is oriented by discrete tube-block movement. One tube-block movement is about 15˚–22˚ based on the process parameters. If it requires any angle between 15˚ and 75˚, the tube-block must be moved by one, two, or three tube distance. A small angle changes have been identified from the loom state to the out-of-loom state at an average of 46˚ to 42˚.

The multiaxis weaving width is not equal to that of the preform as shown in Figure 24. This difference is defined as the width ratio (preform width/weaving width). This is not currently the case in the 2D or 3D orthogonal weaving. The width ratio is almost 1/3 for multiaxis weaving. This is caused by an excessive filling length during insertion. It is reported that the fiber density and pick variations are observed. Some of the warp yarns accumulated at the edges are similar to those of the middle section of the preform. When the preform cross-section is examined, a uniform yarn distribution is not achieved for all the preform volume as shown in Figure 22. These indicate that the light beat-up did not apply enough pressure to the preform, and the layered warp yarns are redistributed under the initial tension. In part, the crossing of bias yarn prevents the Z-yarn from sliding the filling yarns towards the fabric line where the filling is curved. Probably, this problem is unique to

multiaxis weaving. Hence, it can be concluded that the rigid beat-up is necessary. This unique problem can be solved by a special type of open reed, if the width ratio is considered the main design parameter (Bilisik, 2010d). Dry volume fraction in the fabricated preform shows that increasing the fiber content in the warp or ±bias and filling fiber sets results in a high total preform volume fraction and porosity in the crossing points of fiber sets in the preform is reduced (Bilisik, 2009a).

Fiber waviness is observed during weaving at the bias and filling yarn sets. The bias yarn sets do not properly compensate for excessive length during biasing on the bias yarns. Variable tensioning may be required for each bias bobbin. The filling yarn sets are mainly related to the width ratio and level of tension applied. A sophisticated tensioning device may be required for filling yarn sets. On the other hand, the brittle carbon fiber characteristics must be considered. The bias fiber waviness is observed during weaving in the loom state. First of all, this is because of the variable tension in the bias fiber sets. Secondly, other fiber sets affect the bias waviness in the fabric formation zone. Thirdly, because of the rotatable creel used for the ± bias fiber sets, there is an excessive bias fiber on the preform surface. This causes the ± bias waviness, and it is eliminated by the compensation system connected to the rotational bias creels. The filling waviness mainly depends on the width ratio, and the related processing parameter is the selvage transfer system. The Z-fiber waviness depends on the Z-fiber path which is different during the half cycle of the weaving and another half cycle. This is because Z-fiber needles, means, open needle shed and it is a part of the processing parameter.

The parameters related with the multiaxis 3D circular woven fabric-process are bias orientation, radial and circumferential yarn insertion, beat-up and take-up. It is found out that the bias yarns are on the outer and inner surfaces of the structure form helical paths and there is a slight angle difference between them especially producing the thick wall preforms. There is a certain relation between preform density (fiber volume fraction), bias yarn orientation and take-up rate. More researches may be required to understand the relations between those processing parameters and preform structural parameters. In circumferential yarn insertion, the excessive yarn length during circumferential yarn insertion occurs due to diameter ratio (preform outer diameter/outermost ring diameter)which is not 1. The amount of the diameter ratio depends on the number of the rings. When the excessive circumferential yarn is not retracted, this causes waviness in the structure. However, there must be adequate tension applied on the circumferential yarns to get proper packing during beat-up. The circumferential yarn ends in each layer, which are equivalent to filling in the flat weaving, are six during insertion. This is resulted in high insertion rate. It is realized that there is a relation between the number of layers and radial yarn retraction. If the number of layers in the preform increases, yarn retraction in the radial carrier increases. The retraction must be kept within the capacity of the radial carrier. It is also observed that the tension level in the radial yarn is kept high compared to that of the circumferential yarns because of easy packing and applying tensioning force to the bias crossing points which resists the radial yarn movements during structure formation at the weaving zone. However, there is a certain relation between radial yarn tension and beat-up force. There must be an optimum tension level and beat-up force between them during the weaving for proper structural formation. It is observed that the radial yarn in the structure is at a slight angle. This depends partly on the structure wall thickness and partly on the weaving zone length during structure formation. In this point, the take-up rate is a crucially important process parameter. Also, a high beat-up force causes local yarn distortion in the structure. It

is understood that the beat-up unit in the experimental loom must be modified to get consistent volume fraction, especially when the brittle fibers are used. It is understood that two types of take-up are necessary. A part manufacturing needs mandrel and is adapted to the take-up unit. A continuous manufacturing needs a pair of coated cylinders. For both take-up units, the important process parameter is take-up rate during delivering the fabric from the weaving zone. The rate affects the fabric volume fraction and the bias angle, and relations between preform structural parameters and processing parameters must be analyzed. This is addressed for future analytical research in take-up rate (Bilisik, 2010c).

4.4 Multiaxis 3D and 3D orthogonal fabric composites

Cox et al. (1993) stated that low volume fraction 3D woven preform may be performed well under the impact load compare to that of the tight volume fraction 3D woven preform. Dickinson (1990) studied on 3D carbon/epoxy composites. It is realized that the amount of Z-yarn and the placement of Z-yarn in the 3D woven preform influence the in-plane properties of the 3D woven structure. When the Z-yarn volume ratio increases, the in-plane properties of the 3D woven structure decrease. The placement of the Z-yarn in unit cell of the 3D woven fabric decreases, failure mode of the 3D woven composite changes and a local delamination occurs. Babcock and Rose (2001) explained that under the impact load, 3D woven or 2D fabric/stitched composites confines the impact energy due to the Z-yarn.

A five-axis 3D woven fabric composite was characterized by Uchida et al. (2000). Tensile and compression results of multiaxis weave and stitched 2D laminate are comparable. Open hole tensile and compression results of multiaxis woven structure look better compared to that of the stitched 2D laminated structure. Compression After Impact (CAI) test shows that the 5-axis 3D woven composite is better than that of the stitched 2D laminated structure. Also, damaged area in terms of absorbed energy level is small at the 5-axis 3D woven composite compared to that of the stitched 2D laminated composite. The multiaxis 3D knitted fabric suffers from limitation in fiber architecture, through-thickness reinforcement due to the thermoplastic stitching thread and three dimensional shaping during molding.

For this reasons, multiaxis 3D knitted fabric is layered and stitched to increase damage resistance and to reduce production cost (Dow and Dexter, 1997).

Another experimental research was conducted on multiaxis and orthogonal 3D woven composites by Bilisik (2010d). Bending strength and modulus of the multiaxis and orthogonal woven composites were 569 and 715 MPa, and 43.5 and 50.5 GPa, respectively. Bending strength and modulus of the 3D orthogonal woven composites were higher than those of multiaxis 3D woven composites by about 20% and 14%, respectively. This indicates that the ±bias yarn orientations on both the surfaces of multiaxis woven composite cause a reduction in bending properties. Bending failure in the multiaxis 3D woven composite is shown in Figure 29, where there is a bias yarn breakage at the outside surface of the warp side and a local delamination is seen between the filling and ±bias yarns in places where it is restricted by Z-yarn. In the 3D orthogonal woven composite, bending failure occurs at the outside surface of the structure. Initially, matrix and yarn breakages are in normal direction of yarn but later on these breakages turns and propagates in parallel to the yarn direction. Crack propagation is restricted by Z-yarn.

Interlaminar shear strengths were determined as 47.1 MPa for multiaxis woven composite and as 52.2 MPa for orthogonal woven composite. Interlaminar shear strength of the 3D orthogonal woven composite was higher than that of multiaxis 3D woven composites

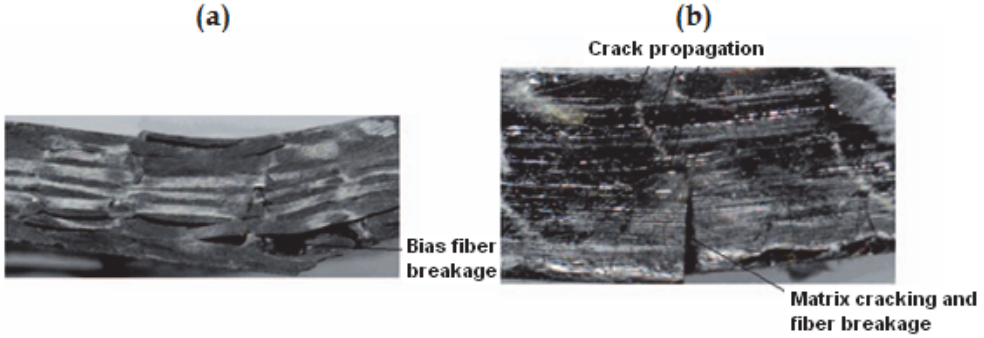

Fig. 29. Bending failure on the warp side of the multiaxis 3D woven composite (a) and bending failure on the warp side of the 3D orthogonal woven composite (b). Magnifications: x6.7 (a), x18 (b) (Bilisik, 2010d).

almost by 10%. The ±bias yarns have no considerable effect on interlaminar shear strength of the multiaxis 3D woven composite. There is a shear on directional yarn breakages mainly at bias and warp yarns and some local yarn–matrix splitting on the warp side of the structure. On the surface, local yarn crack occurs throughout the normal direction of the warp yarn. In the 3D orthogonal woven composite, yarn and matrix cracks are observed at the shearing load on warp side and filling yarn direction of the surface of the structure as shown in Figure 30.

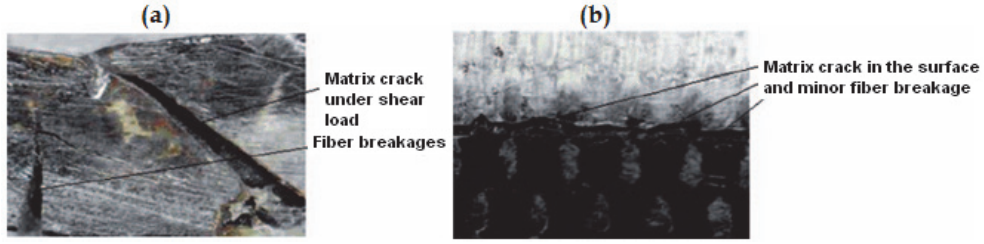

Fig. 30. Interlaminar shear failure on the warp side (a) and on the outside surface (b) of 3D woven composite. Magnifications: x20 (a), x6.7 (b) (Bilisik, 2010d).

In-plane shear strength and modulus of the multiaxis and orthogonal woven composites were measured as 137.7 and 110.9 MPa, and 12.1 and 4.5 GPa, respectively. In-plane shear strength and modulus of the multiaxis 3D woven composites were higher than those of multiaxis 3D woven composites almost by 25% for in-plane shear strength and 170% for in-plane shear modulus due to the addition of the ±bias yarns on the surface of the multiaxis 3D woven composites. There is a local delamination on the warp-filling yarns and local breakages on ±bias yarns through-the-thickness direction and surface of the multiaxis 3D woven composites for in-plane shear failure as seen in Figure 31. For 3D orthogonal woven composite, there is a local yarn breakage between the warp and filling yarns and a local delamination between the warp and filling yarns through-the-thickness direction.

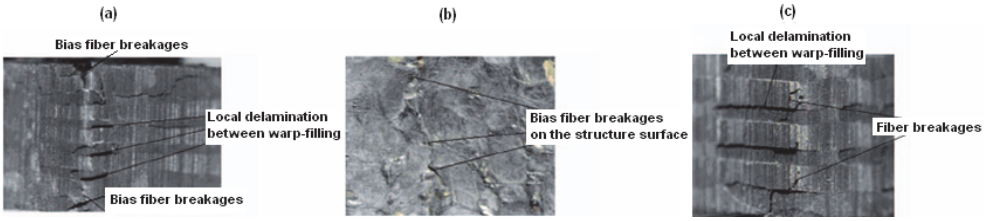

Fig. 31. In-plane shear failure (a), in-plane shear failure at surface (b) of the multiaxis 3D woven composite and in-plane shear failure (c) of the 3D orthogonal woven composite. Magnifications: x13 (a), x6.7 (b), x18 (c) (Bilisik, 2010d).

			Carbon Fiber	**Epoxy Matrix**
			Thornel™ T-300 PAN	(Tactix™ 123)[3]
Material Properties	Tensile Strength (MPa)		3450	76.50
	Tensile Modulus (GPa)		230	3.45
	Modulus of Rigidity (GPa)		88.50	1.30
	Elongation (%)		1.62	5.70
	Poisson's ratio (v)		0.27	0.31
	Density (g/cm^3)		1.76	1.16
			Preform 1	**Preform 2**
Bias angle (°), (measured)			30°	40°
Fractional volume (%), (measured at preform)	+Bias		9.43	11.7
	–Bias		9.43	11.7
	Warp		10.5	13.7
	Filling		5.42	4.77
	Z-yarn		3.67	5.61
	Total Volume (%)		38.4	47.5
Elastic constants (Calculated)	Modulus of elasticity (GPa)	E_{11}	48.33	48.00
		E_{22}	19.87	23.85
		E_{33}	9.86	14.24
	Modulus of rigidity (GPa)	G_{12}	10.42	15.65
		G_{23}	2.78	3.47
		G_{31}	2.80	3.47
	Poisson's ratio	v_{12}	0.446	0.530

Table 3. Multiaxis 3D woven preform elastic constants from multiaxis 3D weaving (Bilisik & Mohamed, 2010).

Gowayed and Pastore (1992) reviewed on computation methods for 3D woven fabric. The developed analytical methods are stiffness averaging, fabric geometry and inclination models. They are based on the classical lamination theory, and micro mechanic approach is considered. Bilisik & Mohamed (2010) applied stiffness averaging method to multiaxis 3D

carbon/epoxy composites. Table 3 shows the directional tensile and shear elastic constants of multiaxis carbon/epoxy composite structure. It is demonstrated that yarn orientation in the preform influences the shearing properties of the multiaxis 3D woven composite structure.

4.5 Applications

Traditional as well as contemporary fabric structures are increasingly gaining acceptance due to their attractive specific performances and low cost in use for the technical textiles (Hearle, 1994) such as defense and civilian areas as transportation, automobile, energy and marine industries (Mouritz et al., 1999). Biaxial, triaxial and more sophisticated multiaxis 3D fabric structures are used as structural elements in medical, space and rocket propulsions (Beyer et al., 2006). Examples of these elements are plate, stiffened panel and beams and spars, shell or skin structures (Yamamoto and Hirokawa, 1990), hip and medical devices and prosthesis (Donnet and Bansal, 1990; Bilisik, 2009b). Recently, Atkinson et al., (2008) explored that using the nano based high modulus fibers in 3D fabrics results 10-fold increase of their mechanical properties.

5. Conclusion

3D fabrics, methods and techniques have been reviewed. Biaxial 2D fabrics have been widely used as structural composite parts in various technical areas. However, composite structures of biaxial 2D fabrics have delamination between layers due to the lack of fibers. Biaxial methods and techniques are well developed. Triaxial fabrics have delamination, open structure and low fabric volume fractions. But, in-plane properties of the triaxial fabrics become homogeneous due to the ±bias yarn orientations. Triaxial weaving methods and techniques are also well developed. 3D woven fabrics have multiple layers and no delamination due to the Z-fibers. But, the 3D woven fabrics have low in-plane properties. 3D weaving methods and techniques are commercially available. Multiaxis 3D knitted fabrics which have four layers and layering is fulfilled by stitching, have no delamination and in-plane properties are enhanced due to the ±bias yarn layers. But, it has a limitation for multiple layering and layer sequences. Multiaxis 3D knitting methods and techniques have been perfected. Multiaxis 3D woven fabrics have multiple layers and no delamination due to the Z-fibers and in-plane properties enhanced due to the ±bias yarn layers. Also, layer sequence can be arranged based on the requirements. But, multiaxis 3D weaving technique is at its early development stages and needs to be fully automated. This will be the future technological challenge in this area.

6. Acknowledgements

The author thanks the Research Assistant Gaye Yolacan for her help during the preparation of this book chapter.

7. References

Abildskow, D. (1996). *Three dimensional woven fabric connector*, US Patent 5533693.

Anahara, M. & Yasui, Y. (1992). *Three dimensional fabric and method for producing the same*, US Patent 5137058.

Atkinson, K. R., Skourtis, C. & Hutton, S. R. (2008). Properties and applications of dry-spun carbon nanotube yarns, *Advances in Science and Technology*, 60: 11-20.

Babcock, W. & Rose, D. (2001). Composite preforms, *The AMPTIAC Newsletter*, 5(1): 7-11.

Beyer, S., Schmidth, S., Maidi, F., Meistring, R., Bouchez, M. & Peres, P. (2006). Advanced composite materials for current and future propulsion and industrial applications, *Advances in Science and Technology*, 50: 178-171.

Bilisik, A. & Mohamed M. H. (1994). Multiaxis 3D weaving machine and properties of Multiaxial 3D woven carbon/epoxy composites, *The 39th International SAMPE Symposium*, Anaheim, USA.

Bilisik, K. (1991). *Three dimensional (3D) weaving and Braiding*, PhD Thesis, University of Leeds, Leeds, UK.

Bilisik, K. (2000). *Multiaxial three dimensional (3D) circular woven fabric*, US Patent 6129122.

Bilisik, K. (2009a). Multiaxis three dimensional (3D) flat woven fabric and weaving method: Feasibility of prototype Tube Carrier Weaving, *Fibres and Textiles in Eastern Europe* 17(6): 63-69.

Bilisik, K. (2009b). Multiaxis Three-Dimensional (3-D) Woven and Braided Preform Unit Cells and Implementation of Possible Functional Characterization for Biomedical Applications, *Artificial Organs*, 33(8): A101.

Bilisik, K. (2010a). Multiaxis 3D Weaving: Comparison of Developed Two Weaving Methods-Tube-Rapier Weaving Versus Tube-Carrier Weaving and Effects of Bias Yarn Path to the Preform Properties, *Fibers and Polymers*, 11(1): 104-114.

Bilisik, K. (2010b). Dimensional Stability of Multiaxis 3D Woven Carbon Preform, *Journal of the Textile Institute*, 101(5): 380–388.

Bilisik, K. (2010c). Multiaxis Three Dimensional (3D) Circular Woven Preforms-Radial Crossing Weaving and Radial In-Out Weaving: Preliminary investigation of feasibility of weaving and methods, *Journal of the Textile Institute*, 101(11): 967-987.

Bilisik, K. (2010d). Multiaxis 3D woven preform and properties of multiaxis 3D woven and 3D orthogonal woven carbon/epoxy composites, *Journal of Reinforced Plastics and Composites*, 29(8): 1173-1186.

Bilisik, K. & Mohamed, M. H. (2010). Multiaxis Three Dimensional (3D) Flat Woven Preform-Tube Carrier Weaving, *Textile Research Journal*, 80(8): 696-711.

Bhatnagar, A. & Parrish, E. S. (2006). *Bidirectional and multiaxial fabric and fabric composites*, US Patent 7073538.

Brandt J., Drechsler, K. & Filsinger, J. (2001). Advanced textile technologies for the cost effective manufacturing of high performance composites, *RTO AVT Specialist Meeting on Low Cost Composite Structures*, Norway, RTO-MP-069(II).

Bryn, L., Islam, M. A., Lowery, W. L. & Harries, H. D. (2004). *Three-dimensional woven forms with integral bias fibers and bias weaving loom*, US Patent 6742547.

Chen, X. (2007). *Technical aspect: 3D woven architectures*, NWTexNet 2007 Conference, Blackburn, UK.

Chou, T. W. (1992). *Microstructural Design of Fiber Composites*, UK: Cambridge University Press.

Cox, B. N., Dadkhah, M. S., Morris, W. L. & Flintoff, J. G. (1993). Failure mechanisms of 3D woven composites in tension, compression and bending, *ACTA Metallurgica et Materialia* 42: 3967-84.

Cox B.N. & Flanagan, G. (1997). *Handbook of analytical methods for textile composites*, NASA Contractor Report 4750.

Crawford, J. A. (1985). *Recent developments in multidirectional weaving*, NASA Publication No. 2420, pp. 259-269.

Deemey, S. (2002). The new generation of carpet weaving machines combines flexibility and productivity, *Technical notes*, Van de Wiele Incorporations.

Dexter, H. B. & Hasko G. H. (1996). Mechanical properties and damage tolerance of multiaxial warp-knit composites, *Composites Science and Technology* 51: 367-380.

Dickinson, L. C. (1990). *Evaluation of 3D woven carbon/epoxy composites*, MSc Thesis, NCSU, USA.

Donnet, J. B., Bansal, R. C. (1990). *Carbon Fibers*, Marcel Dekker Inc., New York, USA.

Dow, M. B. & Dexter, H. B., (1997). *Development of stitched, braided and woven composite structures in the ACT Program and at Langley Research Center (1985 to 1997). NASA/TP-97-206234.*

Dow, N. F. (1969). *Triaxial fabric*, US Patent 3446251.

Dow, N. F. & Tranfield G. (1970). Preliminary investigations of feasibility of weaving triaxial fabrics (Doweave), *Textile Research Journal* 40(11): 986-998.

Edgson, R. & Temple, S. (1998). *Fibre preforms for structural composite components*, US Patent 5783279.

Evans, R.G. (1999). *Air jet machine and diagonal Z loop fabric pattern for three dimensional fabrics*, US Patent 5924459.

Fukuta, K., Nagatsuka, Y., Tsuburaya, S., Miyashita, R., Sekiguti, J., Aoki, E. & Sasahara, M. (1974). *Three dimensional fabric, and method and loom construction for the production thereof*, US Patent 3834424.

Goldstein, A. D. (1939). *Textile material*, US Patent 2244835.

Gowayed, Y. A. & Pastore, C. M. (1993). Analytical techniques for the prediction of elastic properties of textile reinforced composites, *Mechanics of composite materials*, 28(5): 393-408.

Gu, P. (1994). *Analysis of 3D woven preforms and their composite properties*, PhD Thesis, NCSU, College of Textiles, Raleigh.

Hearle, J. W. S. (1994). Textile for composites, Textile Horizons, 11: 11-15.

Homma, K. & Nishimura, A. (1992). *Reinforcing woven fabric and preformed material, fiber reinforced composite material and beam using it*, US Patent 5100713.

Hutson, H. K. (1985). *Biased multilayer structural fabric composites stitched in a vertical direction*, US Patent 4550045.

Jonas, P.J. (1987). *Method for fastening aircraft frame elements to sandwich skin panels covering same using woven fiber connectors*, US Patent 4671470.

Kamiya, R., Cheeseman, B. A., Popper, P. & Chou, T. W. (2000). Some recent advances in the fabrication and design of three dimensional textile preforms: A review, *Composite Science and Technology* 60: 33-47.

Kazumara, M. (1988). *Tetraxial fabric and weaving methods*, European Patent 0263392.

Khokar, N. (2001). 3D-Weaving: Theory and Practice, *Journal of the Textile Institute*, 92(2): 193-207.

Khokar, N. (2002a). Noobing: A nonwoven 3D fabric-forming process explained, *Journal of the Textile Institute*, 93(1): 52-74.

Khokar, N. (2002b).*Woven 3D fabric material*, US Patent 6338367.

Kimbara, M., Fukuta, K., Tsuzuki, M., Takahama, H., Santo, I., Hayashida, M., Mori, A. & Machii, A. (1991). *Three dimensional multi-axis fabric composite materials and methods and apparatuses for makinf the same*, US Patent 5076330.

King, R. W. (1977). *Three dimensional fabric material*, US Patent 4038440.

Ko, F.K. & Chou, T.W. (1989). *Textile Structural Composites*, New York: Elsevier.

Lida, S., Ohmori, C. & Ito, T. (1995). *Multiaxial fabric with triaxial and quartaxial portions*, US Patent 5472020.

Mamiliano, Dini. (1994). *Tetraxial fabric and weaving machine for its manufacture*, US Patent 5351722.

Mohamed, M. H. (1990). Three dimensional textiles, *American Scientist* 78: 530-541.

Mohamed, M. H. & Bilisik, A. K. (1995). *Multilayered 3D Fabric and Method for Producing*, US Patent 5465760.

Mohamed, M. H. & Zhang, Z. H. (1992). *Method of forming variable cross-sectional shaped three dimensional fabrics,* US Patent 5085252.

Mood, G. I. (1996). *Multiaxial yarn structure and weaving method*, US Patent No 5540260.

Mouritz, A. P., Bannister, M. K., Falzon, P. J. & Leong K. H. (1999). Review of applications for advanced three dimensional fiber textile composites, *Composites Part A: Applied Science and Manufacturing*, 30: 1445-1461.

Naumann, R. and Wilkens, C. (1987). *Warp knitting machine*, US Patent 4703631.

Nayfeh, S. A., Rohrs, J. D., Rifni, O., Akamphon, S., Diaz, M. & Warman, E. (2006). *Bias Weaving Machine*, US Patent No. 7077167.

Ruzand, J. M. & Guenot, G. (1994). *Multiaxial three-dimensional fabric and process for its manufacture*, International Patent WO 94/20658.

Scardino, F. L. & Ko, F. K. (1981). Triaxial woven fabrics: Part I Behavior under tensile, shear and burst deformations, *Textile Research Journal*, 51(2): 80-89.

Schwartz, P. (1981). The mechanical behavior of fabrics having three, non-orthogonal thread directions (triaxial) and the equivalence of conventional fabrics, *PhD thesis*, NCSU.

Skelton, J. (1971). Triaxial woven fabrics: Their structure and properties, *Textile Research Journal*, 41(8): 637-647.

Uchida, H., Yamamoto, T., Takashima, H., Otoshima, H., Nishiyama, S. & Shinya, M. (1999). *Three dimensional weaving machine*, US Patent 6003563

Uchida, H., Yamamoto, T. & Takashima, H. (2000). Development of low cost damage resistant composites, In: *Muratec Murata Machinery Ltd*, 14 May 2008, Available from: http://www.muratec.net/jp.

Wilkens, C. (1985). *Warp knitted ware with reinforcing thread*, US Patent 4518640.

Wunner, R. (1989). *Apparatus for laying transverse weft threads for a warp knitting machine*, US Patent 4872323.

Yamamoto, T. & Hirokawa T. (1990). Advanced joint of 3D composite materials for space structure, *35th International Sampe symposium*, pp. 1069-1077.

Yasui, Y., Anahara, M. & Omori, H. (1992). *Three dimensional fabric and method for making the same*, US Patent 5091246.

Part 3

Design and Appearance of Woven Fabrics

6

Functional Design of the Woven Filters

Cioară Lucica and Cioară Ioan
Technical University "Gheorghe Asachi" Iassy/Faculty of Textiles and Leather Engineering
România

1. Introduction

The filtration process implies the physical separation of one or more components of a fluid that passes through or over a barrier which is permeable to only one or some of the fluid components. Therefore the fundamental element of the filtration process is the barrier which is permeable to only a part of the suspension or the solution applied to filtration. This barrier is named filter medium and the mechanical structure used to support it is named filter. The statement the heart of any filter is the filter medium is fully justified. The most ingenious filter is useless if does not have an adequate filter medium. A specific shape of a filter can use a wide variety of filter mediums to do the same or different separation.
Function of their purpose filtration processes are used to separate solid – gas, solid – liquid, liquid – liquid or solid – solid mixtures. Solid – gas separation domain is represented mainly by air filters also including gas processing. Solid – liquid separation is the usual area of mechanical filters from which a relevant part is the inertial separators. Liquid – liquid and solid – solid separations are complex and specialized areas of filters or separators typology.
Industrial installations frequently use as filtration media technical textiles obtained by weaving i.e. woven filters (Adanur, 1995; Harracks&Anand, 2000). To respond to imposed exigencies by the use in industrial installations, the fabrics utilized as filter media must comply with a wide range of demands which are for the most part determined by the fabrics own structural characteristics and partially by the fabric finishing methods (Marchiş et al.,1991; Cioară et al., 1991; L.Cioară&I.Cioară, 2001). Among these requirements the following are mentioned:

- high filtration capacity, high degree of filtered elements purification and minimum hydraulic resistance;
- good mechanical resistance and stability to chemical, thermal, corrosive and biological agents;
- a high degree of the filtering surface smoothness allowing an easy and total residue separation and filter regeneration;
- a firm and homogenous structure allowing a high filtering process fineness and quality throughout the service life of the filtering element.

The fields having a vital requirement for woven textile media filtration are in a continuous diversification and specialization. It is widely known that technical textiles represent viable alternatives for all economic and social life sectors. In this context the woven textiles filter media, a significant representative of technical textiles, find their application in various

fields from automobiles to space industries, in construction, in agriculture and environment protection (Adanur, 1995; Harracks&Anand, 2000).
Filtration processes are accomplished following two basic principles: depth filtration and surface filtration (Medar&Ionescu, 1986). Both forms of the filtering process imply the simultaneous occurrence, in different ratio of two physical phenomena:

- direct particles retention – do to this process filter medium stand for a mechanical barrier for particles bigger than the restriction;
- adsorption – particles retention by electrostatic forces or molecular attraction of the filter medium.

Principle of **depth filtration** and the specific mechanisms through which the particles are retained are shown in Figure 1.a. Direct interceptions take place when particles of a certain size are passing through larger pores and are trapped in the filter medium structure when meet smaller pores. Inertial forces cause particles to hit filter medium fibers the particles retention being obtained due to their penetration into the body of fibers or due to the fiber deformation.

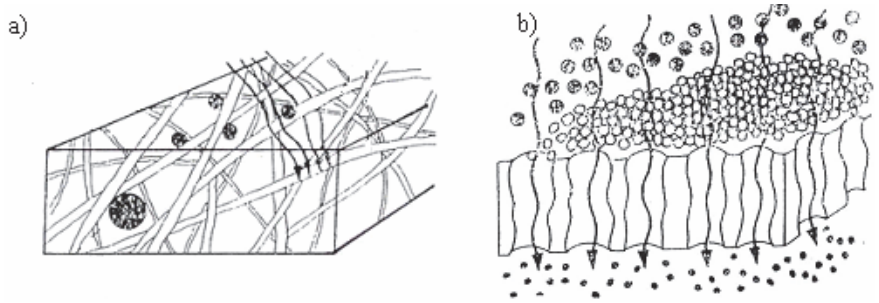

Fig. 1. Filtrations mechanisms

Inertial impaction is predominant when high fluid velocity or very dense filter medium is present. This type of filtration mechanism is most predominant when high gas velocity and/or dense packing of the filter media is present. Inertial impaction occurs also when an abrupt change in streamline take place. In this case the particle, due to its inertia, will continue along its original path and could be retained by the filter medium
Adsorption phenomena determine the attraction of small size particles by the filter medium fibers. The adsorption is favored by particles Brownian movement of the particles during the filtration process. Textile filter media that work by the depth filtration principle are: nonwoven fibrous layers, simple textiles made of spun or filamentary yarn, pile or felted, composite fabrics made as semi double, double or multiple layers structures.
Surface filtering implies that particles larger than the pore size are retained on the filter medium surface (Figure 1.b) Due to the adsorption forces particles smaller than pore size can be retained along the pore wall, reducing its transverse dimension causing blocked pores and filter medium clogging as a result. In the first phase of the clogging nominal fineness of filtration is reduced, the pressure difference increases and a combination of surface filtration with a pseudo-depth filtration take place (occurs).
Later on, as the degree of clogging increases, fluid flow through the filter medium is significantly reduced. Textile filter media which operate by surface filtration are monofilament yarns woven textiles.

The comparative analysis of the woven filter media working according to these two principles highlights their advantages and disadvantages (Table 1). In all cases the filter media is considered within the conventional filtering range ensuring the separation of particles over 1 μm in size (Rouette, 2001).
Filtration fineness is influenced by filter medium structure. Pore size distribution is Gaussian for filter media that operates on depth filtering principle and covers a narrower range around the mean value for filter media that works on surface filtration principle. As a result, the particles retention set in the case of surface filtration is much more restrictive than in the case of depth filtration.

Depth filtration		**Surface filtration**	
advantages	disadvantages	advantages	disadvantages
low cost	hard to clean	possibility of cleaning and reuse	high cost
high efficiency	filter medium particles migration is possible	filter medium particles migration is excluded	low initial efficiency
high capacity to retain impurities	filtering performance is depending on the fluid viscosity	fatigue resistance, resistance to temperature or corrosive agents	limited capacity to retain impurities
	relatively large pressure drop	lower pressure drop	
	increased clogging	reduced clogging	

Table 1. Comparative analysis of filter media

2. Analysis of woven filter media functionality

Woven filter media are products that are differentiated by structure and properties in strict accordance with the requirements and particularities of the process in which they operate. The filter medium structure is necessarily associated with the principle used to separate the mixture particles (surface filtration or depth filtration).

2.1 Features woven filter media

The result of filter medium different properties combination sets up its quality and respectively its functionality. For an objective assessment of filter media quality (functionality) three groups of properties have been identified as follows:

- properties related to filter medium mounting system type. Those properties are important for the mechanical implementation of the filter respectively the filter medium set up on the support frame. Among the key properties of this group stated: stiffness, tensile strength, tear resistance, burst strength, abrasion resistance, vibration stability, elongation, the edges stability;
- properties related to the application type that are taking in consideration the compatibility between the filter medium and the processed medium. In this category falls the following properties: chemical stability, thermal stability, biological stability, dynamic stability, adsorption, absorption, operational safety and security, electrostatic characteristics, reuse capability, price;

- properties addressing specific filtrations process particularities underlining the filter medium capacity to comply with required demands. The most important properties of this group are: the smallest particle retained, retention efficiency, the structure of filter media, particle shape, filtering mechanisms used, flow resistance, porosity of filter media, permeability, tendency to clog, filter-cake discharge characteristics.

Symbol	Function name	Technical dimension	Function type
F1	to separate the phases of a heterogeneous mixture	porosity permeability	primary, objective, necessary, general
F2	to ensure filtration fineness	shape, size and pore distribution	primary, objective, necessary, specific to filter principles
F3	to be dimensionally stable during operation	elastic and residual tensile strain	primary, objective, necessary, specific to filter principles
F4	to withstand the action of mechanical factors during operation	tensile strength burst resistance	primary, objective, necessary, specific to filtration process
F5	to withstand the erosive effects of the environment	chemical resistance	primary, objective, necessary, specific to filtered fluid
F6	to ensure filtration velocity	active filtration surface	primary, objective, necessary, specific to filter principle
F7	to withstand the erosive action of the filtered fluid	abrasion resistance	secondary, objective, necessary, specific to filtration process
F8	mechanical durability	fatigue resistance	secondary, objective, necessary, specific to filter type
F9	shouldn't clog	filter structure, pores shape	secondary, objective, necessary, specific to filter type
F10	easy to clean and rebuild	filter structure raw material	secondary, objective, necessary, specific to filter type
F11	easy to fabricate	filter structure, fabrication technology	secondary, objective, necessary, specific to filter type
F12	easy to install and replace	filter shape and dimensions	secondary, objective, necessary, specific to filter type

Table 2. The functions of woven filter media

For each filter medium, depending on field of use and the requirements in service only some of these properties are necessary. As a result, the design of woven textiles intended to be used as filter media must be made in accordance with functionality criteria ensuring priority to the properties requested by the process utilized.
The relation structure – properties – use value is the design criterion for woven filters. Value engineering is a method of research and systemic design according to which the functions of the product studied (filter medium) must be designed and carried out with minimum expenditure in terms of highest quality, reliability and performance (Condurache et al., 2004). Value engineering instrumentation methodology implies the following stages:

- functional analysis: answers the questions what is and what the product does; the function list of the analyzed product is completed;
- classification of functions: answers the question how important the function is and how well meets the user requirements; function's relative importance, intrinsic and technical dimension terms are ascertained; functions classification for the analyzed product is finalized;
- product design or redesign based on required functions.

Function is considered an essential attribute of the studied product expressed in terms of medium and user. In the same time, the function can be regarded as a characteristic of the product that determines a particular utility. The list of function classification is the starting point of value engineering studies.
Product functions are determined by importance, the measurement method, its contribution to achieving use value and the degree of generality.
Drawing up the list of filter medium functions is based on defining the filter medium and the conditions under which it works. In principle woven filters are intended to be used in filtration.
Based on such considerations the functions considered to be necessary for the filter medium, their technical elements of assessment and their typology classified by standard criteria are shown in Table 2 (I.Cioară&L.Cioară, 2009).

2.2 The hierarchy functions woven fabrics filter

After developing the list of all functions their classification is done in order to establish the importance and weightiness of each function in rapport to all functions the product offers. The classification of the function is done using Value Engineering methods such as the Expertise Method or Imposed Decision Method. Regardless of the method used the classification is done considering all filter media functions or, selectively, group of functions, classified according to their typology.
Imposed Decision Method presents a high degree of objectivity (Condurache et al., 2004). To apply this method the following steps must be achieved: comparing the functions in pairs, calculating the importance coefficient for each function and classifying the functions by their importance coefficient value. By comparing the environmental functions as a filter to obtain decisions (0-1), (0.5-0.5) or (1-0). Scoring are considered: 0 considered less important function, 1 for the function considered more important, compared to 0.5 when the functions are valued as important. D total number of decisions resulting from the comparison of the n features of the filter is calculated with:

$$D = C_n^2 = \frac{n \cdot (n-1)}{2} \tag{1}$$

I importance factor for each sample is calculated function the relationship:

$$I = \frac{N}{D} \tag{2}$$

where: N is the sum of points awarded;
D - total number of decisions.
The filter media 12 functions obtained by weaving defined in Table 2 were divided into two groups: 6 primary and 6 secondary functions. Apply for group relationship of the main functions, which will be used to design, to establish the number of decisions as follows:

$$D = C_6^2 = \frac{6 \cdot (6-1)}{2} = 15 \tag{3}$$

Function	**Decisions**															**N**	**I**
	1	2	3	4	5	6	7	8	9	10	11	12	13	14	15		
F1	0.5	0.5	1	1	0.5											3.5	0.233
F2	0.5					0.5	1	1	0.5							3.5	0.233
F3		0.5				0.5				0.5	0.5	0.5				2.5	0.166
F4			0				0			0.5			0.5	0		1	0.066
F5				0				0			0.5		0.5		0	1	0.066
F6					0.5				0.5			0.5		1	1	3.5	0.233

Table 3. Coefficient calculation Ranking

The name of the function	**Specific technical dimension**	**Structural characteristics of fabric**
to separate the phases of a heterogeneous mixture	pore size	fineness and density of yarns
to ensure filtration fineness	pore shape and distribution, filter medium fineness	fineness and density of yarns, weave
to ensure filtering velocity	adequate filtering active area	fineness and density of yarns
to be dimensionally stable during operation	structural and mechanical characteristics of yarn and fabric	the mechanical characteristics of the of yarns
to withstand the action of mechanical factors during operation	tensile strength burst resistance	the mechanical characteristics of the of yarns
to withstand the erosive effects of the environment	chemical resistance	the nature of raw material

Table 4. Priority functions of the filter media and their assessment criteria

In Table 3 are comparative analysis, two by two principal functions. The last column of the table are shown the importance scores and values of each corresponding functions. Based on

the values of the coefficients of importance to obtain the hierarchy of the main functions in the following sequence: F1, F2, F6, F3, F4, F5.
Priority functions set out in this way are taken into consideration when designing or redesigning filter media weaved in accordance with functionality criteria. In this respect the assessing criteria of woven filter media priority functions are summarized in Table 4.
The parameters specific to the woven filter with simple structure that will provide functional design criteria are: the relative porosity, pore shape and size, the pore distribution, the active filtering surface.
The structural characteristics of woven fabric,which determine the parameters of filter fabric are: yarns count, thread density and weave.

3. Structural and functional characteristics of the fabric filters with simple structure

Characterization and use of the fabric estimating filters with simple structure can be made by means of specific structural and functional characteristics (Behera, 2010; Cioară, 2002). Among these characteristics are mentioned: porosity, pore size and architecture, active filtering surface environment and filter fineness.

3.1 Porosity

Porosity, feature size filter material is the property of having pores in their structure (Medar&Ionescu, 1986; Cay et al., 2005). In connection with the porosity are two distinct notions:

- relative porosity, apparent or open, when taking into account only pores that communicate with each other;
- absolute porosity, effective or real, if we take into account all the pores, i.e. those who are isolated.

  Fluid flow through uniform or uneven spaces created by the filter medium, while maintaining the quality of filtration, filtration efficiency and smoothness and filtering capacity are issues directly related to the porosity of filter media.

  Fluid movement across the filter medium is described by the filtration rate, defined as the maximum volume of fluid passing per unit time through unit area of filter. Porosity refers to the filter media pore volume per unit volume and is typically seen in relative units. Generally, the textile filtering media are inhomogeneous because the filter permeability changes during the exploitation. The medium in homogeneity can be bigger or smaller, depending on the structure of woven filter.

3.2 Pore dimensions and architecture

An important feature of each filter surfaces is the existence of pores which penetrate the entire thickness of the filter and retain solid particles larger than the pores in the cross section of their most narrow, but allow passage of fluid that carried them. Small pore is a void within a solid body. After dimensions are distinguished (Medar&Ionescu, 1986) : fine pores with a diameter greater than 20 μm (invisible to the naked eye) and coarse pore diameter greater than 20 μm (visible to the naked eye). The way of communication with the outside pores can be:

- open, when communication with the outside;
- closed, when no communication with the outside.

Dimensional uniformity and stability of pores of a filter medium directly influences the process of filtering performance (Gabrijelcic et al., 2009). Pore size and shape of woven textile filter media are dependent on the basic structural parameters of fabric: the fineness of yarns, thread density and the weave.
Pore's characteristics which is assessed functional performance of a fabric filter are: side pore, pore area, architecture and distribution of pores in the fabric plane.
Side and pore area are geometric features of woven fabric due to its basic structural parameters.
In terms of basic structural parameters, the woven fabrics with simple structure can be balanced or unbalanced in fineness and density yarns, and the resulting pores have square or rectangular form.
In Figure 2 are defined pore geometry of a woven fabric with simple structure. In the balanced woven fabric (Figure 2.a), the warp and weft, have the same fineness and density, the same diameter d and the same density P. Therefore to obtain a filter fabric with square pores. In the unbalanced woven fabric (Figure 2.b), the warp and weft have different count, expressed by d_u, d_b, and different density threads expressed by Pu, Pb. As a consequence to obtain a fabric filter with rectangular pores.

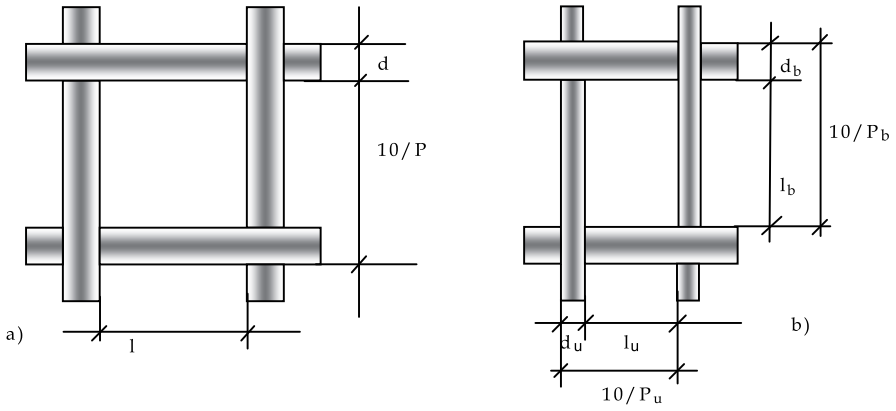

Fig. 2. Pore geometry

3.2.1 Pore side

Pore side is the distance between two consecutive threads of the fabric measured in the projection on the horizontal fabric's plan.
For structures balanced (Figure 2.a), pore side it could be calculated with:

$$l = \frac{10}{P} - d \quad \text{(mm)} \tag{4}$$

For structures unbalanced (Figure 2.b), pore sides, l_u and l_b, is defined by relations:

$$l_u = \frac{10}{P_u} - d_u \text{ (mm)}; l_b = \frac{10}{P_b} - d_b \text{ (mm)} \tag{5}$$

3.2.2 Pore area

Pore area is defined as the projection on the horizontal plan of the fabric's pore.
For balanced structure (Figure 2.a) the pore area A_p is calculated with:

$$A_p = l^2 \text{ (mm}^2\text{)} \tag{6}$$

For unbalanced structure (Figure 2.b) pore area is calculated by the relationship:

$$A_p = l_u \cdot l_b \text{ (mm}^2\text{)} \tag{7}$$

3.2.3 Pores architecture

Pores architecture is a characteristic determined by the fineness of yarns, threads density, mechanical and rheological characteristics of yarns and weave used. The segments of the yarn which constitute the pore sides can be considered, like a beam in one of two situations:
- passing from one side to another fabric,
- above or under the opposite yarn system.

Under these circumstance, the pores` shape and size depend not only on yarn count and density, but also on the positions of the yarns in the weave.
For this purpose an analysis is presented which highlights the fact that the weave determines the distribution of requests in the yarns and the default form of pores. The analysis is done on three woven fabrics filter, whose characteristics are presented in Table 5.
The weave used in implementing the three fabrics are shown in Figure 3. To the right of each weave are represented by pores with a distinct architectural (Cioara et al., 2003).

Woven filter	Weave	Raw material	Yarn diameter (mm)	Thread density (yarns/cm)
Filter 50 mesh	Plain	Polyamide	0.14	20
Filter 22 mesh	Twill D2/2	Polyamide	0.45	9
Filter 24 mesh	Twill D3/1	Polyamide	0.45	9.5

Table 5. Variants of filter fabrics

After examining the shape of pores in the three weave can be made the following observations and interpretations:
- at the fabric filter with plain weave (Figure 3.a) all the pores have the same architecture; the threads have a similar position in the pore sides (all threads are crossing from one side to another of the fabric). Under these conditions the fabric structure creates the potential formation of uniform pores in the shape of their; the pores I, is identical in structure with pores II;
- at the fabric filter with twill weave D 2/2 (Figure 3.b) pores of the report have the same structure. Shapes and sizes of the four types of pores are identical. It creates the conditions to achieve a uniform structure with a high degree of homogeneity to ensure a quality filter; pores numbered I, II III IV is identical in structure;
- at the fabric filter with twill weave D 1/3 (Figure 3.c) is classified in four types of pores. The four distinct architecture creates pores with different shapes and volumes that the

conditions for the flow through it are differentiated; pores numbered II, is identical in structure with pores IV, pores I and III is different.

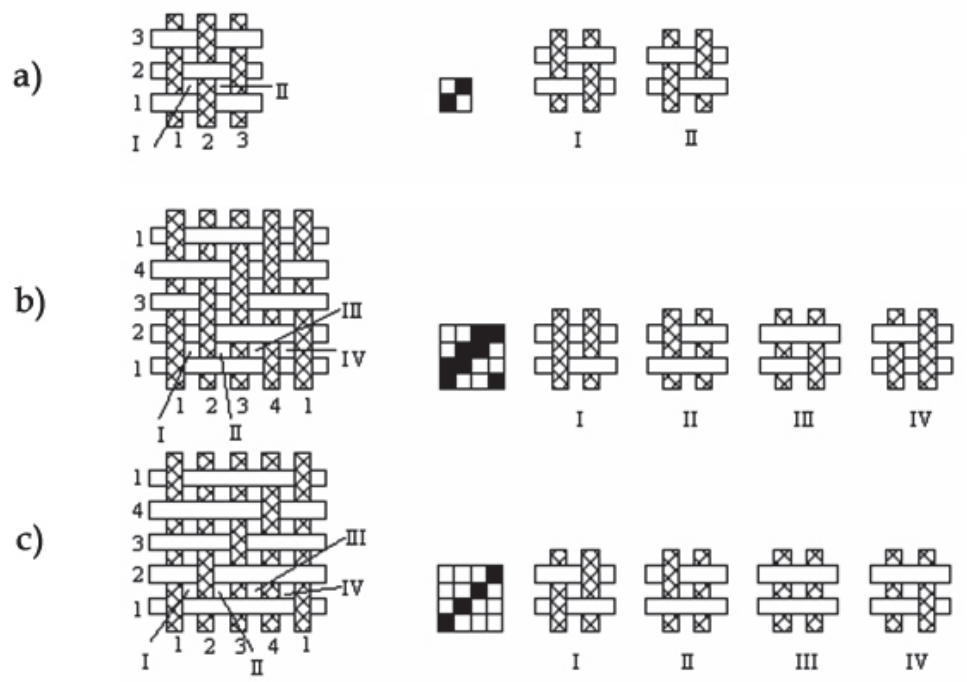

Fig. 3. Type of pores

To support these interpretations, on the three types of fabric filter were performed measurements of area pores, using a specialized program. Measurements were made on the fabric images captured with a stereo microscope with digital camera.
These images are presented in Figure 4, 5 and 6. In each figure is shown a fragment of the microscopic image of the fabric filter with the contours measured pore, the statistics of individual value of area and pore distribution curve.
To facilitate analysis of information provided by research, in Table 6 were centralized statistical processing on the string values of individual values of the areas measured.

Weave	Mean area (mm^2)	Min. value (mm^2)	Max. value (mm^2)	Range (mm)	Std.Dev. (mm)	CV (%)
Plain	0.1021164	0.0841335	0.1120637	0.0279302	0.0064476	6.31
Twill D2/2	0.2104919	0.1555840	0.2731934	0.1176094	0.0310180	14.73
Twill D3/1	0.3233822	0.1810607	0.4755648	0.2945041	0.0722753	22,34

Table 6. Statistical evidence

The analysis of microscopic images shows that the filter fabric with plain weave (Figure 4) pores are relatively uniform shapes and sizes. This is supported on the one hand, the low dispersion of individual values (s=0.00644) and, on the other hand, the restricted

distribution of individual values around the average. Extreme values, minimum and maximum, with reduced weight, have a deviation of up to 10% of the average pore area.
At the fabric filter with twill weave D 2/2 (Figure 5) is observed as architecture, two types of pores with greater irregularity than plain weave. Pore area shows a greater variation, which is confirmed by the dispersion value (s=0.03101) and the pore distribution curve shape. Even if the pore area varies widely, up to 25% from the mean, the woven filter is estimated that the structure is uniform. Extreme values are numerous and, consequently, the distribution curve is wider.

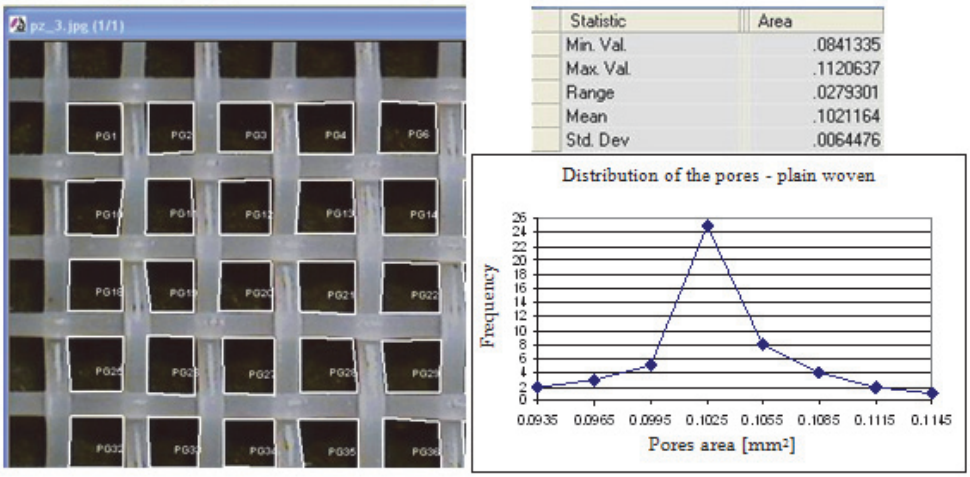

Fig. 4. Pore architecture of the woven filter - plain weave

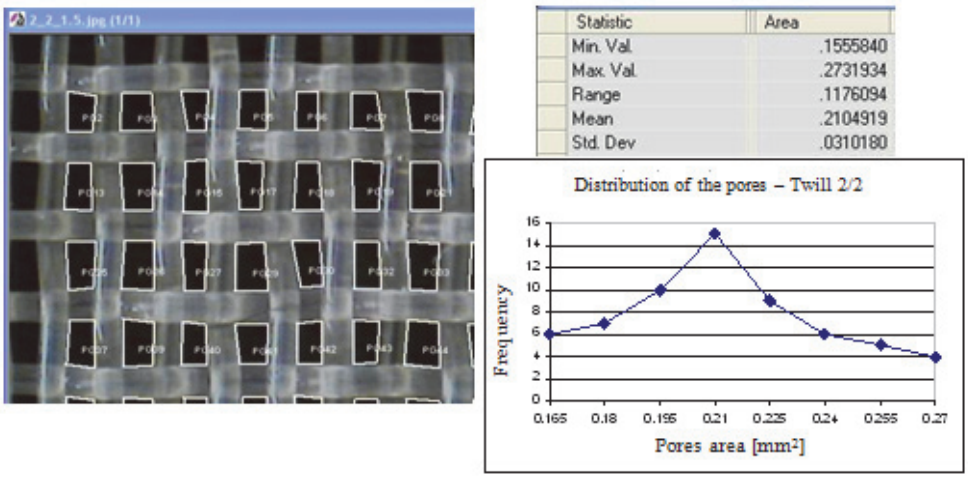

Fig. 5. Pore architecture of the woven filter - twill D 2/2

At the fabric filter with twill weave D 3/1 (Figure 6) is observed as architecture, the four specific types of pores. The dispersion of measured values (s=0.07227) indicates large variation in pore area, which is emphasized by the distribution curve. Pore area varies widely, with over 50% of the mean value and the structure of a fabric filter has emphasized the uneven character.

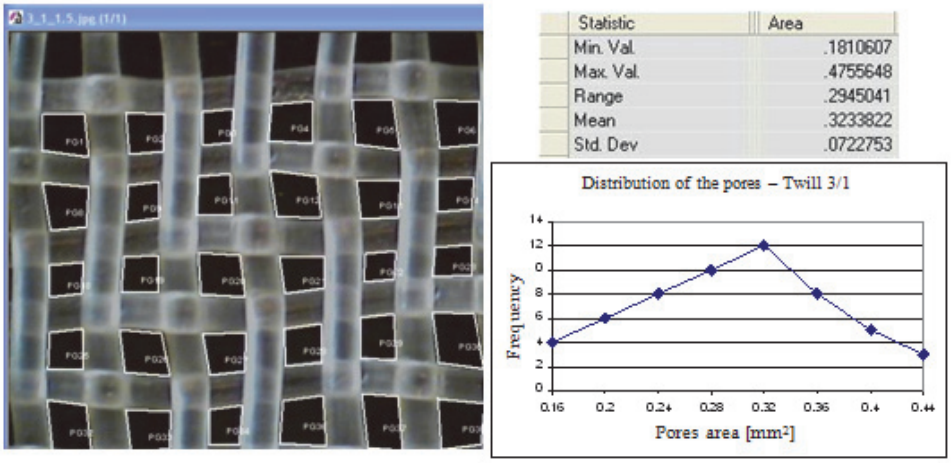

Fig. 6. Pore architecture of the woven filter - twill D 3/1

3.3 The active filtering surface

This parameter provides information about the porosity of the woven filter and resistance to fluid flow through it. Active filtering area was defined as the ratio of pore area, A_P, and area of fabric element, A_{et}, is calculated from the relationship:

$$S_a = \frac{A_p}{A_{et}} \cdot 100\ (\%) \tag{8}$$

3.4 Filter fineness

The woven filter fineness is a nominal identification, which is expressed by the number of pores per unit length or number of pores per unit area. The filter fineness is calculated by the following relations:
balanced woven filter fabrics:

$$F = P\ (\text{pores} / \text{cm}) \tag{9}$$

$$F_m = 2.54\ P\ (\text{pores} / \text{inch}) \tag{10}$$

$$F_d = P^2\ (\text{pores} / \text{cm}^2) \tag{11}$$

unbalanced woven filter fabrics:

$$F_d = P_u P_b \left(pores / cm^2 \right) \quad (12)$$

4. Algorithms for functional design of filter. Examples of application

The last stage of the value engineering technique is to design or redesign based priority functions. Based on the conclusions presented in the above analysis were developed five functional design algorithms for simple structure filter fabrics balanced and unbalanced in fineness and/or density (I.Cioara & L.Cioara, 2010). Always choose the algorithm is done according to known elements (input data) and the requirements process of filtering (output data) to design, redesign or verification. Following the sequence of calculation steps is different from one algorithm to another.

4.1 Algorithms for functional design of filter

In Tables 7 and 8 shows the deployment of the calculations according to data input and output, these calculations are completed to the mass of fabric filter.

In the relationships of calculating the parameters of qualitatively appraising the simple structure woven fabrics used as filtering media the significance of the employed symbols is the following: d - yarn diameter in the balanced structures (mm); d_u, d_b - warp and weft diameter (mm); A - tabled constant for the diameter calculating; A_p - pore area, (mm^2); A_{et} - woven fabric element area, (mm^2); T_{tex} - yarn count in the balanced structures, (g/km); T_{texu}, T_{texb} - warp and weft count, (g/km) ; P - threads density in the balanced structures, (yarns/cm); P_u, P_b - warp density and weft density, (yarns/cm); l - square pore side, (mm); l_u, l_b - the pore side in the warp and weft direction, (mm); F - balanced structure filter fineness, (pores/cm); F_m - balanced structure filter fineness, (pores/inch); F_d - filter fineness, ($pores/cm^2$); M - woven fabric mass, (g/m^2); a - crimp yarn in the woven fabric, (%); m – factor of unbalanced for threads density.

4.1.1 Algorithm I. Design of simple filters based on the density and fineness of yarn (Table 7)

In this case we consider as known the basic structural characteristics of fabric: warp and weft yarn diameters (d_u, d_b) and their densities (P_u, P_b). The algorithm is used to identify specific characteristics of woven fabrics filters: the filter fineness, the pore side and area, the active filtering surface.

Based on of factors identified can be appreciated if appropriate filter fabric filtration process characteristics. Depending on the conclusions formulated after verification can be redesign the fabric to match the outlays.

4.1.2 Algorithm II. Design of simple filters based on the yarn diameter and filter fineness (Table 7)

In this case it is considered known diameters of the warp and weft of yarns (d_u, d_b) and fineness filter fabrics. The algorithm is used to design a filter of woven fabrics density unbalance. The yarns density, the pores sides and surface, the active filter area and the fabric weight are determined by calculations.

Since by changing the density unbalance factor the pores shape and dimensions are also modified ensuring an appropriate filtering fineness. The algorithm can be additionally used to re-design according to given requirements.

4.1.3 Algorithm III. Design of simple filters based on the yarn diameter and side of pore (Table 7)

Algorithm I	Algorithm II	Algorithm III
1. Input data: d_u, d_b, P_u, P_b	1. Input data: d_u, d_b, F_d	1. Input data: d_u, d_b, l_u,l_b
2.Yarn count $T_{tex} = \frac{d^2}{A^2}$	2. Yarn count $T_{tex} = \frac{d^2}{A^2}$	2. Yarn count $T_{tex} = \frac{d^2}{A^2}$
3. Filter fineness balanced structures $F = P_u = P_b \;\; pores/cm$ $F_m = F \cdot 2.54$ pores/inch unbalanced structures $F_d = P_u \cdot P_b$ pores/cm²	3. Thread density $P = f(F_d)$ $P_u \cdot P_b = F_d$ $\frac{P_u}{P_b} = m$ $P_u = \sqrt{F_d \cdot m}$ $P_b = \frac{P_u}{m}$	3. Thread density $P = f(l_p, d)$ $P_u = \frac{10}{l_u + d_u}$ $P_b = \frac{10}{l_b + d_b}$
4. Pore side $l_u = \frac{10}{P_u} - d_u$ $l_b = \frac{10}{P_b} - d_b$	4. Pore side $l = f(P, d)$ $l_u = \frac{10}{P_u} - d_u$ $l_b = \frac{10}{P_b} - d_b$	4. Filter fineness balanced structures $F = P_u = P_b \;\; pores/cm$ $F_m = F \cdot 2.54$ pores/inch unbalanced structures $F_d = P_u \cdot P_b$ pores/cm²
5. Pore area $A_p = f(P, d)$ $A_p = \left(\frac{10}{P_u} - d_u\right) \cdot \left(\frac{10}{P_b} - d_b\right)$		
6. Filtering active surface $S_a = f(P, d)$ $S_a = (10 - P_u \cdot d_u) \cdot (10 - P_b \cdot d_b)$		
7. Woven fabric mass $M = \frac{P_u \cdot T_{texu}}{10} \cdot \frac{100}{100 - a} + \frac{P_b \cdot T_{texb}}{10} \cdot \frac{100}{100 - a}$		

Table 7. Specific elements for algorithms design I, II, III

Algorithm IV	Algorithm V
1. Input data: d_u, d_b, S_a	1. Input data: l_u, l_b, S_a
2. Yarns count $T_{tex} = \frac{d^2}{A^2}$	2. Pore area $A_p = l_u \cdot l_b$
3. Thread density for balanced structures of cover factory: $P_u \cdot d_u = P_b \cdot d_b$ $P = f(S_a, d)$ $P_u = \frac{10 - \sqrt{S_a}}{d_u}$ $P_b = \frac{10 - \sqrt{S_a}}{d_b}$	3. Thread density $P = f(S_a, l_p)$ $S_a = \frac{A_p}{A_{et}} \cdot 100 \Rightarrow A_{et} = \frac{A_p \cdot 100}{S_a} = \frac{10}{P_u} \cdot \frac{10}{P_b}$ $P_u \neq P_b \; ; \; \frac{P_u}{P_b} = m$ $P_b = \sqrt{\frac{S_a}{m \cdot A_p}}$ $P_u = P_b \cdot m$
4. Filter fineness balanced structures $F = P_u = P_b \;\; pores / cm$ $F_m = F \cdot 2.54$ pores/inch unbalanced structures $F_d = P_u \cdot P_b$ pores/cm²	4. Filter fineness balanced structures $F = P_u = P_b \;\; pores / cm$ $F_m = F \cdot 2.54$ pores /inch unbalanced structures $F_d = P_u \cdot P_b$ pores/cm²
5. Pore side $l = f(P, d)$ $l_u = \frac{10}{P_u} - d_u$ $l_b = \frac{10}{P_b} - d_b$	5. Yarns diameter $d_u = \frac{10}{P_u} - l_u$ $d_b = \frac{10}{P_b} - l_b$
6. Pore area $A_p = f(P, d)$ $A_p = \left(\frac{10}{P_u} - d_u\right) \cdot \left(\frac{10}{P_b} - d_b\right)$	6. Yarns count $T_{tex} = \frac{d^2}{A^2}$
7. Woven fabric mass $M = \frac{P_u \cdot T_{texu}}{10} \cdot \frac{100}{100 - a} + \frac{P_b \cdot T_{texb}}{10} \cdot \frac{100}{100 - a}$	

Table 8. Specific elements for algorithms design IV, V

The algorithm is used to design the fabric characteristics in compliance with the parameters of the filtering process. The input data are warp and weft yarn diameters (d_u, d_b) and pore sizes (l_u, l_b). Imposing pore side means the particle to be retained is known, the filter being a calibrated restriction. The required yarn density and all the specific characteristics of the filter are obtained by calculations.

4.1.4 Algorithm IV. Design of simple filters based on the yarn diameter and active filter area (Table 8)

Active filter area is a feature that determines the permeability of the fabric and filter potential to withstand the fluid flow. This algorithm is considered known following elements: the warp and weft yarn diameters (d_u, d_b) and active filtering surface (S_a).
The algorithm allows the calculation of specific characteristics of the filter: pore area and pore side, which determines the filtration fineness and efficiency.

4.1.5 Algorithm V. Design of simple filters based on the pore side and active filter area (Table 8)

In this case filter fabrics design is based on filtering process requirements. Input data are: pore sizes (l_u, l_b) and active filtering surface (S_a). Active filter area determines the filter permeability and influences the flow velocity. The pore side determines the size of the retained particle and influences the filtration fineness and efficiency. The structural characteristics of the fabric are obtained by calculations.

4.2 Examples of application

Further gives examples of the implementation of the five algorithms to design filter woven fabrics with simple structure made from monofilament yarns.
To facilitate the calculation has been made a computer assisted design program (Cioara et al., 2008).
Sequence with the principal program menu is shown in Figure 7. At the top of the screen, interactive buttons, the corresponding input data are highlighted five algorithms. The dates presented in Figure 7 are typical application example of the algorithm I (Table 9).

Sample filter	Parameter	Symbol	Value	UM
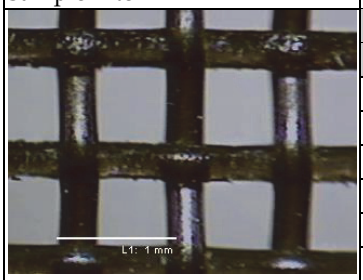	Yarns diameter	d	**0.31**	mm
	Thread density	P	**11.0**	threads/cm
	Filter finess	F	11.0	pores/cm
	Filter finess mesh	F_m	27.94	pores/inch
	Pore side	l	0.599	mm
	Pore area	A_p	0.3589	mm^2
	Filtering active surface	S_a	43.43	%
	Dimensional factor	A	**0.0392**	-
	Yarns count	T	62.54	tex
	Crimp yarn	a	4	%
	Woven fabric mass	M	143.32	g/m^2

Table 9. Balanced structure - designed with algorithm I (weave plain)

The program has the possibility of saving data Input and account for the different variants. These data are provided to the operator in the form of tables. In this way the designer can to compare specific elements of the different variants and select the variant that best corresponds to requirements process of filtering.

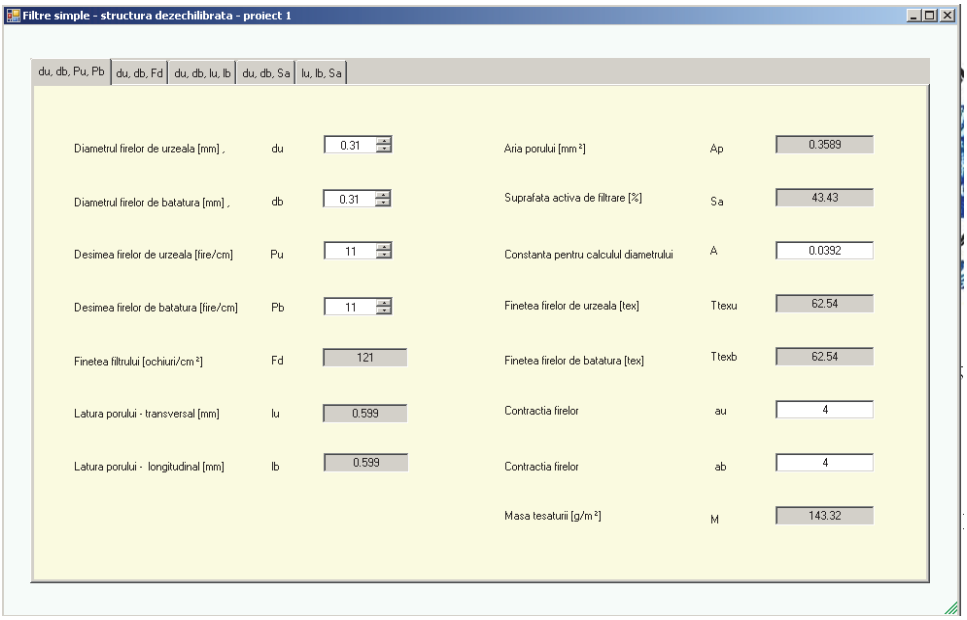

Fig. 7. The main menu of the program

Sample filter	**Parameter**	**Symbol**	**Value**	**UM**
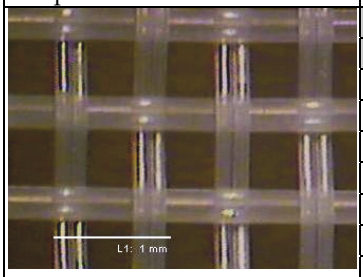	Yarns diameter	d	**0.29**	mm
	Filter finess mesh	Fm	36	pores/inch
	Filter finess	F	14.2	pores/cm
	Thread density	P	14.2	threads/cm
	Pore side	l	0.414	mm
	Pore area	A_p	0.1716	mm^2
	Filtering active surface	S_a	34.6	%
	Dimensional factor	A	**0.0392**	-
	Yarns count	T	54.73	tex
	Crimp yarn	a	2	%
	Woven fabric mass	M	158.61	g/m^2

Table 10. Balanced structure - designed with algorithm II (weave – hopsack 2/2)

The applications are presented in Tables 9, 10, 11, 12, 13. These applications are made for woven fabrics filters with finesse and densities balanced structures, made with weave plain, weave – hopsack 2/2, weave- irregular sateen and weave – twill 2/2.

Sample filter	Parameter	Symbol	Value	UM
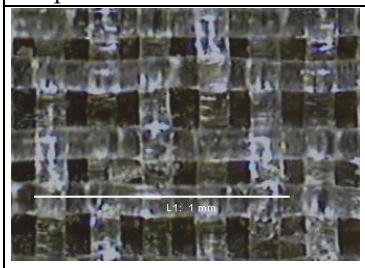	Yarns diameter	d	**0.11**	mm
	Pore side	l	**0.11**	mm
	Thread density	P	45.5	threads/cm
	Filter finess	F	45.5	pores/cm
	Filter finess mesh	Fm	115.57	pores/inch
	Pore area	Ap	0.0121	mm^2
	Filtering active surface	Sa	24.95	%
	Dimensional factor	A	**0.0392**	-
	Yarns count	T	7.87	tex
	Crimp yarn	a	4	%
	Woven fabric mass	M	74.6	g/m^2

Table 11. Balanced structure - designed with algorithm III (weave- irregular sateen)

Sample filter	Parameter	Symbol	Value	UM
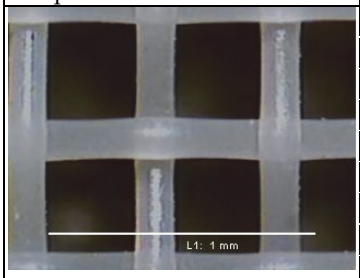	Yarns diameter	d	**0.14**	mm
	Filtering active surface	S_a	**49**	%
	Thread density	P	21.4	threads/cm
	Filter finess	F	21.4	pores/cm
	Filter finess mesh	F_m	54	pores/inch
	Pore side	l	0.327	mm
	Pore area	A_p	0.107	mm^2
	Dimensional factor	A	**0.0392**	-
	Yarns count	T	12.76	tex
	Crimp yarn	a	5	%
	Woven fabric mass	M	57.49	g/m^2

Table 12. Balanced structure - designed with algorithm IV (weave – plain)

Sample filter	Parameter	Symbol	Value	UM
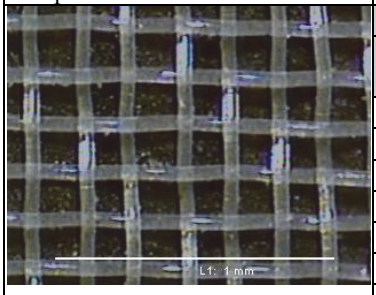	Pore side	l	0.1	mm
	Filtering active surface	S_a	**31**	%
	Pore area	A_p	0.01	mm^2
	Thread density	P	55.7	threads/cm
	Filter finess	F	55.7	pores/cm
	Filter finess mesh	F_m	141.4	pores/inch
	Yarns diameter	d	0.08	mm
	Dimensional factor	A	**0.0392**	-
	Yarns count	T	4.16	tex
	Crimp yarn	a	6	%
	Woven fabric mass	M	49.3	g/m^2

Table 13. Balanced structure - designed with algorithm V (weave – twill 2/2)

Each table is presented as a fabric filter microscopic image and the list of parameters supplied by the computer program. Same time, the tables are highlighted input data specific to each algorithm separately.
In each example there is a good correlation between the elements provided by the computer program and structural characteristics shown on the microscopic image of the fabric made. This aspect allows us to say that the proposed algorithms achieve a better modeling of the structural parameters and specific functional of woven fabrics filters with simple structure.

5. Conclusion

The woven fabrics which are used as filter fabrics, have the functionality imposed for the filtration process. Structure and properties of the woven filter fabrics are adequately differentiated, for the principles of the filtering process. The paper defines the structural and functional elements that are specific to the filtering woven fabrics, which have a structure that is simple, balanced and unbalanced in yarn count and thread density.
The methods of filter design for the fabrics with simple structure is based on the specific geometry of the structure elements fabrics. To achieve filter fabric with uniform pore (size and shape), is recommended of use, weaves balanced with equal segments and uniform distribution (plain, twill D 2/2, hopsack 2/2). Five algorithms of designing the filtering woven fabrics having a simple structure were elaborated, which can be differentially applied depending on the initially introduced elements.
By using computer aided design program to obtain a set of variations of the designer select the optimal variant, which corresponds better to the needs of field exploitation.

6. Acknowledgment

The paper was developed in the research program PNCDI II no.31-088/2007 contract, financed by the Romanian government, which the Technical University "Gheorghe Asachi" of Iassy was a partner. Research presented in this work were performed at the Faculty of Textiles and Leather Engineering of Iassy, Department Technology and Design of Textile Products, laboratory TEXTILEXPERT.

7. References

Adanur, S.(1995).Handbook of Industrial Textiles, Technomic Publishing Company, ISBN 1-56676-340-1, Lancester, U.S.A.

Behera, B.K.&Hari,P.K.(2010).Woven textile structure, Woodhead Publishing Limited, ISBN 978-1-84569-514-9, Cambridge, UK

Cay, A.; Vassiliadis, S; Rangoussi, M.&Tarakcioglu, I.(2005).On the use of image processing techniques for the estimation of the porosity of textile fabrics, World Academy of Science, Engineering and Technology, no.2, pp.76-79, ISSN 2010-3778

Cioară, I.& Cioară, L.(2010).Algorithms design of the filtering woven fabrics with simple structure, Annals of the University of Oradea- fascicle of Textiles Leatherwork, volume XI, pp.41-46, ISSN 1582-5590, Oradea, Romania

Cioară, I.& Cioară, L.(2009).Criteria for estimating the functionality of the filtering mediaobtained by weaving, Industria Textilă, No. 1, pp. 21-25, ISSN 1222-5347, Bucharest

Cioară, I.; Cioară, L.&Cascaval, D.(2008).Method and software design woven filter media, The VI National Conference of Virtual Learning (CNIV), University of Bucharest Publishing, pp.60-65, ISSN 1842-4708, Constanţa, România

Cioară, I.; Cioară, L.& Onofrei, E. (2003). Aspects regarding the architecture of the filtering woven fabrics, UNITEX, No.1, pp. 28-30, Belgium

Cioară, L. (2002).Woven fabric structure, Performantica Publishing House, ISBN 973-8075-16- 15, Iassy, România

Cioară, L.& Cioară, I.(2001). Optimization of the technical parameters in processes of filter weaving, Proceedings vol.I, 1st Autex Conference Technitex-Technical Textiles: Designing Textiles for Technical Applications, ISBN 972-98468-3-9, pp.467-470, Minho

Cioară, L.; Cioară, I.& Marchiş, O.(1991). The influence of certain technical parameters onthe capacity of filtering the woven textile planes, Industria Uşoară, No.4, pp.239-241, ISSN 1222-5347, Bucharest, România

Condurache, G.; Ciobanu, R.& Niculae, M.(2004).Analysis and value engineering, Performantica Publishing House, ISBN 973-730-022-x, Iassy, România

Gabrijelcic, H.; Urbas, R.; Sluga, F.&Dimitrovski, K.(2009).Influence of Fabric Constructional Parameters and Thread Colour on UV Radiation Pretection, FIBRES&TEXTILES in Eastern Europe, vol.17, no.1(72), pp.46-54, ISSN 1230-3666, Lodz, Poland

Harracks, A.R. & Anand, S.C. (2000). Handbook of technical textiles, Woodhead Publishing Limited, ISBN 1-85573- 385-4, England

Marchiş, O.; Cioară, L. & Cioară, I.(1991).Considerations on certain factors that influence the porosity of filtering planes, Industria Uşoară, No.4, pp.237-238, ISSN 1222-5347, Bucharest, România

Medar, S.& Ionescu, F.(1986). Filters for hydraulic and pneumatic drives, Technical Publishing House, Bucharest, România

Rouette, H.K., (2001), Encyclopedia of Textile Finishing, Woodhead Publishing Limited, ISBN 1-84569- 065-6, England

7

Color and Weave Relationship in Woven Fabrics

Kavita Mathur[1] and Abdel-Fattah M. Seyam[2]
[1]*Precision Fabrics Group Inc., Greensboro NC*
[2]*College of Textiles, North Carolina State University, Raleigh NC*
USA

1. Introduction

In woven designs from colored threads, a colored pattern is a consequence of two possible arrangements where warp is over the weft or vice versa. Thus the primary elements of woven fabric design are combination of weaves and blending of colors using such weaves. Weave is the scheme or plan of interlacing the warp and weft yarns that produce the integrated fabric. Weave relates specially to the build or structure of the fabric. Color is differently related to effects of weave and form. The methods of utilization of color in woven textiles depend upon the composition of the weave design to be woven and the structure parameters of the cloth.

Color and ornamentation in woven fabrics is imparted through the pre-determined placement and interlacing of particular sequences of yarns. A solid color is produced by employing the same color in warp and weft. On the other hand, different colors may be combined to produce either a mixed or intermingled color effect in which the composite hue appears as a solid color. Figured ornamentation is created through the selection of different groups of colored yarns, placed in the warp and/or in the weft; while in certain patterns, textural effects may be created entirely through the use of different values and closely associated hues of certain colors. The figure is formed for the purpose of displaying different pattern formations, adding dimension or color reinforcement and for enhancing a particular motif.

Modern CAD systems provide a variety of design tools that are supported by standardized color databases that allow simulation of weave structures on the computer monitor that could be printed on paper. However, deviations of the color values of these simulations still occur. Also, the color on fully flat fabric simulations on paper or computer screen is two-dimensional that differs from the real three-dimensional nature of fabrics and yarns.

In textile wet processing, the uses of colorimetry systems and associated software have proven their worth over the years, in objective estimation of color, and have minimized misunderstandings between textile manufacturers and their customers. However, color communication within textile design is largely a subjective process. Recent experimental studies (Osaki 2002; Dimitrovski & Gabrijelcic 2001, 2002, 2004) have revealed that the use of colorimetry has helped to achieve better reproducibility and accuracy in the shade matching of textiles products. Colorimetry is, however, less used when fabrics are made from colored

yarns than when yarns and fabrics are dyed to a solid color, or are printed. Recent research work (Mathur et. al. 2005, 2008, 2009 and 2011) provided a model that involves colorimetry for color prediction and is discussed briefly in section 4.

Several measuring and imaging systems are now available commercially that can record colorimetric data and convert these data into visual images. Hence, the designer can generate a numerical color specification that can be visualized accurately on a suitably calibrated monitor. Recent advances in color curve generation and image processing provide opportunities for additional improvements in the areas of collaborative color development, color marketing, and color prediction in multi-step processes. Contemporary techniques of computer-aided fabric design offer new possibilities for using colorimetry in weaving practice.

Along with the fundamental description of weave and color relationship, and recent advances in woven fabric design, this chapter also includes the research models developed to quantify the color proportion and color values, in effort to eliminate the expensive and time consuming process of prototyping and color matching in woven fabric design.

2. Woven fabric design and structure

This section introduces the reader to the basic knowledge of woven fabrics design and structure and the concept on how colored patterns are created using colored yarns. It sets the stage for the next sections that deal with objective evaluation of color in woven structures.

Woven fabrics are formed by interlacing two orthogonal sets of yarns; warp yarns that are vertically arranged and weft yarns that are horizontally placed. While all weave structures are created from a binary system (that is a warp yarn is over or under a weft yarn at the crossover areas), infinite number of weaves can be formed. The distribution of interlacement is known as weave design or pattern. There are three types of weaves that are known as basic weaves, which include plain weave (the simplest and smallest repeat size possible; 2 warp yarns x 2 weft yarns) and its derivatives, twill weaves and their derivatives, and satin/sateen weaves and their derivatives. These basic weaves are characterized by their simplicity, small size, ease of formation, and recognition. However, they form the base for creating any complex/intricate structures (such as multi-layer fabrics and pile weave structures) and weaves with extremely large patterns that are known as Jacquard designs. Figures 1-3 show examples of basic weaves. More on the rules to construct basic weaves and their derivatives can be found in Seyam 2001.

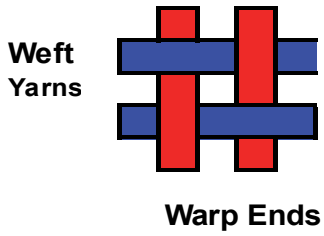

(a) Flat view

(b) Weave design

Fig. 1. Plain weave

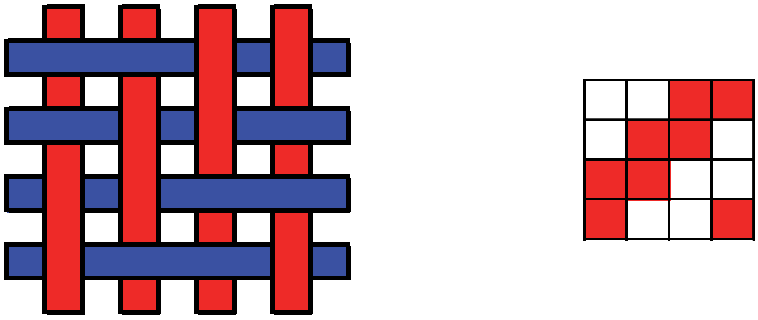

(a) Flat view (b) Weave design

Fig. 2. Example of twill weave (2x2 Right Hand Twill weave)

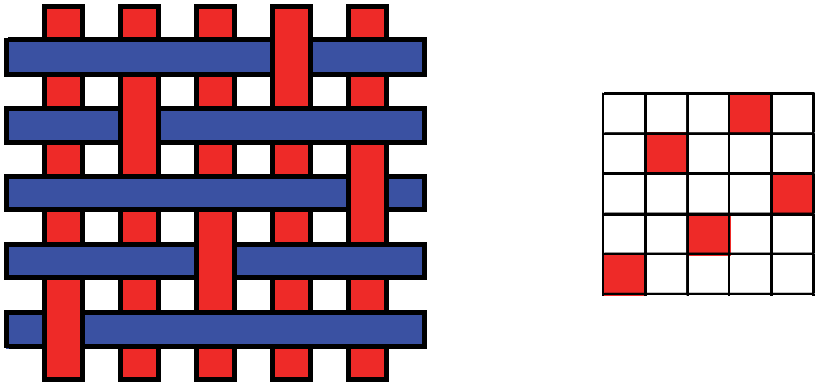

(a) Flat view (b) Weave design

Fig. 3. Example of sateen weave (5-Harness Sateen Weave)

Figures 1-3 depict two methods of presenting weaves namely flat view and weave design. While the flat view presentation provides better understanding in regards to the warp and filling yarn interlacing, it takes time to draw especially for large size repeats. The weave design presentation was created to communicate in a much simpler and easy to draw weave illustration using weave design paper (squared paper). In the weave design presentation the spaces between yarns are eliminated and only the squares where warp yarns are over the weft yarns are shown, which is reasonable since in most of woven fabrics the yarns cover most of the fabric surface. Any color or marks (such X, /, or \, etc.) can be used to indicate where a warp yarn is over a weft yarn. The squares that are left blank indicate otherwise.

2.1 Color/weave relationship

Figure 4 shows another illustration of the weaves of Figure 1-3. In Figure 4 all the squares of the weave design presentations are painted using the color of warp and weft yarns (red and blue). This is known as color effect presentation. It should be pointed out that a square in the

design paper represents extremely small size area in the woven cloth. The colors of Figure 4 will be perceived by human eye as a mixture of two colors with different ratios.

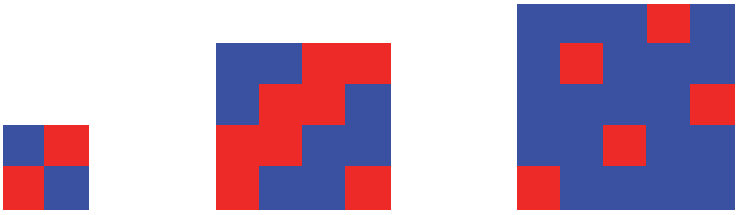

(a) (b) (c)

Fig. 4. Color effects

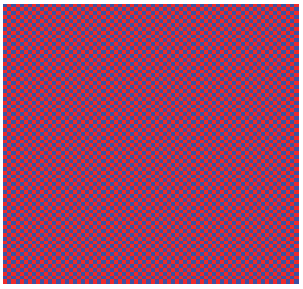

Fig. 5. Color simulation of the plain weave of Figure 1

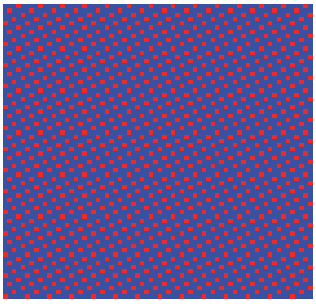

Fig. 6. Color simulation of the sateen weave of Figure 3

Thus, the use of colored warp and weft yarns combined with the weave structures permit the development of striking patterns. For a given pattern with multi-color, a color can be strategically placed in the pattern by merely using the binary system of warp and weft interlacing. The desired color of a yarn appears when the yarn is over the crossing yarns for a desired length and small or large area if several yarns are used. Moreover, numerous mixtures of colors to produce other colors can be obtained from few colors of the warp and weft yarns through proper weave interlacing. Figures 5 and 6 are two examples of such mixtures. They were produced using many repeats in warp and weft directions, thread count close to real cloth, and assuming there are no spaces between the yarns, which is reasonable assumption

for most woven fabrics. Figure 5 is the color simulation produced from red warp yarns and blue weft yarns and plain weave of Figure 4(a). While the color simulation of Figure 5 is produced from red warp yarns and blue weft yarns woven in sateen of Figure 4(c). These two examples indicate that numerous purple colors can be produced from only two colors (red and blue). Using this concept striking patterns can be created using few colors in warp and weft directions such as the Jacquard design of Figure 7.

Pattern is courtesy of Manual Woodworkers and Weavers, Hendersonville, N.C., USA

Fig. 7. Color simulation of Jacquard faric

2.2 CAD and woven fabric design

Designing fabrics is a creative/technical process that is dependent upon the ability of the textile designer to combine aesthetic sensibility with a strong knowledge of the technology of materials and fabric production machinery. Most Dobby and Jacquard fabrics producers' facilities are now equipped with Computer Aided Textile Design systems. In the pre-computer era, the designing process was done in the following manner: (a) a piece of artwork was created on paper, (b) the artwork was then rendered as a scaled grid (known as squared paper or design paper), whose columns and rows represented warp and weft yarns, respectively, (c) weaves were then assigned to specific areas to represent the original pattern, and (d) a technician then punched cards, direct from this technical design layout, in which each card represent one pick of the actual fabric.

Computers have been utilized in woven textile design for almost 25 years, and this has revolutionized the entire design process. They have revolutionized the entire thought-process from the initial artwork to final production. CAD systems in woven designing operate in a series of basic steps. The first step is that of digitizing the artwork. This feature allows the designer to see the artwork on a computer monitor by scanning the original piece or creating a design using the CAD system drawing tools directly. This is generally done in 8-bit format (256 colors) and allows the designer to modify patterns and reduce the number of colors to a manageable number as he/she wishes. The second step is fabric designing, in which the artwork image data is transformed (i.e. the grid system, above) into weaving

information for fabric production. Weave allocation is the third step, in which information from the artwork image can be converted into a woven fabric. The designer created the appropriate weave structure or chooses one (from a weave library) to match the desired color, shape or texture in the artwork. This part of the program also helps the designer to see a simulation of the final fabric on the display monitor. By looking at the preview, the designer can easily modify the design, and can change the weaves to recolor the design as required. All these developments have greatly increased the ease of woven fabric designing. It is now possible to perform the entire process on a personal computer, and then transfer the ready-to-weave file (electronic punch-card file) via the internet, direct to the dobby or Jacquard controller at the loom, or to some interim storage area.

Textile CAD/CAM systems are mainly modular in structure and, in addition to covering yarn and fabric design may also include very realistic 3D simulation packages. A complete automated process with immediate response to the customer's demand seems to be a reality in the near future with these systems (Dolezal & Mateja 1995; Bojic 1999; Dimitrovski & Bojic 1999). Moreover, developments of powerful modem systems and electronic controls have brought the weaving machine into the design studio. This evolution has, in turn, given an entirely new meaning to the term *Quick Response*.

The impetus for use of CAD in the textile industry was to improve efficiency in the production process. Initial textile designing software packages were mainly derived from graphic design software, without putting much emphasis upon the underlying fabric structures. CAD systems have evolved, however, by considering the designing process and technical limitations. These systems are now extensions of creative expression which comply with technical requirements (Doctor 1997). Numerous descriptions of this process exist within the computer environment (Lourie 1969, 1973; Lourie & Bonin 1968; Lourie & Lornzo 1966) addressing, algorithmically, the problems that arise when one attempts to harmonize visual pattern with the notational point paper diagrams of those used for warp and weft interlacing.

Innovation in the field of textile design CAD systems for woven fabrics has provided the opportunity to design intricate fabrics with the use of a variety of tools. There is also the possibility of seeing the resultant fabric on a computer monitor that gives the visualization of real fabric prior to weaving. There is constant improvement and development in the CAD system to develop several design features (CAD tools) to keep pace with new market demands. At ITMA 2003, 40 companies exhibited CAD systems. Most of the weaving machinery companies showed CAD systems as an accessory. Many CAD companies (UVOD, Fractal Graphics, Yxendis, ScotWeave, EAT, NedGraphics, Pointcarré, Mucad, Informatical Textil, Booria CAD/CAM systems, Arahne etc.) showed constant improvement in the quality of CAD systems such as, easy-to-use software modules, flexibility of changing constructional parameters, speed of defining technical data and enhanced visualization of fabric structures (Gabrijelcic 2004, Seyam 2004).

3. Color visualization in woven fabrics

In pre-colored yarn or fabric, when light falls on the colorants (dyes or pigments), the white light is broken into its component wavelengths. Depending upon the particular molecular structure of a colorant and surface, light may be reflected back to the viewer, absorbed into the molecular surface, scattered by the molecular surface, transmitted through the surface or be subjected to some combination of reflection, absorption and transmission. One of the three processes always dominates; however, this in turn produces color effects (Lambert,

Staepelaere & Fry 1986; Menz 1998). The color effect of perceived color is a consequence of three types of color mixing principles:

a. **Additive Color mixing** is a basic phenomenon for color perception, which involves addition of wavelengths of light to create higher-value colors. The broadest bands of color seen in the visible spectrum are those belonging to red-orange, green and blue-violet, known as *Primaries*. When all these colors are projected and overlapped, their specific wavelength mix together and produce white light (Figure 8). Magenta, cyan and yellow are known as *Secondary* colors where only two colors overlaps and their respective wavelengths add together.

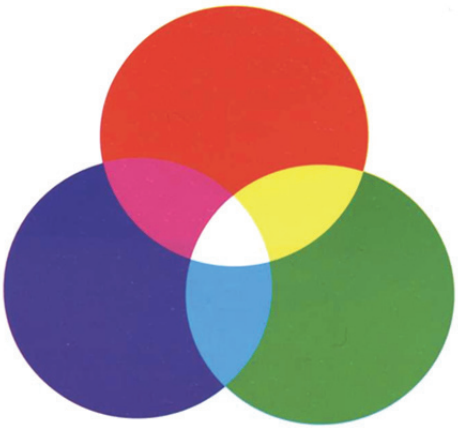

Fig. 8. Additive color mixing (McDonald 1997)

b. **Subtractive Color Mixing** is created by the addition of pigment materials such as dyes, inks, and paints that remove reflecting wavelengths from light from each other, allowing us to see new color. When the pigment primaries that are cyan, magenta and yellow are mixed together, they culminate in black (Figure 9).

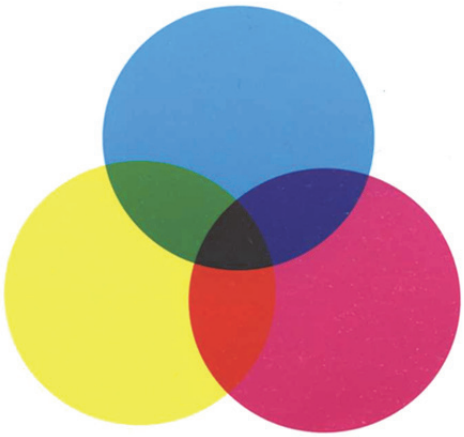

Fig. 9. Subtractive Color Mixing (McDonald 1997)

c. **Optical Color Mixing** is also known as *Partitive* Color Mixing because optical mixtures combine additive and subtractive color mixing phenomenon. This is an effective method of creating mixtures that appear to vibrate and mix at particular distances when small areas of color are juxtaposed as shown in Figure 10.

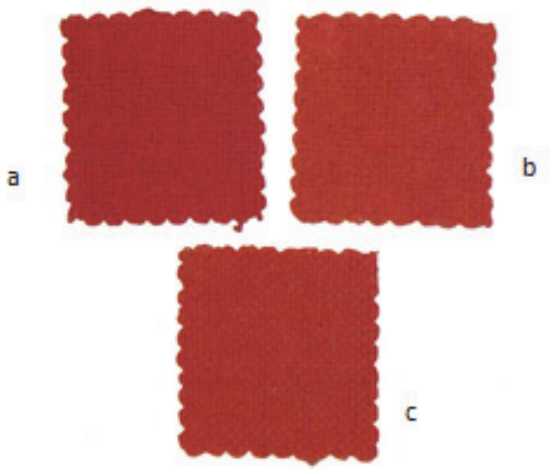

Fig. 10. The Optical mixture (c) is a result of weaving the yarn used in sample (a) with yarn used in sample (b) (Lambert, Staepelaere & Fry 1986)

Partitive color achieved in woven fabrics does not follow the same rules as the other cases (such as in additive and subtractive color mixing), presumably because the individual yarns are not completely opaque and moreover the fabrics are made from blends of several colored yarns with different weave effects.

Furthermore, the relation between the color values of different colors and their size must be carefully considered. When two colors are in juxtaposition with each other, each takes on the complement of its neighbor. This is known as law of 'Simultaneous Contrast'. In woven fabrics, the appearance of the color is a consequence of light reflected back from different areas of color surface of the yarns involved in the fabric structure. Looking at the color wheel (Figure 11), if color values of warp and weft are taken into account, behavior of the color contrast and harmony can be well understood.

Complementary colors lie on the opposite sides of the color circle, and their sum of reflected light gives an unsaturated color, which can be observed as a grayish hue on the fabric. On the other hand, the close positioning of two harmonic colors gives similar color value.

In woven designs, in case where fabric is made of multi-colored yarns, the final visualized color is a contribution of each color component present on the surface of the structure. Individual color components are blended and seen as one solid color. This blending of color is governed by the above mentioned color mixing principles. Blending of fibers has been very well studied in the past (Pierce 1997, Burlone 1990, Friele 1965, Miller 1979, Guthrie 1962, Burlone 1983, Walowit 1987, 1988, Burlone 1984, Reed et. al. 2004, Amisharhi & Pailthorpe 1994), but very few literatures have discussed the blending of yarns in fabric structure (Mathur 2007).

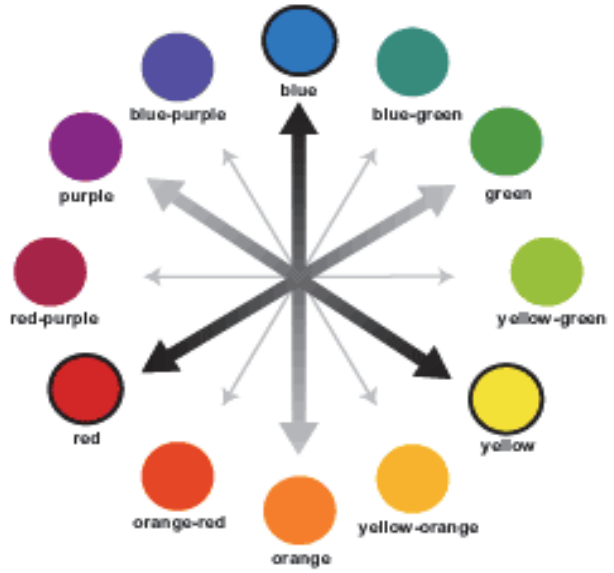

(a) Color wheel

(b) OPTICAL COLOR MIXING (ANALOGOUS) juxtaposition of small areas of analogous colors forces viewer to mix them optically, creating a blend on a very small scale

(c) OPTICAL COLOR MIXING (COMPLIMENT) juxtaposition of small areas of complimentary colors forces viewer to mix them optically, canceling each other out

Fig. 11. Optical Color Mixing (Richard & Struve 2005)

3.1 Color visualization in CAD systems

In computer-aided design, there is a popular acronym called "wysiwyg", which means "what you see is what you get". Unfortunately, the wysiwyg concept often fails when dealing with the issue of color and reproducing color for different output devices. For example, it is difficult to match three different fabrics, all of which have different fiber content, because each fiber requires a different dye formulation. The same concept holds true in the world of computer generated color. Each color device used in CAD and production, including monitors, desktop printers, and commercial four-color process printers, have unique definitions and limitations for color by virtue of their own unique technology (Ross 2004).

Hoskins et al. (1983, 1985) developed an algorithm to analyze the color of woven structures. Since size of the design and restricted color sets were the limitation for the industry requirements, this algorithm was developed to provide the possibility of capturing any kind

of image by the system. The system could then provide important elements of color in the image without compromising the storage requirements or degrading the system's response time. Rich (1986) discussed the basic colorimetry of CRT (Cathode Ray Tube) displays, both instrumental and visual, as applied to textile design systems. His paper emphasized CRT-based graphical displays to generate colored images. He also suggested some technical aspects for accurate and repeatable representation of the weave and color of the textile on display. Similarly, Takatera and Shinohara (1988) developed a search algorithm to determine the color-ordering of the yarns and weave, to obtain a given pattern of color-and-weave effect. Dawson (2002) examined color-and-weave effects with small repeat sizes. He studied the effects of yarn color sequences over several weave repeats. Grundler and Rolich (2003) proposed an evolution algorithm to combine the weave and color, in order to have a predetermined idea of the appearance of the fabric to be produced. Based on the algorithm, software was then developed to access different fabric patterns and allowed the creation of new patterns, based on the user's choice.

Colors displayed via computer monitors cannot be specified independently. Therefore, color is considered as one of the major aspects of a user-centered design process. Most current CAD systems use uncalibrated color and, in consequence, designers are unable to define or communicate accurately the color of the image-design effect that they produce on the computer screen. A system with calibrated colors gives precise definitions for all colors seen. The numerical specifications for colors used in current CAD systems are expressed in terms of red, green, and blue (RGB) or hue, value, and saturation (HVS) combinations. Importantly, the CIE system of color specification (via tristimulus values, XYZ) is independent of any specific reproduction system and is widely used to specify color in textile manufacturing (Polton & Porat 1992).

The color issue represents not only one of the most frustrating aspects of CAD, but the area with the most rapidly advancing technology. A color management system, or CMS can be used to create color for specific output devices. Theoretically, this allows for more consistent and accurate color results between different output devices. A CMS works in the background and translates colors based upon pre-defined color profiles for specific output devices, allowing for more consistent color viewing and output. CMS's provide new possibilities for accurate color communication, but they cannot be considered an ultimate solution (Ross 2004).

Since the introduction of spectral-based imaging systems some years ago, algorithmic data communication of color standard and production 'submits', between retailers and suppliers, has proven to be one of the primary economic applications of the technology. Recent advances in color curve generation and image processing provide opportunities for additional improvements in areas of collaborative color development, color marketing, and color prediction in multi-step. At the same time, there are other aspects of imaging technology that have strong economical implications in other areas besides color communication. The other applications are derived from what is considered the very heart of such a system – the spectral base for color. Contrary to most CAD type systems, the input and output channels are spectral reflectance values either measured or generated and are largely device and illuminant independent. The spectral data are by far the most basic characterization of an object's color. From these spectral values, we derive all the other higher level output forms such as colorimetric values (X, Y, Z, L*, a*, b*, C*, H*), output to the monitor in calibrated color (R, G, B), and to the calibrated printer in C, M, Y, K. By

combining the spectral base, colorimetric functions, and an image processor, the color imaging system is a powerful tool for color management (Randall 2004).

4. Advances in color and weave design

Recently, a number of technological advancements have been introduced by weaving machine producers, such as: high speed weaving, higher levels of automation, new shedding concepts, automatic (on the fly) pattern change, and filling color selection. Along with the advances in weaving, significant development has also occurred in the field of CAD systems, which enables automation in the design process. Despite this automation, the process of assigning weaves/colors is still done by the designers or CAD operator, which therefore requires physical sampling prior to production. This section includes the recent research work done to automate the process of assigning weaves/colors in order to reduce or even eliminate the need for physical sampling and to assist woven fabric designers in the creation of pictorial fabrics that are a very close match to the original "artwork" or target.

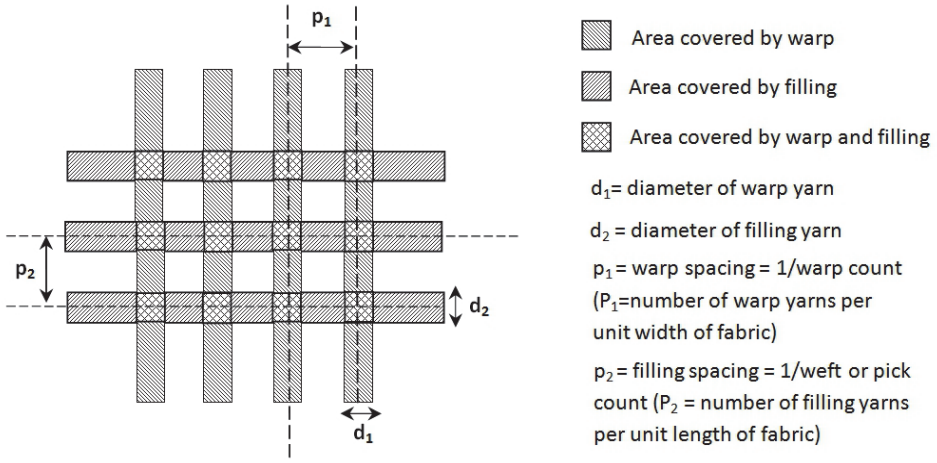

Fig. 12. Cover factor calculation for a Plain weave fabric

In woven fabrics, which are highly textured, various patterns become visible through their different structures. The color of such patterns also depends upon the color of the yarns involved, their combinations and different structures on the pattern surface. The final visible color on the fabric surface is mainly due to the contribution of fabric covering properties, namely optical cover and geometric cover (Lord 1973; Adanur 2001, Peirce 1937). The optical cover properties are defined as the reflection and scattering of the incident light by the fabric surface and are a function of the fiber material and fabric surface. Geometric cover (characterized by fabric cover factor) is defined as the area of fabric actually covered by fibers and yarns. Fabric cover factor is the ratio of surface area actually covered by yarns, to the total fabric surface area (shown in Figure 12).
The following Equations are used to calculate total fabric surface area covered by warp and weft yarns;

$$\text{Warp cover factor } C_1 = P_1 \times d_1 \quad (1)$$

$$\text{Filling cover factor } C_2 = P_2 \times d_2 \quad (2)$$

$$\text{Total cover factor } C_f = (C_1 + C_2 - C_1.C_2) \times 100 \quad (3)$$

Using the fundamental theory as discussed above, Dimitrovski & Gabrijelcic (2002) developed a method for predicting color values on woven fabric surfaces by calculating the color values from the known color values of the used yarns and the constructional parameters based on the cover factor Equations. The author estimated the deviation of the calculated fabric color values and measured fabric simulation color values from the measured color values of a real fabric with identical parameters. Theoretical calculations of color values of a fabric made from single colored warp and filling yarns were reported, based on constructional parameters of each yarn in the fabric. By using fabric geometry, fractions of individual color components in a color repeat was calculated and CIELAB color space was then used to calculate color difference tolerance. This method was experimented for the fabrics composed from single colored warp and filling yarns, where the weave design is divided into two units (when warp is interlaced with weft and vice versa. However, a weave design with varying warp/filling colors and diameters will have more than two units, which was not explained in this study. Also, no specific explanation (assumptions) regarding yarn diameter and yarn spacing was provided. For their calculation purpose, yarn diameter was measured (using microscope), which actually requires weaving a fabric and hence, defeat the purpose of predicting color proportions.

Dimitrovski & Gabrijelcic (2002) also discussed that the accuracy of prediction greatly depends upon the type of yarn. Multifilament yarn with relatively small number of twists tends to relatively big deformations of the diameter in the interlacing points, where deformations depend upon the type and the parameters of the yarns with which they interlace on the fabric surface. Deformation in the yarn diameter at interlacing points also depends upon the constructional and technological parameters the warp and the weft tension and reed plan are most important. Due to considerable deformability of such yarns their spectrophotometrically measured color values vary as well, so that it is difficult to accurately predict the color values of the woven surfaces. The effect of the technological parameters on the color values discussed in the paper was not, however, experimentally verified.

Mathur et. al. 2007, developed a model using the same cover factor principle discussed above that enables calculation of color proportions on the fabric surface in terms of weave pattern and color sequence of warp and weft yarns. The following assumptions were made for the calculations: yarn diameters were uniform cylinders, warp spacing at the weave intersection and under the float are of same value, pick spacing at the weave intersection and under the float were of same value, the projection (two-dimensional) of the fabric on a plane parallel to fabric plane is considered, and yarns are uniformly colored. Geometric calculations obtained from the model were employed in the number of Kubelka-Munk based models to predict the final colorimetric value of the woven design. The colorimetric values obtained were compared with spectrophotometric values for the color difference. Further, the color values obtained from the Kubelka-Munk based color models were simulated on the color calibrated monitor and compared with real woven samples for visual comparison. The detailed test method and results of this model is published elsewhere (Mathur et. al. 2005, 2008, and 2009).

Apart from the work that directly addresses the issue of representing color in interwoven yarns, there is another class of work, based on the influence of various fabric parameters that also addresses the problem of color reproduction in woven fabrics. Yarn count and density have a direct influence on the visible fractions of each individual color component within a color repeat, and consequently on resultant color values of that fabric surface (Gabrijelcic & Dimitrovski 2004). However, during the different stages of producing fabric (spinning, weaving, knitting, etc.), color change evolves due to different surface textures (Menz 1998). Dupont et al (2001) proposed a model of color evolution during the spinning stage, when the roving is transformed into yarn. After spinning, if the yarn is not dyed, the color depends uniquely on the initial color of the roving. Study done by Dimitroviski et al, concluded that the colored yarns used in weaving, if dyed by different methods, also affect the fabric color woven from the same yarns (Dimitrovski & Gabrijelcic 2001).
The optical color values in a fabric depend on the shape of the structural units, such as length of the fiber, yarn floats, diameter of the fiber and the yarn, cross-sectional shape of the fiber, and the longitudinal shape of the fiber and the yarn. Each of these structural units provides surface that reflect and absorb light, and the configuration of these surfaces dictates both the total light reflectance possible from the finished fabric and the direction in which the light is reflected. The amount and direction of reflectance is in turn responsible for the perceived value of the fabric color. A high level of total light reflectance results in a high value (or light color), while a low level of total light reflectance results in a low value (or dark color). If light from a surface is organized and reflected in a single direction, as happens with light from a single large flat shape, the surface appears either very light (if it is reflecting toward the viewer) or dark (if it is reflecting away from the viewer). If light is scattered from a surface in many directions, as happens with light from a curved surface, a uniform value will be seen from all points of view (Lambert, Staepelaere & Fry 1986; Berns 2000; McDonald 1997).

4.1 Color prediction model

Recent research (Mathur et. al. 2005, 2008, and 2009) provided a method to calculate the contribution of each color in an area of a pattern through numerical examples. The method utilized in this research is tedious, especially in the case of large patterns with numerous warp and filling yarns, colors, and weaves. Additionally, the method cannot be programmed to enable the automatic calculations of color contribution from basic design parameters. In this section, a generalized model is discussed briefly that enables the user of a computer simulation to input basic design parameters. The basic parameters used in the generalized model are warp and filling yarns linear densities, warp and pick densities, weave, color arrangements of warp and filling yarns, and color of the background. With proper computer programming of the model, a suitable color mixing equation (Mathur 2007), and databases of yarns colors, yarns, and weave, the process of color/weave selection could be automated without operator/designer intervention and without the need to weave color gamut (Seyam and Mathur 2008).
Figure 13 demonstrate an example to provide a clear understanding of the parameters involved the modeling and the contribution of each color component. Figure 13 is a flat view of 2x2 L.H. Twill with various warp and filling colored yarns (warp color arrangement: 1 purple, 1 light blue, 1 red and filling color arrangement: 1 dark blue, 1 green, 1 black). Using the generalized model, area of each color in the pattern can be calculated using Equations 4-6.

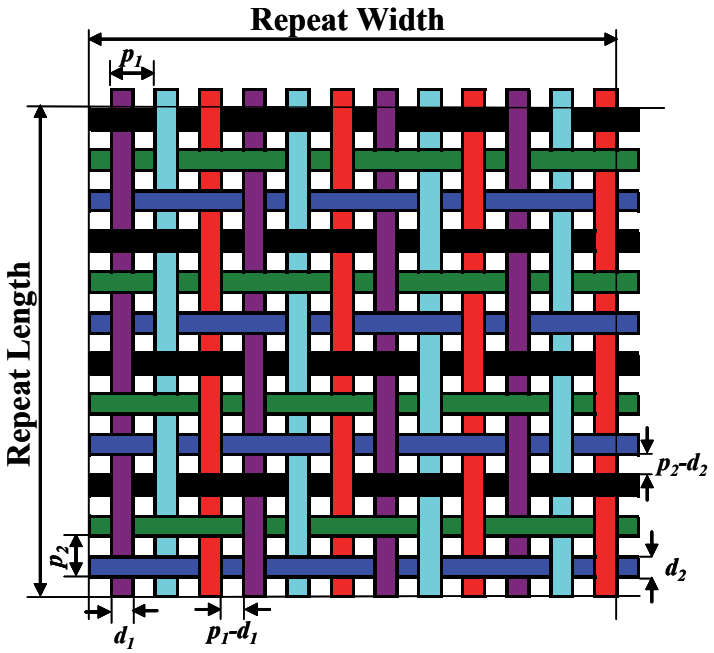

Fig. 13. An example of a weave with colored warp and filling yarns (Seyam and Mathur 2008)

General fraction cover of warp yarns of the i^{th} warp color is;

$$c_{1i} = \frac{m_{1i} l_2 d_1 (p_2 - d_2) + m_{1i} (l_2 / n_2) n_{co1} d_1 d_2}{p_1 l_1 p_2 l_2} \tag{4}$$

General fraction cover of weft yarns of the j^{th} weft color is;

$$c_{2j} = \frac{m_{2j} l_1 d_2 (p_1 - d_1) + m_{2j} (l_1 / n_1) n_{co2} d_1 d_2}{p_1 l_1 p_2 l_2} \tag{5}$$

The fraction of the area covered by the background color (white in Figure 2) is,

$$c_b = \frac{(p_1 - d_1)(p_2 - d_2) l_1 l_2}{p_1 l_1 p_2 l_2} = \frac{(p_1 - d_1)(p_2 - d_2)}{p_1 p_2} = 1 - c_f \tag{6}$$

Where,
m_{1i} = number of warp yarns of warp color *I*
m_{2j} = number of filling yarns of filling color *j*
l_1 = number of ends/weave and color combined repeat = LCM (n_1, m_1); where LCM is Least Common Multiple
l_2 = number of picks/weave and color combined repeat = LCM (n_2, m_2); where LCM is Least Common Multiple;
n_1 = number of ends/weave repeat

n_2 = number of picks/weave repeat
m_1 = number of warp yarns
m_2 = number of weft yarns

d_1 = warp yarn diameter, cm = $\frac{1}{280.2}\sqrt{\frac{N_1}{\varphi_1 \rho_{f1}}}$; N_1 = Warp yarn linear density (g/km or tex);

ρ_{f1}= warp fiber density in g/cm^3; ρ_{y1}= warp yarn density in g/cm^3; φ_1 = warp yarn packing fraction/factor = ρ_{y1}/ρ_{f1};

d_2 = filling yarn diameter, cm = $\frac{1}{280.2}\sqrt{\frac{N_2}{\varphi_2 \rho_{f2}}}$; N_2 = Filling yarn linear density (g/km or tex);

ρ_{f2}= filling fiber density in g/cm^3; ρ_{y2}= filling yarn density in g/cm^3; φ_2 = filling yarn packing fraction/factor = ρ_{y2}/ρ_{f2}
P_1= warp density, ends/cm
P_2 = Pick density, picks/cm
p_1 = warp spacing = $1/P_1$
p_2 = pick spacing = $1/P_2$
d_1 d_2 = cross over area where a warp (or filling) yarn is over a filling (or warp) yarn
n_{co1} = number of cross over areas where warp is over filling/weave repeat
n_{co2} = number of cross over areas where filling is over warp/weave repeat

The detailed discussion of the generalized model along with derivation and examples are discussed elsewhere (Seyam and Mathur 2008). A numerical example is provided in Appendix 1 to demonstrate the use of Equations 4-6 and to investigate the effect of weave and color pattern of warp and filling yarns on the contribution of each color used to construct the weave design.

The color proportion data obtained from this model can be employed in color models to obtain colorimetric calculation to predict the final color values of woven structures. Kubelka-Munk theory (K/S model) is commonly used to model the color of various forms of textile materials, with applications including computer color matching formulation, paints, printing and plastics coloration. To determine the most appropriate color model to use with different structures, a number of Kubelka-Munk theory based approaches were employed (Mathur 2007). In terms of textile structures, these previous works dealt with dye formulation for color matching of woven and knitted structures made from uncolored yarns. Other workers dealt with homogeneous mix of colored fibers to obtain a set color target for fabrics made from such fibers including nonwovens. In the following equations, the color contributions of dyes were replaced with the color contribution of each colored yarn a woven pattern as predicted from the model (Equations 4-6), and therefore the derived equations can be used to calculate the colorimetric values as:

$$\left(K/S\right)_{mix} = \sum_{i=1}^{\nu}\left(K/S\right)_{si} + \sum_{j=1}^{\lambda}\left(K/S\right)_{sj} + \sum_{i=1}^{\nu} c_{1i}(K/S)_{1i} + \sum_{j=1}^{\lambda} c_{2j}(K/S)_{2j} + c_b(K/S)_b \tag{7}$$

$$log\left(K/S\right)_{mix} = \sum_{i=1}^{\nu} c_{1i}\ \log(K/S)_{1i} + \sum_{j=1}^{\lambda} c_{2j}\ \log(K/S)_{2j} + c_b \log(K/S)_b \tag{8}$$

Where,
K = Light Absorption coefficient

S = Light Scattering coefficient
$(K/S)_{mix} = \left(K/S\right)$ of the woven area
$(K/S)_{s_i} = \left(K/S\right)$ of the undyed yarn substrate in warp
$(K/S)_{s_j} = \left(K/S\right)$ of the undyed yarn substrate in filling
$(K/S)_{1i} = \left(K/S\right)$ of the of i^{th} colorant in the mixture
$(K/S)_{2j} = \left(K/S\right)$ of the of j^{th} colorant in the mixture
$(K/S)_b = \left(K/S\right)$ of the background
c_{1i} = fraction cover of warp with warp color i (proportion of i^{th} colorant in the mixture)
c_{2j} = fraction cover of filling with color j (proportion of j^{th} colorant in the mixture)

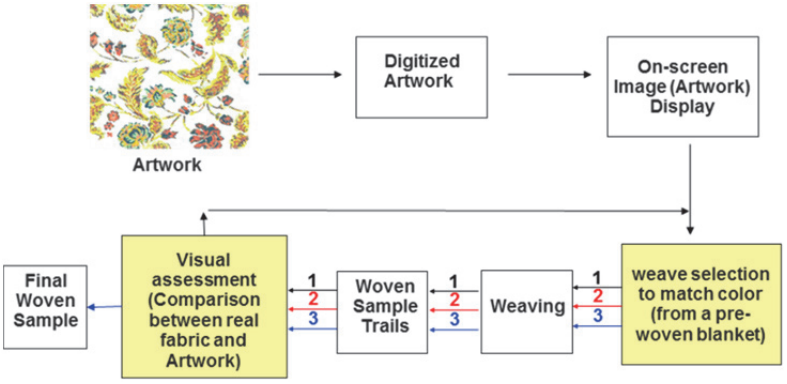

Fig. 14. a) Current/Traditional Design Process - Weave selection and sample matching still require the intervention of designer, who works from color gamut (blanket)

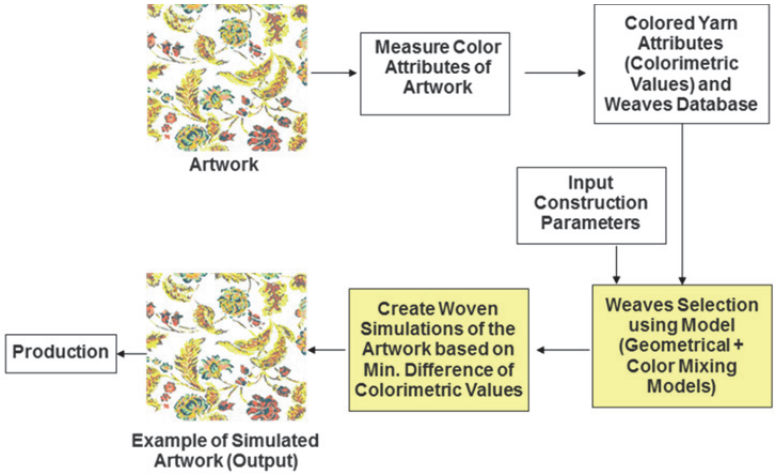

Fig. 14. b) Implementation of the Model in the scheme of the design process

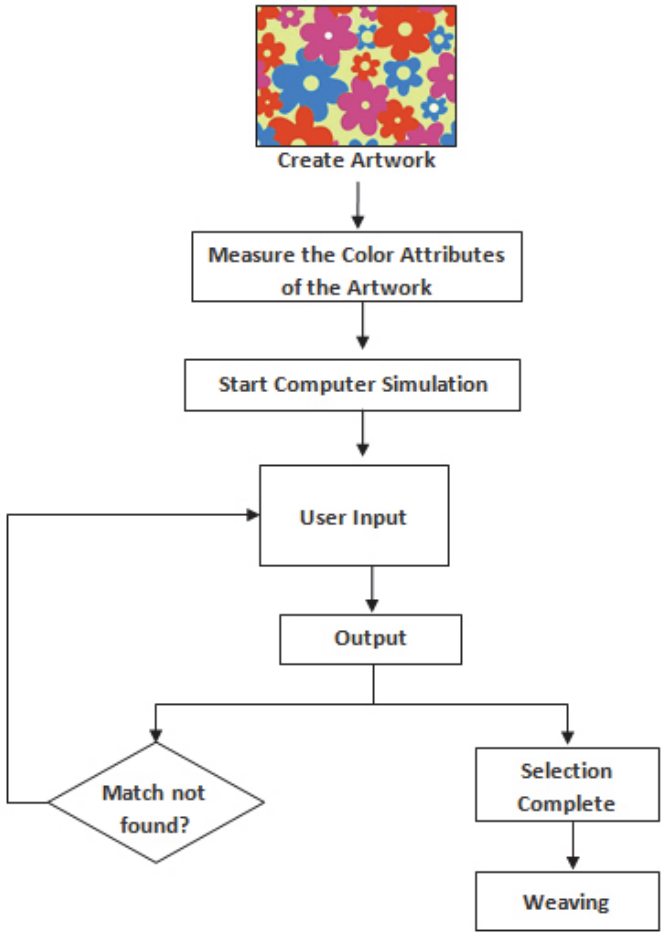

Fig. 15. Implementation of the Model in the scheme of design of patterned woven fabric (Seyam and Mathur 2008)

The color values obtained from these color equations (Equations 7 and 8) were analyzed statistically to validate the predicted color using the CIELAB ΔECMC(2:1) color difference equation (McDonald 1997). Also, extensive visual assessment experiments were designed and conducted for assessing the visual difference between the predicted and the actual color appearance of the woven structure. The results obtained from statistical analysis and visual assessment are reported elsewhere (Mathur et. al. 2008) The equations show how the geometric model and color model are combined to obtain the final color prediction in an objective way so the woven fabric color for each part of the design can be calculated using computer programming to automate the process of weave selection, which is currently (traditionally) decided subjectively by the designer which leads to more trials, high cost and long lead time to achieve the final target fabric (Figure 14a and b). Figure 14 a shows that three trials were conducted to reach to the target artwork while Figure 14 b indicates the

benefit of employing geometric and color models to automate the process of weave (color) selection.

The schematic flow of the design process using the model is illustrated in Figure 15. The process starts from creating artwork and measuring color attributes (defined in CIELAB color space (McDonald 1997)) for each color in the artwork. The computer simulation of the model allows the user to enter the design parameters. Next, the developed geometrical model calculates the contribution of each color and in combination with the color mixing equation, the final color of an area in the pattern can be obtained. The calculated color attributes are compared to the measured from the artwork. The difference of color attributes between the measured and calculated is checked. If the difference is within the tolerance, the program reports output that include the color attributes for calculated and actual, color arrangement, specific weaves within the classified weaves.

In case if the color differences are out of tolerance, the program reports to the user and suggests possible changes to the input parameters. This iteration continues until a reasonable match for each color in the artwork is achieved.

Below is an example to demonstrate the use of Equations 4-6 and to investigate the effect of weave and color pattern of warp and filling yarns on the contribution of each color used to construct the weave as shown in Figure 13. In this example, there are seven colors and the contribution of each color can be calculated from Equations 4-6. From the design parameters of Table 1, the parameters required for the color contribution can be calculated as shown below.

Construction Parameters									
Fabric ID	**Warp Yarn**		**Filling Yarn**		**Warp Density (end/cm)**	**Pick Density (picks/cm)**	**Weave**	n_{co1}	n_{co2}
	tex	**Material**	**tex**	**Material**					
A	30	Cotton, Ring Spun	30	Cotton, Ring Spun	41	24	1x3 Twill	1	3
B							2x2 Twill	2	2
C							3x1 Twill	3	1

Color Arrangement				
Warp		**Filling**		**Background**
Color	**Number**	**Color**	**Number**	**Color**
Purple	1	Dark Blue	1	White
Light Blue	1	Green	1	
Red	1	Black	1	

Table 1. Construction and color parameters of fabrics with different weaves

d_1 = warp yarn diameter, cm = 0.020469 cm; d_2 = filling yarn diameter, cm = 0.020469 cm; p_1 = warp spacing = $1/P_1$ = 1/41 cm; p_2 = pick spacing = = $1/P_2$ = 1/24 cm; c_1 = warp fraction cover = d_1/p_1 = 0.020469*41 = 0.839; c_2 = filling fraction cover = d_2/p_2 = 0.020469*24 = 0.491; c_f = fabric fraction cover = $c_1 + c_2 - c_1 c_2$ = 0.839 + 0.491 – (0.839) (0.491) = 0.918; ν = number of warp colors = 3; λ = number of filling colors = 3; l_1 = number of ends/weave and color; combined repeat = LCM (n_1, m_1) = LCM (4, 3) = 12; l_2 = number of picks/weave and color combined repeat = LCM (n_2, m_2)= LCM (4, 3) = 12; The values of n_{co1} and n_{co2} (defined below) are weave dependent as shown in Table 1.

n_{co1} = number of cross over areas where warp is over filling/weave repeat
n_{co2} = number of cross over areas where filling is over warp/weave repeat
The example under consideration has equal number of warp (or filling) yarns per color, thus,
m_{1i} = number of warp yarns of the i^{th} warp color = 4; m_{2j} = number of filling yarns of the j^{th} filling color = 4
Now all the parameters needed for the calculations of each color contribution are known. Since there are three warp colors, three filling colors, and a background color, seven color contributions are required. These are:
c_{11} = fraction cover of warp with warp color 1 (Purple); c_{12} = fraction cover of warp with warp color 2 (Light Blue); c_{13} = fraction cover of warp with warp color 3 (Red); c_{21} = fraction cover of filling with filling color 1 (Dark Blue); c_{22} = fraction cover of warp with filling color 2 (Green); c_{23} = fraction cover of warp with filling color 3 (Black); c_b = fraction cover of background (White). The seven parameters are calculated from Equations 4-6. Their values for the three fabrics of Table 1 are shown in Table 2. The total color contribution for each fabric (must be 1.0) is also shown to validate the correctness of the calculations.

Color	Weave		
	1x3 Twill	**2x2 Twill**	**3x1 Twill**
Purple	0.177	0.211	0.245
Light Blue	0.177	0.211	0.245
Red	0.177	0.211	0.245
Dark Blue	0.129	0.095	0.061
Green	0.129	0.095	0.061
Black	0.129	0.095	0.061
White	0.082	0.082	0.082
Total	**1.000**	**1.000**	**1.000**

Table 2. Color contribution of different weaves

The results of Table 2 indicate that the weave has a significant effect on the contribution of colors. For example, the purple color appeared on an area on the fabric surface of 17.7% for 3x1 twill weave. The same color covered 24.5% of the fabric surface by changing the weave to 2x2 twill. These two weaves are of the same size and interlacing (same tightness), but differ only in the number of crossover areas where warp yarn is over filling yarns. The effect of spacing can also be seen from the results of Table 2. For each weave of Table 2, a warp color dominated more area than a filling color. This is attributed to the fact that warp density (ends/cm) is higher than the pick density (picks/cm).

5. Conclusion

Color blending in woven fabrics is defined as the process of mixing color by combining different colored yarn components to produce a homogenous color appearance. Different colored yarns are mixed in certain proportion to obtain a required color. The final color is a function of the constructional parameters that manifest changes in the area of each yarn on the surface. The colorimetric data of the weave structures can be calculated by using the combined effect of the two aspects of fabric covering power, the optical (reflectance) and the

geometric. The geometric model is discussed in this chapter combined with suitable color mixing model can be used to calculate colorimetric attributes on the surface of the woven fabric. These calculations can be easily programmed and the process of assigning weaves/colors can now be automated and therefore the subjective intervention of the designer is no longer needed. This will help in eliminating the need for physical sampling prior to production and the subjective opinions as the color/weave selection will be done automatically by computer based on the colorimetric values that are very close match to the original artwork.

6. Acknowledgement

The authors express their sincere appreciation to National Textile Center and North Carolina State University for funding this research.

7. References

Adanur, S. 2001, Handbook of Weaving, Technomic Publishing Co., USA.

Amisharhi, S. & Pailthorpe, M.T. 1994, "Applying the Kubelka-Munk Equation to Explain the color of blends prepared from pre-colored fibers", Textile Research Journal, vol. 64, no. 6, pp. 357-364.

Berns, R.S. 2000, Billmeyer and Saltzman's Principles of Color Technology, 3rd edn, John Wiley & Sons Inc., New York, USA. Bojic, M.B. 1999, "CAD/CAM systems for Dobby and Jacquard Weaving", Tekstilec, vol. 42, pp. 77.

Burlone, D. 1984, "Theoritical and Practical aspects of selected fiber blend color-formulation functions", Color Research and Application, vol. 9, no. 4, pp. 213-219.

Burlone, D. 1983, "Formulation of Blends of Precolored Nylon Fibers", Color Research and Application, vol. 8, no. 2, pp. 114-120.

Burlone, D.A. 1990, "Effect of Fiber Translucency on the Color of Blends of Precolored Fibers", Textile Research Journal, vol. 60, pp. 162-166.

Dawson, R.M. 2002, "Color and Weave effects with some small weave repeat sizes", Textile Research Journal, vol. 72, no. 10, pp. 854-863.

Dimitrovski, K. & Gabrijelcic, H. 2004, "Corrections of color values of woven fabrics using changes to constructional parameters", AUTEX Research Journal, vol. 4, no. 4, pp. 187-193.

Dimitrovski, K. & Gabrijelcic, H. 2002, "Predicting of Color Values of Jacquard Fabrics", Tekstilec, vol. 45, no. 7-8, pp. 179-194.

Dimitrovski, K. & Gabrijelcic, H. 2001, "Calculating and measuring the fabric colour for fabrics woven from yarns dyed in different ways", Tekstil, vol. 50, no. 11, pp. 558-567.

Dimitrovski, K. & Bojic, M.B. 1999, "Changes of Dobby and Jacquard Weaving in Last Decade", Tekstilec, vol. 42, no. 11-12, pp. 371-375.

Doctor, V. 1997, "Selecting Aesthetically Imaginative and Technically Sound "CAD" System for Textiles", 42nd Joint Technological Conference.

Dolezal, B. & Mateja, B.B. 1995, "Computer Aided Design in Jacquard Weaving", Tekstilec, vol. 38, no. 9, pp. 237-247.

Dupont, D., Steen, D. & Caze, C. 2001, "Modeling color alterations after the spinning process", Textile Research Journal, vol. 71, no. 9, pp. 755-761.

Friele, L.C.F. 1965, "The application of colour measurement in relation to fibre-blending", Journal of Textile Institute, vol. 43, pp. 604.

Gabrijelcic, H. 2004, "ITMA 2003 – CAD/CAM Systems for Weaving", Tekstilec, vol. 47, no. 3-4, pp. 95-104.

Gabrijelcic, H. & Dimitrovski, K. 2004, "Influence of yarn count and warp and weft thread density on color values of woven surface", Fibers and Textiles in Eastern Europe, vol. 12, no. 1(45), pp. 32-39.

Grundler, D. & Rolich, T. 2003, "Matching Weave and Color with the help of Evolution Algorithm", Textile Research Journal, vol. 73, no. 12, pp. 1033-1040.

Gutherie, J.C., Moir, J. & Oliver, P.H. 1962, "Two problems associated with the blending Blending of colored fibers", Journal society of Dyers and Colour, , pp. 27-34.

Hoskins, J.A. & Hoskins, W.D. 1983, "Algorithms for the design and analysis of woven textiles", Proceedings of the 1983 ACM Conference on Personal and small computers, pp. 153.

Hoskins, J.A., Hoskins, W.D. & May, J.L.W. 1985, "Algorithms for color analysis", Proceedings of the 1985 ACM SIGSMALL symposium on Small systems, pp. 42.

Lambert, P., Staepelaere, B. & Fry, M.G. 1986, Color and Fiber, Schiffer Publishing Ltd.

Lourie, J.R. 1969, "Loom-constrained designs: An algebraic solution", Proceedings of the ACM National Conference, pp. 185.

Lourie, J.R. & Bonin, A.M. 1968, "Computer-controlled textile designing and weaving", Proceedings-IFIPS, pp. 884.

Lourie, J.R. & Lornzo, J.J. 1966, "Online Textile designing", Proceedings of the ACM National meeting, pp. 573.

Mathur, K. 2007, Color Prediction Model for Jacquard Tapestry Woven Fabrics, Ph.D. Dissertation, NCSU, North Carolina, USA.

Mathur, K., Seyam, A.M., Hinks, D., Donaldson, R.A. 2008, Prediction of Color Attributes through Geometric Modeling, Research Journal of Textile and Apparel, Vol. 12, No. 1, pp 19-31.

Mathur, K., Seyam, A.M., Hinks, D., Donaldson, R.A. 2008, Towards Automation of Color/Weave Selection in Jacquard Designs: Model Verification through Visual Assessment, Coloration Technology, Vol. 124, pp 48-55.

Mathur, K., Hinks, D., Seyam, A.M., Donaldson, R.A. 2009, Towards Automation of Color/Weave Selection in Jacquard Designs: Model Verification, Color Research and Application, Vol. 34, No. 3, pp 225-232.

Mathur, K., Donaldson, A., Hinks, D., Seyam, A.M. 2005, Color on Demand for Jacquard Fabrics, Research Journal of Textile and Apparel , Vol. 9, No.4, pp 26-37, Invited.

Miller, A. 1979, "A Computed Colour Catalogue of Fiber Blends and its use in Match Prediction", Journal society of Dyers and Colour, vol. 79, pp. 604-612.

Seyam, A.M. and Mathur, K., A General Geometrical Model for Predicting Color Mixing of Woven Fabrics from Colored Warp and Filling Yarns, The Proceedings of the 2nd International Scientific Conference, Textiles of the Future, Kortrijk, Belgium, November 13-15, 2008.

McDonald, R. 1997, Color Physics for Industry, 2nd edn, Society of Dyers and Colourists, Staples Printers Rochester Ltd.

Menz, D. 1998, Color in Spinning, Interweave Press. Lourie, J.R. 1973, Textile Graphics/Computer Aided, Fairchild Publications Inc., New York.

Osaki, K. 2003, "High Quality Color Reproduction on Jacquard Silk Textile from Digital Color Images", AUTEX Research Journal, vol. 3, no. 4, pp. 173-179.

Osaki, K. 2002, "Reproduction of Various colors on Jacquard textiles by only eight kinds of color wefts", Proceedings of SPIE, pp. 740.

Peirce, F.T. 1937, "The Geometry of Cloth Structure", Journal of Textile Institute, vol. 28, T45.

Pierce, P.E. & Marcus, R.T. 1997, "Radiative Transfer Theory Solid Color –matching Calculations", Research and Application, vol. 22, no. 2, pp. 72-87.

Pulton, D.P. & Porat, I. 1992, "The control of color by using measurement and feedback", Journal of Textile Institute, vol. 83, no. 3.

Randall, D.L. 2005, Digital Imaging for Textiles- Next Generation. Available: Techexchange.com [2004, December 20].

Reed, J., Jasper, W. & Hinks, D. 2004, "Quantitative measurement of Web Uniformity of Blended Fibers", INTC.

Rich, D.C. 1986, "Colorimetry in Textile Design Systems", Textile Chemist and colorist, vol. 18, no. 6, pp. 16-18.

Richards, R. & Struve, G. 2005, Color Theory. Available: http://abacus.bates.edu/ils/ctd/resources/design/color.html [2005, July 13].

Ross, T. 2005, CAD and Color. Available: Techexchange.com [2004, December 20].

Seyam, Abdel-Fattah 2001, "Structural Design of Woven Fabrics: Theory and Practice." Textile Progress. UK: The Textile Institute. 31, pp. 1-36.

Seyam, A.M. 2004, "ITMA 2003: Weaving Technology", Textile World, pp. 34-39.

Takatera, M. & Shinohara, A. 1988, "Color Order and Weave On a Given Color-And-Weave Effects", Sen-I Gakkaishi, vol. 44, no. 7, pp. 339-345.

Walowit, E. 1988, "Spectrophotometric color matching based on two-constant Kubelka-Munk theory", Color Research and Application, vol. 13, no. 6, pp. 358-362.

Walowit, E. 1987, "An algorithm for the optimization of Kubelka-Munk Scattering and Absorption Coefficients", Color Research and Application, vol. 12, no. 6, pp. 340-343.

Part 4

Advanced Properties of Woven Fabrics

8

Sensory and Physiological Issue

Laurence Schacher[1], Sourour Bensaid[2], Selsabil El-Ghezal Jeguirim[1]
and Dominique Adolphe[1]
[1]*Laboratoire de Physique et Mécanique Textiles, University of Haute Alsace*
[2]*Ecole Nationale d'Ingénieurs de Monastir, Unité de Recherche*
Textile de Ksar Hellal, University of Monastir
[1]*France*
[2]*Tunisia*

1. Introduction

1.1 Economical, social, environmental, and industrial contexts

A significant added value of textiles is sensory in nature. During garment handling in a shop, the customer engages a selection process that involves touching and trying on clothing. A multifaceted multi-sensory, emotional and psychological experience occurs. A decision is made and motivations are based on anticipated reality of preference, personality, and emotion.

The Integration of sensory feeling in product development was not only focused in textile industry. The use of sensory analysis methods started in the sixties for food products and has been extended to many non-food products including personal care, pharmaceutical and paper products. New design processes integrating the designers' constraints and the consumers' expectations for better qualities perception have therefore been proposed in other industries. Sensory analysis methods have been widely used as market research tools in recent times and significant examples of application can be found in automotive industry. The latter has recently performed several attempts to understand and characterise the sensory preferences of end-users and to translate these features into technical specifications for new products development (Giboreau et al., 2001). However, this trend may be more prominent for textile industry as many factors can be given for conferring "character" to a material observed through handling. Micro fibres, silk-like and peach-like, cool or soft touches have been successfully developed in the past and new and exciting textile products. Hence, finishing treatments are still studied and launched on the market for that purpose. This phenomenon has been largely increased nowadays by the new textile industry developments in terms of globalization and new virtual-environment applications demand for variety and personalization. The main objective is to tailor products to the preferences of each consumer (Nakano, 1994), (Okamoto, 1991).

2. Scientific context – State of the art

Recently, industrialists have moved away from usability-based approaches and towards different ones to defining user requirements. This strategy provides a framework for

considering the sensory, hedonic and practical user's requirements within the product design or product evaluation process. Therefore, considering the benefits that a product should bring to its users, the next step is to determine the design characteristics through which the product can deliver these benefits. It can be considered to referring to *kansei engineering* which has been pioneered by Nagamachi (Nagamachi, 1995) in Japan since the 1970s. *Kansei* is a Japanese term for consumers' psychological impressions and feelings about a product. This approach encompasses physical, physiological, and psychological point of views.

2.1 Physical point of view

More than eighty years have passed since the earliest efforts of Peirce (Peirce, 1930) in the textile field to evaluate fabric hand thanks to physical measurement data. Several studies have then been undertaken to use instruments to measure fabric hand, notably Kawabata's method of the Japanese Hand Evaluation and Standardization Committee (HESC) in the 1970s (HSEC, 1980; Kawabata, 1988), and a number of mechanical devices, including KES (Kawabata Evaluation System), FAST (Fabric Assurance by Simple Testing), and UST (Universal Surface Tester), have been developed to objectively characterize fabric hand quality (Pan & Yen, 1992; Pac et al., 2001; Fontaine et al., 2005; Issa et al., 2008; Maâtoug et al., 2009). Along the instrumental tests, all fabrics are subjected to deformations similar to those applied by the hand experts, using the same modes and rates. These tools are usually fast, repeatable and well understood; however, they may not represent the textile good in use as the measured mechanical parameters cannot directly reflect human sensation in a precise way. Indeed, fabric perception, which can be defined as the human sensory response towards fabric, obviously involves not only physical and mechanical factors, but also physiological, perceptional and social factors.

2.2 Physiological point of view

Physiological approach is focused on the body - information derived from the sensory organs. This information covers tactile, visual and olfactory properties. Tactile pleasures concern holding and handling a textile product. This might be relevant in the context of garments shopping. Olfactory pleasures concern the smell of the new product: the smell inside a new car may be a factor that effects how pleasurable it is for the owner. Hedonic characteristics of fabrics and garments are therefore to be considered by textile manufacturers.

2.3 Psycho-physical point of view

The psycho-physical point of view relates to how the consumer mood is affected by interaction with a product. It might be expected, for example, that a new garment would provide a higher level of psychological pleasure than the old casual one. In the context of textile products it would relate to, for example, the aesthetics of a product and the values that a product embodies.

3. Methods to assess human perceptions: sensory analysis

In the 50s, sensory analysis emerged, first by the development of methods used by food industry and in 1974 in USA; a complete methodology for descriptive analysis was

proposed (Stone et al., 1974). The sensory analysis has shown a promising tool for taste and smell in food industry and has been applied with success in cosmetic industries such as Nestle, L'Oreal, Dior, (Young et al., 2005; Stone & Sidel, 2007). Textile materials have been a subject of interest concerning sensory analysis. The first attempt is reported by Binns (Binns, 1926). Since the early 80s, standard methods have been developed and published. They are customization of methods established in food science (Depledt, 1998); Barthelemy et al., 1990; Meilgaard et al., 1991). A methodology for sensory analysis of tactile feeling of textile fabrics was developed in France and the results reported a creation of tactile sensory profile (Depledt, 1998; Cardello et al., 2003; Philippe et al., 2003; Chollakup et al., 2004 a; 2004 b; Bensaid et al, 2006). Automotive industry has also applied sensory methods for their own products. Sensotact® reference frame is a commercial example of an attempt to formalize and calibrate descriptions of tactile perceptual dimensions. It was developed by French Renault Automotive Company (Sensotact, 2008). Italian Fiat Company (Bandini et al., 1997) has also shown some relevant sensory design engineering examples for their products.

3.1 Definition of sensory analysis

The basic assumption of sensory evaluation is the ability to perform objective measurements of sensations using a panel of people as an instrument. The sensory analysis is defined as « the examination of the organoleptical properties of a product using the human senses » (ISO 5492, 1992). Fortin and Durand (Fortin & Durand, 2004) give the following assertion « The sensory analysis can be defined as the study of the human response to a stimulus (…) The sensory analysis qualifies and quantifies the felt perceptions of persons called judges or panelists when they evaluate products or materials inducing our reactions senses. These methods could be applied to food, perfumes, cosmetics, textiles, automotives… Based on these definitions, it can be assumed that the sensory analysis of the products consists in the description or their evaluation through words called descriptors or attributes linked to each of our senses (sight, hearing, taste, smell, touch).

3.2 Measurement principle

The evaluation starts with the contact between the body and the environment and the interaction of the product with the judge. It is the "sensorial stimuli", which will be analyzed in different manners regarding the personal history of the "judge" and will be linked with the relationship existing between him or her and the evaluated object. The analysis of the "sensorial stimuli" is a unique function dedicated to the human being and no measurement device could reproduce it" (Fortin & Durand, 2004). In other words, the sensory analysis method uses the human senses as measurement device. In this way, it is essential to understand how the senses are working in general and the tactile sense in particular. Every sensory information is issued from a stimulus applied on the sensorial receptors by the environment. Generally, the stimulus feeling unrolls the following procedure (Rosenweig & al., 1998; Richard & Orsal, 2001).

Signal reception: every sensorial system is activated when a stimulus is generated by an external event applied on an organ. These sensory organs select stimuli, it is the filter phase.

Transduction: the human sensors convert the external event in electric signals understood by the nervous system. This step is followed by the transmission of this signal to the nervous centers.

Integration: The different information will be treated and computed by the central nervous system which will generate the response in relation to the solicitation.
The sensorial sensors are usually grouped in sensorial organs and are specialized in one particular sensorial solicitation.
A feeling is beginning when a stimulus activates a sensory organ. The sensory responses are generated after 0.1 to 0.2 second after the stimulation. First, the stimulus is coded in terms of quality and intensity. The response to a sensory stimulation could be physiological, behavioral, verbal, or psychological; taken into consideration that, at least, only the three first responses are observable (SSHA, 1998).
Generally, as a first step in fabric sensory analysis, monosense approach is preferred. Usually, tactile only or visual only examinations are performed by panelists: for tactile evaluation, tests are carried out in "blind" conditions in order to reduce biases that could be induced by seeing the fabric such as subjective preference of a special colour or material. However, human beings are equipped with multiple sensory channels through which they experience objects in the environment. There is obvious evidence that perception of information provided within one sensory modality can be greatly influenced by stimuli caused by another modality. It is true that consumer can see the fabric when touching it and tactile exploration of a textile surface is usually accompanied by visual sensory inputs and in a context of purchase. In such conditions, the consumer has the possibility to see the colour of the fabric and to know which kind of material it has been made from as well as its context of use. During tactile exploration, one can also sometimes hear the sounds made as the fingers explore the fabric. One can sometimes smell the odour of the fabrics. For all possible combination, the correlation between visual and tactile properties has mainly been studied (Lederman et al., 1981; Konyo et al., 2002, Cinel & al., 2002, Guest & Spence, 2003, Mucci et al., 2005, Bensaid & al., 2008). In these studies, the superiority of vision in the multi-modal sensational perception has been somehow demonstrated (Konyo et al., 2002). This first modality corresponds to several marketing results showing that vision is the very first data required by consumers and that the risk of not feeling, and trying on clothing before purchase may be the greatest challenge for Internet clothing sales, and is an issue that must be addressed. Some companies are developing Virtual 3-D try-on technology that might reduce the risk of ill-fitting or inappropriately styled clothing for one's body type, by providing the consumer with a view of the garment on his/her body. Inappropriate tactile or sound or smell feelings would be more complex to address with such technologies. However, Lederman et al. (Lederman, 1981; Lederman & al., 1986) have shown that the extent to which the data from one modality is preferred over the other depends on the nature of the task to be performed. Consequently, some tasks appeared best suited to vision (e.g. determining the spatial density of texture elements), and some to touch evaluation (e.g. determining the roughness of fine textures).
The touch feeling is known to be one of the most important senses. The skin which is the main organ of the tactile sensibility covers our body with an average surface of 1.7m² for an adult person. It is made of two layers: a top layer called epidermis which is renewed every 20 days and a bottom layer called dermis which contains nerves and blood vessels. The touch feeling groups three main modalities: mechanical sensibility, thermal sensitivity and pain.
The mechanical sensibility: also called touch sensibility corresponds to the response to pressure, touch and vibration solicitations. This sensibility depends on numerous

parameters such as shape, surface, duration and intensity of the stimulus. The mecano-receptors are the key elements of this sensibility.
Six kinds of receptors have been listed, the Merkel disks, the tactile disks, receptors of the hair follicles, the Meissner corpuscles, the Ruffini corpuscles and the Pacini corpuscles as shown in the figure 1.

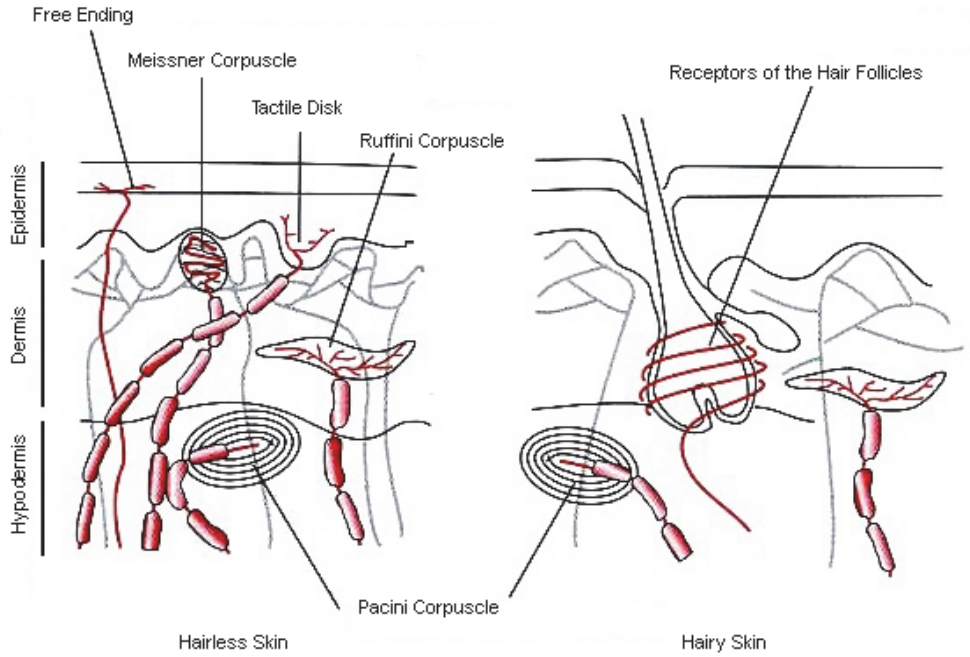

Fig. 1. Scheme of the skin and location of the touch sensors (Richard & Orsal, 2001)

The figure 2 displays the location (a), the size and the density (b) of the four kinds of receptors in the internal face of the hand (Richard & Orsal, 2001). Every cerebral region manages a precise skin part. This repartition has been presented in a caricature manner through the "homoculus" display (figure3) where every organ is represented with a surface in relation with its touch sensors density (Richard & Orsal, 2001). Nevertheless, the tactile sensibility is not fully linked with the density of the touch sensors but it is more driven by the number of connections in the sensitive cortex of the brain. On apes, some studies have shown that the sensitive surface could be increased or decreased thanks to training. Figure 4 represents a map of the spatial discrimination for the different organs. The more sensitive parts are the fingers tips and the tongue end.
Thermal sensitivity corresponds to two opposite sensibilities, the sensitivity to warm and the sensitivity to cold. These feelings are detected by some specific points which are sensitive to hot and warm and that are scattered all over the skin with a lower density than those dedicated to mechanical stresses. Moreover, the sensitive points to cold are more numerous than those sensitive to hot.

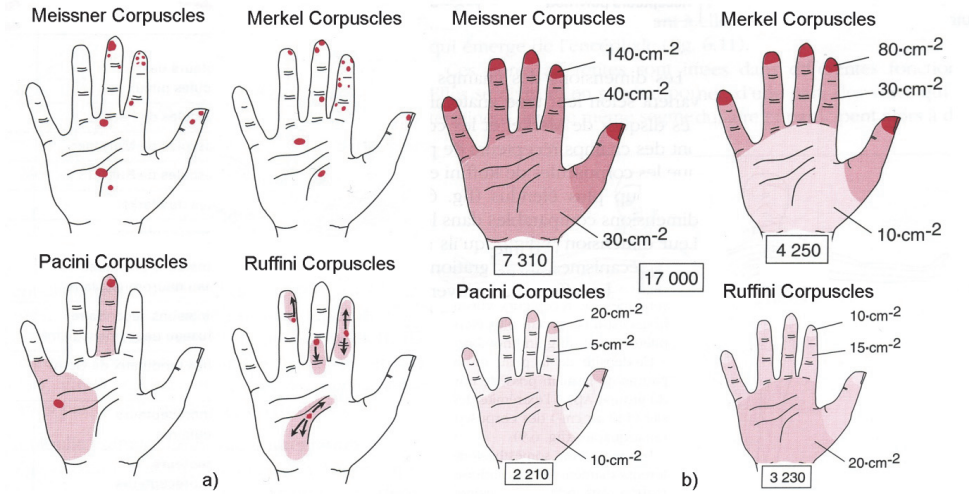

Fig. 2. Touch Sensors location a) and density b) in the inside hand

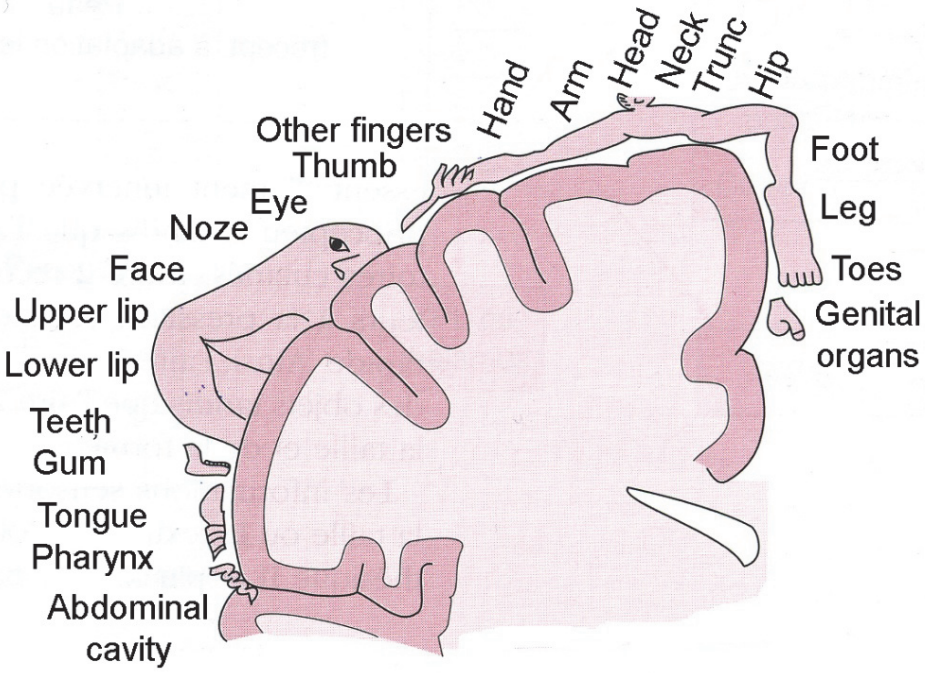

Fig. 3. Homoculus caricature display

Pain is a feeling generated by a high level stimulation called "novice" because it induces injuries in the organism. Different kinds of pain can be detailed: superficial pain which is

coming from the skin, deep pain coming from the bones, from the muscles, from the joints or the tendons. The receptors involved in this feeling are called "nocireceptors".

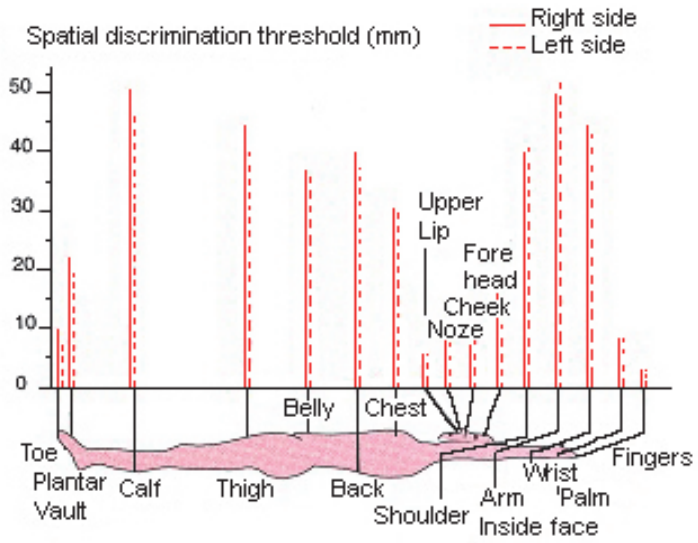

Fig. 4. Spatial discrimination threshold of human organs

3.3 Sensory analysis: Methodology

In regard to the final goal of the evaluation, comparison, quality measurement, new product characterization, etc, different kinds of tests issued of the sensory analyze set could be performed (AFNOR V09-001, 1983; AFNOR XP V 09-501, 1999; ISO 6658, 1985). One of the most frequently used, the descriptive test allows characterizing, comparing and quantifying differences between tested products. The method requires a group of trained judges (panelists), who are intensively trained to qualify and quantify their feeling and hedonic judgment in an objective way. The product characteristics are dissected through their expertise. The panelists first agree on specific and objective sensory vocabulary (ISO 11035, 1995) to describe the feeling of a product range (Nogueira & al., 2009).

Continuous training enables them to sharpen their perceptions and to perceive differences of intensity between products for every criterion. Training the panels also leads to homogeneity and reproducibility in the ratings (ISO 8586, 1993). Finally, a final grading enables to build out product sensory *identity maps* or *profiles*, or *fingerprints*. The obtained results are rich and powerful as they allow identifying all of a product's perception characteristics along with measures of the importance of those characteristics.

Figure 5 represents a sensory map of raw cotton woven fabrics before (non-treated) and after various commercial post-treatments (m, sd, sp, k) evaluated by 11 trained panelists. The tests were replicated twice and the order of presentation of the samples was randomized for each assessor. The displayed differences on figure 5, even the smallest one, are significant in regards to statistical analysis.

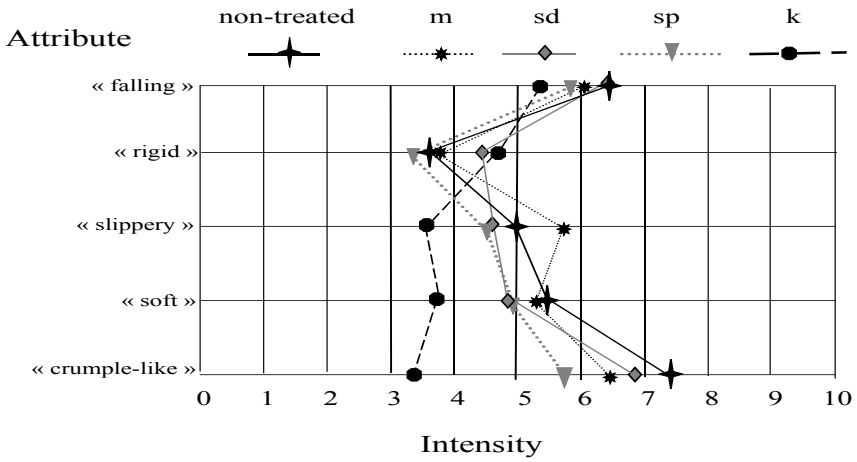

Fig. 5. Example of tactile sensory profiles of textile woven fabrics

However, the panelists are not representative of the end-users and therefore are not asked to perform the hedonic studies. The complete sensory methodology process involves another group of persons: the final consumers. This group is not trained, the persons being merely questioned on their preferences (like-dislike). Both approaches lead to *preference mapping* (Schlich, 1995) that allows specifying preferred sensory characteristics of products for given groups of end-users. Figure 6 represents the main methods in sensory analysis.

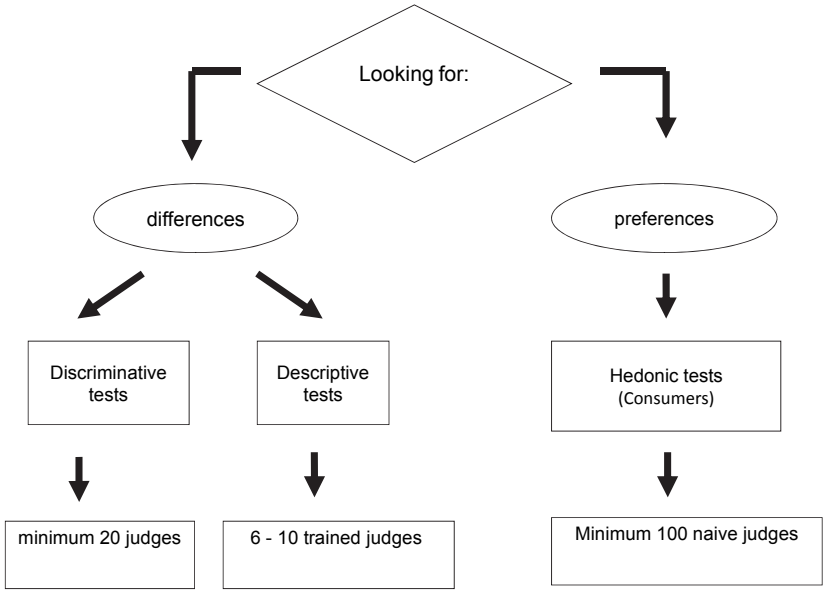

Fig. 6. Methods of sensory analysis

Sensory analysis is using "human beings" as a tool but it is employing objective methods to collect their subjective sensory responses. One disadvantage of the sensory methodology is the time consuming due to the panel recruitment, training and the validations of each step of the methods using the appropriate statistical tools.

4. Innovating method and numerical tool to simulate complex systems

Several attempts have been made to model the relationship between tactile sensory attributes of fabrics and their production parameters, or their instrumental measurements. Hence, statistics and multivariate analysis (Bishop, 1996) and methods based on intelligent techniques (neural networks, fuzzy logic...) have been used (Vassiliadis et al., 2010). The intelligent techniques have proven a very efficient tool for the fast and precise solution. Therefore, they have found increasing applications in the textile field such as properties prediction and process optimization.

4.1 Artificial Neural Network

An artificial neural network (ANN), usually called neural network (NN), is a mathematical model or computational model that tries to simulate the structure and functional aspects of biological neural networks. A neural network consists of an interconnected group of artificial neurons and processes information using a connectionist approach to computation. Neural networks are non-linear statistical data modelling tools. They can be used to model complex relationships between inputs and outputs or to find patterns in data.
There are many different ANN structures and learning algorithms available in the literature (Haykin, 2000). Among these algorithms, multilayer perceptron (MLP) has been successfully applied. A typical multi-layer neural network with a single hidden layer is shown in Fig.7. Each neuron receives a signal from the neurons of the previous layer and these signals are multiplied by separate synaptic weights. The weighted inputs are then summed up and passed through a transfer function, which converts the output to a fixed range of values. The output of the transfer function is then transmitted to the neurons of next layer. This process is continued and finally the output is produced at the output node. Predicted output is then compared with the desired output and an error signal is generated.

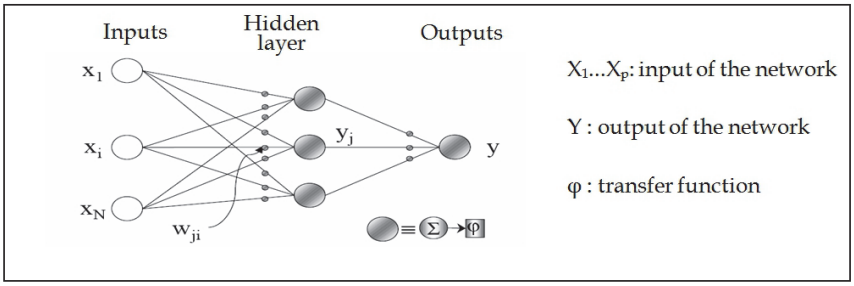

Fig. 7. A multilayer artificial neural network

The error signal is then minimised in iterative steps by adjusting the synaptic weights using a suitable training algorithm (figure 7). Among the various kinds of algorithms for training neural network, the back-propagation algorithm developed by Rumelhart et al. (1986) is the

most widely used. Network weights are adapted iteratively until some appropriate stopping criteria are met and the best weight vector that corresponds to the best generalization is achieved.

4.2 Fuzzy interference system

The foundation of fuzzy logic, which is an extension of crisp logic, was first proposed by Zadeh (Zadeh, 1965). The theoretical aspects of fuzzy logic and fuzzy arithmetic have been explained in many standard textbooks (Zimmerman, 1996). In crisp logic, such as binary logic, variables are true or false, black or white, 1 or 0. In fuzzy logic, a fuzzy set contains elements with only partial membership ranging from 0 to 1 to define uncertainty of classes that do not have clearly defined boundaries. For each input and output variable of a fuzzy inference system (FIS), the fuzzy sets are created by dividing the universe of discourse into a number of sub-regions, named in linguistic terms (high, medium, low etc.). If X is the universe of discourse and its elements are denoted by x, then a fuzzy set A in X is defined as a set of ordered pairs as $A=\{x, \mu A(x) \mid x \in X\}$ where $\mu A(x)$ is the membership function of x in A.

Once the fuzzy sets are chosen, a membership function for each set is created. A membership function is a typical curve that converts the input from 0 to 1, indicating the belongingness of the input to a fuzzy set. This step is known as "fuzzification". Membership function can have various forms, such as triangle, trapezoid, sigmoid and Gaussian.

The linguistic terms are then used to establish fuzzy rules. Fuzzy rules provide quantitative reasoning that relates input fuzzy sets with output fuzzy sets. A fuzzy rule base consists of a number of fuzzy if-then rules. For example, in the case of two inputs and single output fuzzy system, it could be expressed as follows:

$$\text{If x is Ai and y is Bi then z is Ci} \tag{1}$$

where x, y and z are variables representing two inputs and one output; Ai, Bi and Ci, the linguistic values of x, y and z respectively.

The rule base contains linguistic rules that are provided by experts. It is also possible to extract rules from numerical data. Once the rules have been established, the FIS can be viewed as a system that maps an input vector to an output vector.

The output of each rule is also a fuzzy set. Output fuzzy sets are then aggregated into a single fuzzy set. This step is known as "aggregation". Finally, the resulting set is resolved to a single output number by "defuzzification". These main steps involved in modeling a fuzzy system are shown in Fig.8.

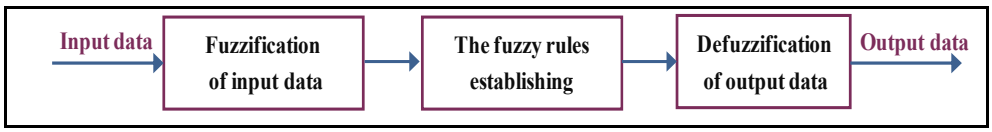

Fig. 8. General depiction of fuzzy system

4.3 Modeling the relationship related to sensory evaluation

4.3.1 Modeling the relationship between sensory properties and production parameters

In order to face the competitive environment, textile companies are interested in designing and producing new industrial products adapted to the specific needs of consumers with a

minimal number of experiments. In fact, specific fabrics tactile properties desired by consumers can be reached by adjusting the process parameters.
Several investigators have used statistics and multivariate analysis, such as multiple factor analysis MFA and principal component analysis PCA for studying the influence of finishing treatments on low stress mechanical properties and sensory attributes (El-Ghezal Jeguirim et al. 2010 a; 2010b; 2011). Although classical computing techniques are relatively efficient to interpret and analyze the relationship between sensory properties and production parameters, some limitation related to the non-linear relations in sensory domain has been reported (Zeng et al., 2008).
New methods based on intelligent techniques (fuzzy logic, neural networks...) are used to treat a great number of textile applications (Dubois & Prade, 1997; Kwak et al., 2000; Jain et al., 2004; Wong et al., 2006; Ertugrul & Ucar, 2000; Vassiliadis et al., 2010). Zeng et al. have used the fuzzy logic technique for modeling the relationship between the production parameters and the physical features of fabrics (Zeng et al., 2004). The instrumental features have been measured on Kawabata Evaluation System. In order to reduce the inputs number, a small number of relevant physical features have been selected using human knowledge on fabric production and fabrics properties. In the modeling procedure, the fuzzy rules have been extracted from measured numerical data. These extracted rules have been validated and adjusted by human knowledge on production processes. In this way, the two information sources (human knowledge and measured data) are both taken into account in the fuzzy rules of this model.
El-Ghezal Jeguirim et al. (El-Ghezal Jeguirim et al., 2009) have developed neural network and fuzzy logic based models to predict the sensory attributes, evaluated by a trained panel, of knitted fabrics from the structure and process parameters. In their further work, the intelligent techniques have been used for modeling the relationship between the instrumental properties measured by Kawabata Evaluation System and the finishing parameters of knitted fabrics (El-Ghezal Jeguirim et al., 2011). The prediction performance of these models was considerably lower than the mean variations of experimental values. These results showed the intelligent techniques ability to model the relationship between manufacturing parameters and instrumental or sensory tactile properties. The fuzzy or neural models provide contribution in industrial products engineering, with minimal number of experiments and short cycles of product design. The prediction performances of neural and fuzzy models were also similar. However, the 'black box' problem associated with neural networks can hinder the widespread adoption of this method. In fact, the fuzzy techniques have two advantages over the neural ones. In fuzzy models, the linguistic rules can be interpreted and the linguistic sensory attributes can be integrated. Thus, it is possible to observe how the fuzzy model performs its computations.
Moreover, better results can be obtained when these techniques are used in combination. In fact, hybrid models based on neuro-fuzzy methodologies combine the self learning ability of neural networks and the human-like reasoning style of fuzzy systems. Hence, neuro-fuzzy models can provide enormous scopes to link sensory attributes or mechanical properties with processes parameters of fabrics.

4.3.2 Modeling the relationship between sensory properties and instrumental measurements

The sensory evaluation method has been adapted to textile products to characterize consumer preference for textile products. However, sensory evaluation is time-consuming

and expensive. Therefore, reliable and practical instrumental methods are needed to accurately predict sensory tactile attributes, at least in the product development and quality control stages. Several instrumental methods (Kawabata, 1975; 1980; Kawabata et al., 1982; Tester and De Boos, 1990; Pan & al., 1993, Pan & Yen., 1992) have been developed for measuring the tactile feeling of fabrics according to their physical mechanical, thermal and surface properties. Hence, modeling the relationship between instrumental measurements and sensory attributes becomes a key problem in tactile quality assessment.

Wide ranges of statistical or multivariate analysis have been proposed for characterizing this relationship and selecting the relevant instrumental and sensory properties. In particular, Weber-Fechner's law (Matsuo et al., 1971; Bishop, 1996; Rombaldoni et al., 2010), Stevens's power law (Bishop, 1996; Elder et al., 1984; Rombaldoni et al., 2010), and PCA (Mackay el al., 1999; El-Ghezal Jeguirim et al., 2010 b) have been usually applied.

Matsuo et al. (Matsuo et al., 1971) used the Weber-Fechner's law to translate instrumental measurements of a wide of fabric mechanical properties into corresponding hand parameters. Although the method has the virtue of independence of fabric type, further work would be needed to check the validity of the Weber-Fechner's law for modeling the complex sensory-instrumental relationship.

Elder et al. (Elder et al., 1984) used Stevens's power law to examine the relationships between subjectively measured softness and a compression and also between subjective stiffness and a flexural rigidity. Excellent correlation was found, correlation coefficients for the Stevens's law being about 0.97. On the evidence of the results of Elder et al., Stevens's law appears to be an excellent model. Although the relationship breaks down in some cases, this fact is probably because the subjective evaluation attribute cannot be adequately represented by a single instrumental parameter. This problem may be overcome by relating each sensory score to the sum of the different contributions made by a number of instrumentally measured properties that are relevant to well-defined fabric types or end uses. Rombaldoni et al. (Rombaldoni et al., 2010) investigated the possibility of predicting the human psychophysical perception of crispness and coolness hand of men's suit woven fabrics made from animal fibers (wool, mohair, cashmere and alpaca) from measurable low-stress mechanical and thermal parameters. In particular, the parameters chosen were weight per unit area, thickness at 9.81 kPa, surface thickness, bending rigidity, extensibility at 98.1 N/m, shear rigidity, formability and thermal absorptivity. The sensory-instrumental relationship was explored using the Stevens's power law. The correlation results were also compared by the predictive power of other mathematical models: a linear function and the Weber–Fechner law. The obtained results showed that the Weber–Fechner-law-based model was the best to predict the sensory hand value.

Mackay el al. (Mackay et al., 1999) used Principal Component Analysis (PCA) to study relationships between sensory and instrumental measurements of the effect of washing processes on 1x1 rib knitwear fabrics. El-Ghezal Jeguirim et al. (El-Ghezal Jeguirim et al., 2010 b) investigated the relationship between instrumental data and sensory attributes, assessed by a trained panel by using PCA. The obtained results have shown that the compression resilience, the geometrical and frictional roughness are significantly correlated with the following sensory parameters thick, heavy, soft, elastic and crumple-like attributes.

The intelligent techniques, including fuzzy logic and neural networks are also used for modeling the relationship between instrumental measurements and sensory properties. Hui et al. have developed a neural network to predict the consumers sensory data from fabric properties (Hui et al., 2004). The predicted results are highly correlated to the targets in the

fabrics made by five materials: cotton, wool, polyester, nylon, and acetate. In the validation, the results show that the proposed network also predicts the hand of linen and silk. Another work for predicting fabric hand from physical measures has been done by combining fuzzy logic and neural networks (Park et al., 2000). The obtained results revealed that the neural networks and fuzzy logic provide an alternative approach for predicting sensory properties from instrumental measurements of fabrics.

5. Applications study cases for cotton/woolen woven fabrics with difference pattern

The main applications of sensory analysis in textile industry are focused on the analysis of the factors affecting fabric hand. Many studies have been conducted to identify the effect of construction factors, such as pattern, yarn properties, fabric materials, or finishing treatments on the fabric tactile quality by using the sensory analysis (Bensaid & al., 2006; El-Ghezal Jeguirim et al., 2010 a; 2010 b).
In order to provide reliable descriptions and evaluation of fabric hand, rigorous procedures have to be implemented i.e. exploratory procedures, samples presentation and data analysis. In this section, a detailed description of the followed procedure is presented before the discussion of some studies' results.

Description of the followed experimental protocol

Sensory analysis method has been developed in the group since 1999. It requires a group of trained persons. In these cases, the sensory panel comprises nine adults between 20 and 50 years old. These persons, called assessors, have been trained according to a previously established methodology (Nicod, 1990; NF-ISO, 1993). The tests are conducted in an environmentally controlled room (20°C and 65% Relative Humidity) (NF EN 20139, 1992). The assessors evaluate the products twice, in particular conditions, in order to avoid some bias due to other senses. The presentation of the fabrics is randomised and the evaluation is done without seeing the fabric using specially designed booth.
Sensory rating is done using a set of 15 individual sensory attributes (Table 1) to build profile consisting of the descriptive, quantitative and objective analysis of the fabric. These attributes have been consensually selected by the assessors and have been used for different types of fabrics (NF-ISO 5492, 1992; NF-ISO 11035, 1995). Quotation is performed on a non-structured scale 0-10.
Before every new product category evaluation, the assessors are retrained for ten sessions. This step allows them to become familiar with the procedure of evaluation and to remember the right meaning and extremes of each attribute.
The pertinence of the attribute is checked later using statistical tools.
In this chapter the effect on the fabric hand of cotton fabrics of three series of parameters will presented: effect of the weaving patterns, effect of the yarn count, and effect of finishing treatments.

5.1 Effect of the weaving patterns on the fabric hand of cotton fabrics

Materials
In order to study the effect of weaving pattern, nine fabrics have been selected. The samples have been woven with nine classical weft effect patterns on a Jacquard loom. The patterns include a plain weave, 3-twill weave, 4-twill weave (Z direction), waved twill weave

Bipolar attributes	Surface attributes	Handle attributes
cold-warm thin-thick light-heavy supple-rigid	pilous soft granulous sticky grooved greasy slippery	falling responsive crumple-like elastic

Table 1. List of the 15 attributes used for the sensory evaluation

(horizontal effect), 4-satin weave, 5-satin weave, 6-satin weave, 12-satin weave and crêpe weave; the yarns are 100% cotton, 14 Tex for the warp and 25 Tex for the weft. In order to highlight the influence of the pattern on the tactile feeling, we tested fabrics having close characteristics. Hence, the saturation index in weft direction was kept equal to 52%. This index is defined as following:

$$I_t = \frac{100 \text{ x D (yarn count within the fabric)}}{D_{max} \text{ (maximum yarn count)}} \quad (2)$$

Microphotographs of the fabrics weaved in different patterns are presented in Figure 9. Their characteristics are presented in Table 2.

Pattern	Weft count (tex)	Warp count (tex)	Area density g/m²	Saturation index (%)
Plain	25	14	124.8	52
3-Twill	25	14	140.0	52
4-Twill	25	14	140.8	52
4-Satin	25	14	141.8	52
5-Satin	25	14	141.6	52
6-Satin	25	14	147.0	52
12-Satin	25	14	147.2	52
Waved twill	25	14	150.2	52
Crêpe	25	14	135.6	52

Table 2. Characteristics of the tested fabrics

Results and discussion

Statistical methods of data analysis have been applied. The ANOVA 2-way test (5%), applied on product across assessor variables, outlined that only 4 attributes are not affected by the fabric pattern (*warm*, *sticky*, *greasy* and *elastic*), the other 11 attributes are significantly affected (Table 3). Four attributes are considered as non pertinent for this study: *cold–warm*, *sticky*, *greasy* and *elastic*. The three first are material dependant and the same weft and warp material (100% cotton) was adopted whatever the pattern is. The last one, *elastic*, could be dependant of the pattern, but in woven fabrics case, the elastic behavior is relatively low in comparison to the knitted fabrics. Hence, the marks given by the panellists are around 0 with a non significant difference between the different samples.

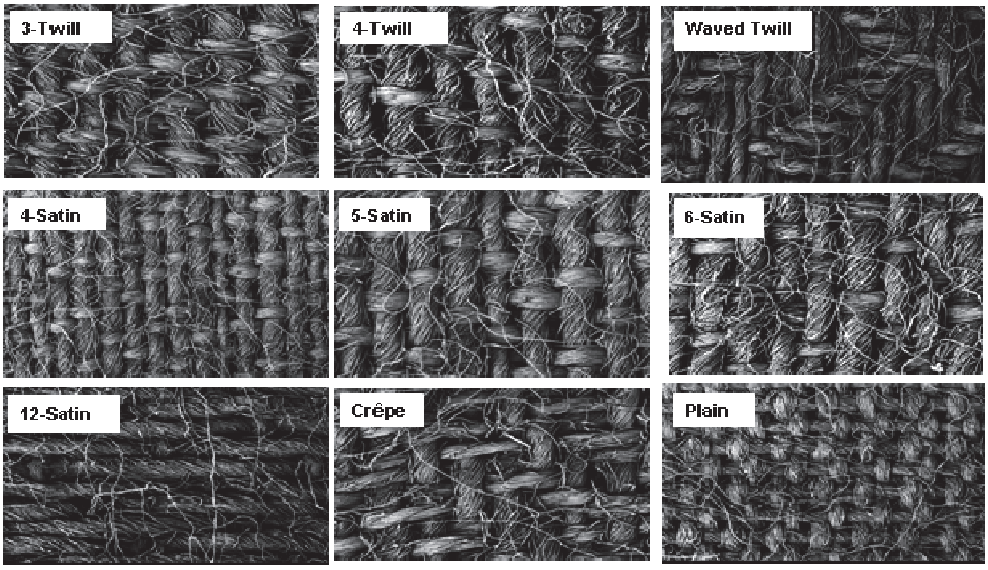

Fig. 9. Microphotographs of the nine different patterns

Attribute	Product	Assessor	PdxAs
Warm	NS	×	NS
Falling	×	×	NS
Thick	×	×	NS
Heavy	×	×	NS
Rigid	×	×	NS
Sticky	NS	×	NS
Slippery	×	×	NS
Soft	×	×	×
Granulous	×	×	×
Greasy	NS	×	NS
Pilous	×	×	×
Grooved	×	×	×
Elastic	NS	×	NS
Responsive	×	×	NS
Crumple-like	×	×	×

Table 3. ANOVA 2-way test (5%) for all the attributes and all the fabrics

According to the column PdxAs, it appears that *soft*, *granulous*, *pilous*, *grooved* and *crumple like* have been marked in a different manner depending of the judges.

The sensory profile is the simplest way to visualize the results. Each horizontal line represents the scale of one attribute, on which the mean score is plotted. All marks related to the same product are joined by a line. Figure 10 shows the profiles of the nine weaving patterns.

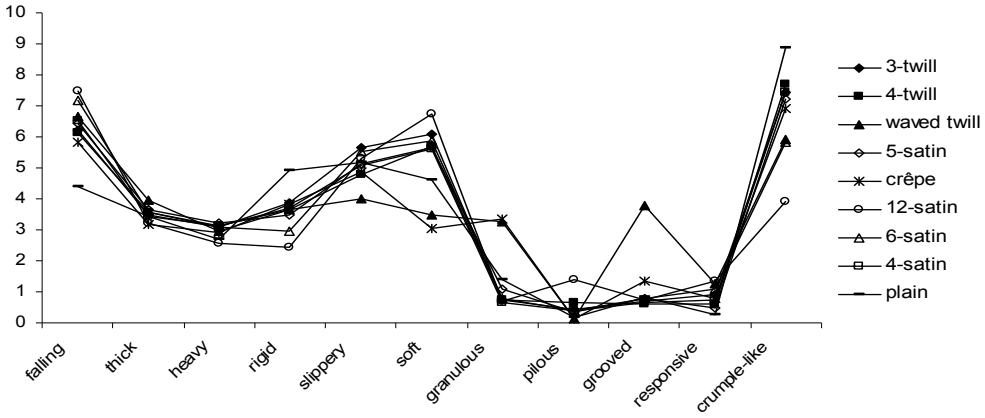

Fig. 10. The sensory profiles of the nine fabrics for the relevant attributes

According to this figure, it can be observed that the waved twill, the crêpe, the plain, and the 12-satin weaves have distinguished profiles.

The Friedman test (5%) ranges the products into groups. The obtained results show that the nine fabrics are close, and they belong to the same group for *cold–warm, light-heavy*, *sticky*, *slippery*, *greasy*, and *elastic* attributes, since the differences between fabrics are not significant. However, the fabrics are divided into several groups for *falling*, *thin-thick*, *supple-rigid*, *soft*, *granulous*, *pilous*, *grooved*, *responsive* and *crumple-like* attributes.

The Principle Component Analysis (PCA) is one of the most frequently used methods for the analysis of data collected from sensory tests. It is applied on the mean score of the panel across replication to analyze the pertinence of the attributes and to obtain graphical displays of the multivariate data simplifying subsequent analysis and highlighting similarities and differences between the woven fabrics. Sensory attributes were abstracted into two sensory independent factors, which explain respectively 46% and 28% of the total variance. These groups are carried to the map of products, in order to see the different correlations between fabrics and attributes. The results are presented in Figure 11.

In this figure, it can be observed that:

- the plain weave is the most *rigid* and *crumple-like* and the least *falling* and *responsive*.
- the waved twill is the most *granulous* and *grooved* and the least *soft* and *slippery*.
- the 12-satin is the most *pilous*, *responsive*, *falling*, *soft*, and *slippery*.
- the crêpe has a rigid *feeling*; it is also less *pilous*, *soft*, and *responsive* than most of the other fabrics.

Conclusion

Based on the obtained results, and as predicted, it is seen that the pattern strongly influences tactile feeling. Several attributes have been affected: *soft*, *slippery*, *grooved*, *granulous*, *pilous*, *rigid*, and *falling*. These results are in accordance with textile professionals' expectations.

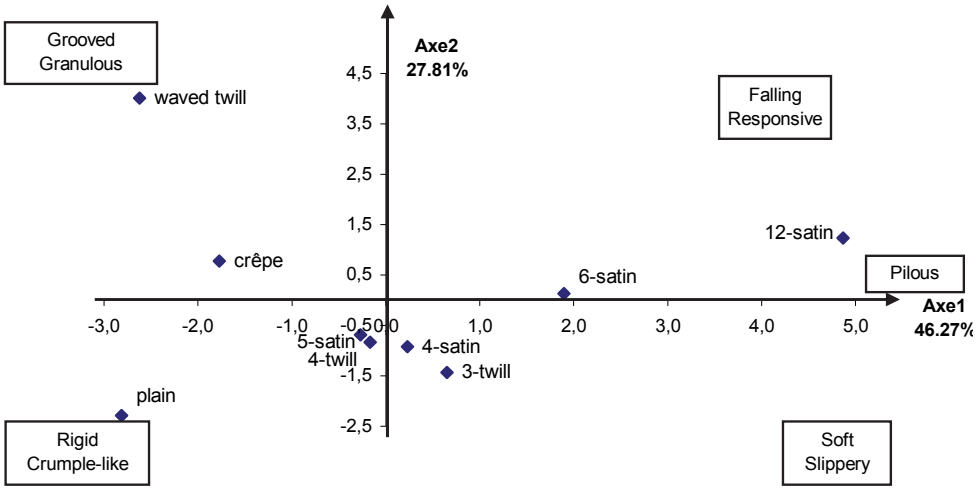

Fig. 11. Principle Component Analysis, map of products

Plain weave, waved twill, crêpe and 12-satin have very distinguished tactile profiles as compared to the other fabrics.

Knowing the correlations that may exist between fabric pattern and tactile properties, manufacturers would be able to design specific touch by the weaving process instead of using finishing treatments. This may be interesting in order to develop an environmental friendly process and avoid the use of chemical products.

5.2 Effect of the yarn count on the fabric hand of cotton woven fabrics

All woven fabrics are made by yarns. It is therefore interesting to study the effect of yarn properties on fabric hand. In this paragraph, on yarn property, the yarn count is studied. The impact of this factor on fabric sensory properties is underlined.

Materials

The study is carried out on 4 fabrics having different weft counts: 25 Tex, 50 Tex, 71 Tex and 100 Tex. The other parameters are unchanged: 100% cotton, Warp count (14 Tex) and Index of saturation (52%).

The experiment is applied on nine different patterns. Only the results of the plain weave are presented in this paragraph.

Results and discussion

The ANOVA 2-way test (5%) revealed that 9 attributes are significantly affected. These attributes are: *thin-thick*, *light-heavy*, *supple-rigid*, *soft*, *granulous*, *grooved*, *falling*, *responsive* and *elastic*.

The sensory profiles are presented in Figure 12. It can be noticed that some attributes are positively correlated to the yarn count. These attributes are: *thin-thick*, *light-heavy*, *supple-rigid*, *granulous* and *responsive*.

On the map of products obtained by the Principle Component Analysis (Figure 13), it can be noticed that fabrics are ranked on one principle axe (79.53%). On the left side of the axe, there are fabrics with high yarn counts and they are correlated to *thick*, *heavy*, *rigid*,

granulous, *grooved*, *elastic* and *responsive* attributes. The right side contains fabrics with low yarn counts which are positively correlated to *falling*, *thin*, *light*, *supple* and *soft* attributes. Those results are proven for the all other patterns: twills, satins and crêpe.

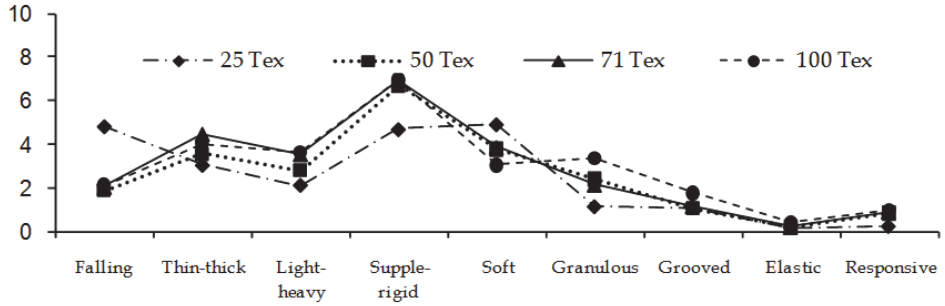

Fig. 12. Sensory profiles of plain weave fabrics with different yarn counts

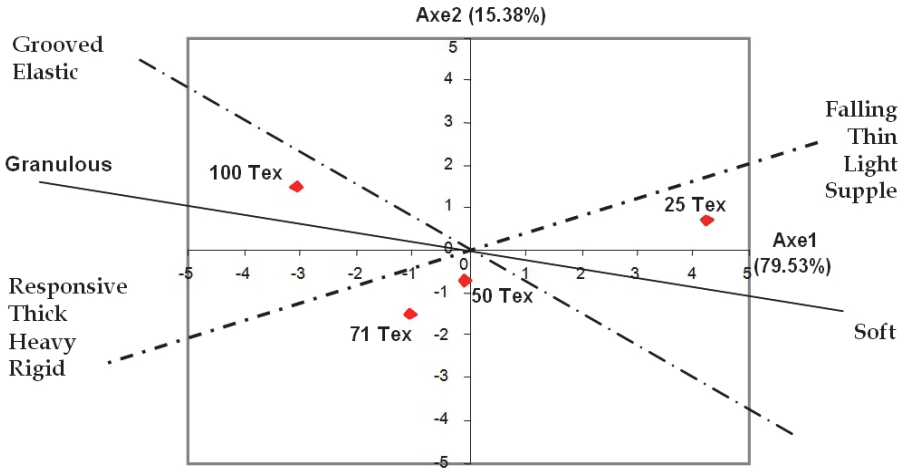

Fig. 13. Map of products, yarn count effect

Conclusion

The study of the influence of yarn count on the touch quality of fabrics has been proven as very important and has shown very interesting results. Surface properties as well as full hand properties are strongly affected by the yarn count. The more the yarn count is important, the more the fabric is *granulous*, *grooved*, *thick*, *heavy*, *rigid* and *responsive*.

This may help to control and evaluate fabric tactile properties by modifying the yarn characteristics and parameters.

5.3 Effect of finishing treatment on the fabric hand of cotton woven fabrics

In order to confer a variety of looks and effects on fabrics, there are many new finishing products and treatments proposed by chemical suppliers. This investigation was aimed by

the fact that differences between fabric treatments technologies could be distinguished more evidently than it was done before thanks to sensory evaluation methods.

Testing methods and materials

The tests are carried out on 100% cotton plain weave fabric, 24 yarns/cm weft and warp, 160 g/m², scoured and bleached. Two finishing products were studied: the crease-resistant finishing Knittex "K" and the softener macro silicone Ultratex® "Ul".

Knittex® FEL: a nonionic crosslinking resin based on a modified dimethyloldihydroxyethylene, allows bringing properties of anti-crease and anti-shrink to the fabric.

Ultratex® UM: cationic emulsion of functional polydimethylsiloxane, allows bringing a very soft touch to the fabric.

The products were processed using semi-industrial range and with varied concentrations of the two products (Table 4). Fabrics were tested and evaluated under controlled environmental conditions following the previously described procedure.

Product	Product code	Concentration (g/l)
Non treated fabric	0	0
Knittex® FEL "K"	21	20
	22	50
	4	80
Ultratex®UM "Ul"	23	5
	24	20
	17	40

Table 4. Different finishing treatments

Results and discussion

Seven attributes are significantly affected by the treatments. Table 5 shows the mean scores for the tested fabrics and the 7 pertinent attributes. For the silicone finishing, the *slippery* and *greasy* attributes change clearly with the concentration of the product. This result was expected as Ul treatment was known to soften the fabric and with the increase of concentration fabric becomes more *greasy* and *slippery*. It is also worth noting that the panel greatly perceived the modifications obtained by this treatment for the different concentrations.

For the resin treatment it is expected to have more *responsive* and less crumple-like fabrics. This is confirmed by the obtained results, since fabrics treated with a high concentration of resin finishing were significantly more *nervous* and less *crumple-like* than the non-treated fabric.

These results show that both treatments changed the hand-feel of the fabric in the expected direction and that the panel clearly perceived the modifications. Figure 14 shows the variation of sensory attributes according to the concentration of the finishing product.

The analysis of the results shows that the sensory evaluation ranges the treated fabrics as follows:

- for the resin finishing we have in terms of *responsiveness* 4<22<21<0, and for the *crumple-like* attribute 0<21<22<4;

- for the silicone treatment *greasy* and *slippery* attributes are ranged: 0<23<24<17.

Conclusion

The effects of finishing products' concentrations were found in accordance with the manufacturers' technical specifications and with the finishing industrialists' expectations. The evaluation of this effect was carried out by the sensory evaluation. The panel was able to detect the modifications and to evaluate them in the right sense.

	Non treated	K			UI		
Fabric code	0	21	22	4	23	24	17
Concentration	0	20	50	80	5	20	40
Falling	7.31	6.71	6.29	6.49	7.34	7.37	7.26
Rigid	3.09	3.90	4.01	4.38	3.18	2.78	2.99
Slippery	5.01	4.48	4.16	4.84	5.73	6.77	7.67
Soft	5.73	4.48	3.62	3.84	5.28	5.83	6.65
Greasy	2.14	1.81	1.55	1.70	2.98	4.77	5.52
Responsive	1.29	1.35	1.79	2.26	2.00	2.77	2.84
Crumple-like	7.60	6.98	6.06	4.47	7.32	7.67	7.40

Table 5. Mean values for the attributes according to the finishing treatments

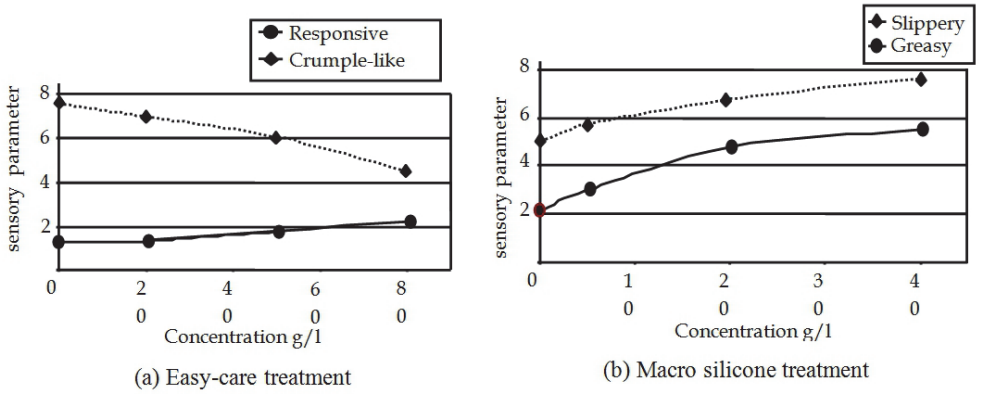

(a) Easy-care treatment (b) Macro silicone treatment

Fig. 14. Variation of the effected attributes according to the concentration of the finishing product

6. Conclusion

Sensory analysis has become a powerful tool for helping textile industries in product design and marketing tasks. In fact, haptic perceptions, including both cutaneous and kinesthetic perceptions, guide consumers' choice for clothes as well as textile manufacturers for

development of new products. Our studies on woven fabric have shown that modification of structure parameters or finishing treatments have a significant effect on sensory feeling. The trained panelists have detected those modifications. Sensory analysis methods provide quantification of tactile feeling. Moreover, sensory analysis approach allows understanding some complex sensation such as softness, comfort and well-being. It can therefore be concluded that sensory analysis has a solid future into the next century. In the meantime, development of dedicated devices for modeling of human perception and use of intelligent techniques which can be used in a complementary way for that purpose can be helpful and a promising approach.

7. References

AFNOR V09-001, (1983). Analyse sensorielle – Méthodologie - Directives générales

AFNOR XP V 09-501, (1999). Sensory Analysis-General Guidance for Sensory Evaluation-Description, Differentiation and Hedonic Measurement

Bandini-Buti, L.; Bonapace, L. & Tarzia, A. (1997). Sensorial Quality Assessment: a method to incorporate perceived user sensations in product design. Applications in the field of automobiles. In IEA '97 Proceedings (Helsinki: Finnish Institute of Occupational Health), 186–9

Barthelemy, J.; Danzart M.; MacLeod, P.; Sauvageot, F. & Sztrygler, F. (1990) - Evaluation sensorielle. Manuel méthodologique, Ed. Technique et Documentation Lavoisier, Paris

Bensaid, S.; Osselin, J-F.; Schacher; L. & Adolphe, D. (2006). The effect of pattern construction on the tactile feeling evaluated though sensory analysis. *Journal of the Textile Institute*, Vol.97, pp. 137-145

Ben Said, S.; Schacher, L. & Adolphe, D. C. (2008). Touch and sight interaction in fabric sensory analysis" *Tekstil*, 57(8), pp 383-389

Binns, H. (1926). The discrimination of wool fabrics by the sense of touch. *British Journal of Psychiatry*, 16, pp. 237–247

Bishop, D.P. (1996). Fabrics: Sensory and Mechanical Properties, *Textile Progress*, The Textile Institute 26

Cardello, V.A.; Winterhalter, C. & Schutz, G. H., (2003). Predicting the Handle and Comfort of Military Clothing Fabrics from Sensory and Instrumental Data: Development and Application of New Psychophysical Methods," *Textile Research Journal*, 73(3), 221-237

Chollakup, R.; Sinoimeri, A.; Philippe; F. Schacher, L. & Adolphe, D. (2004 a). Tactile sensory analysis applied to silk/cotton knitted fabrics. *International Journal of Clothing Science and Technology*, Vol.16, pp. 132-140

Chollakup, R.; Sinoimeri, A., Philippe, F. Schacher, L. & Adolphe, D. (2004 b). Tactile feeling: sensory analysis applied to textile goods. *Textile Research Journal*, Vol.74, pp.1066-1072

Cinel, C.;. Humphreys G. W. & Poli R., (2002). Cross-Modal Illusory Conjunctions between Vision and Touch. *Journal of Experimental Psychology: Human Perception and Performance*, Vol. 28, No. 5, pp. 1243–1266

Depledt, F., (1998). Société Scientifique d'Hygiène Alimentaire (SSHA) : Evaluation sensorielle-Manuel méthodologique, Lavoisier, Paris.

Dubois, D. & Prade, H. (1997). Fuzzy criteria and fuzzy rules in subjective evaluation – a general discussion, *Proceedings of EUFIT'97*, Aachen, Germany, 975-979

Elder, H.M.; Fisher, S.; Armstrong, K. & Hutchison, G. (1984). Fabric Softness, Handle and Compression, *Journal of Textile Institute*, 75, 37-46

El-Ghezal Jeguirim, S.; Babay Dhouib, A.; Sahnoun, M.; Cheikhrouhou, M.; Schacher, L.&Adolphe, D. (2009). The use of fuzzy logic and neural networks models for sensory properties prediction from process and structure parameters of knitted fabrics, *Journal of Intelligent Manufacturing*, Under press, DOI 10.1007/s10845-009-0362-y

El-Ghezal Jeguirim, S.; Babay Dhouib, A.; Sahnoun, M.; Cheikhrouhou, M.; Schacher, L. & Adolphe, D. (2010 a). The tactile sensory evaluation of knitted fabrics: effect of some finishing treatments, *Journal of the Sensory Studies*, Volume 25, Issue 2 April 2010, pages 201-215

El-Ghezal Jeguirim, S.; Babay Dhouib, A.; Sahnoun, M.; Cheikhrouhou, M.; Schacher, L. & Adolphe, D. (2010 b). Sensory and instrumental techniques evaluating the effect of structure parameters on the tactile properties of knitted fabrics, *Journal of Texture Studies*, 41(5), 714 – 735

El-Ghezal Jeguirim, S.; Sahnoun, M.; Babay Dhouib, A.; Cheikhrouhou, M.; Schacher, L. & Adolphe, D. (2011). Predicting compression and surfaces properties of knits using fuzzy logic and neural networks techniques, *International Journal of Clothing Science and Technology*, Under press

Ertugrul, S. & Ucar, N. (2000). Predicting bursting strength of cotton plain knitted fabrics using intelligent techniques. *Textile Research Journal*, 70, 845–851

Fontaine, S.; Marsiquet, C.; Nicoletti, N.; Renner, M. & Bueno, M.A. (2005). Development of a sensor for surface state measurements using experimental and numerical modal analysis. *Sensors and Actuators* A, vol. 120, pp. 507–517

Fortin, J. & Durand, N. (2004). De la perception à la mesure sensorielle, La fondation des gouverneurs, Saint-Hyacinthe, Québec

Giboreau, A.; Navarroa. S.; Fayeb P. & Dumortier J. (2001). Sensory evaluation of automotive fabrics: the contribution of categorization tasks and non verbal information to set-up a descriptive method of tactile properties. *Food Quality and Preference* Volume 12, Issues 5-7, July-September 2001, Pages 311-322

Guest, S. & Spence, C. (2003).What role does multisensory integration play in the visuotactile perception of texture? *International Journal of Psychophysiology* 50 pp. 63–80

Haykin, S. (2000). Neural Networks: A Comprehensive Foundation, Prentice Hall, New Jersey, 2nd edition, 1999. Presented at the ASME ICE Division Fall 2000 Technical Meeting September 25-27, Peoria

HSEC A New Approach to the Objective Evaluation of Fabric Handle from Mechanical Properties Part I: Objective Measure for Total Handle Evaluation," 2nd ed., The Textile Machinery Society of Japan, Osaka, Japan, 1980, pp. 7, 28

Hui, C.L.; Lau, T.W. & Ng, S.F. (2004). Neural network prediction of human psychological perceptions of fabric hand, *Textile Research Journal*, 74(5), 375-383

Issa, M.; Schacher, L. & Adolphe, D. (2008). Development of a New Experimental Technique for Mechanical Characterization of Fabric, *Experimental Techniques* November/December, pp 24-29

ISO 1992 ISO 5492 : (1992). Analyse sensorielle – Vocabulaire

ISO 11035-1995 (F), (1995), Sensory analysis - Identification and selection of descriptors for establishing a sensory profile by a multidimensional approach

ISO 8586. International Standard ISO 8586-1993 (F), (1993), Assessors for Sensory Analysis, Part 1: Guide to the selection, training and monitoring of selected assessors

ISO 6658. International Standard ISO 6658-1985 (F), (1985), "Sensory analysis - Methodology - General guidance"

Jain, V.; Tiwari, M. K. & Chan, F. T. S. (2004). Evaluation of the supplier performance using an evolutionary fuzzybased approach. *Journal of Manufacturing Technology Management*, 15(8), 735–744

Kawabata, S. (1975). The standardisation and analysis of Hand Evaluation, Journal of the Textile Machinery Society of Japan', Osaka, Japan

Kawabata, S. (1980). The Standardisation and Analysis of Hand Evaluation (2nd Edition), Textile Machinery Society of Japan, Osaka, Japan

Kawabata, S. (19882). The Development of the Objective Measurement of Fabric Handle, Proceedings of the First-Japan Australia Symposium on Objective Specification of Fabric Quality, Mechanical Properties and Performance, Kyoto, Japan, pp. 31-59

Kawabata, S., (1988). The Standardization and Analysis of Hand. *Textile Research Journal*, pp 438- 444

Konyo M.; Tadokoro S.; Hira M.; & Takamori T. (2002). Quantitative Evaluation of Artificial Tactile Feel Display Integrated with Visual Information Proccedings of 2002 IEEE/RSJInternational Conference on Intelligent Robots and Systems EPFL, Lausanne October 2002 pp 3060-3065

Kwak, C.; A.Ventura, J. & Tofang-Sazi, K. (2000). A neural network approach for defect identification and classification on leather fabric, Journal of Intelligent Manufacturing, 11, 485-499

Lederman, S.J., & Abbott, S.G. (1981). Texture perception: Studies of intersensory organization using a discrepancy paradigm and visual versus tactual psychophysics. *Journal of Experimental Psychology*: *Human Perception & Performance*, 7(4), 902-915

Lederman, S.J; Thorne & G; Jones, B. (1986) Perception of texture by vision and touch: Multidimensionality and intersensory integration. *Journal of Experimental Psychology*: *Human Perception & Performance* 12:169–180

Maâtoug, N.; Sahnoun, M. & Sakli, F. (2009). Banc d'essais pour la mesure des caractéristiques physiques d'état de surface des tricots. Tunisian Patent 19934, January, 12,.2009

Mackay, C., Anand S. C. & Bishop, D. P. (1999). Effects of laundering on the sensory and mechanical properties of 1x1 rib knitwear fabrics. Part II: Changes in sensory and mechanical properties, *Textile Research Journal* 69(4), pp. 252–260.

Matsuo, T.; Nasu, N. & Saito, M. (1971). Study on the Hand, part 2: The Method for Measuring Hand, *Journal of the Textile Machinery Society*, 24(4), 58-68.

Meilgaard M.; Civille G. & Carr B. (1991). Sensory evaluation techniques. - 2e éd., CRC Press Inc., Boca Raton, Floride, p. 354

Mucci A.; Garitta L.; Hough G. & Sampayo S. (2005). Comparison of Discrimination Ability Between a Panel of Blind Assessors and a Panel of Sighted Assessors, *Journal of Sensory Studies* Vol. 20 pp. 28–34

Nagamachi, M. (1995). Kansei engineering: A new ergonomic consumer-oriented technology for product development. *International Journal of Industrial Ergonomics*, 15(1), 3-11

Nakano H. (1994). Product Development of Clothes by Kansei Engineering. *J. Soc. Fib. Sci. Tech Japan* [Sen-i Gakkaishi] 50 [8], pp. 473-478

NF EN 20139, 1992. Textiles – Atmosphères normales de conditionnement et d'essai

NF-ISO 5492, (1992). Analyse sensorielle – Vocabulaire

NF–ISO 8586-1, (1993). Analyse sensorielle – Guide générale pour la sélection, l'entraînement et le contrôle des sujets – Partie1: sujets qualifiés

NF-ISO 11035, (1995). Analyse sensorielle – Recherche et sélection de descripteurs pour l'élaboration d'un profil sensoriel, par approche multidimensionnelle

Nicod, H., (1990). Evaluation Sensorielle, manuel méthodologique, SSHA, Technique and Documentation, Lavoisier, Paris, 2nd édition, pp. 46–63Nogueira, C.; Cabeço-Silva, M. E.; Schacher, L. & Adolphe, D. (2009). Textile Materials: Tactile Describers. *Journal of Food Technology* 7(3): 66-70, ISSN: 1684-8462

Okamoto, M. (1991). Some Attempts at Quantification of Sensibility" Toray Ind. Inc. *J. Soc. Fib. Sci. Tech.*, Japan [Sen-i Gakkaishi] 47 [11], pp. 617-623

Pac, M.J.; Bueno, M.A.; Renner, M.; & Elkasme, S. (2001). Warm- Cool Feeling Relative to Tribological properties of Fabrics, *Textile Research Journal*, vol. 71, no. 7, pp. 806-812

Pan, N.; & Yen, K.C. (1992). Physical Interpretations of Curves Obtained Through the Fabric Extraction Process for Handle Measurement. *Textile Research Journal* 62: 279–290

Pan, N., Zeronian, H., & Ryu H.S., (1993) An Alternative Approach to the Objective Measurement of Fabrics, Textile Research Journal , V.63, p.33 -43

Park, S. W.; Hwang, Y. G. & Kang, B. C. (2000). Applying fuzzy logic and neural networks to total hand evaluation of knitted fabrics. *Textile Research Journal*, 70(8), 675–681

Peirce, F. T. (1930). The "Handle" of Cloth as a Measurable Quantity. *J. Textile Inst. 21,* T377

Philippe F.; Schacher, L.; Adolphe D. & Dacremont C., (2003). The sensory panel applied to textile goods: a new marketing tool, *Journal of Fashion Marketing and Management* 7, pp. 235–248

Richard, D. & Orsal, D. (2001). Neurophysiologie, Organisation et Fonctionnement du Système Nerveux, Dunod, Paris

Rombaldoni, F.; Demichelis, R. & Mazzuchetti, G. (2010). Prediction of human psychophysical perception of fabric crispness and coolness hand from rapidly measurable low-stress mechanical and thermal parameters. *Journal of Sensory Studies*, 25 (2010) 899–916

Rozenweig M.; Leiman, A. & Breedlove, S.M. (1998) Psychobiologie, De Boeck Université, ISBN : 978-2-7445-0025-1, Paris, France

Rumelhart, D. E.; Hinton, G. E. & Williams, R. J. (1986). Learning Representations by Back-propagating errors, *Nature* 323, pp. 533–536

Schlich P., (1995), Preference Mapping: Relating Consumers Preferences to Sensory or Instrumental Measurements. *Bioflavour*, INRA Dijon, pp. 135-150

Sensotact (2008). http: //www.sensotact.com

SSHA. (1998). Société Scientifique d'Hygiène Alimentaire : Evaluation Sensorielle – Manuel méthodologique. Technique & Documentation. ISBN 2-7430-0124-0, Lavoisier, Paris

Stone, H.; Sidel, J.L.; Oliver, S.; Woolsey, A. & Singleton R.C. (1974). Sensory Evaluation by Descriptive Analysis. *Food Technology*, Vol. 28 No. 11, pp. 24-34

Stone, H. & Sidel, J.L. (2007) Sensory research and consumer-led food product development. In MacFie, H. (ed), Consumer-led Food Product Development. Boca Raton, FL: CRC Press; ISBN: 90-73592 -18-6, pp 307-320

Tester, D. & De Boos, A. 1990. Get it right FAST time. Textile Horizons, 10(8), 13

Vassiliadis, S.; Rangoussi, M.; Cay, A. & Provatidis, C. (2010). Artificial Neural Networks and Their Applications in the Engineering of Fabrics. *Woven Fabric Engineering*, Polona Dobnik Dubrovski, pp. 111-134, Sciyo, ISBN 978-953-307-194-7, Croatia.

Wong, A. S. W.; Li, Y.; Yeung, P. K. W. & Lee, P. W. H. (2003). Neural network predictions of human psychological perceptions of clothing sensory comfort. *Textile Research Journal*, 71, pp. 331–337

Wong, W. K.; Kwong, C. K.; Mok, P. Y. & Ip, W. H. (2006). Genetic optimization of JIT operation schedules for fabric-cutting process in apparel manufacture. *Journal of Intelligent Manufacturing*, 17, pp. 341–354

Young N. D.; Sanders, T.; Drake, M.A.; Osborne, J. & Civille, G. (2005). Descriptive analysis and US consumer acceptability of peanuts from different origins. *Food quality and preference*, Vol. 16 (1), pp. 37-43

Zadeh, L. A. (1965). *Information and Control*, 8, pp. 338

Zeng, X.; Koehl, L.; Sahnoun, M.; Bueno, M.A. & Renner, M. (2004). Integration of human knowledge and measured data for optimization of fabric hand. *International Journal of General Systems* 33 (2–3), pp. 243–258

Zeng, X.; Ruan, D. & Koehl, L. (2008). Intelligent sensory evaluation: Concepts, implementations and applications. *Mathematics and Computers in Simulation*, 77, pp. 443–452

Zimmerman, H. J. (1996). *Fuzzy Set Theory and Its Applications*, 2nd Ed., Allied Publishers Limited, New Delhi

9

Superhydrophobic Superoleophobic Woven Fabrics

Hoonjoo Lee[1] and Jeffery Owens[2]
[1]*North Carolina State University*
[2]*Air Force Research Laboratory*
U.S.A.

1. Introduction

Technologies related to superhydrophobic and superoleophobic treatments have recently attracted considerable attention in the textile industry due to their potential applications in medical devices as well as industrial materials. A surface whose water contact angle exceds150° is called a superhydrophobic surface, and we define a surface with an oil contact angle of over 150° as a superoleophobic surface. Since the wettability of a solid surface is determined by two parameters, the chemical composition and the geometrical structure of a rough surface, the combination of these two factors are often used to design superhydrophobic and superoleophobic textiles. More specifically researchers employ two predominant rough surface wetting models, the Wenzel model and the Cassie–Baxter model compared to the wetting behaviour of a smooth surface to predict the requirements for imparting a fabric with superhydrophobic and superoleophobic character. However, not all surfaces having high contact angles to liquids possess low roll-off angles. Rather, roll-off angles are highly dependent on the mass and density of the droplet, the surface tensions of both the liquid and the surface the droplet is sitting atop of, and the geometrical morphology and degree of roughness of that surface. Typically, unless a surface possesses a very low surface tension that is approximately one forth the surface tension of the liquid, droplets of less than 50 μL are not mobile when the surface is tilted.
In this chapter, the relationships amongst contact angles, surface tension, and surface roughness are reviewed; the wetting behaviour of a rough surface is compared with that of a smooth surface; the relationships between contact angle hysteresis and roll-off angles are analysed, and finally superhydrophobic, superoleophobic woven fabric is designed and developed using chemical and geometrical surface modifications.

2. Design and preparation of superhydrophobic superoleophobic woven fabric

Although it is hard to measure the surface tension of a solid directly, it is easy to measure the contact angles of liquid droplets sitting atop its surface (Fig. 1). By obtaining the contact angle data for liquids with varying surface tensions and inserting the data into select equations predictions of a surface's wetting characteristics to other liquids can be obtained.

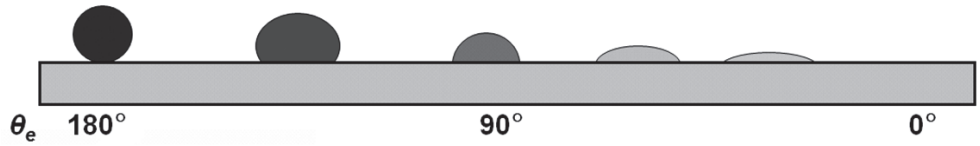

Fig. 1. Contact angle and wettability

2.1 Wetting behavior of smooth and rough surfaces

The relationship between surface tension and contact angle is obtained by the Young equation:

$$\frac{\gamma_{SV} - \gamma_{SL}}{\gamma_{LV}} = \cos\theta_e \tag{1}$$

where γ is the surface tension; and SV, SL, and LV are the solid-vapour, the solid-liquid, and the liquid-vapour interfaces, respectively (Fig. 2). According to Young's equation, the contact angle is a well-defined property that depends on the surface tension coefficients that exist between the solid−liquid and the liquid−gas interface.

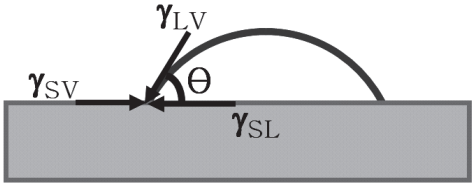

Fig. 2. A drop on a flat surface

The right hand side of equation (1) and γ_{LV} can be obtained from experimental measurements, leaving two unknowns, γ_{SV} and γ_{SL}. When θ_e for a test liquid is> 20°, it is assumed that $\gamma_{SV} \approx \gamma_S$ and $\gamma_{LV} \approx \gamma_L$. On the other hand, the thermodynamic work of adhesion, W_{SL}^a can be explained by the Dupre equation as:

$$W_{SL}^a = \gamma_{SV}^a + \gamma_{LV}^a - \gamma_{SL}^a \tag{2}$$

Combining equation (1) and (2) results in the Dupre-Young equation:

$$W_{SL}^a = \gamma_{SV}^a + \gamma_{LV}^a - \gamma_{SL}^a = \gamma_{LV}^a(1 + \cos\theta_e) \tag{3}$$

According to Fowkes, when only dispersion interactions are present, the interfacial tension between the solid and liquid is $\gamma_{SL}^{LW} = (\sqrt{\gamma_{SV}^{LW}} - \sqrt{\gamma_{LV}^{LW}})^2$ and the geometric mean of the liquid and solid surface tension is:

$$W_{SL}^{LW} = 2\sqrt{\gamma_{SV}^{LW}\gamma_{LV}^{LW}} \tag{4}$$

where W_{SL}^{LW} is the thermodynamic work of Lifshitz–van der Waals (LW) components.
Meanwhile, the addition of intermolecular forces at the interface is equal to the surface tension of the material, as shown in equation (5).

$$\gamma = \gamma^{d} + \gamma^{p} + \gamma^{H} + \gamma^{ind} + \gamma^{m} + \ldots \quad (5)$$

where d, p, H, ind, and m mean London dispersion forces, permanent dipoles, hydrogen bonds, induced dipoles and metallic interaction, respectively. Therefore, we can determine γ_{SV} and γ_{LV} as:

$$\gamma_{SV} = \gamma_{SV}^{d} + \gamma_{SV}^{p} + \gamma_{SV}^{H} + \gamma_{SV}^{ind} + \gamma_{SV}^{m} + \ldots \quad (6)$$

$$\gamma_{LV} = \gamma_{LV}^{d} + \gamma_{LV}^{p} + \gamma_{LV}^{H} + \gamma_{LV}^{ind} + \gamma_{LV}^{m} + \ldots \quad (7)$$

Combining equation (3), (4), (6) and (7) gives:

$$\begin{aligned} &\gamma_{LV}(1+\cos\theta_e) \\ &= \gamma_{LV}^{d}(1+\cos\theta_e) + \gamma_{LV}^{p}(1+\cos\theta_e) + \gamma_{LV}^{H}(1+\cos\theta_e) + \gamma_{LV}^{ind}(1+\cos\theta_e) + \gamma_{LV}^{m}(1+\cos\theta_e) + \ldots \\ &= 2(\sqrt{\gamma_{SV}^{d}\cdot\gamma_{LV}^{d}} + \sqrt{\gamma_{SV}^{p}\cdot\gamma_{LV}^{p}} + \sqrt{\gamma_{SV}^{H}\cdot\gamma_{LV}^{H}} + \sqrt{\gamma_{SV}^{ind}\cdot\gamma_{LV}^{ind}} + \sqrt{\gamma_{SV}^{m}\cdot\gamma_{LV}^{m}} + \ldots) \end{aligned} \quad (8)$$

Since the surface tensions of dodecane and most polymeric surfaces are determined by London dispersion forces, this equation can be simplified to:

$$\gamma_{LV}(1+\cos\theta_e) = 2(\sqrt{\gamma_{SV}^{d}\cdot\gamma_{LV}^{d}}) \quad (9)$$

An oil, such as dodecane has a very low surface tension, ~24.5 dyne/cm. Substituting γ_L = 24.5 dyne/cm for dodecane into Eq. 9 suggests γ_S must be smaller than 6.3 dyne/cm, and a smooth surface having $\gamma_{SV} \leq 6.3$ dyne/cm is oleophobic ($\theta_e > 90^o$) under these conditions. The Young equation and Dupre-Young equation are valid only for the wetting of smooth surfaces, but real solids are not perfectly flat and surface structure greatly effects wettability, e.g. when a rough surface of a solid is very hydrophobic, liquid droplets are in contact with the upper part of a rough surface and the lower part is filled with air.

In order to design a superhydrophobic superoleophobic surface, two predominant rough wetting models are used: the Wenzel model and the Cassie–Baxter model. In the Wenzel model a liquid fills the grooves of a rough surface and completely wets the surface, whilst in the Cassie–Baxter model, a liquid sits on top of the surface and repels the liquid. To create a Cassie–Baxter surface, the Young contact angle of a liquid, θ_e, must be greater than 90^o as shown in Fig. 3.

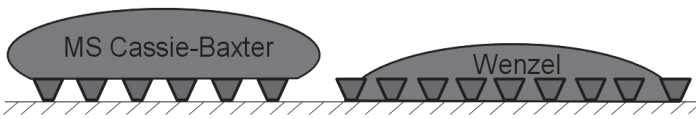

Fig. 3. A drop on a rough surface

In Wenzel's approach the liquid fills the grooves on the rough surface, and the liquid contact angle on a rough surface, θ_r^W, can be described as:

$$\cos\theta_r^{W} = r\cos\theta_e \quad (10)$$

where r is roughness — the ratio of the total wet area of a rough surface to the apparent surface area in contact with the water droplet (r > 1). According to equation (10), for a rough

surface (r > 1) a hydrophilic surface becomes more hydrophilic while a hydrophobic surface does more hydrophobic, e.g. for a material with $\theta_e \approx 120^o$, r must be greater than 1.79 to make the surface superhydrophobic. Since most solid surfaces typically possess $\gamma_{SV} > 6.3$ dyne/cm, the Cassie–Baxter model does not allow for stable superoleophobicity under normal circumstances. On a metastable Cassie–Baxter surface, a liquid initially sits atop of the surface since air pockets inside the grooves of the rough surface provides lower Gibbs free energy than that when the liquid penetrates the rough surface. However, the liquid can be potentially drawn into contact with the rough surface over time, with the time to absorption dependent on the surface tension, volume, and density of the liquid, and the surface tension and morphology of the surface. Hence, a superoleophobic surface can be produced by designing a metastable Cassie–Baxter surface.

The Cassie and Baxter model is an extended form of the Wenzel model to include porous surfaces. In this model a liquid sits on a composite surface made of a solid and air. Therefore, the liquid does not fill the grooves of a rough solid. In their paper published in 1944, Cassie and Baxter suggested that the liquid contact angle at on such a rough surface, θ_r^{CB}, is:

$$\cos\theta_r^{CB} = f_1\cos\theta_e - f_2 \tag{11}$$

where f_1 is the surface area of the liquid in contact with the solid divided by the projected area, and f_2 is the surface area of the liquid in contact with air trapped in the pores of the rough surface divided by the projected area. When there is no trapped air, f_1 is the same with r in the Wenzel model. In the Cassie-Baxter model, the smooth surface can become more hydrophobic or oleophobic by surface roughening, regardless of θ_e. However, in the Wenzel model, θ_e has to be greater than 90^o in order for a smooth surface to be more hydrophobic or oleophobic after roughening. This statement reinforces the concept of the metastable Cassie–Baxter model, i.e. a surface having $\theta_e < 90^o$ with a liquid, when roughened, will immediately wet (Wenzel behaviour) or the liquid will sit on top of the surface due to air pockets inside the grooves which result in a local minimum in the surface energy (meta-stable Cassie-Baxter behaviour). In addition, since the surface tension of an oil such as dodecane is lower than that of water (γ = 72.8 dyne/cm), the θ_r^{CB} of water is higher than θ_r^{CB} of oil. Hence, according to equations (10) and (11), all superoleophobic surfaces should be superhydrophobic, but not all superhydrophobic surfaces exhibit superoleophobicity.

2.2 Preparation of superhydrophobic and superoleophobic woven fabric

Superhydrophobicity has gained a great deal of interest and has been studied extensively since one of the most-prized features of superhydrophobic surfaces is their ability to self-clean — that is the ability of water to collect and remove dirt and debris as the water droplet rolls off of the surface. The roll-off angle of a droplet, α, on a smooth surface can be described as:

$$mg\sin\alpha \approx -2R_w\gamma_{LV}(\cos\theta_A - \cos\theta_R) \tag{12}$$

where m is the mass of the droplet, g is the gravitational acceleration, R_w is the radius of the wetting area, θ_A is the advancing contact angle, and θ_R is the receding contact angle. Meanwhile, contact angle hysteresis, $\Delta\theta_H$, is defined as the difference between advancing and receding contact angles, i.e. $\Delta\theta_H = \theta_A - \theta_R$. The gain factor, which is often used to

understand the relationship between contact angle hystereses and roll-off angle, is considered as the rate of variation of the contact angle hysteresis at any operating point. The radius of the wetting area, R_w, on a surface is:

$$R_w = \sqrt[3]{\frac{3V}{\pi(2-3\cos\theta+\cos^3\theta)}}x\sin\theta \tag{13}$$

Based on equation (13), the radius of the wetting area can be predicted as shown in Table 1.

θ (°)	R_c (mm)			
	5μL	10 μL	20 μL	50 μL
10	3.31	4.17	5.26	7.14
20	2.62	3.30	4.15	5.63
30	2.27	2.85	3.60	4.88
40	2.03	2.56	3.23	4.38
50	1.86	2.34	2.94	4.00
60	1.71	2.15	2.71	3.68
70	1.58	1.99	2.50	3.40
80	1.46	1.83	2.31	3.13
90	1.34	1.69	2.12	2.88
100	1.22	1.54	1.94	2.63
110	1.10	1.39	1.75	2.37
120	0.97	1.23	1.55	2.10
130	0.84	1.06	1.33	1.81
140	0.69	0.87	1.10	1.49
150	0.54	0.67	0.85	1.15
160	0.37	0.46	0.58	0.78
170	0.19	0.23	0.29	0.40

Table 1. Radius of wetting area of liquid droplets

The Wenzel equation gives a change in the Wenzel contact angle, $\Delta\theta_H^W$, caused by a change in the contact angle on the smooth surface, $\Delta\theta_H$, as:

$$\Delta\theta_H^W = r\left(\frac{\sin\theta_e}{\sin\theta_r^W}\right)\Delta\theta_H \tag{14}$$

The gain factor, which is the change in $\cos\theta_r^W$ relative in $\cos\theta_e$ (i.e. the derivative of $\cos\theta_r^W$ with respect to $\cos\theta_e$) is very useful since it separates the idea of the equilibrium contact angle increase occurring by surface topography from the observed contact angle. Using the Wenzel equation we can obtain the Wenzel gain factor as follows:

$$G_e^W = \frac{r\sin\theta_e}{\sin\theta_r^W} \tag{15}$$

Since the effect of roughness is proportional to the radian contact angle changes, the Wenzel gain factor is approximately unity when a contact angle θ_e is close to 90°, but the Wenzel

gain factor rapidly increases as the roughness factor increases. Likewise, Cassie-Baxter equation gives a change in the Cassie-Baxter contact angle, $\Delta\theta_H^{CB}$, caused by a change in the contact angle on the smooth surface, $\Delta\theta_H$, as:

$$\Delta\theta_H^{CB} = (1 - f_2)\left(\frac{\sin\theta_e}{\sin\theta_r^{CB}}\right)\Delta\theta_H \tag{16}$$

Similarly, a Cassie-Baxter gain factor, G_e^{CB}, can be obtained by the Cassie-Baxter equation as:

$$G_e^{CB} = (1 - f_2)\left(\frac{\sin\theta_e}{\sin\theta_r^{CB}}\right) \tag{17}$$

Since $1 - f_2 \leq 1$, $G_e^{CB} \leq 1$. According to McHale, the Cassie-Baxter gain factor, G_e^{CB}, is an attenuation of any contact angle hysteresis, whilst hysteresis increases on a Wenzel-type surface. As a numerical example, if a water droplet is deposited on a rough nylon surface having $\theta_e = 68°$, $\Delta\theta_H = 150°$ and r = 3, the apparent contact angle, θr^W, will be ~ 0° and thus the contact angle hysteresis on this Wenzel surface, $\Delta\theta_H^W$, will be greater than 150°, i.e., the droplet will be adsorbed onto the rough structure and will not be able to roll off such a hydrophilic rough surface. However, if a water droplet is deposited on a poly(tetrafluoroethylene) (PTFE) having $\theta e = 120°$, $\Delta\theta_H = 80°$ and $f_2 = 0.74$, the apparent contact angle, θ_r^{CB}, will be 150° and the contact angle hysteresis, $\Delta\theta_H^{CB}$, on this C−B surface will be less than 80°, i.e. the surface will become superhydrophobic and liquid droplets will readily roll off at a certain roll-off angle. In the case of dodecane, whose $\theta_e < 90°$ and $\theta_r^{CB} > 90°$, the situation is less favorable, and equations (16) and (17) cannot be used to predict α of dodecane since the sine curve has a bilateral symmetry with respect to 90°. Hence, equations (16) and (17) have to be modified for a metastable CB surface as:

$$\Delta\theta_H^{\text{metastable-CB}} = (1 - f_2)\left(\frac{1 + \cos\theta_e}{1 + \cos\theta_r^{CB}}\right)\Delta\theta_H \tag{18}$$

$$G_e^{\text{metastable-CB}} = (1 - f_2)\left(\frac{1 + \cos\theta_e}{1 + \cos\theta_r^{CB}}\right) \tag{19}$$

Hence, if there is a surface having surface properties as shown in Table 2, α can be predicted by equations (12), (16), and (18).

The predicted values of α are 15° and 10° for 50 μL and 100 μL water droplets, and 45° and 26° for 50 μL and 100 μL dodecane droplets, respectively. If liquids having different γ_{LV} are deposited on a solid surface, the roll-off angles of the liquids are strongly influenced by the mass and the surface energy of each liquid.

2.3 Preparation of superhydrophobic and superoleophobic woven fabric

Again, the wettability of a solid surface is determined by two parameters: the chemical composition and the geometrical structure of a rough surface. Therefore, in this chapter, we design a metastable superoleophobic surface via chemical and geometrical modifications. The surface energy of the fibres are reduced by grafting 1,1,2,2,-tetrahydrodecyltrimethoxysilane (FS) onto nylon and cotton fibres composing nylon cotton

Parameters	Water on PTFE (CB)		Dodecane on PTFE (metastable CB)	
	50 μL	100 μL	50 μL	100 μL
θ_e (°)	120	120	50	50
$\Delta\theta_H$ (°)	110	110	168	168
f_2	0.74	0.74	0.74	0.74
θ_r^{CB} (°)*	150	150	124	124
$\Delta\theta_H^{CB}$ (°)	50	50	163	163
θ_A^{CB} (°)	180	180	180	180
θ_R^{CB} (°)	30	30	17	17
R_w (mm)	2.5	3.3	3.7	4.5
α (°)	**15**	**10**	**45**	**26**

* Approximate values if $f_1 + f_2 \sim 1$.

Table 2. Predicted roll-off angles of water and dodecane on a very hydrophobic and oleophobic rough surface. Here, since the droplet shape begins to deform when m > 10 μL caused by gravity, we use real R_w that is not a predicted value based on equation (13) but a real R_c which has been measured on the surface.

blended woven fabric (NyCo). Macro scale roughness of the NyCo can be controlled via choice of fabric construction, yarn type (mono or multi-filament), and fibre diameter. Additionally, micro and nano scale roughness on the fibres can be achieved by allowing partial condensation of the FS prior to treating the NyCo, thus resulting in deposition of FS particulate condensates over the fibre surface. First, we review how to lower the surface tension of fibres chemically.

2.3.1 Chemical modification

Lowering surface tension of NyCo begins by grafting low-surface-tension material on the surface of NyCo such as replicating the FS grafting process developed by Hoefnagels et al., and Stoeber et al. except that the technique was modified to use microwave radiation in this research. A swatch of NyCo fabric is saturated in a solution containing FS, squeezed at 100 % wet pick-up to remove excess liquid, and cured in a conventional microwave oven at 1250 W, with irradiation times varying time from 0 to 60 sec. Whilst the surface energy of NyCo decreases by FS grafting, silane can form micro- and nano-scale roughness on NyCo and create a high surface area if the FS imparts particulate condensation to the NyCo — the self-condensation of FS will be discussed later in this chapter. Such treatment methods correlate easily to a wide variety of textiles that have –OH and –NH groups such as cotton, polyamides, polyaramids, etc. Fluoroalkyl chains can be attached to the –OH or –NH site via a siloxane or silazane linkage as shown in Fig. 4.

where XH is —OH, —SH, —NH—, and —NH_2, etc. Use of microwave radiation in this process greatly enhances the reaction rate of the covalent attachment of silanes to the reactive substrates, as does the presence of acid or base. Since treatment at low pH is avoided for the treatment of cotton and other cellulose derivatives due to the instability of the β-acetal bonds in acidic solutions, this reaction was processed using neutral and basic solutions.

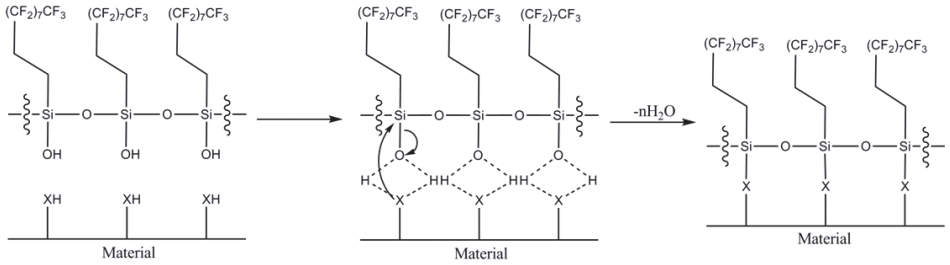

Fig. 4. Reaction mechanism of FS condensation onto a surface

Again, we chemically grafted FS onto a NyCo surface to reduce the surface tension of NyCo and to make the surface less oleophilic. In order to obtain the Young contact angles for water and dodecane, nylon 6,6 film was treated with FS. The Young contact angles of water on a FS-grafted nylon film were 109° – 112°, whilst the Young contact angles for water on an unmodified nylon surface were 70° – 73°. Grafting FS to a nylon film also increased dodecane contact angles. The Young contact angles for dodecane on a FS-grafted nylon film were 73° – 75°, whilst the Young contact angle for dodecane on an unmodified nylon surface was < 5°. The measured values of $\theta_{e\text{-water}}$ and $\theta_{e\text{-dodecane}}$ on FS-treated nylon are critical parameters to consider when designing superoleophobic surfaces using the Wenzel and Cassie–Baxter models. FS-grafting onto a nylon film successfully generated a surface having a low surface energy, as shown in Fig. 5.

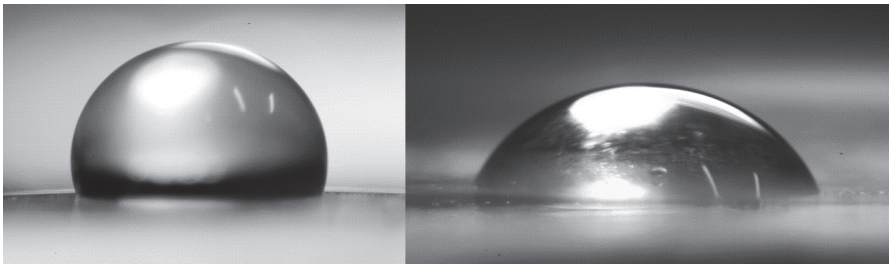

Fig. 5. 10 μL water and dodecane droplets on a FS-grafted nylon film

2.3.2 Geometrical modifications

The wetting behavior of a solid surface is also controlled by the geometrical structure of a surface as mentioned in the beginning of this chapter. In this section, we study how to model and modify a rough surface to make the surface highly hydrophobic and oleophobic using plain woven, woven twill, and 3/1 satin woven constructions.

2.3.2.1 Superhydrophobic oleophobic plain woven structure

To obtain the true surface area we use a flux integral. Fig. 6 shows a cross-sectional view of a model of a NyCo plain woven fabric made of monofilament fibres. The distance from the centre of a weft (or warp) yarn to the centre of an adjacent weft (or warp) yarn is 4R; and the distance from the centre of a weft (or warp) yarn to the centre of an adjacent warp (or weft) yarn is 2R. Hence, according to the Pythagorean Theorem, the vector from the centre of one weft yarn to the centre of an adjacent weft yarn makes a 30° angle to the plane of the fabric.

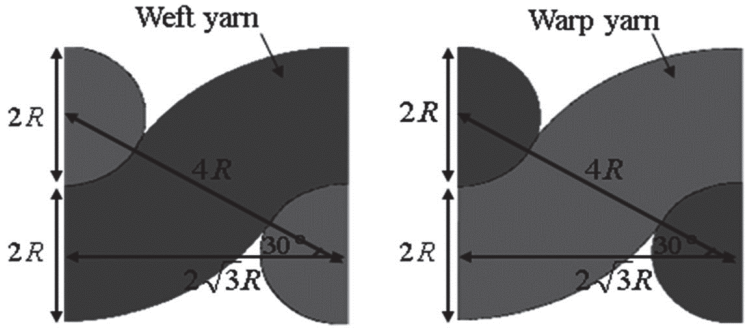

Fig. 6. Cross-section views of a plain woven fabric (source: Lee and Owens, 2011)

Using the flux integral, the area of one yarn in the unit fabric is calculated as:

$$r(u,v) = (2R + Rcosv)cosui + (2R + Rcosv)sinuj + Rcosvk \tag{20}$$

$$\left|r_u \times r_v\right| = R(2R + Rcosv) \tag{21}$$

$$A_{\text{yarn in unit area}} = \frac{\int_0^{2\pi}\int_0^{2\pi} R(2R + Rcosv)dudv}{3} = \frac{8\pi R^2}{3} \tag{22}$$

where R is the radius of yarn; A is the area; i, j and k are the vectors to x, y, and z axis direction, respectively; u and v are the notations for the variables of integration. Then, we determine the true fabric surface area as follows:

$$A_{\text{fabric}}^{\text{true}} = 2A_{\text{yarn in unit area}} = 52.64R^2 \tag{23}$$

where A^{true}_{fabric} is the intrinsic area of the unit fabric determined by the area of yarn surfaces. The apparent surface area is equal to the area of a plane tangent to the top surface.

$$A_{\text{fabric}}^{\text{apparent}} = \left(2\sqrt{3}R\right)^2 = 12R^2 \tag{24}$$

where $A^{apparent}_{fabric}$ is the apparent area of the unit fabric shown in Fig. 6. Finally, the roughness, r, is:

$$r = \frac{52.64R^2}{12R^2} = 4.39 \tag{25}$$

As shown in equation (25) the plain woven rough surface has high enough r to achieve a metastable CB surface.

Next, we look at a plain woven fabric made with multi-filament yarns. Clearly, a multi-filament yarn will have even higher values of r, because the space between the fibres will increase the true surface area whilst the apparent surface area remains the same. In this case, equation (23) becomes:

$$A_{\text{fabric}}^{\text{real}} = A_{\text{multi}} \approx 52.64R \times NR_f \tag{26}$$

where N is the number of filament fibres, R_y is the radius of the yarn, and R_f is the radius of the filament fibres. Substituting equation (26) into equation (25) yields:

$$r \approx 4.39\frac{NR_f}{R_y} \tag{27}$$

For example, a plan woven fabric could have, $R_y \approx 200$ μm, $N > 50$, and $R_f \approx 10$ μm. Substituting these values into equation (27) gives $r > 11$. Since $r > 11$ for the multi-filament fabric, we again expect that the surface is adequately rough and that the roughness is composed of the appropriate geometrical structures so as to be superhydrophobic.

Now, we model a Cassie-Baxter (CB) plain woven fabric. In Fig. 6, the centre-to-centre distance is $2\sqrt{3}R$ and the contact angle on a CB NyCo surface, θ_r^{CB}, is defined as:

$$\cos\theta_r^{CB} = \frac{(\pi - \theta_e)}{\sqrt{3}}\cos\theta_e + \frac{\sin\theta_e}{\sqrt{3}} - 1 \tag{28}$$

based on equation (11). Substituting Young contact angles into equation (28) along with the measured contact angles from the flat nylon film provides θ_r^{CB}. In addition, if the fabric consists of multi-filament yarns whose $D_f \sim R_f$, as shown in Fig 7, where R_f is the fibre radius and $2D_f$ is the distance between two adjacent fibres, the contact angle on CB multi-filament yarn, $\theta_r^{multi\text{-}filament}$, is defined as:

$$\cos\theta_r^{multi\text{-}filament} = \frac{(\pi - \theta_e)}{2}\cos\theta_e + \frac{1}{2}\sin\theta_e - 1 \tag{29}$$

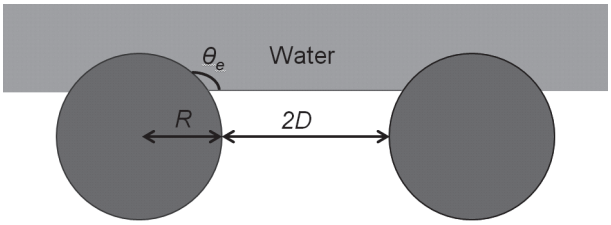

Fig. 7. A water droplet on two filament fibres

For $\theta_e > 90°$, θ_r^{CB} increases with increasing D. For example, if a fabric material is made of PTFE, ($\theta_e = 120°$) and the fibres are closely packed, $\theta_r^{CB} = 131°$; for D = R, $\theta_r^{CB} = 146°$; and for D = 2R, $\theta_r^{CB} = 152°$ on the multi-filament yarn.

As mentioned above, $109^o \le \theta_e$ (water) $\le 112^o$ and $73^o \le \theta_e$ (dodecane) $\le 75^o$ on a surface grafted with FS. By substituting these numbers into equation (28), we find $133° \le \theta_r^{CB}$ (water) $\le 136°$ and $98° \le \theta_r^{CB}$ (dodecane) $\le 100°$ for the FS-grafted mono-filament plain woven fabric. In the same manner, substituting the same θ_e into equation (29), we obtain $142° \le \theta_r^{multi\text{-}filament}$ (water) $\le 144°$ and $114° \le \theta_r^{multi\text{-}filament}$ (dodecane) $\le 115°$ for the FS-grafted multi-filament yarns. Using these values as the effective contact angles for the yarns in the plain woven structure and re-solving equation (28), i.e., substituting these values into θ_e (water) and θ_e (dodecane) in equation (28), we predict $161° \le \theta_r^{CB}$ (water) $\le 163°$ and $138° \le \theta_r^{CB}$ (dodecane) $\le 139°$ for the FS-grafted multi-filament plain woven fabric. According to our prediction, properly constructed NyCo multi-filament plain woven fabric can be

superhydrophobic and highly oleophobic once the fabric is treated with a low-surface-tension material such as FS.

2.3.2.2 Superhydrophobic oleophobic twill woven structure

Fig. 8 shows a cross-sectional view of a model of a NyCo twill woven fabric made of monofilament fibres. Flux integral can be used to obtain true area of twill woven fabric as well. The area of one yarn in the unit fabric is:

$$A_{\text{yarn in unit area}} = \frac{\int_0^{2\pi}\int_0^{2\pi} R(2R + R\cos v)\,du\,dv}{3} + \frac{\pi R^2}{2} = \left(\frac{8\pi^2}{3} + \frac{\pi}{2}\right)R^2 \tag{30}$$

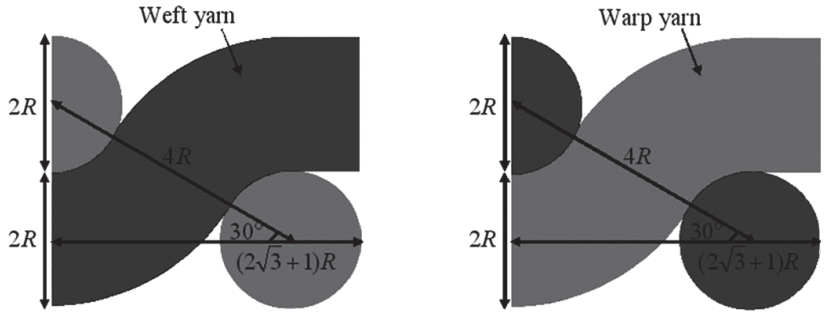

Fig. 8. Cross-section view of a twill woven fabric (source: Lee and Owens, 2010)

The area of one yarn in the unit fabric is applied to both weft and warp yarns, and a twill fabric in Fig. 8 consists of four yarns in the unit area. Therefore, the true fabric area is:

$$A_{\text{fabric}}^{\text{true}} = 4x\,A_{\text{yarn in unit area}} = 111.56R^2 \tag{31}$$

where A^{true}_{fabric} is the intrinsic area of the unit fabric determined by the area of yarn surfaces. The apparent surface area is equal to the area of a plane tangent to the top surface.

$$A_{\text{fabric}}^{\text{apparent}} = \left[R(2\sqrt{3}+1)\right]^2 = 19.93R^2 \tag{32}$$

where $A^{apparent}_{fabric}$ is the apparent area of the unit fabric. Based on equation (10), the roughness, r, is 5.59. If this twill woven fabric is made of yarns having multi-filament fibres as shown in Fig 7, the fabric will have even higher values of roughness and r > 5.59, since the space between the fibres will increase the intrinsic surface area whilst the apparent surface area remains the same. Therefore, the twill woven rough surface has high enough r to exist as a metastable Cassie–Baxter surface regardless of the structure of yarns.

Now, we model a Cassie–Baxter twill woven fabric. In Fig. 8, the centre-to-centre distance is $(2\sqrt{3}+1)R$. Thus, a Cassie–Baxter NyCo surface is defined as:

$$\cos\theta_r^{CB} = \frac{4(\pi - \theta_e) + 1}{2\sqrt{3}+1}\cos\theta_e + \frac{4\sin\theta_e + 1}{2\sqrt{3}+1} - 1 \tag{33}$$

Substituting the same Young contact angles, $109^o \le \theta_e$ (water) $\le 112^o$ and $73^o \le \theta_e$ (dodecane) $\le 75^o$, into equation (29), we obtain $142° \le \theta_r^{\text{multi-filament}}$ (water) $\le 144°$ and $114° \le \theta_r^{\text{multi-filament}}$

(dodecane) ≤ 115° for the FS-grafted multi-filament yarns. Using these values as the effective contact angles for the yarns in the twill woven structure and re-solving equation (33), i.e., substituting these values into θ_e (water) and θ_e (dodecane) in equation (33), we predict 150° ≤ θ_r^{CB} (water) ≤ 152° and 118° ≤ θ_r^{CB} (dodecane) ≤ 119° for the FS-grafted multi-filament twill woven fabric. According to our prediction, properly constructed NyCo multi-filament twill woven fabric can also be superhydrophobic and highly oleophobic once the fabric is treated with a low-surface-tension material such as FS.

2.3.2.3 Superhydrophobic oleophobic satin woven structure

Fig. 9 shows a cross-sectional view of a model of a NyCo 3/1 stain woven fabric made from monofilament fibres. The surface area of a single round monofilament fibre in the unit fabric can be calculated using flux integral in order to obtain r as shown above.

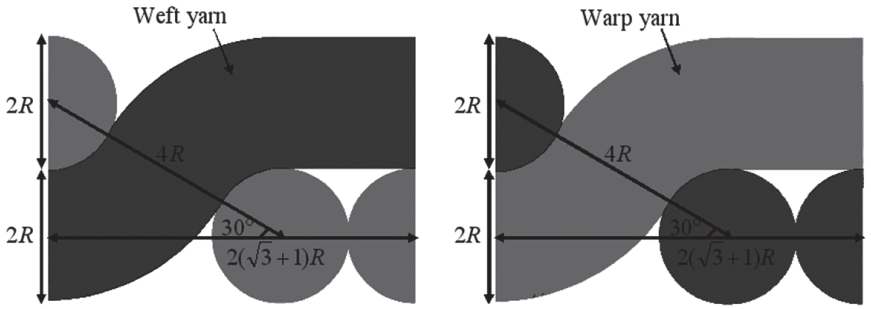

Fig. 9. Cross-section view of a 3/1 satin woven fabric

The area of one yarn in the unit fabric is:

$$A_{\text{yarn in unit area}} = \frac{\int_0^{2\pi}\int_0^{2\pi} R(2R + R\cos v)\,du\,dv}{3} + \pi R^2 = \left(\frac{8\pi^2}{3} + \pi\right)R^2 \tag{34}$$

The area of one yarn in the unit fabric is applied to both weft and warp yarns, and the satin fabric in Fig. 9 consists of six yarns in the unit area. Therefore, the true fabric area is:

$$A_{\text{fabric}}^{\text{real}} = 4\,A_{\text{yarn in unit area}} = 176.76R^2 \tag{35}$$

where A^{true}_{fabric} is the intrinsic area of the unit fabric determined by the area of yarn surfaces. The apparent surface area is equal to the area of a plane tangent to the top surface.

$$A_{\text{fabric}}^{\text{apparent}} = \left[2R(\sqrt{3}+1)\right]^2 = 29.85R^2 \tag{36}$$

where $A^{apparent}_{fabric}$ is the apparent area of the unit fabric. Based on equation (10), the roughness, r, is 5.92. If this satin woven fabric is made of yarns having multi-filament fibres as shown in Fig 9, the fabric will have even higher values of roughness and r > 5.92, since the space between the fibres will increase the intrinsic surface area whilst the apparent surface area remains the same. Therefore, the stain woven rough surface has high enough r to exist as a metastable Cassie–Baxter surface regardless of the structure of yarns.

Now, we model a Cassie–Baxter 3/1 satin woven fabric. In Fig. 9, the centre-to-centre distance is $(2\sqrt{3}+1)R$. Thus, a Cassie–Baxter NyCo surface is defined as:

$$\cos\theta_r^{CB} = \frac{2(\pi-\theta_e)+1}{\sqrt{3}+1}\cos\theta_e + \frac{2\sin\theta_e+1}{\sqrt{3}+1} - 1 \tag{37}$$

Again, substituting the same Young contact angles above, $109^o \le \theta_e$ (water) $\le 112^o$ and $73^o \le \theta_e$ (dodecane) $\le 75^o$, into equation (29), we obtain $142° \le \theta_r^{multi\text{-}filament}$ (water) $\le 144°$ and $114° \le \theta_r^{multi\text{-}filament}$ (dodecane) $\le 115°$ for the FS-grafted multi-filament yarns. Using these values as the effective contact angles for the yarns in the 3/1 satin woven structure and re-solving equation (37), we predict $149° \le \theta_r^{CB}$ (water) $\le 151°$ and $117° \le \theta_r^{CB}$ (dodecane) $\le 118°$ for the FS-grafted multi-filament 3/1 stain woven fabric. According to our prediction, properly constructed NyCo multi-filament satin woven fabric can also be superhydrophobic and highly oleophobic once the fabric is treated with a low-surface-tension material such as FS.

NyCo multi-filament woven fabric can be superhydrophobic but cannot be superoleophobic by itself, even if the fabric is treated with a low-surface-tension chemical. In order to achieve superoleophobicity as well as superhydrophobicity, the fabric morphology has to be manipulated by creating bigger spaces between fibres, loosening the fabric structure, or providing more roughness to the surface of NyCo multi-filament fibres. Considering the manufacturing process of woven fabrics, providing more roughness by adding protuberances to the surface of NyCo fibres seems the easiest way to achieve superhydrophobicity and superoleophobicity. Fig. 10 shows a NyCo surface covered with protuberances in micro and nano size FS. In the next section, we study how to create such a multi-scale roughness on the NyCo surface to prepare a metastable CB superhydrophobic and superoleophobic woven fabric.

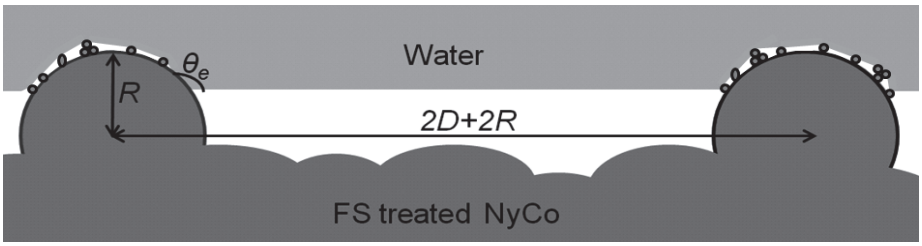

Fig. 10. A water drop on top of a NyCo fibre treated in a 10% FS solution consisting of base catalyst.

2.3.2.4 Superhydrophobic superoleophobic woven fabric

By using FS in conjunction with corrugated, rough surfaces, FS can build multi-scale roughness having low surface energy. Indeed, the previous research presented that the use of condensed silanes increases micro and nano structure corrugation and results in increased hydrophobicity and oleophobicity of so-treated cotton. A superhydrophobic and superoleophobic NyCo woven fabric can be developed in the same manner by covalently binding silanes onto the NyCo surface.

Although any soluble base can be an efficient catalyst, we use ammonium hydroxide as a base catalyst to accelerate the displacement of the methoxy or ethoxy substituent, and to facilitate the formation of the corrugated micro and nano-structure (Fig. 11).

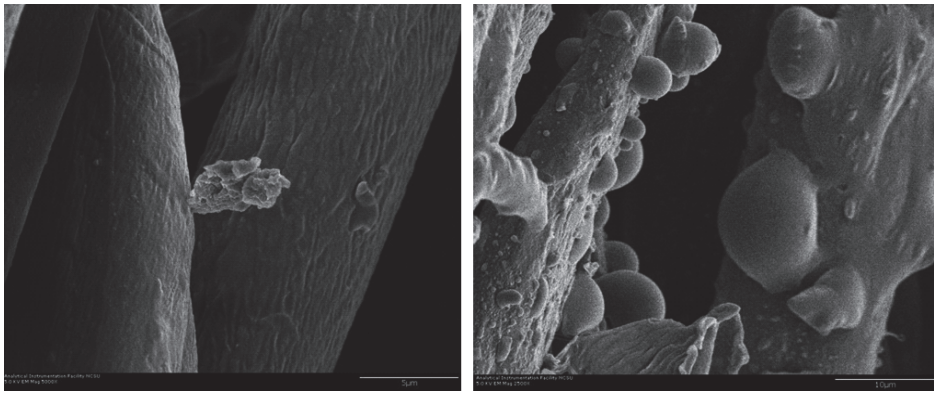

Fig. 11. Mult-scale protuberances on the FS-grafted NyCo surface. NyCo woven fabric was treated in a 10% solution of FS with catalytic water (left) and NyCo fibres treated in 10% FS with NH_4OH (right)

Since FS-treated NyCo without catalytic base has a relatively smooth surface whilst NyCo treated with FS in the presence of 1% catalytic base has multi-scale roughness on the surface, the X-ray photoelectron spectroscopy (XPS) of both FS treated NyCo with and without base catalyst was measured and compared with the XPS of untreated NyCo. Table 3 shows the XPS atomic composition of C, N, O, F, and Si and the ratio of F/O, F/C, and F/Si at the surface of three materials: (a) NyCo treated in a 10% solution of FS with catalytic water, (b) NyCo treated in a 10% solution of FS in the presence of 1% NH4OH, and (c) untreated NyCo. Both (a) and (b) have almost the same amount of fluorine regardless of the presence of base catalyst. However, as shown in Fig. 11, NyCo treated in a 10% solution of FS with water exhibits very different surface morphology compared to (b) although they possess almost the same atomic composition of F and nearly the same values of F/O, F/C, and F/Si ratios at the surface. As expected, based on the atomic composition of (c), the untreated NyCo does not have fluorine on the surface.

Fabric	Atomic composition (%)				Ratio		
	C	O	F	Si	F/O	F/C	F/Si
FS treated NyCo with water	39.1	8	50.2	2.7	6.3	1.3	18.4
FS treated NyCo with NH_4OH	38.4	8.6	50.5	2.5	5.9	1.3	20.4
Control NyCo	77	20.5	0	1.4	0	0	0

Table 3. XPS atomic composition of FS treated and untreated NyCo

By changing FS concentration, curing time, and the number of cures, we can control the morphology of FS protuberances on the NyCo surface and eventually prepare superhydrophobic and superoleophobic woven fabric (Fig. 12). The FS-treated NyCo plain woven fabric shown in Fig. 12 is superhydrophobic and superoleophobic. The fabric prevents the absorption of not only water but also dodecane with almost no change of contact angles.

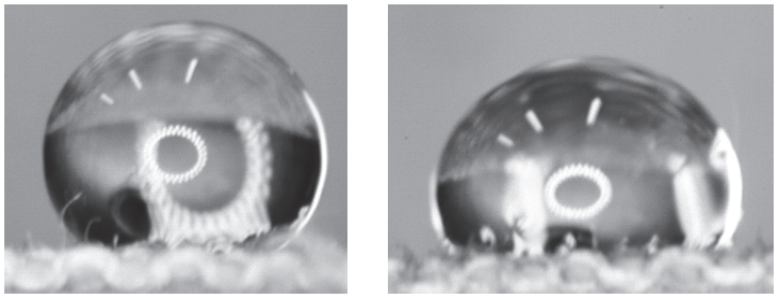

Fig. 12. 10 μL water (left) and dodecane (right) droplets sitting on top of FS-grafted NyCo plain woven fabric treated via microwave synthesis

The FS concentration, curing time, and the number of cures absolutely affect the wetting behaviour of FS-treated NyCo woven fabric. This indicates that oil contact angles can be greatly improved by varying such parameters. We suggest that improving the macro-scale geometric morphology of the woven fabric, such as controlling the fibre spacing, manipulating the yarn structure, and choosing the proper woven construction are also necessary to design and prepare superhydrophobic and superoleophobic fabrics.

3. Conclusion

In this chapter, we studied how to create superhydrophobic and superoleophobic woven fabric. A superhydrophobic superoleophobic surface is obtained by two criteria: a low surface tension and a properly designed rough surface having appropriate surface roughness and morphology. In order to make woven fabric superhydrophobic and superoleophobic, NyCo multi-filament plain woven fabric was treated with FS which has a very low surface tension and provides more roughness to the fabric by generating micro and nano-size protuberances in the form of FS condensates on the fibre surfaces. From the Young contact angles of water and dodecane on a FS-grafted nylon film, we could predict the apparent contact angles on FS-grafted NyCo multi-filament plain, twill, and 3/1 satin woven fabrics. Forming multi-scale geometric structure on the NyCo was also important to improve hydrophobicity and oleophobicity of the fabric, and consequently this treatment resulted in a highly hydrophobic and oleophobic woven fabric material. Finally, superhydrophobic superoleophobic plain woven fabric has been prepared using the Wenzel and the Cassie-Baxter equations. Although superoleophobicity is achieved via the metastable Cassie-Baxter model, the fabric can prevent the absorption of oil as well as water with almost no change of contact angles.

4. Acknowledgment

We appreciate support from the Defense Threat Reduction Agency-Joint Science and Technology Office for Chemical and Biological Defense (contract numbers BA07PRO102 and HDTRA1-08-1-0049) and Air Force Research Laboratory (grant number FA8650-07-1-5903). The U.S. Government is authorized to reproduce and distribute reprints for Governmental purposes notwithstanding any copyright notation thereon. The views and conclusions contained herein are those of the authors and should not be interpreted as necessarily

representing the official policies or endorsements, either expressed or implied, of Air Force Research Laboratory or the U. S. Government.

5. References

Balkenede, A. R, Boogaard, H. J. A. P. van de, Scholten, M., Willard, N. P. (1998), 'Evaluation of different approaches to assess the surface tension of low-energy solids by means of contact angle measurements', *Langmuir*, 14, 5907-5912.

Barton, A. F. M. (1983), *CRC Handbook of solubility parameters and other cohesion parameters*, Boca Raton, CRC Press, Inc.

Barthlott, W., Neihuis, C. (1997), 'Purity of the sacred lotus, or escape from contamination in biological surfaces', *Planta*, 202, 1-8.

Bico, J., Tordeux, C., Quere, D. (2001), 'Rough wetting', *Europhys Lett*, 55, 214-220.

Brar, T., France, P., Smirniotis, P. (2001), 'Heterogeneous versus homogeneous nucleation and growth of zeolite A', *J Phy. Chem B*, 105, 5383-5390.

Chhowalla, M., Amaratunga, G. A. J., Milne, W. I., McKinley, G. H., Gleason, K. K. (2003), ' Superhydrophobic carbon nanotube forests', *Nano Lett*, 3, 1701-1705.

Fowkes. F. M. (1963), 'Additivity of intermolecular forces at interfaces: I. Determination of the contribution to surface and interfacial tensions of dispersion forces in various liquids', *J Phys Chem*, 67, 2538-2541.

Fuerstner, R., Barthlott, W., Neinhuis, C., Walzel, P. (2005), 'Wetting and self-cleaning properties of artificial superhydrophobic surfaces', *Langmuir*, 21, 956-961.

Han, J. T., Xu, X., Cho, K. (2005), 'Diverse access to artificial superhydrophobic surfaces using block copolymers', *Langmuir*, 21, 6662-6665.

Hayn, R., Owens, J., Boyer, S., McDonald, R., Lee, H. (2011), 'Preparation of highly hydrophobic and oleophobic textile surfaces using microwave-promoted silane couling', *Journal of Materials Science*, 46, 2503-2509.

Hoefnagels, H., Wu, D., With, G., Ming, W. (2005), 'Biomimetic Superhydrophobic and Highly Oleophobic Cotton Textiles', *Langmuir*, 23, 13158-13163.

Jopp, J., Gruell, H., Yerushalmi-Rozen, R. (2004), 'Wetting behavior of water droplets on hydrophobic microtextures of comparable size', *Langmuir*, 20, 10015-10019.

Kim, J., Kim, C. (2002), 'Nanostructured surfaces for dramatic reduction of flow resistance in droplet-based microfluidics', *J Microelectromechanical System*, 11(5), 454-464.

Kim, S. H., Kim, J., Kang, B., Uhm, H. (2005), 'Superhydrophobic CF_x coating via in-line atmospheric RF plasma of He-CF_4-H_2', *Langmuir*, 21, 12213-12217.

Kovats, E. (1989), 'Wetting of low energy model surfaces', *Pure and App Chem*, 61, 1937-1944.

Krevelen, D. W. van, Hoftyzer, P. J. (1980), *Properties of Polymers*, New York, Elsvier/North-Holland Inc.

Krupenkin, T. N., Taylor, J. A., Schneider, T. M., Yang, S. (2004), 'From rolling ball to complete wetting: The dynamic tuning of liquids on nanostructured surface', *Langmuir*, 20, 3824-3827.

Kwong, V. H., Mossman, M. A., Whitehead, L. A. (2004), 'Control of reflectance of liquid droplets by means of electrowetting', *App Optics*, 43(4), 808-813.

Lau, K. K. S., Bico, J., Teo, K. B. K., Chhowalla, M., Amaratunga, G. J., Milne, W. I., McFinley, G. H., Gleason, K. K. (2003), 'Superhydrophobic carbon nanotube forests', *Nano Lett.*, 3, 1701-1705.

Lee, H., Michielsen, S. (2006), 'Lotus effect: superhydrophobicity', *Journal of Textile Institute*, 97, 455-462.

Lee, H., Owens J. (2010), 'Design of superhydrophobic ultraoleophobic nyco', *Journal of Materials Science*, 45, 3247-3253.

Lee, H., Owens J. (2011), 'Motion of liquid droplets on a superhydrophobic oleophobic surface', *Journal of Materials Science*, 46, 69-76.

Liu, H., Feng, L., Zhai, J., Jiang, L., Zhu, D. (2004), 'Reversible wettability of a chemical vapor deposition prepared ZnO film between superhydrophobicity and superhydrophilicity', *Langmuir*, 20, 5659-5661.

Marmur, A. (2004), 'The Lotus effect: superhydrophobicity and metastability', *Langmuir*, 20, 3517-3519.

McHale, G., Shirtcliffe, N. J., Newton, M. I. (2004), 'Contact-angle hysteresis on super-hydrophobic Surfaces', *Langmuir*, 20, 10146-10149.

Miwa, M., Nakajima, A., Fujishima, A., Hashimoto, K., Watanabe, T. (2004), 'Effects of the surface roughness on sliding angles of water droplets on superhydrophobic surfaces', *Langmuir*, 16, 5754-5760.

Nakajima, A., Hashimoto, K., Watanabe, T. (2005), 'Transparent superhydrophobic thin films with self-cleaning properties', *Langmuir*, 16, 7044-7047.

Ostrovskaya, L., Podesta, A., Milani, P., Ralchenko, V. (2003), 'Influence of surface morphology on the wettability of cluster-assembled carbon films', *Europhys Lett*, 63(3), 401-407.

Otten, A., Herminghaus, S. (2004), 'How plants keep dry: A physicist's point of view', *Langmuir*, 20, 2405-2408.

Pal, S. Weiss, H., Keller, H., Mueller-Plathe, F. (2005), 'Effect of nanostructure on the properties of water at the water-hydrophobic interface: a molecular dynamics simulation', *Langmuir*, 21, 3699-3709.

Patankar, N. A. (2003), 'On the modeling of hydrophobic contact angles on rough surfaces', *Langmuir*, 19, 1249-1253.

Roura, P., Fort, J. (2002), 'Comment on "Effects of the surface roughness on sliding angles of water droplets on superhydrophobic surfaces" ' *Langmuir*, 18, 566-569.

Sun, M., Luo, C., Xu, L., Ji, H., Ouyang, Q., Yu, D., Chen, Y. (2005), 'Artificial lotus leaf by nanocasting', *Langmuir*, 21, 8978-8981.

Sun, T., Feng, L., Gao, X., Jiang, L. (2005), 'Bioinspired surfaces with special wettability', *Acc Chem Res*, 38, 644-652.

Tadanaga, K., Morinaga, J., Matsuda, A., Minami, T. (2000), 'Superhydrohpobic-superhydrophilic micropatterning on flowerlike alumina coating film by the sol-gel method', *Chem Mater*, 12, 590-592.

Yoshimitsu, Z., Nakajima, A., Watanabe, T., Hashimoto, K. (2002), 'Effects of surface structure on the hydrophobicity and sliding behavior of water droplets', *Langmuir*, 18, 5818-5822.

Zhai, L., Cebeci F. C., Robert E. C., Rubner M. F. (2004), 'Stable superhydrophobic coatings from polyelectrolyte multilayers', *Nano Lett*, 4, 1349-1353.

Zhang, X., Sato, O., Taguchi, M., Einaga, Y., Murakami, T., Fujishima, A. (2005), 'Self-cleaning particle coating with antireflection properties', *Chem Mater*, 17, 696-700.

10

The Flame Retardant Nomex/cotton and Nylon/Cotton Blend Fabrics for Protective Clothing

Charles Q. Yang and Hui Yang
Department of Textiles, Merchandising and Interiors,
The University of Georgia,
U.S.A.

1. Introduction

Due to its excellent fire-resistant property, Nomex has commonly been used to produce protective clothing [1, 2]. However, the high cost and low comfortability of Nomex have limited its wider uses. Blending Nomex with cotton not only reduces the cost but also improves comfortability of the fabrics. Because cotton is a highly flammable fiber, the Nomex/cotton blend fabric containing more than 20% cotton is not self-extinguishable [3-4]. Therefore, a durable flame-retardant finishing treatment becomes necessary to make the Nomex/cotton blend flame-resistant if it contains more than 20% cotton fiber.

Previously we developed a flame retardant finishing system for cotton based on a hydroxy-functional organophosphorus oligomer (HFPO) shown in Scheme 1. Because HFPO does not have a reactive functional group for cotton, it is necessary to use a bonding agent, such as dimethyloldihydroxyethyleneurea (DMDHEU), trimethylolmelamine (TMM), or 1,2,3,4-butanetetracarboxylic acid (BTCA), to make the flame retardant resistant to hydrolysis [5-12]. In this research, we developed a nonformaldehyde flame retardant finishing system for the Nomex/cotton using BTCA to bond HFPO to cotton by esterifying both HFPO and cotton.

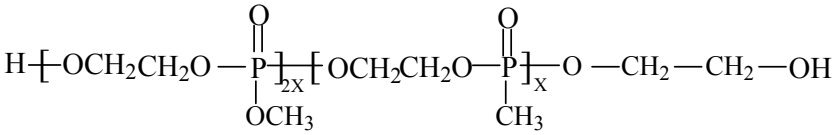

Scheme 1. A hydroxy-functional organophosphorus oligomer (HFPO)

Considering the high cost of Nomex, nylon/cotton blend is a more attractive alternative for use in protective clothing if the nylon/cotton fabric can be successfully flame retardant finished. The industry is still not able to produce flame-resistant nylon fabrics in spite of significant efforts made in the past 40 years [13-16]. It is even more difficult to impart flame retardancy to a blend of cotton and a synthetic fiber, such as cotton/nylon blend, than to each individual component fiber due to "scaffolding effect" [17]. The industry has yet to

develop effective, practical and commercially feasible flame retardant finishing system for nylon/cotton blend fabrics.

In this study, we investigated the bonding of HFPO onto nylon by DMDHEU, and found that HFPO can be bound to the nylon fabric in the presence of DMDHEU by forming a polymeric HFPO/DMDHEU system shown in Scheme 2. We also evaluated the performance of two 50/50 nylon/cotton batter dress uniform (BDU) military fabrics treated with HFPO/DMDHEU flame retardant finishing system.

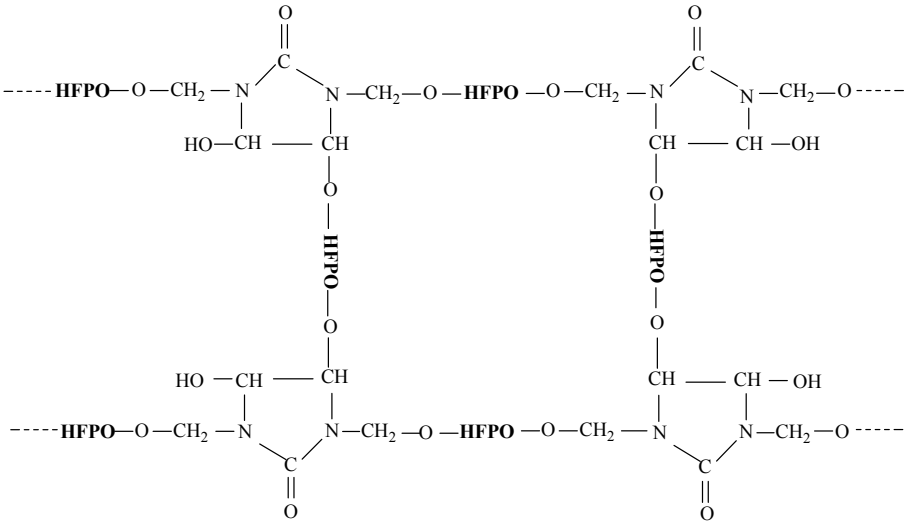

Scheme 2. Formation of a Crosslinked Polymeric Network on Nylon

2. Experimental

2.1 Materials

The Nomex/cotton (35%/65%) blend fabric with woodland camouflage was a twill weave fabric weighing 219 g/m^2 produced in China. The nylon fabric was a 100% nylon 6.6 woven fabric (Testfabrics Style 306A) weighing 59 g/m^2. Two nylon/cotton blend BDU fabrics were used in this study: (1) a 50%/50% nylon/cotton BDU pure finish ripstop fabric printed with three-color "day desert" camouflage weighing 216 g/m^2 (military specification: MIL-C-44031 CL1); (2) a 50%/50% nylon/cotton BDU pure finish twill fabric with three-color "woodland" camouflage weighing 220 g/m^2 (military specification: MIL-C-44436 CL3), both supplied by Bradford Dyeing Association, Bradford, Rhode Island. HFPO under the commercial name of "Fyroltex HP" (also known previously as "Fyrol 51", CA Registry No. 70715-06-9) was supplied by Akzo Nobel Phosphorus Chemical Division, Dobbs Ferry, New York. N-methylol dimethylphosphonopropionamide (MDPA) under the trade name of "Pyrovatex CP New" (CA Registry No. 20120-33-6) was supplied by Ciba Specialty Chemicals, High Point, North Carolina. DMDHEU was a commercial product (44% agueous solution) under the trade name of "Freerez 900" supplied by Noveon, Cleveland, Ohio. BTCA, triethanolamine (TEA) and hypophosphorous acid (H_3PO_2) were reagent-grade chemicals supplied by Aldrich, Wisconsin.

2.2 Fabric treatment and laundering procedures

The fabric was first immersed in a finishing solution, then passed through a laboratory padder with two dips and two nips, dried at 90°C for 5 min and finally cured in a Mathis curing oven. All concentrations presented here were based on weight of bath (w/w %). The wet pick-up of the nylon/cotton blend fabrics was 77±2% whereas that of the Nomex/cotton blend fabric was approximately 60±2%. After curing, the treated fabric was subjected to a specified number of home laundering cycles using a standard reference detergent (AATCC Detergent 1993) according to AATCC Test Method 124. The water temperature for laundering was approximately 46°C.

2.3 Evaluation of the flame retarding performance and stiffness of the fabric

The vertical flammability of the fabrics was measured according to ASTM Standard Method D6413. The limiting oxygen index (LOI) of the fabrics was measured according to ASTM Standard Method D2863. The fabric stiffness was measured according to ASTM Standard Method D6828 using a "Handle-O-Meter" tester (Model 211-300) manufactured by Thwing-Albert, Philadelphia. The slot width was 5 mm, and the beam size was 1000 grams. The fabric stiffness presented in this paper was the mean of measurements of 5 specimens.

2.4 Determination of phosphorus concentration on the treated fabric

Approximately 2 g of a treated fabric sample taken from three different parts of a "10 inches × 12 inches" fabric specimen were ground in a Wiley mill into a powder to improve sample uniformity. 2 ml of concentrated H_2SO_4 were added to 0.1 g of the powder in a beaker. 10 ml of 30% H_2O_2 were added dropwise to the mixture, allowing the reaction to subside between drops. The reaction mixture was heated at approximately 250°C to digest the powder and to evaporate the water until dense SO_3 vapor was produced. The completely digested sample as a clear solution was transferred to a 50 ml volumetric flask, then diluted with distilled/deionized water. The sample thus prepared was analyzed with a Thermo-Farrell-Ash Model 965 inductively coupled plasma atomic emission spectrometer (ICP/AES) to determine the phosphorus concentration. The percent phosphorus retention is calculated by: (the phosphorus concentration of the fabric after laundering) ÷ (that of the fabric before laundering) x 100%.

3. Results and discussion

3.1 Flame retardant finishing of the 65/35 nomex/cotton blend military fabric

The phosphorus concentration of Nomex/cotton blend fabric treated with 24% HFPO, 8% BTCA and 2.5% H_3PO_2 in combination with TEA at different concentrations and subjected to different home laundering cycles is presented in Figure 1. The data presented here show that the phosphorus concentration on the treated Nomex/cotton blend fabric first increased, then decrease as the TEA concentration increases in the range from 1.0% to 10.0% and the maximum phosphorus concentrations on the treated fabric are achieved at 4% TEA (Figure 1). The data indicate that the use of TEA also increases the percent phosphorus retention on the fabric after multiple laundering cycles. TEA has three hydroxyl groups in its molecule and is able to react with carboxylic acid groups of BTCA by esterification. BTCA also reacts with HFPO and cotton to form a BTCA/HFPO/TEA/cotton crosslinked network as shown

in Scheme 3, thus improving the laundering resistance of the HFPO on cotton. The data presented in Figure 1 also show that further increasing TEA concentration from 4% to 10% reduces the retention of HFPO after multiple launderings on the treated fabric. Because TEA, HFPO and cotton all have hydroxyl groups and they compete to react with BTCA, the presence of excessive amount of TEA reduces the reaction of BTCA with HFPO and cotton, thus reducing the bonding of HFPO on cotton as shown in Figure 1.

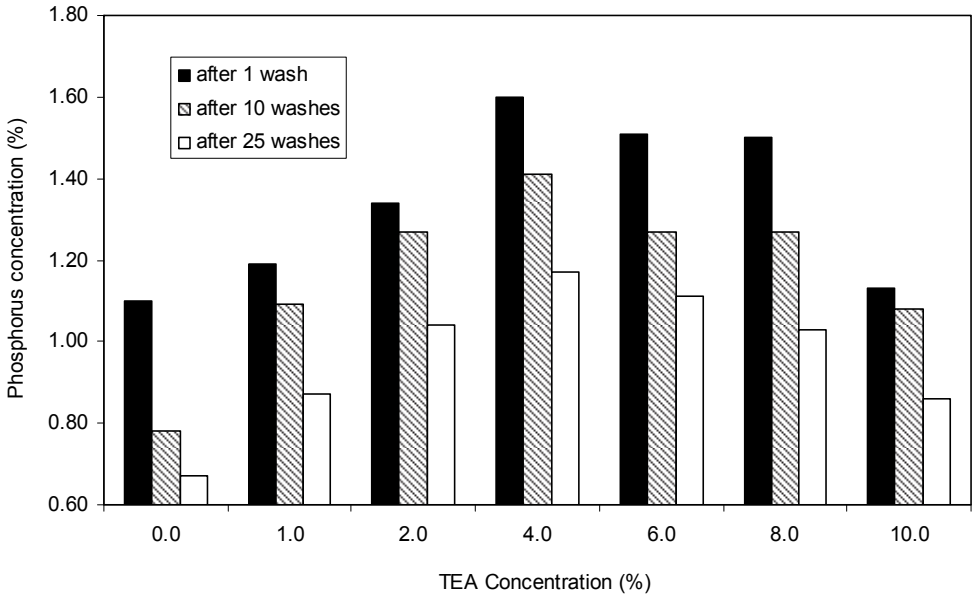

Fig. 1. The phosphorus concentrations of the Nomex/cotton blend fabric treated by 24% HFPO, 8%BTCA and 2.5% H_3PO_2 as a function of TEA concentration.

The Nomex/cotton fabric is treated with 24%HFPO, 8%BTCA, 2.5% H_3PO_2 and TEA at different concentrations. The fabric thus treated is cured at 180ºC for 3 min. The LOI of the fabric thus treated (before washing) is plotted against the TEA concentration in Figure 2. Without being subjected to laundering, all Nomex/cotton fabric samples have the same HFPO and H_3PO_2 concentrations but different TEA concentrations. The LOI (%) of the fabric increases from 37.2 to 40.6 as the TEA concentration (%) increases from 0.0 to 8.0% (Figure 2). Thus, the data demonstrate the phosphorus-nitrogen synergistic effect of TEA in the HFPO/BTCA/ H_3PO_2/TEA system on the Nomex/cotton blend fabric.

Previously, we found that calcium deposit formed on the cotton treated with HFPO/BTCA during laundering diminishes the flame retardant performance of the treated cotton fabric [11, 12]. We also studied the effects of TEA on the calcium deposit on the cotton fabric treated with HFPO/BTCA [12]. The calcium concentration on the treated Nomex/cotton blend fabric increases after multiple launderings is due to the formation of insoluble calcium salt of those free carboxylic acid groups of BTCA bound to cotton. We also found that the calcium concentration on the fabric after multiple launderings decreases as the TEA concentration is increased. The reduction of the calcium concentration on the treated

Nomex/cotton blend fabric as a result of the presence of TEA is attributed to esterification of the free carboxylic acid groups of BTCA on cotton by TEA as shown in Scheme 3.

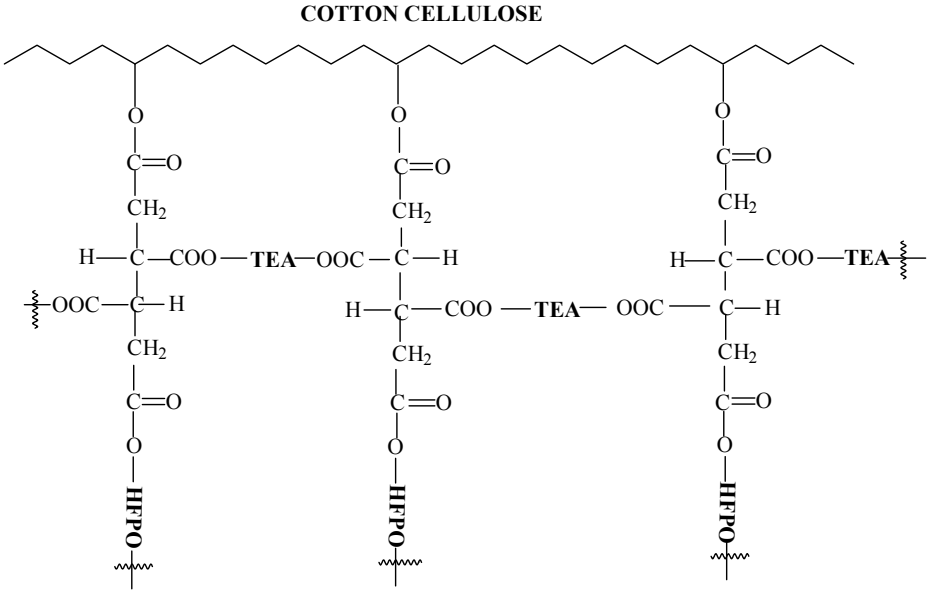

Scheme 3. Formation of BTCA/HFPO/TEA crosslinked network on cotton

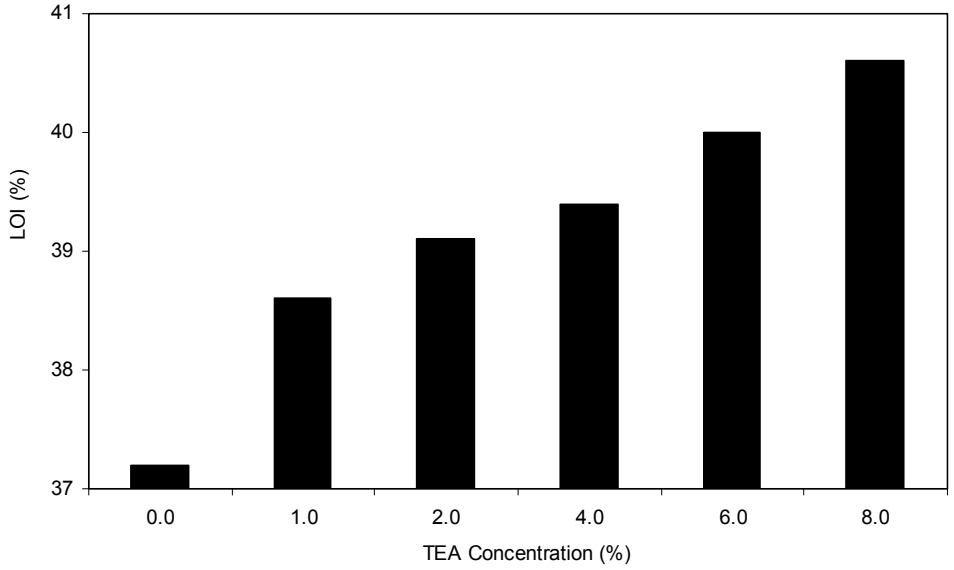

Fig. 2. LOI of the Nomex/cotton blend fabric treated by 24% HFPO, 8% BTCA and 2.5% H_3PO_2 in combination with TEA as a function of TEA concentration.

The Nomex/cotton blend fabrics were treated with 24% HFPO, 8% BTCA, 2.5% H_3PO_2 and TEA at different concentrations. The Nomex/cotton blend fabric thus treated was cured at 180°C for 3 min and finally subjected to 1, 10 and 25 laundering cycles. The LOI (%) of the fabric thus treated is shown against the TEA concentration (Figure 3). After 1 laundering cycle, the LOI of the treated Nomex/cotton blend fabric first increases from 32.1% without TEA to its maximum (36.3%) when 6.0% TEA is used. Further increasing TEA concentration reduces the LOI of treated Nomex/cotton blend fabric. Similar trends are observed on the treated fabric subjected to 10 and 25 laundering cycles. The optimum TEA concentration for the finish solution is in the 4.0-6.0% range. After 25 laundering cycles, the LOI of the fabric treated using 6.0% TEA is 30.5%.

The Nomex/cotton blend fabrics was treated with HFPO/BTCA/TEA (weight ratio: 3.0/1.0/0.75) at different concentrations and curried at 180°C for 3 min. The HFPO concentration increases from 12% to 24%, and the BTCA and TEA concentration are increased accordingly. The LOI and vertical flammability (char length) of the treated fabric after different laundering cycles are presented in Tables 1 and 2, respectively. The LOI of the Nomex/cotton blend fabric without treatment is 22.9% and it fails the vertical flammability test. All the Nomex/cotton fabric samples treated with the four HFPO/BTCA/TEA formulas pass the vertical flammability test after 30 laundering cycles (Table 2). The fabric treated with 12% (w/w) HFPO finishing solution (approximately 8% [w/w] HFPO on the fabric) has LOI of 26.5% and char length of 48 mm after 30 laundering cycles, demonstrating excellent flame retardant performance and superior laundering durability at a small flame retardant concentration on the fabric.

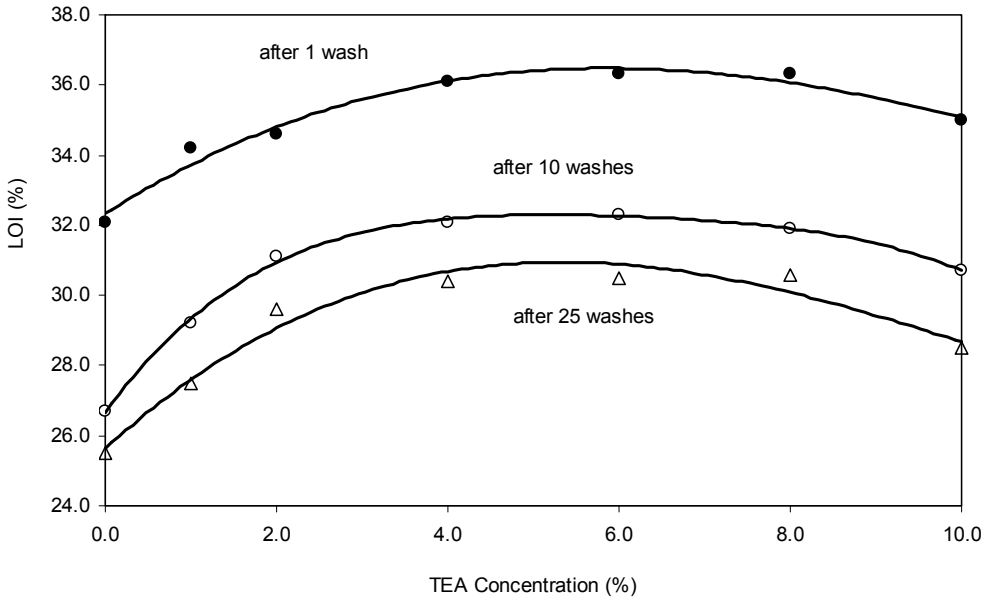

Fig. 3. The LOI of the Nomex/cotton blend fabric treated by 24%HFPO, 8%BTCA and 2.5% H_3PO_2 in combination with TEA as a function of TEA concentration.

HFPO (%)	BTCA (%)	H_3PO_2 (%)	TEA (%)	Number of home laundering cycles				
				before wash	1 wash	10 washes	20 washes	30 washes
12	4	1.25	3.0	35.7	32.7	27.9	27.1	26.5
18	6	1.88	4.5	38.8	35.7	31.1	30.1	28.5
24	8	2.50	6.0	40.7	37.2	32.5	30.5	29.4
30	10	3.13	7.5	40.6	37.8	33.0	32.0	29.5
Control				22.9				

Table 1. The LOI of the Nomex/cotton fabric treated with HFPO/BTCA/H_3PO_2/TEA at the weight ratio of 24/8/2.5/6 and cured at 180°C for 3 min.

HFPO (%)	BTCA (%)	H_3PO_2 (%)	TEA (%)	Number of home laundering cycles				
				No wash	1 wash	10 washes	20 washes	30 washes
12	4	1.25	3.0	37	34	41	44	48
18	6	1.88	4.5	28	29	43	27	35
24	8	2.50	6.0	27	31	35	34	31
30	10	3.13	7.5	27	31	30	38	32
Control				>300				

Table 2. The char length of the Nomex/cotton blend fabric treated with HFPO/BTCA/H_3PO_2/TEA at a weight ratio of 24/8/2.5/6 and cured at 180°C for 3 min.

The tensile strength of the treated Nomex/cotton blend fabric is summarized in Table 3. The tensile strength retention is 73-77% at the warp direction and 77-82% at the filling direction (Table 3). The fabric strength loss is due to acid-catalyzed cellulose depolymerization and crosslinking of cellulose [18]. The fabric strength loss after the flame retardant finishing process is modest. The effect of the treatment on the fabric hand property appears to be negligible. More details about the flame retardant Nomex/cotton blend fabric can be found elsewhere [19].

HFPO (%)	BTCA (%)	H_3PO_2 (%)	TEA (%)	Tensile Strength (N)		Strength Retention (%)	
				Warp	Filling	Warp	Filling
12	4	1.25	3.0	405	262	73	80
18	6	1.88	4.5	414	271	74	82
24	8	2.50	6.0	409	254	74	77
30	10	3.13	7.5	427	270	77	82
Control				556	329	-	-

Table 3. The tensile strength of the Nomex/cotton blend fabric treated with HFPO/BTCA/H_3PO_2/ TEA at the weight ratio of 24/8/2.5/6 and cured at 180°C for 3 min.

3.2 The flame retardant finishing of nylon/cotton blend BDU fabrics

We first studied the bonding of HFPO to nylon fiber using DMDHEU as the bonding agent. The nylon 6.6 fabric was first treated with the combination of 32% HFPO and DMDHEU at

different concentrations, cured at 165 °C for 2 min, and finally subjected to 1 and 10 laundering cycles. The phosphorus concentration and the percent phosphorus retention of the nylon fabric thus treated are shown in Figure 4 and Table 4, respectively. When the DMDHEU concentration is increased from 1% to 8%, the phosphorus concentration of the treated nylon fabric after 1 laundering cycle increases from 0.21% to 1.75%, representing an increase in phosphorus retention from 9% to 75%, respectively. After 10 laundering cycles, 1.04% phosphorus (45% retention) remains on the nylon fabric treated with 8% DMDHEU.

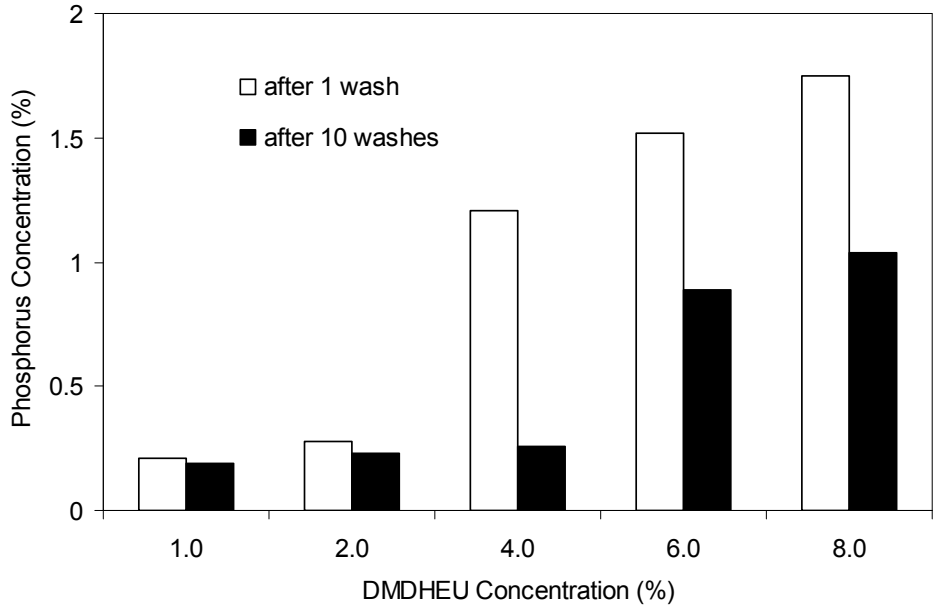

Fig. 4. The phosphorus concentration of the nylon-6.6 fabric treated with 32% HFPO and DMDHEU cured at 165°C for 2 min and finally subjected to 1 and 10 laundering cycles versus TMM concentration.

HFPO (%)	DMDHEU (%)	Molar Ratio (hydroxyl/hemi-acetal*)	Phosphorus Retention (%)	
			1 wash	10 washes
32	1	6.19	9	8
32	2	3.10	12	10
32	4	1.55	52	11
32	6	1.03	65	38
32	8	0.77	75	45

* The molar ratio of the hydroxy group of HFPO to the methylol group of DMDHEU.

Table 4. The percent phosphorus retention of the nylon 6.6 fabric treated with 32%HFPO and DMDHEU at different concentrations, cured at 165°C for 2 min and finally subjected to 1 and 10 laundering cycles.

The concentration of the terminal amine groups of nylon 6.6 in the fiber is small. Due to the poor penetration of the finishing solution into the fiber interior and the low reactivity of the terminal amine groups as a result of a high degree of crystalinity and H-bonding in nylon 6.6, the concentration of phosphorus bound to the fabric by nylon's terminal groups should be even smaller. The phosphorus concentration of nylon fabric treated with 32%HFPO without DMDHEU is 0.20% and 0.17% after 1 and 10 laundering cycles, respectively. The phosphorus concentration on the nylon fabric after 1 laundering reaches 1.21, 1.52 and 1.75 when 4, 6 and 8% DMDHEU, respectively, is used for the treatment. The data indicate that HFPO bound to the fabric is durable to multiple launderings. Therefore, the majority of HFPO on the fabric must be bound to nylon by its reactions with DMDHEU other than its bonding to nylon's terminal groups by a DMDHEU "bridge". DMDHEU has four chemically active methylol groups, and HFPO has two hydroxyl groups. The increase in the phosphorus retention as the DMDHEU concentration is increased shown here suggests the formation of a crosslinked polymeric network. A simplified version of the crosslinked polymeric network is shown in Scheme 2. The bonding of HFPO to the nylon fabric and the retention of HFPO on the fabric after multiple launderings can probably be attributed to the formation of the polymeric network on the fabric.

For the purpose of elucidating the bonding mechanism of HFPO to nylon by DMDHEU, we applied N-methylol dimethylphosphonopropionamide (MDPA, shown in Scheme 4) to the nylon fabric. A MDPA molecule has only one methylol group which may react with the terminal amine groups on nylon but it is not able to from crosslinked network with HFPO. The nylon 6.6 fabric was treated with 32% MDPA and DMDHEU at different concentrations, cured at 165 ^{o}C for 2min and finally subjected to 1 laundering cycle. The phosphorus concentration of the nylon-6.6 fabric thus treated is presented in Table 5. The phosphorus concentration on the nylon fabric treated using MDPA without DMDHEU is 2.53% before laundering, and it becomes 0.23% after 1 laundering (Table 5). Considering the fact that the same fabric treated with 32% HFPO without a bonding agent is 0.20% after 1 laundering, the phosphorus concentration on the fabric thus treated (0.23-0.26%) is negligible. It is also independent of the DMDHEU concentration used (Table 5). The small amount of MDPA bound onto the nylon fabric is possibly due to (1) the reaction between MDPA and the terminal amine group on the nylon fiber and (2) physical adsorption.

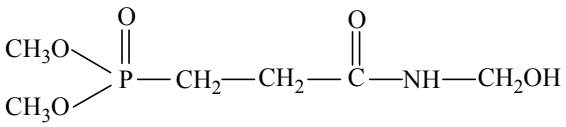

Scheme 4. MDPA

HFPO is a bifunctional compound and it is able to form a crosslinked polymeric network by its reaction with DMDHEU as shown in Scheme 2. Unlike HFPO, MDPA is mono-functional and is not able to form a crosslinked polymeric network in the presence of DMDHEU. The data presented here shows that the amount MDPA bound to nylon is negligible and is independent of the amount of DMDHEU used. Those facts are consistent with the hypothesis that HFPO reacts with DMDHEU on the nylon fabric to form a crossinked polymeric network shown in Scheme 2, which makes HFPO on nylon resistant to laundering.

MDPA (%)	DMDHEU (%)	Phosphorus (%)*
32	0	0.23
32	2	0.26
32	4	0.25
32	6	0.24
32	8	0.23

Table 5. The phosphorus concentration of the nylon 6.6 fabric treated with 32% MDPA and DMDHEU at different concentrations, then cured at 165°C for 2 min, and finally subjected to 1 laundering cycle. (The phosphorus concentration on the fabric was 2.53% before laundering.)

We applied two different formulas (HFPO/DMDHEU and MDPA/TMM) to the 50/50 nylon/cotton fabric (Table 6). The nylon/cotton fabric samples treated with the two formulas have approximately the same phosphorus concentration (~3.80%) before laundering. The fabric was cured at 165°C for 2 min and finally subjected to 10 laundering cycles. The phosphorus concentration, LOI and char length of the fabric thus treated is shown in Table 6. The nylon/cotton fabric treated with MDPA has 1.20% phosphorus retained, and it has LOI of 23.9% and failed the vertical flammability test after 10 launderings. The fabric samples treated with HFPO/DMDHEU has LOI of 27.3% and passes the vertical flammability test. Evidently, the MDPA/TMM system is not suitable for the flame retardant finishing of the nylon/cotton blend fabric.

Flame Retardant	Bonding Agent	Catalyst	Phosphorus (%)	LOI (%)	Char length (mm)
HFPO 32%	DMDHEU 6%	NH_4Cl 0.12%	2.20	27.3	75
MDPA 45%	TMM 6%	H_3PO_4 2.0%	1.20	23.9	>300

Table 6. The LOI and char length of the 50/50 nylon/cotton blend fabric treated with different flame retardants and different binders and subjected to 10 laundering.

The nylon/cotton fabric (woodland) is treated with 32% HFPO and DMDHEU at different concentrations and cured at 165°C for 2 min. The phosphorus concentration of the fabric thus treated and subjected to different numbers of laundering cycles is shown in Table 7. The phosphorus retention of the treated fabric is presented against the DMDHEU concentration in Figure 5. When DMDHEU increases from 1% to 10%, the phosphorus concentration of the treated fabric after one laundering increases from 0.56% (16% phosphorus retention) to 2.69% (78% phosphorus retention). The percent phosphorus retention after one laundering is also called "percent phosphorus fixation" by the industry. A higher percent phosphorus fixation is a indicator of higher relative quantity of the flame retarding organic phosphorus agent bound to the fabric after curing. Similar trend is observed on the treated fabric after 20 and 40 launderings. The phosphorus concentration and phosphorus retention decrease as the number of laundering cycle increases due to the hydrolysis of the HFPO bound to the fabric. It is noticed that the fabric treated with 32% HFPO and 10% DMDHEU after 40 laundering cycles still retains 1.84% phosphorus (54% phosphorus retention).

HFPO (%)	DMDHEU (%)	Phosphorus concentration (%)		
		1 laundering	20 launderings	40 launderings
32	1	0.56	0.30	0.25
32	2	1.34	0.52	0.42
32	4	1.81	0.72	0.64
32	6	2.47	1.79	1.01
32	8	2.59	2.00	1.13
32	10	2.69	2.18	1.84

Table 7. The phosphorus concentration of the nylon/cotton fabric (woodland) treated with HFPO and DMDHEU at different concentrations and cured at 165°C for 2 min. (The phosphorus concentration of the treated fabric before wash is 3.43%.)

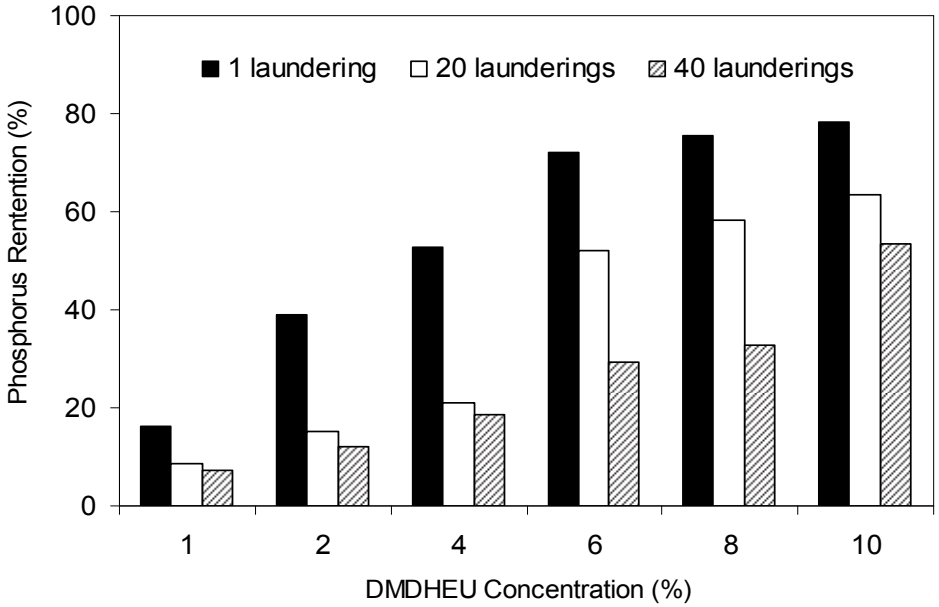

Fig. 5. The percent phosphorus retention of the nylon/cotton fabric (woodland) treated with 32%HFPO and DMDHEU at different concentrations and cured at 165°C for 2 min.

The LOI and vertical flammability of the fabric thus treated is shown in Table 8 and Table 9, respectively. As the DMDHEU concentration is increased from 1 to 10%, the LOI of the treated fabric after 1 laundering cycle increases from 22.9 to 28.0%. The LOI decreases as the number of laundering cycles for the fabric increases. The fabric treated using 6% or higher DMDHEU concentrations passes the test after 40 launderings (Table 9). The LOI of the fabric treated with 32% HFPO and 10% DMDHEU (after 40 laundering cycles) reaches 27.0% with a char length of 81 mm. The data presented here clearly show that DMDHEU concentration plays a critical role in determining the flame retardant performance of the nylon/cotton blend fabric treated with HFPO/DMDHEU. A higher DMDHEU concentration increases the amount of HFPO bound to the treated fabric and it also improves the hydrolysis resistance

HFPO (%)	DMDHEU (%)	LOI (%)			
		1 laundering	10 launderings	20 launderings	40 launderings
32	1	22.9	22.2	21.6	21.2
32	2	25.0	23.2	22.5	22.2
32	4	26.5	25.1	23.0	22.7
32	6	27.7	27.1	26.8	24.8
32	8	27.9	27.5	27.2	25.8
32	10	28.0	28.0	27.4	27.0

Table 8. The LOI (%) of the nylon/cotton fabric (woodland) treated with HFPO and DMDHEU at different concentrations and cured at 165°C for 2 min. (The LOI (%) of the untreated fabric is 20.1.)

of the HFPO bound onto the treated fabric by forming crosslinked HFPO/DMDHEU polymeric network. In our previous research, we have discovered that the nitrogen of DMDHEU does have a synergistic effect for the HFPO-based flame retardant system on cotton [9], but this effect becomes less predominant on the nylon/cotton blends.

We applied the same flame retardant finishing system to a second nylon/cotton BDU fabric ("desert") with the same chemical composition but different structure. The fabric treated with 32% HFPO and DMDHEU at different concentrations is subjected to different numbers of laundering cycles. The LOI (%) and vertical flammability of the nylon/cotton blend fabric (desert) thus treated are presented in Table 10 and 11, respectively. After l laundering cycle, the LOI of the treated fabric increases from 28.0 to 28.5% as the DMDHEU concentration is increased from 6 to 10%, respectively, and all three fabric samples pass the vertical flammability test. As the number of laundering cycle increases, the difference among the fabric samples treated using different DMDHEU concentrations becomes more evident. After 25 launderings, the fabric treated with 6% DMDHEU has LOI of 23.8% and fails the vertical flammability test, whereas that treated with 8% DMDHEU has LOI of 26.1% and passes the flammability test. The fabric treated with 10%DMDHEU has LOI of 24.8% and passes the vertical flammability test after 50 launderings. The data presented here again demonstrate that DMDHEU plays a decisive role in determining the flame retardant performance of the nylon/cotton blend fabric treated with HFPO and DMDHEU.

HFPO (%)	DMDHEU (%)	Char length (mm)			
		1 laundering	10 launderings	20 launderings	40 launderings
32	1	>300	>300	>300	>300
32	2	77	>300	>300	>300
32	4	80	94	>300	>300
32	6	77	99	88	114
32	8	79	66	83	105
32	10	49	62	68	81

Table 9. The vertical flammability of the nylon/cotton fabric (woodland) treated with HFPO and DMDHEU at different concentrations and cured at 165°C for 2 min.(The char length of the untreated fabric is >300 mm.)

DMDHEU (%)	LOI (%)			
	1 laundering	25 launderings	40 launderings	50 launderings
6	28.0	23.8	23.1	22.5
8	28.4	26.1	24.4	23.2
10	28.5	27.1	25.5	24.8

Table 10. The LOI of the nylon/cotton fabric (desert) treated with 32%HFPO and DMDHEU at different concentrations and cured at 165°C for 2 min. (The LOI (%) of the untreated fabric is 20.1.)

DMDHEU (%)	Char Length (mm)			
	1 laundering	25 launderings	40 launderings	50 launderings
6	68	>300	>300	>300
8	74	94	103	>300
10	53	81	92	92

Table 11. The vertical flammability of the nylon/cotton fabric (desert) treated with 32%HFPO and DMDHEU at different concentrations and cured at 165°C for 2 min. (The char length of the untreated fabric is >300 mm.)

The nylon/cotton fabric (woodland) is treated with 32% HFPO and DMDHEU at different concentrations and subjected to 1 laundering cycle. The tensile strength of the fabric thus treated after 1 laundering cycle is shown in Table 12. When DMDHEU concentration increases from 2 to 8%, the tensile strength at the warp direction is in the range from 703 N (98% retention) to 685 N (95% retention), respectively. The tensile strength in the filling direction is in the range from 445 N (97 retention) to 454 N (99% retention). Thus, the data presented in Table 12 demonstrate that the fabric treated with HFPO and DMDHEU has negligible strength loss. More details for the flame retardant finished nylon/cotton blend fabrics can be found in our two recent publications [20, 21].

DMDHEU (%)	Tensile Strength (N)		Tensile Strength Retention (%)	
	Warp	Filling	Warp	Filling
2	703	454	98	99
4	694	449	96	98
6	685	445	95	97
8	701	451	97	98
Control	721	458	--	--

Table 12. The tensile strength of the nylon/cotton fabric (woodland) treated with 32%HFPO and DMDHEU at different concentrations and cured at 165°C for 2 min (after 1 laundering cycle).

4. Conclusions

(1) The HFPO/BTCA/TEA flame retardant finishing system applied to the Nomex/cotton blend fabric significantly enhances the performance of the Nomex/cotton blend fabric. The

Nomex/cotton blend fabric treated with HFPO/BTCA/TEA is able to achieve high levels of the flame retardant performance and laundering durability at relatively low add-on levels. The treated fabric also shows modest strength loss and little change in hand properties. This flame retardant finishing system is a formaldehyde-free and odor-free system.
(2) DMDHEU is able to covalently bond HFPO to nylon 6.6 fabrics probably by the formation of a crosslinked HFPO/DMDHEU polymeric network. The combination of HFPO and DMDHEU is an effective durable flame retardant finishing system for the 50/50 nylon/cotton blend BDU fabrics with negligible fabric strength loss. The MDPA/TMM system is not suitable for the flame retardant finishing of the nylon/cotton blend fabric.

5. Acknowledgement

This paper is based on the data included in the dissertation of Dr. Hui Yang, the University of Georgia. Dr. Hui Yang was a graduate student under my supervision and he received his Ph.D. degree in the summer of 2007.

6. References

[1] Rebouillat, S. *High Performance Fibers*, Woodhead Publishing, Cambridge, U.K., pp23-61 (2001).
[2] Schutz, H. G., Cardello, A. V., Winterhalter, C. *Textile Research Journal*, 75: 223-232 (2005).
[3] Fukatsu, K. *Polymer Degradation and Stability*, 75: 479-484 (2002).
[4] Tesoro, G.C.; Rivlin, J. *J. AATCC*, 5(11):23-26 (1973).
[5] Wu, W.D., Yang, C.Q. *Journal of Fire Science*, 22:125-142 (2004).
[6] Yang, C. Q., Xu, Y. Wu, W.D. *Fire and Materials*, 29:109-120 (2005).
[7] Yang, H., Yang, C. Q. *Polymer Degradation and Stability*, 88:363-370 (2005).
[8] Wu, W.D., Yang, C. Q. *Polymer Degradation and Stability*, 91:2541-2548 (2006).
[9] Wu, W.D., Yang, C. Q. *Polymer Degradation and Stability*, 92:363-369 (2007).
[10] Wu WD, Yang CQ. *Polymer Degradation and Stability*, 85:623-632 (2004).
[11] Yang, C. Q., Wu, W.D. *Fire and Materials*, 27: 223-237 (2003).
[12] Yang, C. Q., Wu, W.D. *Fire and Materials*, 27: 239-25 (2003).
[13] Levchik, S. V., Weil, E. D., *Polymer International*, 49:1033-1073 (2000).
[14] Subbulakshmi, M. S., Kasturiya, N., Hansraj, B. P., Agarwal, A. K., *Journal of Macromolecular Science, Reviews in Macromolecular Chemistry and Physics*, C(40):85-104 (2000).
[15] Lewin, M., In: Lewin, M., Sello, S. B., (ed.), *Handbook of Fiber Science and Technology: Chemical Processing of Fibers and Fabrics*, Vol.2, Part B, New York, Mercel Dekker, pp.117-120 (1984).
[16] Weil, E. D., Levchik, S. V., *Journal of Fire Science*, 22:251-264 (2004).
[17] Horrocks, R. A., In: Heywood, D., editor, *Textile Finishing*. Society of Dyers and Colorists, West Yorkshore, U.K., pp.214-250 (2003).
[18] Kang, I., Yang, C. Q., Wei, W., Lickfield, G. C. *Textile Research Journal*, 68:865-870 (1998).
[19] Yang, H., Yang, C. Q., *Journal of Fire Science*, 25:425-446 (2007).
[20] Yang, H., Yang, C. Q., *Industrial and Engineering Chemistry Research*, 47:2160-2165 (2008).
[21] Yang, H., Yang, C. Q., He, Q., *Polymer Degradation and Stabilization*, 94:1023-1-31 (2009).

11

Liquid Transport in Nylon 6.6. Woven Fabrics Used for Outdoor Performance Clothing

A. B. Nyoni
National University of Science and Technology,
Department of Textile Technology
Zimbabwe

1. Introduction

Humans rely on the evaporation of sweat to remain comfortable and prevent overheating in hot environments and during exercise.[1] Discomfort results from the build up of sweat on the skin and if it doesn't evaporate quickly, the body core temperature heats up producing more sweat exposing the wearer to potential afflictions such as post-exercise chill and even hypothermia. Therefore, with properly engineered dynamic or responsive fabrics [2,3] less energy to cool the body will be required resulting in increased performance and endurance.
Researchers [4,5] generally agree that liquid transport properties are significantly affected by fibre type, yarn construction and fabric construction. The fibre length, width, shape and alignment all have a great influence on the quality of the capillary channels in the inter-fibre spaces and size of the pores present. The density and structure of yarns can greatly influence the dimensions and structure of inter- and intra-yarn pores[4] and pore sizes and distribution are determined by the manner in which fibres are assembled into the woven, nonwoven, or knitted structure.[6] Finishing treatment of the fabric surface and its surface roughness and the bulk properties of the liquid (i.e. viscosity, surface tension, volatility and stability) also play a significant role during wicking.
Additional important variables which exert influence on wicking are the level of physical activity and environmental conditions such as the relative humidity of the atmosphere which combined with the ambient temperature, determine the water vapour pressure of the ambient atmosphere and hence the rate of water vapour transfer through clothing. The wind speed which affects the thermal and water vapour resistance of the air adjacent to the fabric also plays a significant part during wicking.[7] Therefore, to design textile materials with specific functional properties of moisture management, it is essential to establish the relationship between the wicking properties of yarns and the structure of the fabric they are part of. In this chapter the effect of these variables on the wicking performance of a selected fabrics made from a combination of textured and flat continuous Nylon 6.6 yarns[8] were determined by The Longitudinal Wicking "Strip" Test using BS3424 Method 21 (1973).
In all the fabrics, saturated, unsaturated and dry zones were exhibited and the simultaneously occurrence of wetting, wicking, liquid dispersion and evaporation influenced the time exponent values *k* obtained.
The critical volume of liquid at which transfer wicking occurred at yarn cross over regions termed as the "transfer rate" was influenced by two competitive effects, i.e. the tendency to

spread in the capillary space between the filaments of "absorber" textured yarns and the tendency to wick the liquid by the "runner"flat continuous filament yarns yarns

2. Fabric sample preparation and test methods

Fabrics woven from different combinations of nylon 6.6 filament yarns were selected and the characteristics determined as shown in Table 1.

Prior to testing, the samples were conditioned in a standard atmosphere of 20±2°C and 65±2% relative humidity for 24 hours. Sample strips of 3.5cm x 33cm each were cut in the warp and weft directions from the conditioned sample. To aid observation of the wicking distance, a pen filled with water soluble ink was used to mark a graduated scale in 1cm intervals on the strips. The samples were then mounted on the pinned frame for the vertical, horizontal and syphon tests as shown in Figures 1, 2 and 7 respectively. The dipping ends of the samples were aligned leaving a length of 1cm to dip into the infinite reservoir containing distilled water. A ruler with millimeter divisions was placed parallel to the sample strip to enhance the accuracy of the measurement.

For washed fabric tests, the fabric samples were washed with a non-biological detergent in an automatic front loading domestic washing machine and tumble dried according to the ISO 6330:2000 which specifies domestic washing and drying procedures for textile testing. The dry fabrics were then conditioned in a standard atmosphere of 20± 2°C and 65±2% relative humidity for 24 hours before testing. Sample strips of 3.5cm x 33cm each were cut in the warp and weft directions from the conditioned fabric sample and tested with the frame in both the vertical and horizontal positions above the water basin containing distilled water and the results are shown in Table 2.

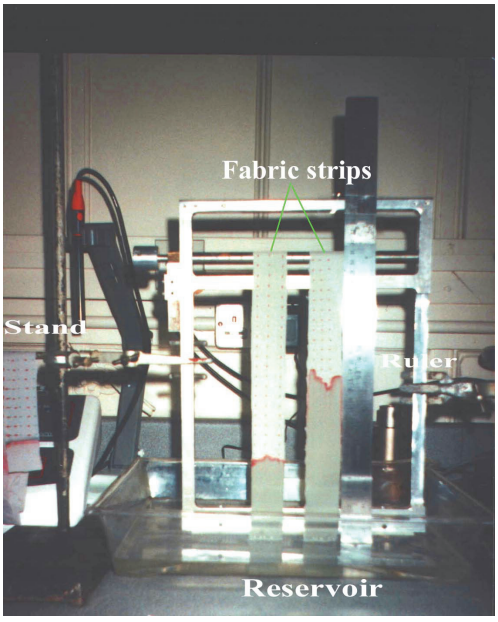

Fig. 1. Vertical Strip Wicking Test

The height of the advancing liquid front as a function of time was recorded by visual observation of the running ink through a travelling microscope at 5 minutes intervals for the first hour, and then at hourly intervals thereafter until the maximum wicking height (equilibrium point) was reached. To avoid contamination by the indicating ink the test liquid was changed after each test. Constant temperature and humidity in the ambient atmosphere were achieved by testing in the conditioned room.
The strip method has been used by Hollmark and Peek[9] to characterize the wicking behaviour of porous materials and they found it readily applicable under different conditions with a relatively high degree of reproducibility. Zhuang[10] also found good correlation between results obtained by manual and automatic testing.

3. Vertical strip wicking test results

3.1 Fabric sample S1F–unwashed

The results obtained from the wicking tests are shown in Table 2 and in Figures 3. Figure 3 shows that there was rapid wicking for the first 5-10 minutes in both the warp and weft directions and then a significant decrease to a slow rate with the lapse of time until it was difficult to note the level of liquid rise in 5 minutes time intervals. Observations done at hourly intervals thereafter tabulated in Table 2 indicate that from 60-180 minutes the fabrics continued wicking at a slow rate until an equilibrium point was reached.

Property	Test Method	Sample S1F	Sample S2F
Ends/cm	BS 2862:1984	70	70
Picks/cm	BS 2862:1984	30	50
Linear Density Warp (dtex)	BS 946:1970	44dtexf34 flat fully dull PA 6.6	44dtexf34 flat fully dull PA 6.6
Linear Density Weft (dtex)	BS 946:1970	195dtexf170 Airjet Textured Bright PA6.6	44dtexf34 flat fully dull PA 6.6
Fabric Weight g / m^2	BS 2471:1978	43.75	26.31
Filaments x-section	Microscopy-SEM	Circular	Circular
Warp FilamentØ	Microscopy-SEM	11.673µm	11.673µm
Weft		11.673µm	11.673µm

Table 1. Fabric and Yarn Characteristics

Multiple comparison between means of the actual liquid advancement in the first 15minutes (1st Quarter) Table 3 and the second 15 minutes (2nd Quarter) Table 4 of the hourly test shown in Tables 5 indicate that that there was a significant difference in the distance moved by the liquid in both the warp and weft direction wicking with the lapse of time. Wicking in the weft direction was more rapid than in the warp direction and multiple comparison of the actual liquid advancement in the first 15minutes (1st Quarter) of the hourly test in Tables 5 show that there was a significant difference in warp and weft direction wicking. Microscopic examination of fabrics during wicking exhibited an almost linear leading edge in the weft direction and a spiked pattern in the warp direction.

Wicking time (t)min	Vertical Wicking								Horizontal Wicking							
	S1F-warp (lmm)		S1F-Weft (lmm)		S2F-Warp (lmm)		S2F-Weft (lmm)		S1F-warp (lmm)		S1F-Weft (lmm)		S2F-Warp (lmm)		S2F-Weft (lmm)	
	Uw	**W**	**Uw**	**W**	**Uw**	**W**	**Uw**	**W**	**Uw**	**W**	**Uw**	**W**	**Uw**	**W**	**Uw**	**W**
5	15	35	40	70	28	37	18	25	25	34	50	73	27	32	9	23
10	30(15)	45(10)	56(16)	100(30)	39(11)	45(8)	23(5)	32(7)	33(8)	49(15)	65(15)	101(29)	32(5)	38(6)	13(4)	30(7)
15	35(5)	55(10)	70(14)	119(19)	41(2)	49(4)	27(4)	39(7)	40(7)	55(6)	80(15)	120(19)	36(4)	41(3)	16(3)	32(2)
20	38(3)	62(7)	80(10)	130(11)	44(3)	50(1)	30(3)	41(2)	43(3)	60(5)	90(10)	135(15)	38(2)	43(2)	18(2)	32(0)
25	40(2)	67(5)	90(10)	140(10)	46(2)	51(1)	31(1)	43(2)	46(3)	66(6)	95(5)	149(14)	39(1)	47(4)	19(1)	36(4)
30	45(5)	70(3)	95(5)	146(6)	49(3)	53(2)	31(0)	44(1)	50(4)	71(5)	100(5)	157(8)	40(1)	49(2)	19(0)	38(2)
35	47(2)	72(2)	100(5)	153(7)	49(0)	54(1)	31(0)	44(0)	51(1)	74(3)	103(3)	166(9)	41(1)	49(0)	19(0)	38(2)
40	48(1)	73(1)	104(4)	157(4)	49(0)	55(1)	31(0)	44(0)	52(1)	75(1)	108(5)	169(3)	41(0)	50(1)	19(0)	39(1)
45	49(1)	74(1)	107(3)	158(1)	49(0)	55(0)	32(1)	44(0)	54(2)	78(3)	109(1)	176(7)	41(0)	52(2)	19(0)	39(0)
50	50(1)	75(1)	110(3)	158(0)	49(0)	55(0)	32(0)	44(0)	55(1)	81(3)	111(2)	182(6)	42(1)	52(0)	20(1)	39(0)
55	51(1)	79(4)	112(2)	163(5)	49(0)	55(0)	32(0)	44(0)	56(1)	81(0)	113(2)	185(3)	42(0)	52(0)	20(0)	40(1)
60	52(1)	80(1)	113(1)	165(2)	49(0)	55(0)	32(0)	44(0)	57(1)	84(3)	114(1)	188(3)	42(0)	50(0)	20(0)	40(0)
120	56(4)	89(9)	121(8)	180(15)	50(1)	55(0)	32(0)	48(4)	58(1)	110(26)	125(11)	220(32)	47(5)	61(11)	23(3)	49(9)
180	56(0)	89(0)	121(0)	180(0)	50(0)	55(0)	32(0)	48(0)	58(0)	110(0)	129(4)	227(7)	50(3)	61(0)	23(0)	49(0)

Note: Figures in parentheses indicate the actual liquid advancement per time interval
Key: Uw-Unwashed
W-Washed

Table 2. Fabric Vertical and Horizontal Wicking Test Results

Sample	Vertical Wicking								Horizontal Wicking							
	S1F-warp (lmm)		S1F-Weft (lmm)		S2F-Warp (lmm)		S2F-Weft (lmm)		S1F-warp (lmm)		S1F-Weft (lmm)		S2F-Warp (lmm)		S2F-Weft (lmm)	
	Uw	**W**	**Uw**	**W**	**Uw**	**W**	**Uw**	**W**	**Uw**	**W**	**Uw**	**W**	**Uw**	**W**	**Uw**	**W**
1	35	55	70	119	41	49	27	39	40	55	80	120	36	41	16	32
2	33	54	72	120	40.5	50	28	39	40.5	55	82.5	126	37.5	39.5	15.5	31.5
3	34.5	53.5	69	123	39	51	25	40	40	55	81	123	36	42	16.5	32
4	33	55.5	70.5	115.5	42	48	25.5	38	39	54	78	120	38	41.5	17	33
5	34	54	69	118.5	42	48	29	37.5	41	55	84	120	36	42	17	31
Mean	33.9	54.4	70.1	119.2	40.9	49.2	26.9	38.7	40.1	54.8	81.1	121.8	36.7	41.2	16.4	31.9
SD	2.6	3.3	3.74	4.88	2.86	3.14	2.32	2.78	2.83	3.31	4.03	4.94	2.71	2.87	1.81	2.53
SE	1.3	1.65	1.87	2.44	1.43	1.57	1.16	1.39	1.42	1.66	2.01	2.47	1.36	1.44	0.91	1.26
CV	7.68	6.06	5.34	4.1	4.1	6.99	8.62	7.19	7.06	6.04	4.97	4.05	7.38	6.97	11.04	7.92

Key: Uw-Unwashed
W-Washed

Table 3. Fabric Wicking Test 1st Quarter (15 minutes).

Sample	Vertical Wicking								Horizontal Wicking							
	S1F-warp (lmm)		S1F-Weft (lmm)		S2F-Warp (lmm)		S2F-Weft (lmm)		S1F-warp (lmm)		S1F-Weft (lmm)		S2F-Warp (lmm)		S2F-Weft (lmm)	
	Uw	**W**	**Uw**	**W**	**Uw**	**W**	**Uw**	**W**	**Uw**	**W**	**Uw**	**W**	**Uw**	**W**	**Uw**	**W**
1	10	15	20	27	8.0	4	4	5	10	16	25	37	4	8	3	6
2	9.5	15	19	25.5	6.5	4	3	3.5	11	16	25	36	4	7.5	4	6.5
3	10	15	20	25	8.0	4.5	3	4.5	11	17	26	37.5	4.5	6.5	2.5	6
4	9.5	14.5	18.5	29	7.5	4.5	4	5.5	11	16.5	24.5	37	4	7.5	3	6
5	9	15.5	18	27.5	7.5	4.5	3	5	10.5	15	25.5	36	4	8.0	3.5	6
Mean	9.6	15	19.1	26.8	7.5	4.3	3.4	4.7	10.7	16.1	25.2	2.71	4.1	7.5	3.2	6.1
SD	1.39	1.73	1.96	2.32	1.23	0.93	0.83	0.97	1.46	1.79	2.25	1.36	0.91	1.23	0.8	1.11
SE	0.69	0.87	0.98	1.16	0.61	0.46	0.41	0.49	0.73	0.9	1.12	7.38	0.45	0.61	0.4	0.55
CV	14.43	11.55	10.23	8.64	16.33	21.57	24.25	20.63	13.67	11.15	8.91	12.78	22.09	16.33	25	18.11

Key: Uw-Unwashed
W-Washed

Table 4. Fabric Wicking Test 2nd Quarter (30 minutes).

Fabric samples	Significance	Difference
V15min-warp-uw Vs.		
V15min-weft-uw	0.000↑	***
H15 min-warp-uw	0.000↑	***
V15min-warp-w	0.000↑	***
V30 min-warp-uw	0.000↓	***
V15min-weft-uw Vs.		
H15 min-weft-uw	0.000↑	***
V15min-weft-w	0.000↑	***
V30 min-weft-uw	0.000↓	***
H15min-warp-uw Vs.		
H15min-weft-uw	0.000↑	***
H15 min-warp-w	0.002↑	***
H30min-warp-uw	0.000↓	***
H15min-weft-uw Vs.		
H15 min-weft-w	0.000↑	***
H30min-weft-uw	0.000↓	***

W = Washed fabric W = Unwashed fabric
H = Horizontal wicking V = Vertical Wicking
↑= Wicking decrease ↓= Wicking increase
Significance of differences of fabric wicking:
*****P≤ 0.001,**P≤0.01,*P≤0.05 and Not significant (ns) at P>0.05.**

Table 5. Multiple Comparison Between Wicking Means of Fabric S1F

Fabric samples	Significance	Difference
V15min-warp-uw Vs.		
V15min-weft-uw	0.000↓	***
H15 min-warp-uw	0.000↓	***
V15min-warp-w	0.000↑	***
V30 min-warp-uw	0.000↓	***
V15min-weft-uw Vs.		
H15 min-weft-uw	0.000↓	***
V15min-weft-w	0.000↑	***
V30 min-weft-uw	0.000↓	***
H15min-warp-uw Vs.		
H15min-weft-uw	0.000↓	***
H15 min-warp-w	0.000↑	***
H30min-warp-uw	0.000↓	***
H15min-weft-uw Vs.		
H15 min-weft-w	0.000↑	***
H30min-weft-uw	0.000↓	***

W = Washed fabric UW = Unwashed fabric
H = Horizontal wicking V = Vertical Wicking
↑= Wicking decrease ↓= Wicking increase
Significance of differences of fabric wicking:
*****P≤ 0.001,**P≤0.01,*P≤0.05 and Not significant (ns) at P>0.05.**

Table 6. Multiple Comparison Between Wicking Means of Fabric S2F

3.2 Vertical wicking fabric sample S2F-unwashed

The results in Table 2 and Figures 4 to 5 show that there was rapid wicking for the first 5-10minutes in both the warp and weft directions which became less rapid with the lapse of time. Multiple comparison of wicking results in Table 6 show a significant decrease in weft direction wicking compared to warp direction wicking. The wicking rate significantly decreased to a slow rate with the lapse of time in the warp and weft directions. The rapid attainment of the equilibrium point when wicking the fabrics in the warp and weft direction indicates that the liquid is rapidly spread over a large area for quick evaporation.

4. Horizontal strip wicking tests

Wicking occurs when a fabric is completely or partially immersed in a liquid or in contact with a limited amount of liquid such as a drop placed on the fabric. In a vertically held substrate, wicking is affected by gravitational forces and ceases when capillary forces are balanced by the hydrostatic head.[11] At that point, the capillary pressure that raises the liquid is balanced by the effect of gravity, that is, by the weight of raised liquid.[12] To determine the extent to which gravity affects wicking, horizontal wicking tests were carried out on nylon 6.6 fabrics samples S1F and S2F and the results are shown in Table 2.

4.1 Horizontal strip wicking test sample S1F-unwashed fabric

The results in Table 2 and Figures 3 to 6 exhibited a similar wicking trend as fabrics wicked in the vertical direction in which wicking in the weft direction was more rapid than in the

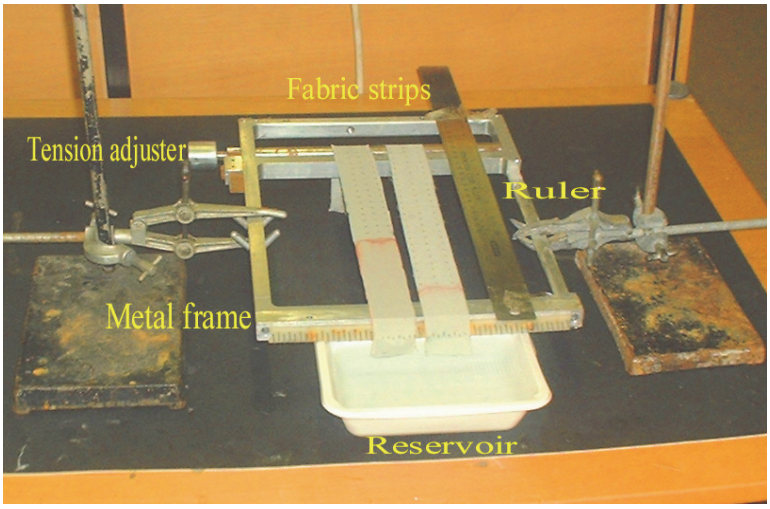

Fig. 2. Horizontal Wicking Test

warp direction. However, even though the trend was similar, there was a significant difference in the distance travelled by the wicked liquid compared to vertically wicking in both the warp and weft directions as shown by the results of multiple comparison of the actual liquid wicked during the 1st and 2nd quarters of an hourly test in Table 5. As was the case with vertical wicking, there was rapid wicking for the first 5-10 minutes in the warp and weft directions.

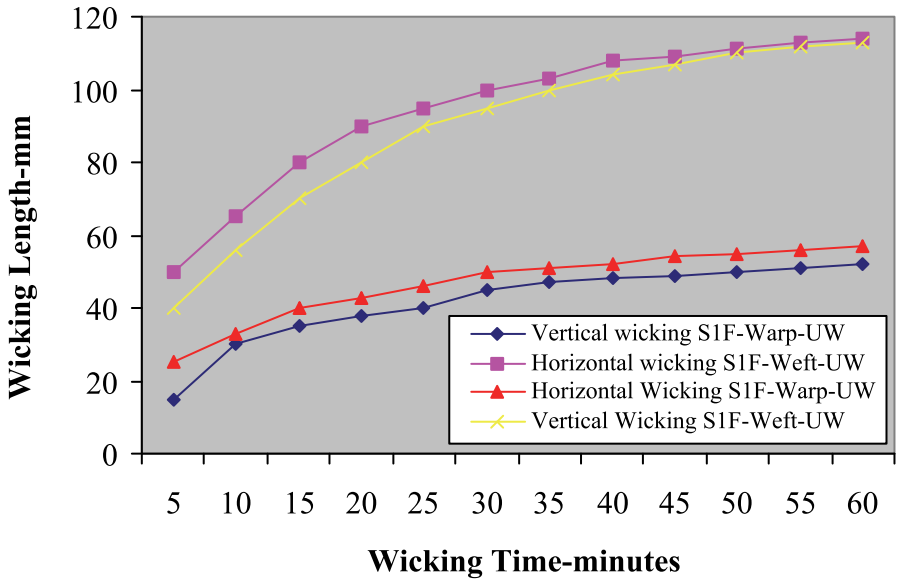

Fig. 3. Wicking test of fabric S1F – unwashed fabric

4.2 Horizontal strip wicking test-sample S2F-unwashed fabric

Table 2 and Figures 4 and 5 shows that there was rapid wicking for the first 5-10 minutes but wicking in the warp direction was more rapid than wicking in the weft direction. At the start of wicking there is a variation in lift off followed by the same wicking trend in both the weft and warp directions. Results of multiple comparison of the actual liquid wicked within the 1st and 2nd quarters of an hourly test in Table 5 show a significant decrease in the liquid wicked in both the warp and weft horizontal directions.

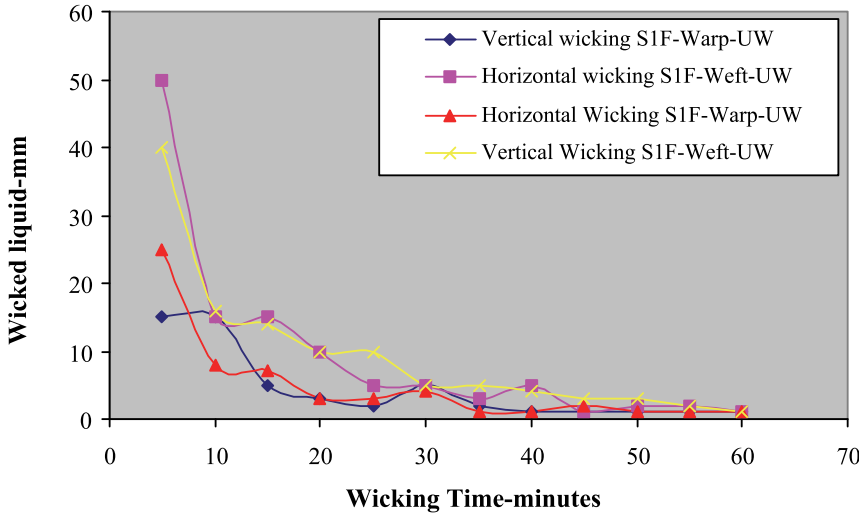

Fig. 4. Actual Liquid Advance Sample S1F - Unwashed Fabric

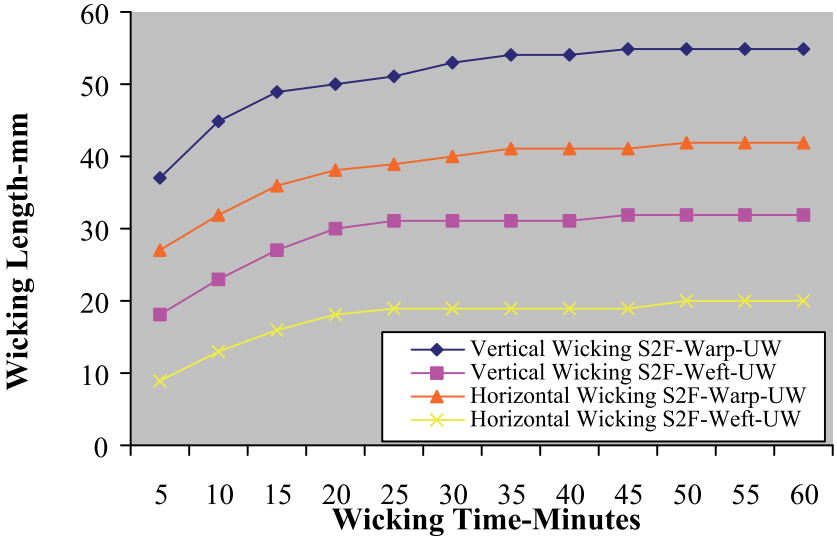

Fig. 5. Wicking Tests of Fabric S2F-Unwashed Fabric

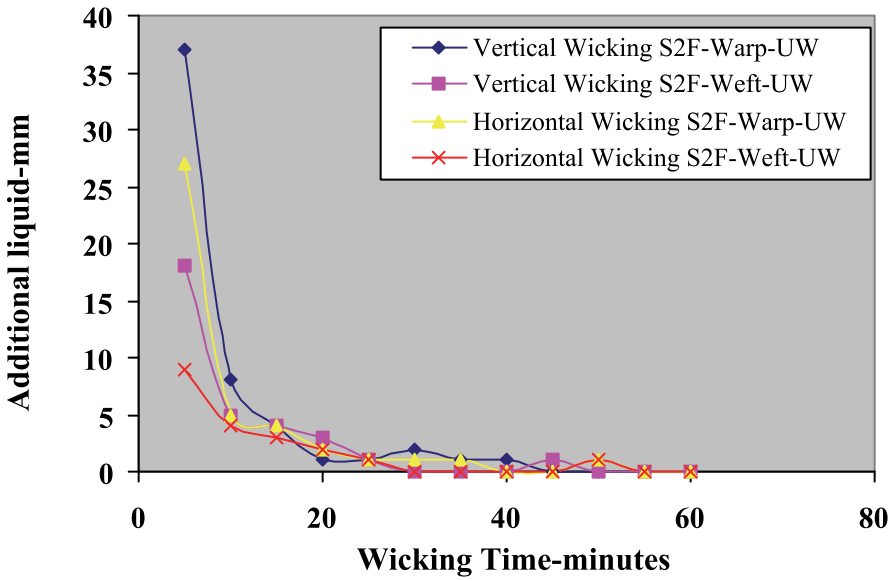

Fig. 6. Actual Liquid Advance S2F-Unwashed Fabric

5. Syphon wicking

It is a known fact that the liquid flow in downward wicking is aided by gravity and occurs more rapidly through an already saturated fabric with a lower resistance to flow than an initially dry fabric.[13] A further study to determine the extent to which the structure of the constituent yarns affects wicking in fabrics S1F and S2F was carried out by wicking washed fabrics in the warp and weft directions using the Syphon[11] Test Method.

In downward wicking, Figure 7 a rectangular strip of the test fabric is used as a syphon, by immersing one end in a reservoir of water or saline solution and allowing the liquid to drain from the other end at a lower level, into a collecting beaker. The amount of liquid transferred at successive time intervals can be determined by weighing the collecting beaker. No published standards exist and evaluation of results differ between researchers with some authors [14] taking the rate of mass transfer of the liquid when a constant flow through the syphon has been attained as an indicator of wickability.

Hardman[14] distinguished this as a "rate of drainage," using the elapsed time between the initial moment of contact between the fabric strip and liquid and the moment when dripping from the lower fabric end commences as a measure of wicking.

Because of the limited amount of liquid retained by the fabrics S1F and S2F due to the effects of rapid evaporation observed in preceding experiments, determination of their downward wicking behaviour was done by observing the actual distance traveled by the liquid towards the bottom end of the fabric as a function of time.

Samples were prepared as in section 2 and the rectangular strip of the test fabric used as a syphon by immersing 1cm of the top end in the liquid reservoir. The distance of water travel as a function of time was taken at 5 minutes intervals for an hour or terminated when the liquid dripped at the bottom of the fabric or when wicking ceased due to evaporation.

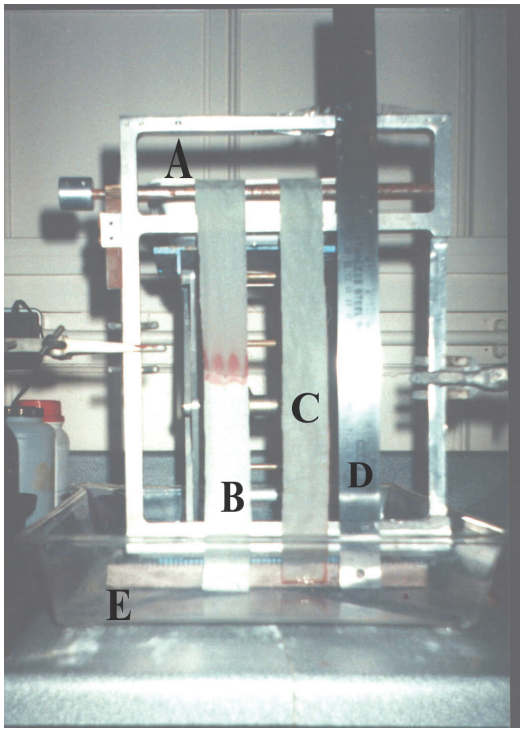

A-liquid reservoir
B/C Strips of Fabrics
D-Ruler
E-Collecting tray

Fig. 4.7. Syphon Wicking Test

5.1 Syphon wicking test- fabric sample S1F and S2F

The results in Tables 7 show the distance travelled by the liquid leading front and the figures in parentheses indicate the actual liquid advancement per time interval.

Fabric sample S1F made from 195f170 weft yarn and 44f34 warp yarn with 70 ends/cm and 30 picks/cm (43.75g/m^2) was wicked in the warp and weft directions. Figure 8 shows that after wicking fabric sample S1F for 50 minutes in the weft direction, the liquid had travelled to the lower end of the fabric strip whereas in the warp direction the leading head was still 202mm from the lower end of the fabric.

When the fabric is wicked in the warp direction, the textured weft yarns cause retardation of the liquid's progress due to their absorption capacity. The absorption of the liquid into the heterogeneous structure of the yarn causes a temporary slowing down of its advancement as it is dispersed in the yarn structure before a critical volume is achieved [15] to enable liquid transfer to the capillaries of the warp yarns. The nature of the liquid flow in the warp direction therefore is in fast-slow fast (warp-weft-warp) steps resulting in a haphazard flow as shown in Figure 9. In wicking the fabric in the weft direction, the high volume textured weft yarns rapidly flood the capillaries of the flat continuous filament yarns and this speeds

Sample	S1F-Warp direction (l -mm)		S1F-Weft direction (l -mm)		S2F-Warp direction (l -mm)		S2F-Weft direction (l -mm)	
Wicking Time-t minutes	Vertical	Syphon	Vertical	Syphon	Vertical	Syphon	Vertical	Syphon
5	35	35	70	42	37	58	25	48
10	45 (10)	47(12)	100(30)	84(42)	45 (8)	69(11)	32 (7)	56(8)
15	55 (10)	60(13)	119(19)	129(45)	49 (4)	74(5)	39 (7)	62(6)
20	62 (7)	69(9)	130(11)	156(27)	50 (1)	79(5)	41 (2)	67(5)
25	67 (5)	78(9)	140(10)	199(43)	51 (1)	81(2)	43 (2)	70(3)
30	70 (3)	98(20)	146 (6)	220(11)	53 (2)	82(1)	44 (1)	71(1)
35	72 (2)	110(12)	153 (7)	253(33)	54 (1)	84(2)	44 (0)	73(2)
40	73 (1)	116 (6)	157 (4)	268(15)	55(1)	*84(0)*	-	-
45	74 (1)	122(6)	158 (1)	282(14)	55(0)	-	-	-
50	75 (1)	128(6)	158 (0)	330(48)	-	-	-	-
55	79 (4)	139(11)	163 (5)	-	-	-	-	-
60	80 (1)	150(11)	165 (2)	-	-	-	-	-
120	89 (9)	-	180(15)	-	-	-	-	-
180	89 (0)	-	180 (0)	-	-	-	-	-

Note:Figures in parentheses indicate the actual liquid advancement per time interval.

Table 7. Washed Fabric Wicking Tests-Vertical Vs. Syphon Wicking

the rate of wicking. The actual advancement of the wicked liquid shown in Figure 9 is directly proportional to the wicking time in both cases (warp and weft) but was found to be 61% more in the weft compared to warp direction wicking. This indicates that for this fabric, the wicking rate does not only depend on the yarn and fabric structure but also on the direction of orientation of the constituent yarns in the structure.

Results in Table 7 show the wicking behaviour of an almost balanced fabric sample S2F made from 44f34 warp and weft flat continuous filament yarns with 70 ends/cm and 50 picks/cm ($26.31\ g/m^2$). The graphical representation in Figures 10-11 plotted from the results tabulated in Table 7 show that the rate of warp and weft wicking follow a similar trend. The difference of the actual liquid wicked was 15% more in the warp direction due to the high number of ends/cm compared to picks/cm therefore the packing of the additional filaments in the warp yarns introduced more capillary spaces between the nylon filaments. Due to its light-weight ($26.31\ g/m^2$), the fabric allowed rapid liquid evaporation. Results in Table 7 show that the wicking rate had significantly slowed down after 20 minutes despite the fact that the liquid flow in this test was through an already saturated fabric with a lower resistance to flow and was also aided by gravity. After 35minutes wicking, liquid advancement had ceased and when the fabric was left to wick to the end of the hour there was no change in the position of the liquid edge. In the absence of gravity, this indicates that there is significant rapid evaporation of liquid from the fabric which is a desired functional property of fabrics designed to rapidly transmit perspiration to the exterior where it can evaporate.

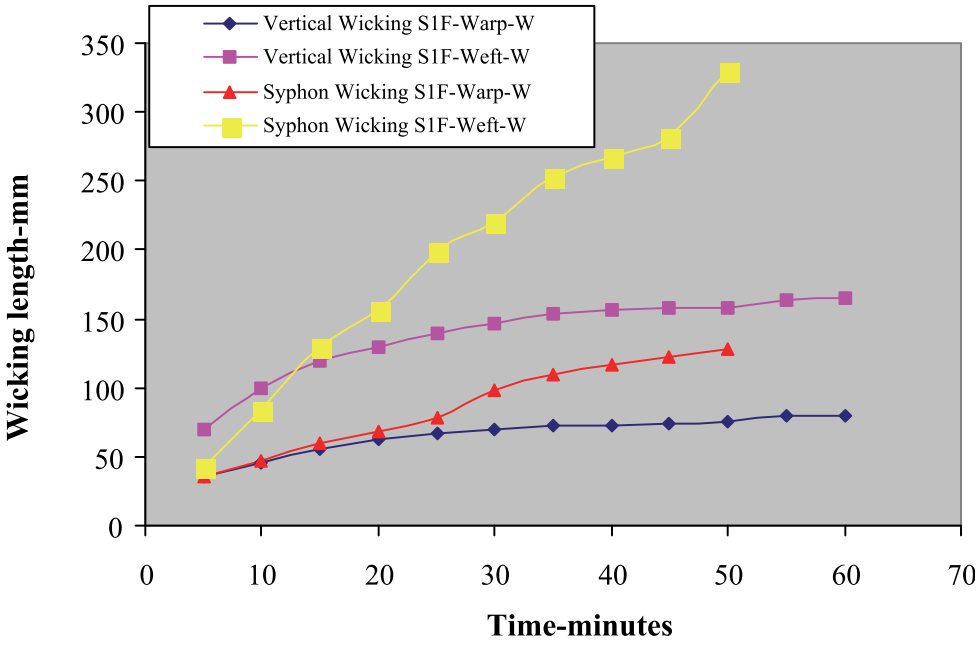

Fig. 8. Vertical Vs Syphon Wicking Fabric S1F-Washed

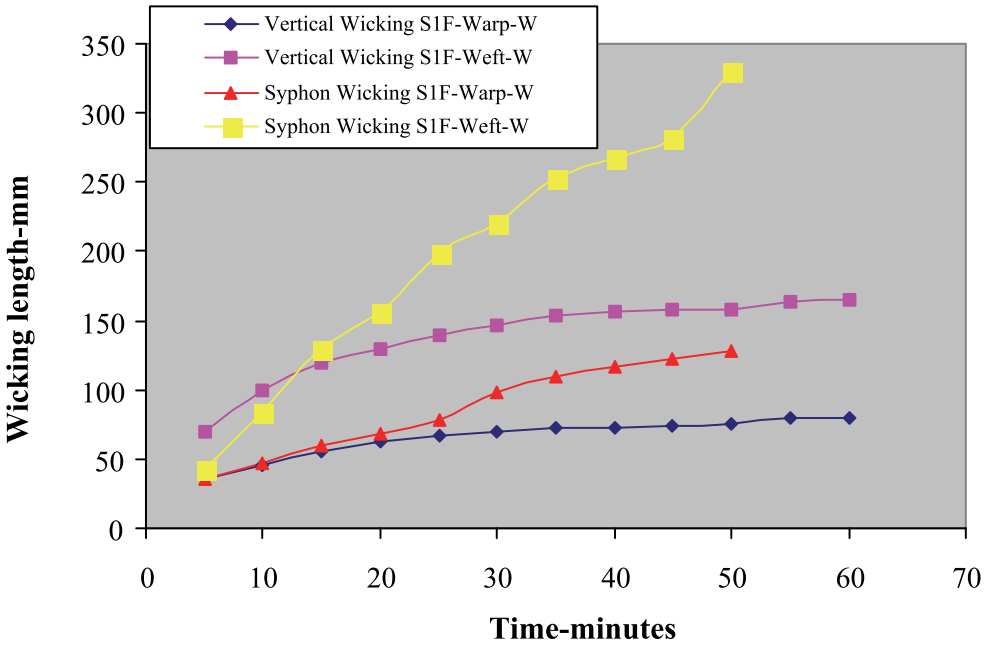

Fig. 9. Actual Liquid Advance-Vertical Vs. Syphon Wicking Fabric S1F-Washed

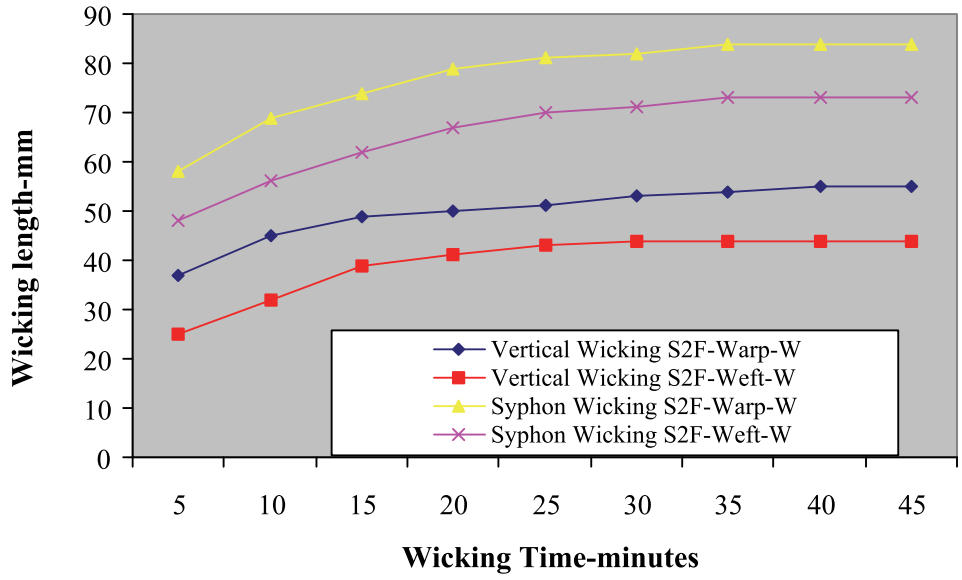

Fig. 10. Vertical Vs. Syphon Wicking-Fabric S2F-Washed

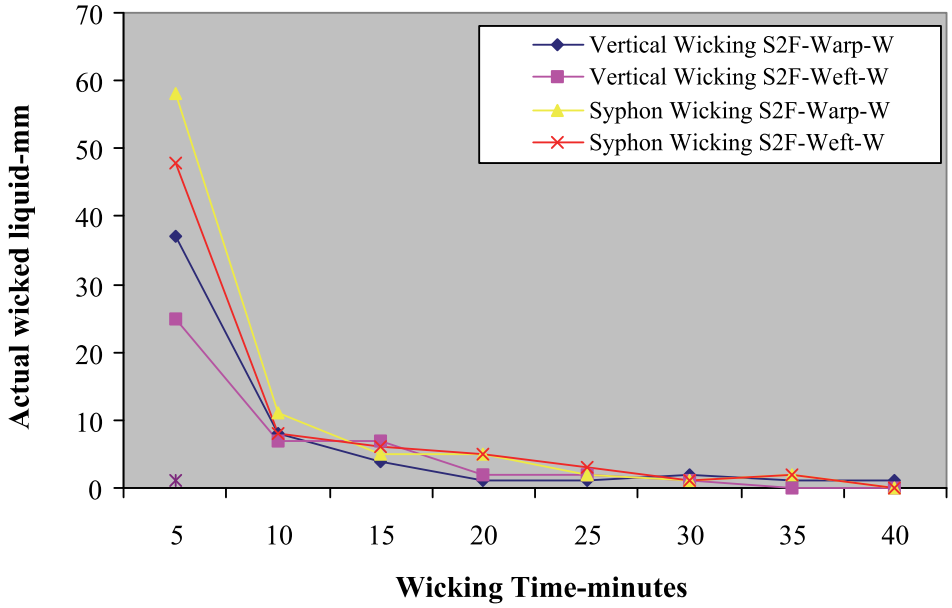

Fig. 11. Actual Liquid Advance: Vertical Vs. Syphon Wicking Fabric S2F-Washed

6. Wicking characteristics of washed fabrics

The ability of a fibre to facilitate migration of liquid water or water vapour molecules depends on its surface hydrophilicity or affinity for water, the textile finish applied and the fibre substrate.[7,16] The surface properties of man-made fibres are generally adjusted with spin finishing agents during the fibre spinning process.[17] Hydrophobic fibres can be modified in finishing to give surface properties which can allow liquid flow.[18] Leijala and Hautojarvi[17] using Scanning Force Microscopy (SFM) studied the structure, distribution, and composition of spin finish layers on a polypropylene fibre surface. They noted that the coverage and homogeneous distribution of the finish on the fibre surface even though only a few nanometers in thickness is an important factor affecting tribological and antistatic properties as well as the wettability of fibres. In another study[14], the wickability attributed to the conventional (non porous) acrylic as was found to be the case with polypropylene was due to spin finish which could be easily removed by washing. Gogalla[4] also noted that the uneven distribution of chemical finish on the surface of a fabric greatly affected its wicking behaviour.
Electron micrographs of yarns from which the fabric samples S1F and S2F were woven in Figure 12 a-c show traces of spin finish on all the yarns which was removed during the scouring process.
During use, out-door and performance textiles fabrics are exposed to soiling which comes from two different sources, namely,

a. from the body of the wearer and
b. from the environment.

therefore, it will be necessary at some stage to wash the fabrics. However, it is important that such a treatment does not alter the functional properties of these garments. Therefore, it

was of interest to study the effect of laundering on the wicking behaviour of fabric samples S1F and S2F.

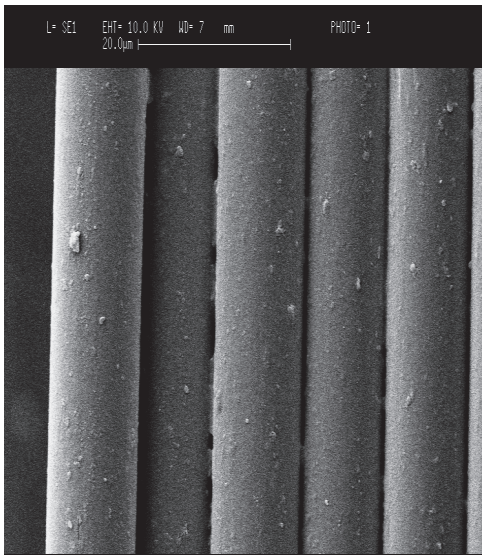

(a) Sample S1Y 44F34 Flat Fully Dull PA 6.6

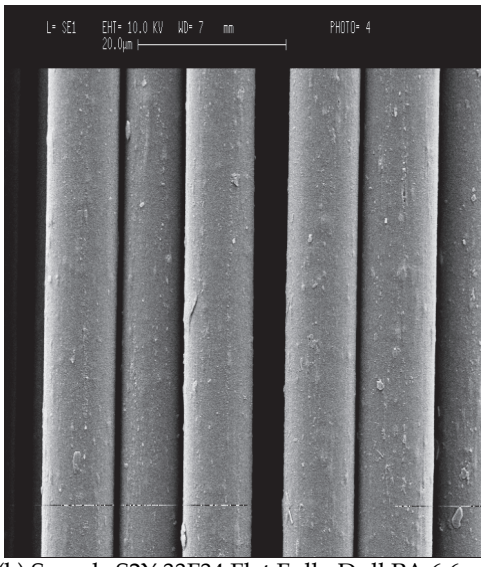

(b) Sample S2Y 33F34 Flat Fully Dull PA 6.6

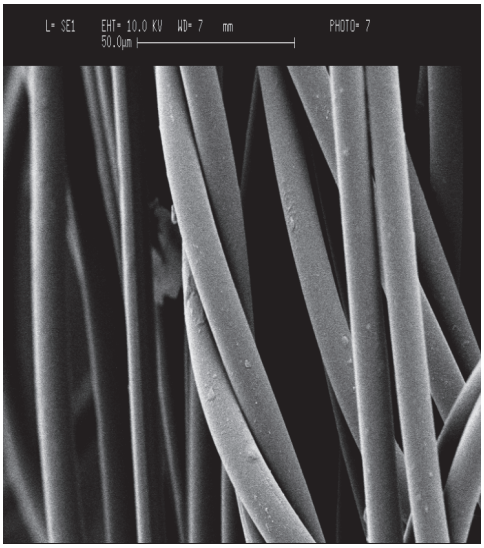

(c) Sample S3Y Air Textured Bright PA6.6

Fig. 12. Nylon 6.6 Yarn Micrographs

6.1 Results and discussion

6.1.1 Vertical wicking sample S1F- washed fabric: Warp and weft directions

Figures 17 to 20 show the graphical representation of the wicking rate of the washed and unwashed fabrics plotted from results in Table 2. Multiple comparison of the fabric wicking behaviour after a single wash in Table 5 show that there was a significant increase in the wicking rate of sample S1F in both the vertical and horizontal directions. In all cases, the weft direction wicking rate of washed fabrics remained higher than warp direction wicking regardless of the orientation of the fabrics as was the case with the unwashed fabric.

6.1.2 Vertical wicking sample S2F -washed fabric: Warp and weft directions

Table 2 and Figures 23 to 24 show the vertical wicking results of sample S2F. Results in Table 6 show that there was a significant increase in wicking in both directions after the fabrics were washed. Wicking in the warp direction was more rapid than in the weft direction and the difference gradually decreased with the lapse of time.

6.1.3 Horizontal wicking of washed fabrics

Fabrics wicked in the horizontal direction (Table 2 and Figures 13 and 19) show a similar change in wicking trend as the fabrics wicked in the vertical direction. Figures 15 to 18 show that there was marked increase in the wicking rate of samples S1F and S2F after a single wash. Results of multiple comparison of the actual liquid wicked within the 1st and 2nd quarters of an hourly test for fabric S2F exhibited a significant decrease in the liquid wicked in the horizontal direction compared to wicking in the vertical direction. This deviation from the general trend that horizontal wicking leads to a significant increase in wicking could not be explained.

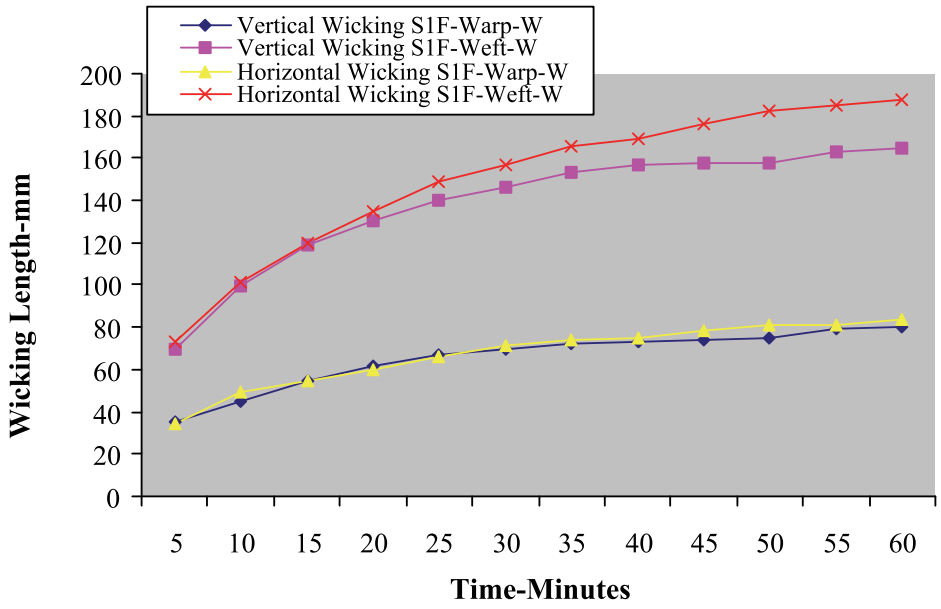

Fig. 13. Wicking Tests Sample S1F- Washed Fabric

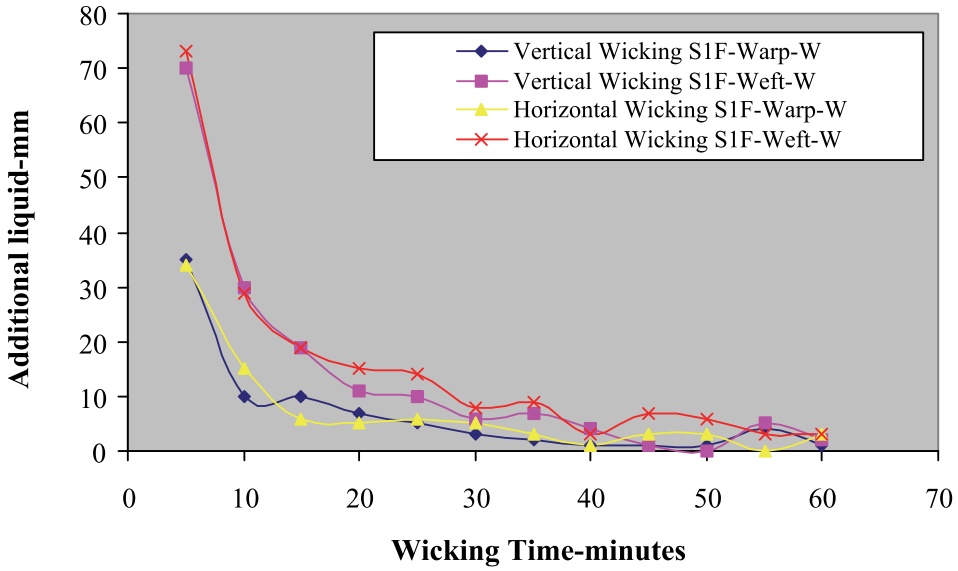

Fig. 14. Actual Liquid Advance Sample S1F-Washed Fabric

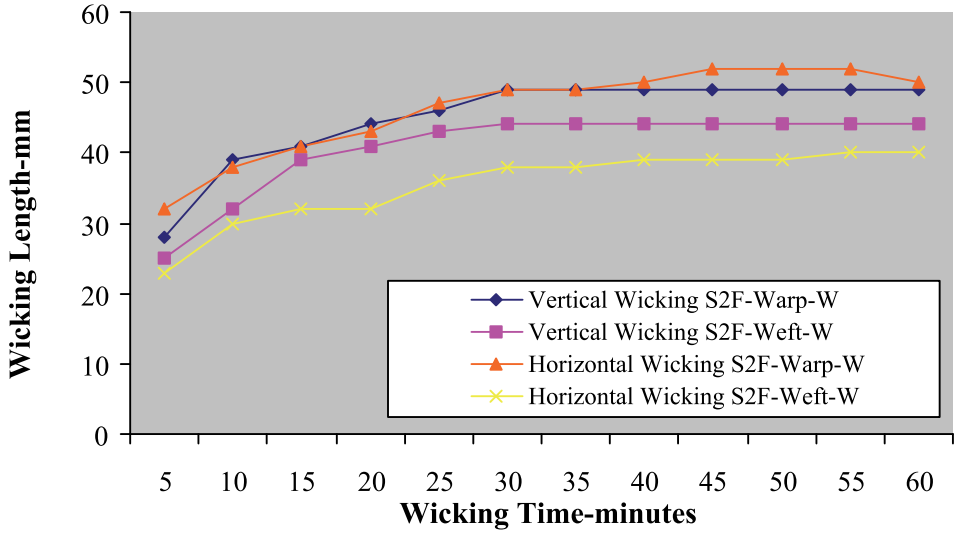

Fig. 15. Wicking Tests Sample S2F-Washed Fabric

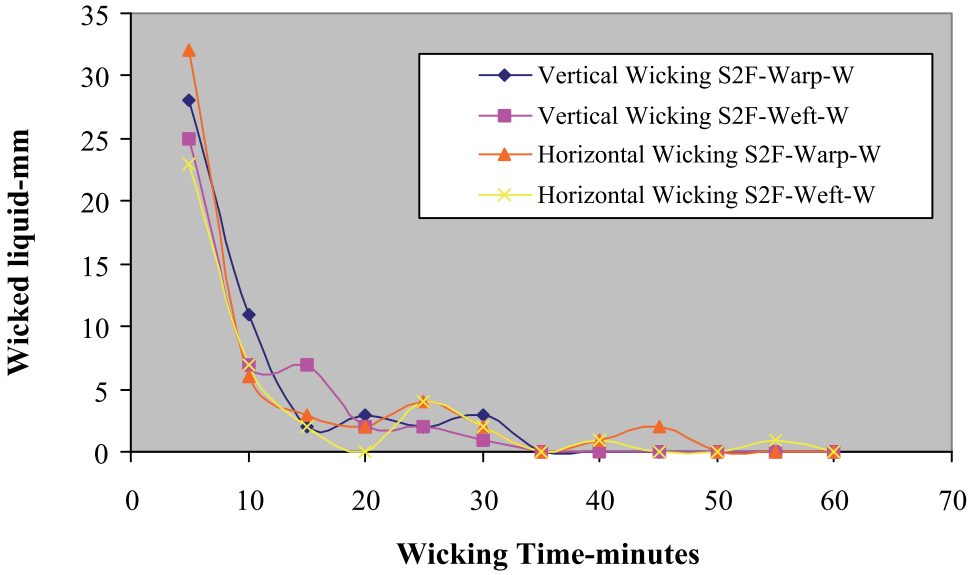

Fig. 16. Actual Liquid Advance Sample S2F- Washed Fabric

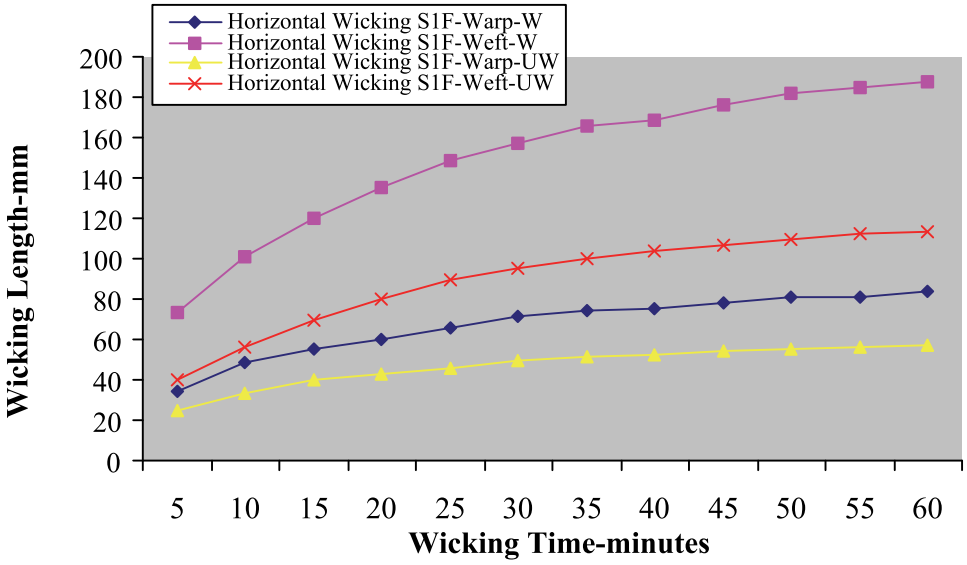

Fig. 17. Wicking Tests Sample S1F-Washed Vs. Unwashed Fabrics

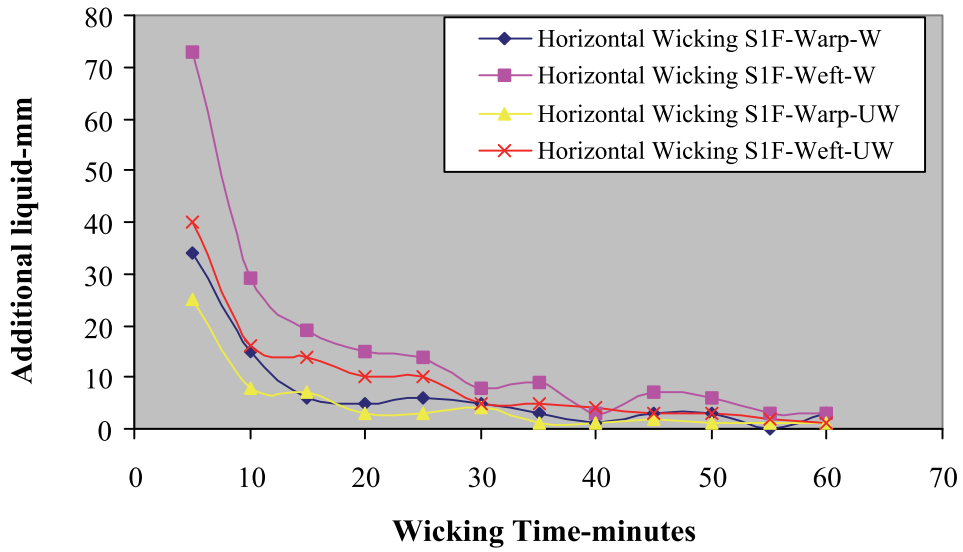

Fig. 18. Actual Liquid Advance Sample S1F-Washed Vs. Unwashed Fabrics

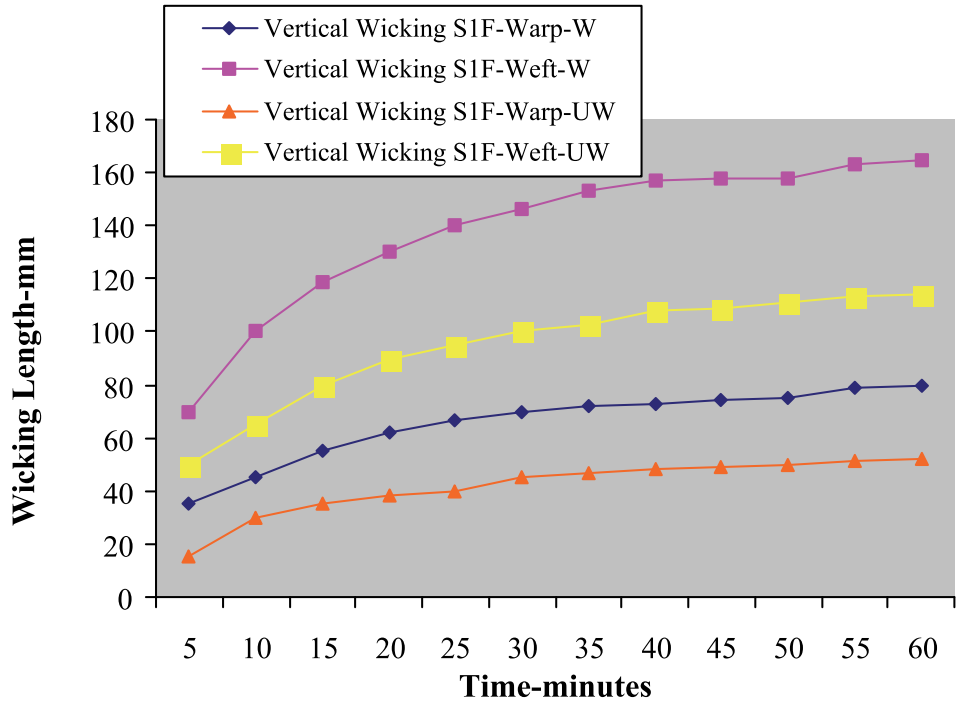

Fig. 19. Wicking Test Sample S1F- Unwashed Vs Washed Fabrics

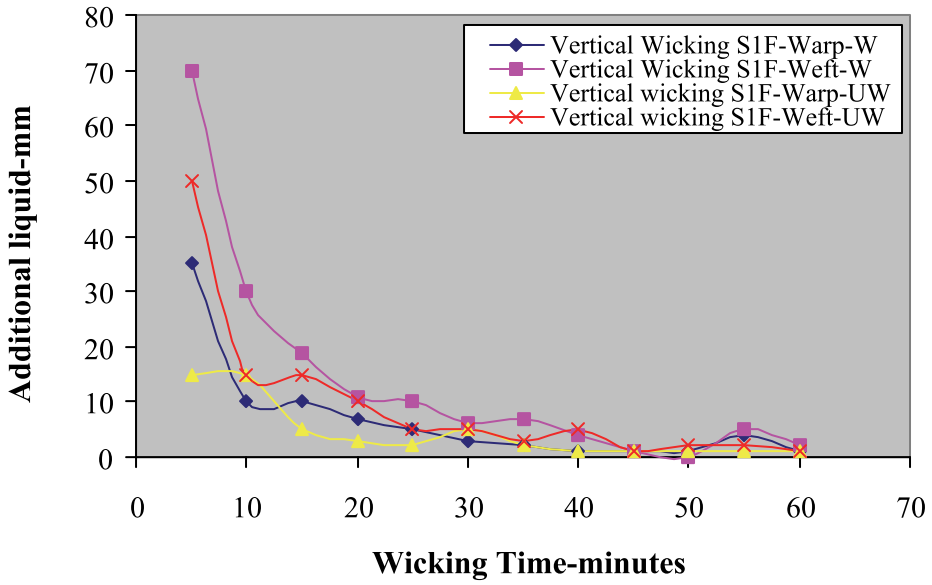

Fig. 20. Actual Liquid Advance Sample S1F -Washed Vs Unwashed Fabrics

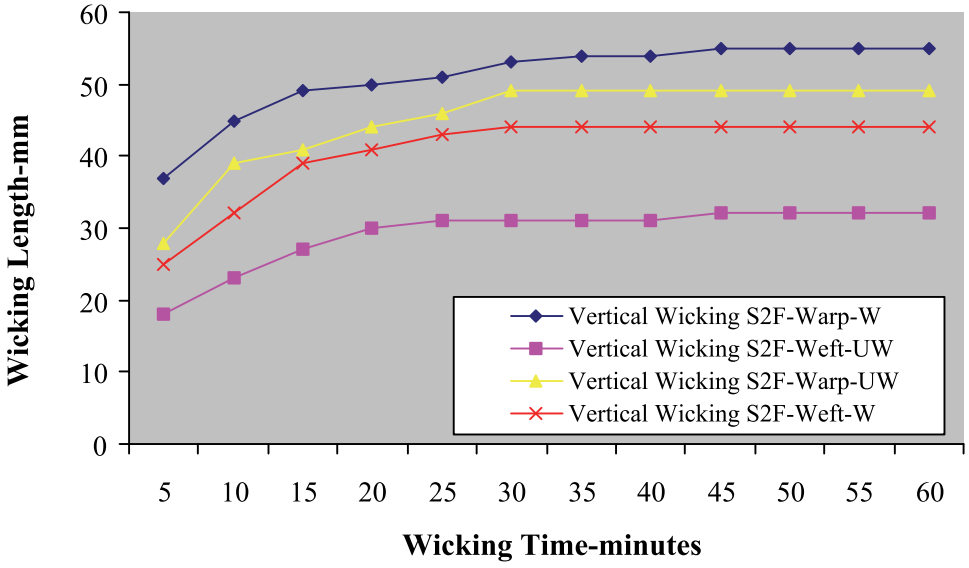

Fig. 21. Wicking Tests Sample S2F-Washed Vs. Unwashed Fabrics

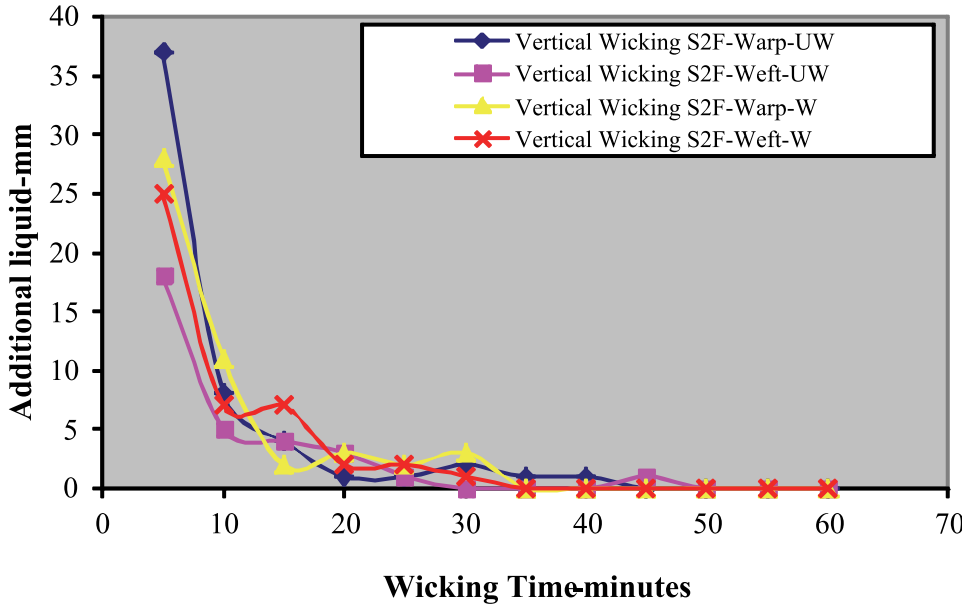

Fig. 22. Actual Liquid Advance Sample S2F -Washed Vs Unwashed Fabrics

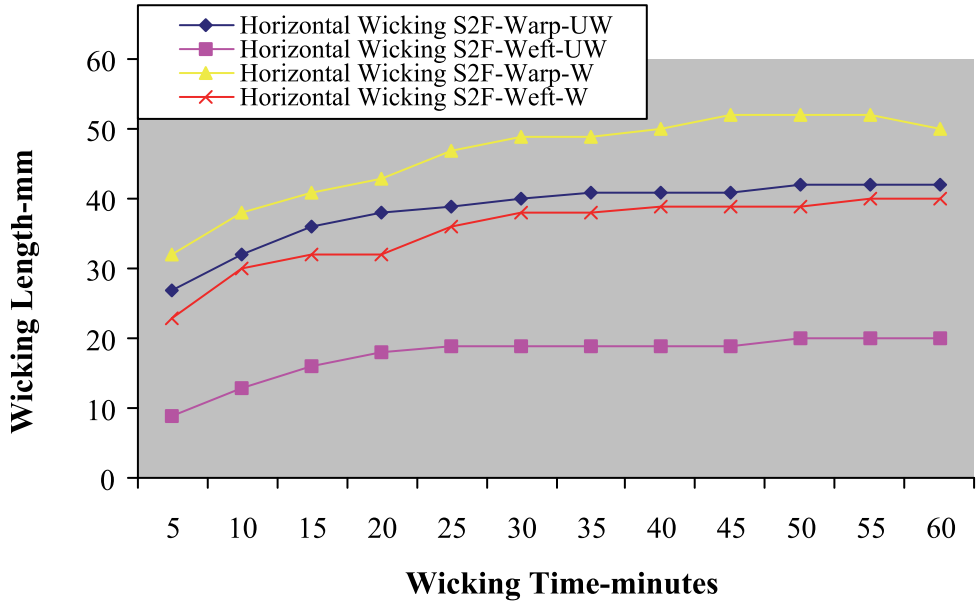

Fig. 23. Wicking Tests Sample S2F-Washed Vs. Unwashed Fabrics

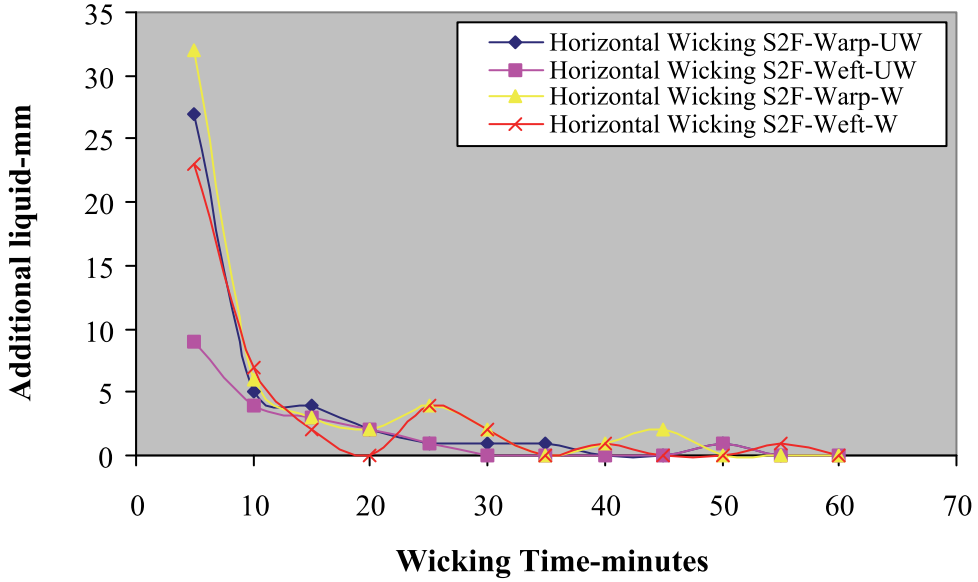

Fig. 24. Actual Liquid Advance Sample S2F -Washed Vs Unwashed Fabrics

7. Consistency with Washburn's equation: Fabrics

The general laws that govern capillary flow in simple cylindrical tubes as expounded by Washburn's well-known equation shown in **(1)** is frequently used to study liquid transport in textile substrates as information obtained from such treatment is useful for the qualitative characterization of the process of liquid transport[13] in complex textile structures.

$$h = Ct^{\frac{1}{2}} \tag{1}$$

Where h is the distance travelled by a liquid in time t and C is proportional to the set of factors

$$\left(\frac{\gamma r \cos\theta}{\eta}\right)^{\frac{1}{2}} \tag{2}$$

Where γ = liquid surface tension, η = viscosity of the wicking liquid, θ = contact angle of the liquid against the fibre substance and r = capillary radius.
Several researchers have modified the expression as a basis for calculation of liquid movement in textiles. Laughlin[19] modified the equation into a general form

$$h = ct^{k} \tag{3}$$

Taking logarithms of both sides of this equation gives

$$\ln(h) = k\ln(t) + \ln c \tag{4}$$

This equation has the form of a straight line.
Plots of the logarithm of the height of rise h and the logarithm of the duration of time t in Figures 19 to 26 have a form of a straight line indicating that the wetting liquid follows diffusive capillary dynamics.[20] The tabulation of the k values of fabric S2F made from flat continuous filament yarns given in Table 8 ranged from 0.1487-0.2925 and for fabric S1F composed of continuous filament warp and textured filament weft yarns the range was from 0.3312-0.4427. In all the cases the time exponents k were less than Washburn's predicted time exponent of 0.5. which was attributed to the non-uniformity of the weft filament arrangement and the simultaneously occurrence of wetting, wicking, liquid dispersion and evaporation. Data points deviating from the trend line (Figures 25-32) mostly towards the end is an indication that with a significantly volatile liquid like water, evaporation from the wet surface of the fabric strip can compete with capillary process that advances the liquid.[12]

Sample	Description	Vertical wicking k-value	Horizontal wicking k-value
S1F-warp direction	Unwashed Washed	0.4427 0.3262	0.3255 0.3478
S1F-weft direction	Unwashed Washed	0.3312 0.3277	0.4217 0.3773
S2F-warp direction	Unwashed Washed	0.1487 0.2051	0.1725 0.1965
S2F-weft direction	Unwashed Washed	0.2179 0.2133	0.2925 0.2125

Table 8. Strip Wicking Test k-values

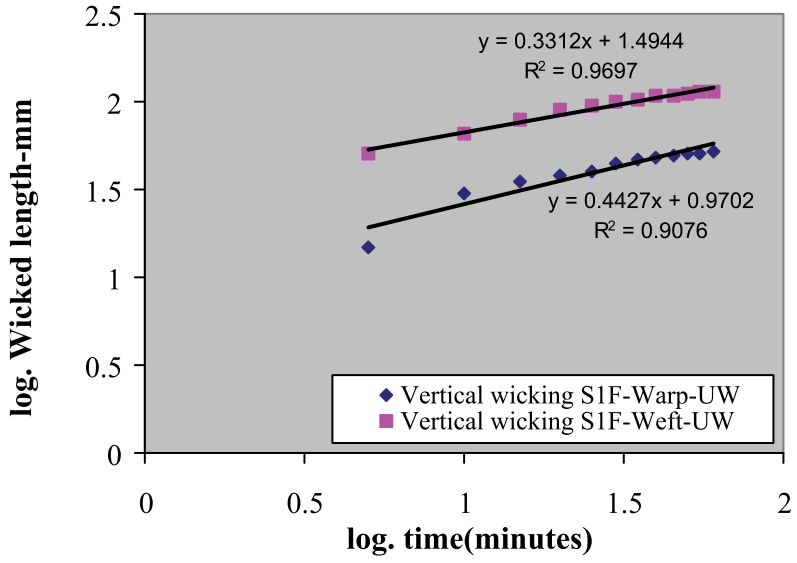

Fig. 25. Vertical Wicking Sample S1F-Unwashed Fabrics

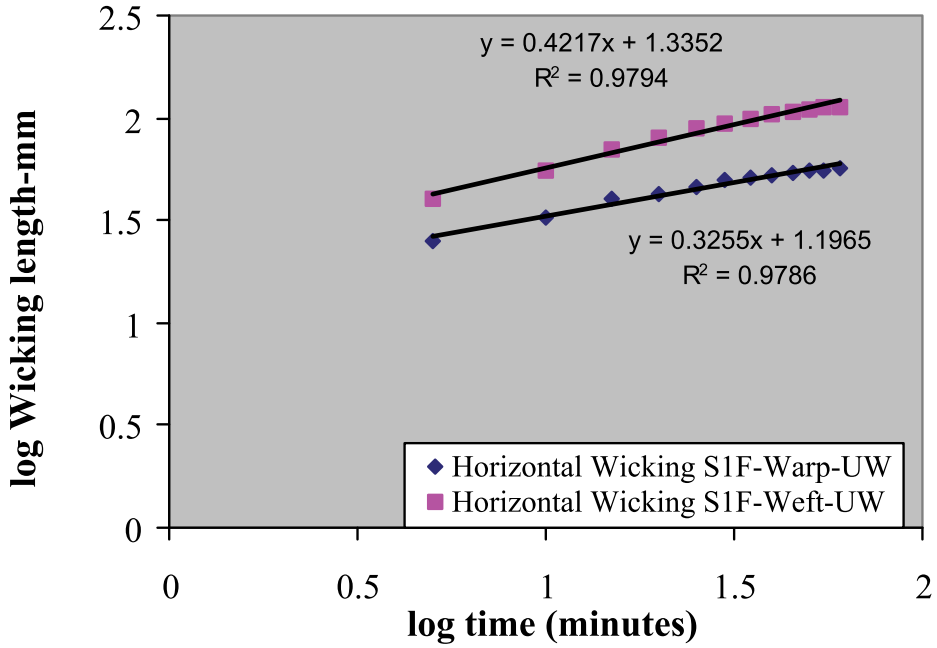

Fig. 26. Horizontal Wicking of Sample S1F -Unwashed Fabrics

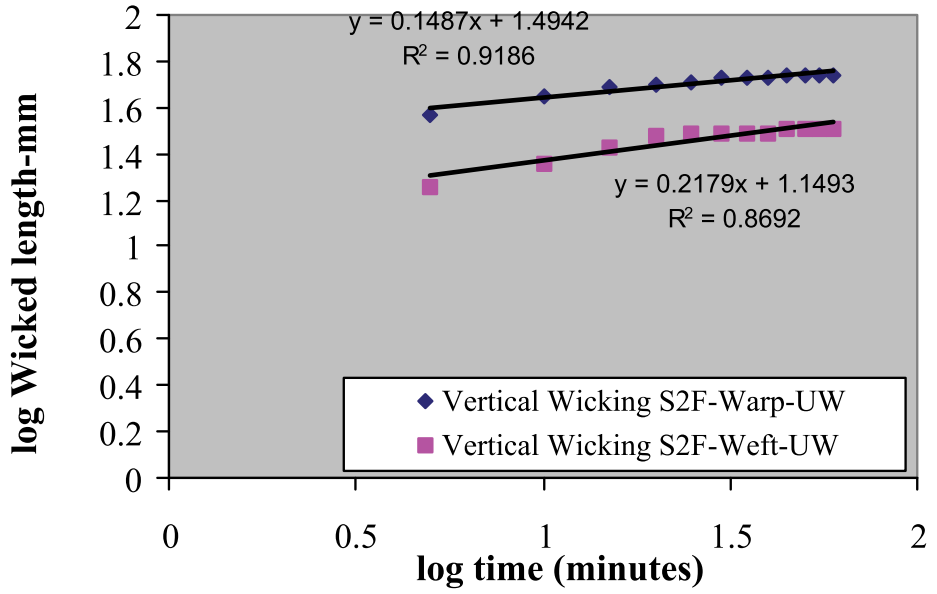

Fig. 27. Vertical Wicking Samples S2F-Unwashed Fabrics

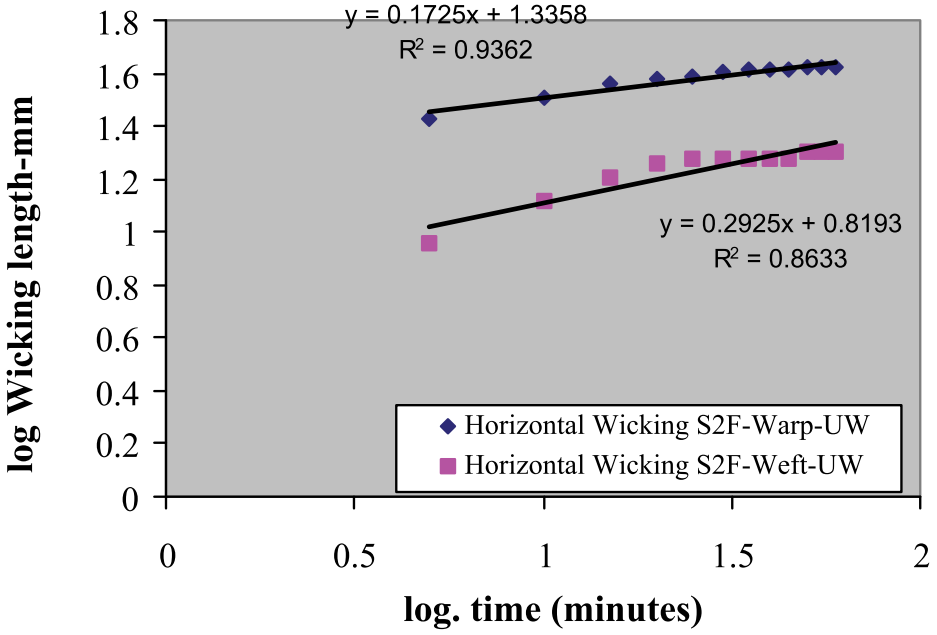

Fig. 28. Horizontal Wicking Sample S2F-Unwashed Fabrics

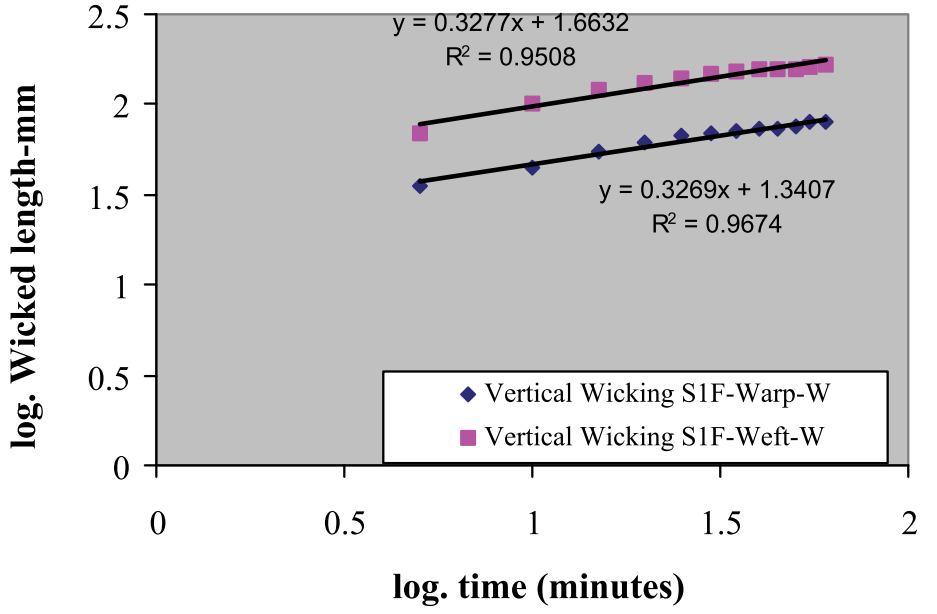

Fig. 29. Vertical Wicking Sample S1F-Washed Fabrics

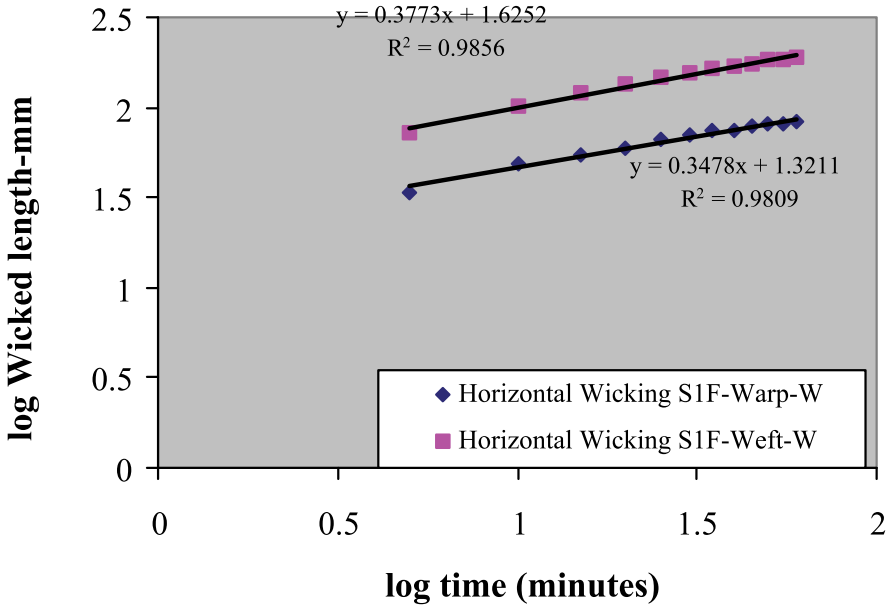

Fig. 30. Horizontal Wicking Sample S1F-Washed Fabrics

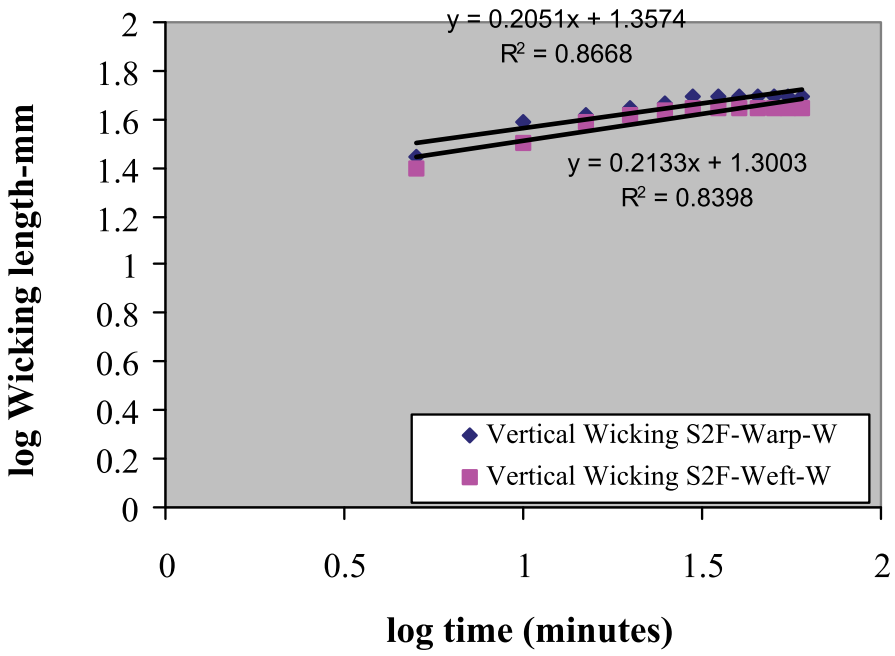

Fig. 31. Vertical Wicking Sample S2F-Washed Fabrics

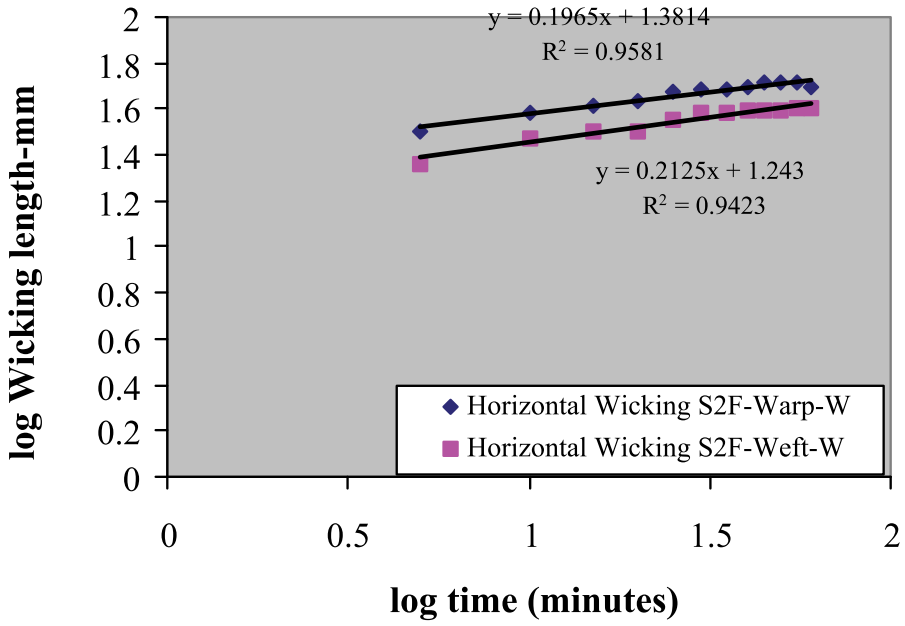

Fig. 32. Horizontal Wicking Sample S2F-Washed Fabric

8. Conclusion

Miller and Tyomkin[21] state that when a porous material such as a fabric is placed in contact with a liquid, spontaneous uptake of liquid may occur. Law[9] observed that if the wicking distance is plotted against time, the graph is expected to have an initial rapid rate of change which decreases subsequently because water is first sucked into wider capillary channels by the action of surface tension. As the wicking process proceeds further, the total viscous resistance to the flow increases and the rate of flow decreases. In the case of the vertical strip test, the height and the mass of the water absorbed in the sample strip will gradually reach a quasi-equilibrium state when they are balanced by the hydrostatic head of water. In the case of the horizontal strip test, if the supply water is unlimited, the rate of penetration will gradually become constant.[9] In thick fabrics vertical wicking would continue with little effect of evaporation until a quasi-equilibrium state is reached when the wicking level in the fabric is balanced by gravity.[10]

In this work vertical and horizontal wicking of samples S1F and S2F did not continue indefinitely indicating that due to the combination of low fabric weight and thickness the maximum wicking height was not only influenced by gravity but also by evaporation. The rate of evaporation of liquid therefore determined the equilibrium point for both vertical and horizontal wicking of samples S1F and S2F indicating good properties required for eliminating perspiration discomfort which would cause fabric wetness with resulting problems of freezing in winter or clamminess[22] in summer. In most cases, the leading front of the water rise observed at the end of each test period felt dry to the touch which can be attributed to the rapid liquid evaporation of the fabrics.

In textured yarns, the manner in which the liquid is transported through the fabric is determined by the minute loops or coils that characterize air –textured yarns which act as pores that vary in shape and distribution and may or may not be interconnected. Hsieh[6] noted that pore variation and distribution leads to preferential liquid movement towards smaller pores, resulting in partial draining of previously filled pores in the fibrous structure. In all cases studied in this work, tests showed that there is a good linear relationship between the logarithm of the wicked liquid (l) and the logarithm of the wicking time (t) indicating that the wetting liquid follows diffusive capillary dynamics[20] even though for sample S1F in most cases the exponential values were high compared to sample S2F due to evaporation from the parallel packed filaments of the yarn structures.

The high **k** values of fabrics containing textured weft yarns indicate the characteristics of a non-homogenous capillary system where wicking is a discontinuous process due to the irregular capillary spaces of varying dimensions.[11] Rapid wicking is retarded by the 'absorber' textured weft yarns which are more bulky and act as temporary liquid reservoirs as all the voids are filled up. On the other hand, the inter-filament wicking rate is increased once the liquid is transferred to the flat 'runner'continuous filament warp yarn due to capillary sorption[11] resulting in spiked wicking behaviour observed.

Wicking is also affected by fabric construction. Fabric sample S2F wicked more rapid in the warp than in the weft direction due to the high density of ends in the fabric. If the filament packing in the yarn is assumed to be an idealized or closely packed assembly[23] there will be more capillaries in the warp than in the weft direction due to the distribution in the number of ends and picks.

Outdoor active wear such as jackets are infrequently washed and research[24] results have shown that a standard 5 washes of vests used for mountaineering resulted in a significant

increase in their wicking performance. Even though a spin finish was applied to fabrics S1F and S2F during finishing to give surface properties which can allow liquid flow, the durability of the spin finish to washing was insignificant since laundering of fabrics resulted in a significant increase in their wicking performance. Washing therefore did not lead to the collapse of the capillary system of the fabric but results in the re-arrangement of the capillaries between filaments due to the washing liquid movements and the relaxation of the textile structure during drying.[24]

9. References

[1] Barnes J.C and Holcombe B.V., Textile Res. J., 66(12), 777-786, 1996
[2] Brownless N.J., Anand S.C., Holmes D.A. and Rowe T., J. Text. Inst., 87 Part 1, No.1, 172-182, 1996.
[3] Brownless N.J., Anand S.C., Holmes D.A. and Rowe T., Textile Asia, August 1996, 77-80.
[4] Slater K.,Comfort Properties of Textiles, Textile Progress, Volume 9, Number 4, 1-91, Textile Institute 1977.
[5] Yoon H.N. and Buckley A., Text. Res. J., 54, 289-298, 1984.
[6] You-Lo Hsieh, Text. Res. J., 65(5), 299-307, 1995
[7] Brownless N.J., S.c. Anand, D.A. Holmes and T. Rowe, World Sports Activewear, Volume 2, No.2, 36-38, 1996
[8] A.B. Nyoni and D. Brook, J. Text. Inst., Vol.97, No.2, 2006, 119-128.
[9] Law Y.M.M., Ph.D Thesis, University of Leeds, 1988.
[10] Zhuang Q., Ph.D. Thesis, University of Leeds, 2001.
[11] Kissa E., Text. Res. J., 66 (10), 660-668, 1998
[12] Miller B., International Nonwovens Journal, Volume 9, No.1, Spring 2000.
[13] Pronoy K. Chatterjee and Hien V. Nguyen., Mechanism of Liquid Flow and Structure Property Relationships., Absorbency, Chapter II., Edited by Pronoy K. Chatterjee, Elsevier Scientific Publishers; Amsterdam; New York, NY: 1985.
[14] Harnett P.R. and Mehta P.N., Tex. Res. J., 54, 471-478, 1984
[15] A.B Nyoni., (2003), PhD Thesis, University of Leeds.
[16] Hepburn C.D., PhD. Thesis, University of Leeds 1998
[17] Leijala A and Hautojarvi. J, Text. Res. J.,68(3), 193-202, 1998.
[18] Blyth G.T., Ph.D. Thesis, University of Leeds, 1984.
[19] Laughlin R.D. and Davies J.E., Text. Res. J., 31,904-910, 1961.
[20] Anne Perwuelz, Mthilde Casetta and Claude Caze, Polymer Testing, Volume 20, Issue 5, 553-561, 2001.
[21] Miller B. and Tyomkin. I., Text. Res. J., Volume 54, 706-712, Nov. 1984
[22] Rees W.H., Text. Month, 59-61, August 1969
[23] Hearle J.W.S., Grosberg P., and Backer S., Structural Mechanics of Fibres, Yarns, and Fabrics. Volume 1, 1969, John Wiley; New York, NY, USA.
[24] A.B Nyoni and D.Brook, Textile Research Journal ,Vol.80(8), 2010, 720-725.